

Uncovering and Functional Analysis of Novel Genes and Potential Genetic Modifiers for Neuromuscular Disorders



Inaugural-Dissertation
zur
Erlangung des Doktorgrades
der Mathematisch-Naturwissenschaftlichen Fakultät
der Universität zu Köln

vorgelegt von
Natalia Mendoza-Ferreira
aus Popayán, Kolumbien

Köln
2018

The Doctoral Thesis “Uncovering and Functional Analysis of Novel Genes and Potential Genetic Modifiers for Neuromuscular Disorders” was performed at the Institute of Human Genetics, Institute of Genetics and Centre for Molecular Medicine Cologne (CMMC) of the University of Cologne from April 2013 to October 2017.

Berichterstatter: Prof. Dr. rer. nat. Brunhilde Wirth

Prof. Dr. rer. nat. Elena I. Rugarli

Tag der mündlichen Prüfung: 12.12.2017

TABLE OF CONTENT

LIST OF FIGURES	VII
LIST OF TABLES.....	IX
ABBREVIATIONS	X
SUMMARY	XII
ZUSAMMENFASSUNG	XIV
1. PREAMBLE AND THESIS OUTLINE	1
2. INTRODUCTION	3
PART I. IDENTIFICATION AND FUNCTIONAL CHARACTERIZATION OF NOVEL NMD-CAUSATIVE GENES.....	3
2.1. Neuronal circuitry of movement control, an overview	3
2.2. Inherited neuromuscular disorders.....	4
2.2.1. Prevalence of NMDs	4
2.2.2. General classification of NMDs	5
2.2.3. Diagnosis of NMDs	6
2.3. Identification of novel disease-causing genes.....	7
2.3.1. Whole Exome Sequencing	7
2.3.1.1. Linkage analysis	8
2.3.1.2. <i>De novo</i> inheritance assumption.....	8
2.4. Calcineurin Homologous Protein-1 (CHP1) is a novel causative gene of Autosomal Recessive Cerebellar Ataxia (ARCA).....	9
2.4.1. Inherited cerebellar ataxias.....	9
2.4.1.1. Autosomal dominant ataxias.....	10
2.4.1.2. X-linked ataxia	11
2.4.1.3. Mitochondrial ataxias	11
2.4.1.4. Autosomal Recessive Cerebellar Ataxias (ARCAs).....	12
2.4.1.4.1. Clinical features of recessive cerebellar ataxias	13
2.4.1.4.2. Common ARCA syndromes.....	14
2.4.2. Calcineurin Homologous Protein-1 (CHP1).....	19
2.4.2.1. CHP1 molecular functions	20
2.4.2.1.1. Regulation of gene transcription	20
2.4.2.1.2. Regulation of intracellular trafficking.....	20
2.4.2.1.3. CHP1 as regulator of integral membrane proteins. The CHP1-NHE1 interaction.	21
2.4.2.2. CHP1 animal models	22
2.5. Functional characterization of a <i>de novo</i> mutation in <i>SLC18A3</i> in a family with distal motor neuropathy (dHMN)	23

2.5.1. Inherited distal motor neuropathies (dHMNs)	23
2.5.1.1. Classification of dHMNs	24
2.5.1.1.1. Autosomal dominant distal HMN	24
2.5.1.1.2. Autosomal recessive distal HMN	25
2.5.1.1.3. X-linked distal HMN	25
2.5.1.2. Molecular pathogenesis of dHMNs	27
2.5.2. Vesicular Acetylcholine Transporter (VACHT)	28
2.5.2.1. The cholinergic neurotransmission	28
2.5.2.2. Animal models of VACHT	29
2.5.2.3. Mutations in VACHT underlie congenital myasthenic syndromes	30
PART II. CHP1 REDUCTION AMELIORATES MOTOR NEURON DEGENERATION IN A ZEBRAFISH MODEL OF SMA	31
2.6. Modifier genes of Spinal Muscular Atrophy	31
2.6.1. Plastin 3	33
2.6.2. Neurocalcin delta	34
3. STUDY AIMS	35
4. RESULTS	37
PART I. IDENTIFICATION AND FUNCTIONAL CHARACTERIZATION OF NOVEL NMD-CAUSATIVE GENES	37
4.1. Calcineurin Homologous Protein-1 (CHP1) is a novel causative gene of autosomal recessive cerebellar ataxia	37
4.1.1. Detailed clinical features of the index family	38
4.1.2. Linkage analysis and WES in the index family	40
4.1.2.1. Whole genome linkage analysis (WGLA).....	40
4.1.2.2. WES identifies CHP1 as the causative gene of autosomal recessive cerebellar ataxia	41
4.1.3. Focused screening for <i>CHP1</i> variants in two large neurodegenerative disease cohorts	45
4.1.4. Generation and validation of V5-tagged CHP1-WT and CHP1-K19 constructs for protein expression analyses	46
4.1.5. The K19del mutation alters CHP1 expression and solubility	48
4.1.6. CHP1-K19del adopts larger protein conformations	50
4.1.7. Mutant CHP1 is prone to aggregation	52
4.1.7.1. Optimization of Neuro2A culture and differentiation.....	53
4.1.7.2. Expression and cellular localization of GFP-tagged CHP1 proteins	55
4.1.7.2.1. CHP1 aggregates colocalize with protein homeostasis markers	57
4.1.8. The K19del mutation potentially alters CHP1 conformational changes	58
4.1.9. Membrane-bound NHE1 is reduced upon overexpression of CHP1 K19del	60
4.1.10. Generation of a zebrafish model for <i>chp1</i>-deficiency analyses	63

4.1.10.1. Description of selected neurological readouts. Why and how to assess motor neuron and cerebellar defects underlying <i>chp1</i> depletion?.....	63
4.1.10.2. Selection of a suitable MO-dosage for phenotypic analyses	64
4.1.10.3. Generation of CHP1 WT and mutant mRNAs for rescue experiments	67
4.1.10.4. <i>chp1</i> downregulation in zebrafish causes motor axon, cerebellar and movement defects, which are rescued by WT but not mutant CHP1 mRNA.....	69
4.1.10.5. Chp1 downregulation do not affect axonal projections of other neuronal populations	72
4.1.10.6. Endocrine dysfunction is independent of CHP1 expression	73
4.2. Functional characterization of a <i>de novo</i> mutation in <i>SLC18A3</i> in a family with distal motor neuropathy	75
4.2.1. Clinical features of the index family and candidate gene identification.....	75
4.2.2. The D147N mutation has no effect in VAcHT subcellular distribution	77
4.2.3. Generation of <i>VAcHT-WT</i> and <i>VAcHT-D147N</i> human mRNAs for protein OE analysis in zebrafish.....	78
4.2.3.1. OE of VAcHT-WT, as well as VAcHT-D147N, increase CaP-MN axonal outgrowth	80
PART II. CHP1 REDUCTION AMELIORATES MOTOR NEURON DEGENERATION IN A ZEBRAFISH MODEL OF SMA	84
4.3. MO-mediated downregulation of <i>chp1</i> restores CaP-MN axonal outgrowth in <i>smn</i> zebrafish morphants	85
4.4. Chp1 is expressed in zebrafish MNs.....	87
5. DISCUSSION	89
5.1. Biallelic mutation of <i>CHP1</i> expands the number of genes causing ARCA	89
5.1.1. <i>CHP1</i> variants are scarce.....	90
5.1.2. Is CHP1-K19del aggregation proneness a disease mechanism?	90
5.1.3. Zebrafish model of <i>chp1</i> downregulation closely recapitulates the phenotype of ARCA-affected patients.....	91
5.1.4. Incomplete phenotypic translation from fish and mouse to human	93
5.1.5. Intracellular pH (pHi) imbalance and neuronal degeneration. A potential molecular mechanism underlying CHP1-related ARCA pathogenesis.....	95
5.1.6. A second WES variant potentially explains endocrine dysfunction in female proband of the CHP1 family.....	97
5.2. Functional characterization of a <i>de novo</i> mutation in <i>SLC18A3</i> (VAcHT) in a family with distal motor neuropathy	98
5.2.1. Is the VAcHT-D147N mutation causative of dHMN?.....	98
5.3. Chp1 reduction ameliorates axonal outgrowth defects in a zebrafish model of SMA	100
5.3.1. CHP1 reduction is ARCA-causative and SMA protective. A matter of protein dosage	103
5.4. Concluding remarks and future outlook.....	104
6. MATERIALS AND METHODS	107

6.1. Materials	107
6.1.1. Laboratory equipment and devices	107
6.1.1.1. Zebrafish equipment	108
6.1.2. Chemicals	108
6.1.3. Reagents	109
6.1.3.1. Molecular biology reagents	109
6.1.3.2. Cell culture reagents and media	110
6.1.3.3. Zebrafish work reagents.....	110
6.1.4. Enzymes	110
6.1.5. Antibodies and staining reagents	111
6.1.6. Routinely used media and solutions	112
6.1.6.1. Cell culture and growth media.....	112
6.1.6.2. Solutions for DNA work.....	112
6.1.6.3. Solution for work with bacteria	112
6.1.6.4. Solutions for immunostaining	112
6.1.6.5. Solutions for protein work.....	113
6.1.7. Cell lines and zebrafish strains	113
6.1.7.1. Cell lines.....	113
6.1.7.2. Zebrafish strains and lines	114
6.1.8. Primers and morpholinos	114
6.1.8.1. Primers for cloning	115
6.1.8.2. Primers for site-directed-mutagenesis	115
6.1.8.3. Primers for Semi-Quantitative RT-PCR	115
6.1.8.4. Morpholinos for zebrafish experiments	116
6.1.9. Plasmids	116
6.1.10. Kits	117
6.1.11. Software packages	117
6.1.12. Internet databases and web applications of routine use	117
6.2. Methods	118
6.2.1. Patient's recruitment and ethics regulations	118
6.2.1.1. The <i>CHP1</i> family	118
6.2.1.2. The <i>SLC18A3</i> family	118
6.2.2. Molecular biology methods	119
6.2.2.1. Isolation of plasmidic DNA from bacteria	119
6.2.2.2. Isolation of RNA from eukaryotic cells	119
6.2.2.3. Polymerase chain reaction (PCR).....	120
6.2.2.3.1. Standard PCR reaction	120
6.2.2.3.2. Site directed mutagenesis PCR.....	121
6.2.2.4. Clean-up of PCR products	122

6.2.2.5. Agarose gel electrophoresis	122
6.2.2.6. Reverse transcription (cDNA synthesis)	122
6.2.2.7. Semi-quantitative Reverse Transcription PCR	123
6.2.2.8. Cloning procedures	123
6.2.2.8.1. Cloning into TOPO vector	123
6.2.2.8.2. Subcloning into PCS2+ vector	124
6.2.2.9. <i>In vitro</i> transcription of mRNA	125
6.2.2.10. DNA sequencing	125
6.2.3. Microbiology work	125
6.2.3.1. Transformation of DNA into competent <i>E.coli</i> cells	126
6.2.3.2. Colony PCR	126
6.2.3.3. Preparation of bacteria glycerol stocks	126
6.2.4. Gene identification methods	127
6.2.4.1. Whole genome linkage analysis	127
6.2.4.2. Whole Exome Sequencing	127
6.2.4.3. Population screening for <i>CHP1</i> variants	128
6.2.4.3.1. Re-sequencing of <i>CHP1</i> exons 2 and 6	128
6.2.4.3.2. Search for <i>CHP1</i> variants in a NMD cohort.	129
6.2.5. Cell culture	129
6.2.5.1. Cultivation of eukaryotic cell lines	129
6.2.5.2. Cell counting	130
6.2.5.3. Cryopreservation of cell lines	130
6.2.5.4. Cell transfection for transient protein overexpression	130
6.2.5.5. Seeding and differentiation of neuron-like cells	131
6.2.6. Protein biochemistry methods	131
6.2.6.1. Protein isolation from eukaryotic cells	131
6.2.6.2. Subcellular fractionation of total protein lysates	132
6.2.6.3. Protein isolation from zebrafish	132
6.2.6.4. Determination of protein concentration with Bradford	132
6.2.6.5. Sodium Dodecyl Polyacrylamide Gel Electrophoresis SDS-PAGE	133
6.2.6.6. Western blot	133
6.2.6.7. Protein immunodetection on Western Blot membranes	134
6.2.6.8. Size Exclusion Chromatography	134
6.2.6.9. Protein modelling	135
6.2.7. Fluorescence immunostaining	135
6.2.7.1. Immunostaining of eukaryotic cells	135
6.2.7.2. Immunostaining of zebrafish	136
6.2.7.2.1. Visualization of Caudal Primary Motor Neurons (CaP-MN)	136
6.2.7.2.2. Cerebellum visualization	137

6.2.8. Microscopy	137
6.2.8.1. Colocalization analysis.....	138
6.2.9. Zebrafish methods	138
6.2.9.1. Zebrafish breeding and egg collection	138
6.2.9.2. Zebrafish injection of Morpholinos (MOs) and mRNAs	139
6.2.9.3. Zebrafish motor analysis	139
6.2.10. Statistical analysis	140
7. REFERENCES	141
8. PUBLICATIONS, PRESENTATIONS, SCHOLARSHIPS AND AWARDS	174
ACKNOWLEDGMENTS	XVII
EIDESSTATTLICHE ERKLÄRUNG	XIX
LEBENS LAUF	XX

LIST OF FIGURES

Figure 1. Neural systems for movement control.	3
Figure 2. Neuroimaging features of three ARCA types.....	14
Figure 3. Molecular pathogenesis of the autosomal recessive ataxias.	19
Figure 4. Main cellular processes regulated by CHP1.	22
Figure 5. Molecular pathomechanisms in dHMNs.....	28
Figure 6. ACh synthesis, packaging and release in cholinergic neuron.....	29
Figure 7. The genetic determinants of SMA.....	33
Figure 8. Kindred structure of the index family.....	38
Figure 9. Brain MRI of male proband at 22 years of age.....	40
Figure 10. Multipoint linkage analysis.....	41
Figure 11. Pedigree of the index family and Sanger confirmation of the CHP1-K19del mutation in affected probands.	43
Figure 12. Time-course protein and mRNA expression analyses from HEK293T cells transiently expressing CHP1-WT-V5 and CHP1-K19del-V5.....	46
Figure 13. Time-course protein and mRNA expression analyses after 48h transfection.....	47
Figure 14. The K19del mutation affects the expression and solubility of CHP1 in HEK293T cells.....	48
Figure 15. The K19del mutation affects the expression and solubility of CHP1 in N2A cells.....	49
Figure 16. K19del mutation alters CHP1 protein conformations and folding.....	50
Figure 17. The K19del mutation alters NHE1 elution in HMW complexes.....	52
Figure 18. Optimization of N2A differentiation.....	54
Figure 19. Protein aggregation in cell lines transiently expressing WT and mutant CHP1-GFP.....	56
Figure 20. CHP1-K19del-GFP aggregates colocalize with proteostasis markers.....	58
Figure 21. CLUSTALW2 alignment of CHP1 from <i>H. sapiens</i> and <i>R. norvegicus</i>	59
Figure 22. K19del mutation potentially compromises CHP1 conformational changes.	60
Figure 23. CHP1-K19del impairs NHE1 membrane targeting in HEK293T cells.....	61
Figure 24. CHP1-K19del impairs NHE1 membrane targeting in N2A cells.....	62
Figure 25. Quantitative analysis of body axis phenotype upon injection of increasing concentrations of <i>chp1</i> MO.....	65
Figure 26. <i>chp1</i> MO dosage optimization.....	66
Figure 27. mRNA quality assessment and WB confirmation of <i>CHP1</i> mRNAs overexpression.....	67

Figure 28. Overexpression of sole <i>CHP1-WT</i> and <i>CHP1-K19del</i> mutant mRNAs has no effect on CaP-MN or cerebellar morphology.....	68
Figure 29. CHP1 downregulation in zebrafish causes CaP-MN, cerebellar and movement defects which are rescued with WT, but not mutant <i>CHP1</i> mRNA.....	70
Figure 30. Injection of 1ng <i>chp1</i> MO do not affect other neuronal populations.....	73
Figure 31. Macroscopic examination of uteri and ovaries from <i>Chp1^{vac/vac}</i> females.	74
Figure 32. Mutant VACHT overexpression has no effect on protein subcellular distribution.....	78
Figure 33. mRNA quality assessment and WB confirmation of <i>VACHT</i> mRNAs overexpression.....	79
Figure 34. OE of VACHT-WT and VACHT-D147N has no effect on CaP-MN morphology.	80
Figure 35. CaP-MN axonal length upon VACHT-WT and VACHT-D147N OE.....	82
Figure 36. Injection of <i>smn</i> and <i>chp1</i> MOs, alone or in combination, efficiently reduce protein expression.	86
Figure 37. Chp1 downregulation ameliorates CaP-MN defects in <i>Smn</i> -depleted zebrafish.....	87
Figure 38. Chp1 is expressed in zebrafish spinal cord MNs at larvae-developmental stage.....	88
Figure 39. CHP1-mediated NHE1 deregulation causes ataxia.	97
Figure 40. A model of CHP1 balance in ARCA and SMA.....	104
Figure 41. CaP-MN axon morphology.	137

LIST OF TABLES

Table 1. General classification of neuromuscular disorders and known causative genes...	5
Table 2. Assumptions for WES variants filtering.....	9
Table 3. Typical signs and symptoms of ARCAs.....	13
Table 4. List of ARCAs with predominant cerebellar involvement.....	17
Table 5. Classification of dHMNs and recently described causative genes.....	26
Table 6. Clinical features and neurophysiological findings of the affected probands.....	39
Table 7. Characteristics of variants segregating in index family.....	44
Table 8. Focused screening of <i>CHP1</i> mutations in ARCA cohort.....	45
Table 9. Clinical features and neurophysiological findings of the affected probands.....	76
Table 10. Standard PCR components.....	120
Table 11. Standard PCR program.....	120
Table 12. PCR components for site-directed-mutagenesis.....	121
Table 13. Reverse transcription set-up for a 20µl reaction.....	123
Table 14. Standard double digestion reaction.....	124
Table 15. Standard ligation reaction with T4 DNA ligase (Promega).....	124
Table 16. Reaction set-up for <i>in vitro</i> mRNA transcription.....	125
Table 17. Cells seeding densities for transfection experiments.....	130
Table 18. Protein standards used for SEC column calibration.....	135

ABBREVIATIONS

A	adenine
AChR	acetylcholine receptor
ALS	amyloid lateral sclerosis
APS	ammonium persulfate
ARCA	autosomal recessive cerebellar ataxia
bp	base pairs
BSA	bovine serum albumin
C	cytosine
CaP-MN	caudal primary motor neuron
cDNA	coding DNA
CMT	Charcot-Marie-Tooth
CNS	central nervous system
CNV	copy number variation
dHMN	distal hereditary motor neuropathy
DMEM	Dulbecco's modified Eagle medium
DMSO	dimethyl sulfoxide
DNA	deoxyribonucleic acid
EDTA	ethylene diamine tetraacetic acid
e.g.	exempli gratia
EMG	Electromyography
et al.	et alii
FCS	fetal calf serum
FL	full length
FWD	forward
G	guanine
GFP	green fluorescent protein
h	hours
HCA	hereditary cerebellar ataxias
HMW	high molecular weight
hpf	hours post fecundation
HSP	hereditary spastic paraplegia
i.e.	id est
indel	insertion or deletion
kb	kilobases
KD	knock-down
kDa	kilodalton
KO	knock-out
L	liter
LINKS	Lichtenstein-Knorr Syndrome
LMN	lower motor neuron
LMW	low molecular weight
LOD	logarithm of the odds
m	mili
μ	micro
M	molar
min	minutes

MN	motor neuron
MO	morpholino
MRI	magnetic resonance imaging
mRNA	messenger RNA
n	number
NGS	next generation sequencing
NMD	neuromuscular disorder
NMJ	neuromuscular junction
NMR	nuclear magnetic resonance
n.s.	not significant
OMIM	Online Mendelian Inheritance in Man
OE	overexpression
o.n.	overnight
<i>P</i>	probability
PAA	polyacrylamide
PBS	phosphate buffered saline
PCR	polymerase chain reaction
PD	Parkinson's disease
PFA	paraformaldehyde
pH	potential of hydrogen
pHi	intracellular pH
pmol	picomol
RNA	ribonucleic acid
REV	reverse
rpm	revolutions per minute
SEC	size exclusion chromatography
SNP	single nucleotide variation
SD	standard deviation
SDS	sodium dodecyl sulfate
sec	seconds
SEM	standard error of means
SMA	spinal muscular atrophy
T	tyrosine
UMN	upper motor neuron
UTR	untranslated region
WB	western blot
WES	whole exome sequencing
WGLA	whole genome linkage analysis
WGS	whole genome sequencing
WT	wildtype

SUMMARY

The inherited Neuromuscular Disorders (NMDs) is an umbrella term that encompasses a plethora of diseases that affect the functioning of the muscles and/or their underlying nervous system control. Although individually uncommon, NMDs collectively are no longer considered rare diseases. Only in Europe, approximately 300,000 people are yearly diagnosed with one NMD. The diagnosis of a neuromuscular condition –successful in less than 50% of the cases- is often devastating to patients and their relatives. No cure is available for most of these disorders, and the few available treatments will at best delay disease progression. To find treatments and to develop methods for the early diagnosis of NMDs is a goal of highest importance, and the recent advances in the NGS technologies are the platform to reach this objective. Particularly, the implementation of WES has not only minimized the time and costs of genetic diagnostics but also provided unique opportunities for the exploration of gene function in NMDs pathogenesis.

The uppermost goal of this PhD project was to identify and characterize novel NMDs-causative genes. Thereby, two novel NMD-causative genes were investigated in this thesis. First, *CHP1* (Calcineurin Homologous Protein-1) was identified as a novel causing gene of Autosomal Recessive Cerebellar Ataxia (ARCA) and second, VACHT (Vesicular Acetylcholine Transporter, encoded by *SLC18A3*) was analysed in the context of distal Hereditary Motor Neuropathy (dHMN).

Following a combination of WES and linkage analysis, we identified a biallelic 3-bp deletion (p.K19del) in *CHP1* that co-segregates with a complex ARCA in two siblings of a consanguineous family exhibiting motor neuropathy, cerebellar atrophy and spastic paraparesis. *CHP1* was selected as a top disease candidate since: (I) the mutation affects an amino acid highly conserved across species, (II) a point mutation in murine *Chp1*, causing aberrant splicing and reduced full-length *Chp1* transcripts, leads to Purkinje cells loss and ataxia, (III) *CHP1* assists posttranscriptional glycosylation and membrane localization of NHE1, a major neuronal Na^+/H^+ exchanger, (IV) KO of mouse *Nhe1* cause ataxia and loss-of-function mutation in *NHE1* (encoded by *SLC19A1*) cause ataxia-deafness Lichtenstein-Knorr syndrome (LINKS). Therefore, we hypothesized that a mutation in *CHP1*, as a crucial regulator of NHE1, could impair expression and targeting of the exchanger resembling the pathogenesis in mice and humans. To further uncover other families carrying *CHP1* mutations, we performed a focused screening for *CHP1* variants in two large ARCA and NMD cohorts (approximately 1000 exomes). No additional variants fulfilling or selection criteria were found, which emphasizes on the scarcity of *CHP1* variants and the reduced tolerability of *CHP1* for mutations.

With the purpose to assess the functional consequences of the *CHP1*-K19del mutation on protein function, size exclusion chromatography (SEC), protein fractionation, 3D-protein modelling, fluorescence microscopy and *in vivo* zebrafish modelling were performed. We demonstrated that mutant *CHP1* fails to integrate into functional protein complexes and is prone to aggregate, thereby leading to diminished levels of soluble *CHP1* and reduced membrane targeting of NHE1 both in neuronal and non-neuronal cells. To analyze the pathogenic consequences of the hypomorphic *CHP1*-K19del mutation *in vivo*, we used morpholinos (MOs) to inhibit *chp1* translation in zebrafish. Closely resembling the clinical features of the ARCA-affected siblings, *chp1* downregulation in zebrafish led to cerebellar hypoplasia, Caudal Primary Motor Neuron (CaP-MN) defects and spastic trunk movements.

All defects were ameliorated by co-injection with WT, but not mutant, human *CHP1* mRNA, hence demonstrating both the specificity of the *chp1*-MO-induced phenotypes and validating the effect of CHP1-K19del on protein expression and/or function *in vivo*. Altogether, our results identified *CHP1* as a novel ataxia-causative gene in humans, further expanding the spectrum of ARCA-causative loci, and highlight the crucial role of NHE1 within the pathogenesis of these disorders.

Moreover, we conducted functional analyses to ascertain the functional basis of a dHMN presented by a family with cranial nerves palsy and vocal cord paresis as an initial feature of a non-progressive infantile onset dominant dHMN. WES analysis of this family led to the identification of a *de novo* dominant missense mutation (c.439 G>A, p.D147N) in VACHT. The mutation occurred first in the affected mother and was inherited by her affected daughter. VACHT controls the storage of the neurotransmitter Acetylcholine (ACh) by synaptic vesicles, hence it plays a fundamental role in cholinergic neurotransmission and therefore, in the plethora of processes reliant on it, which include: neuronal development and maturation, synaptic transmission and plasticity, patterning of the neuromuscular junction (NMJ), among others. The potential effect of the D147N mutation on VACHT subcellular distribution was analysed in neuron-like NSC-34 cells transiently overexpressing WT or mutant VACHT-GFP tagged proteins. No significant differences were observed in protein expression or localization, thus a detrimental effect of VACHT-D147N mutation at this level was not possible. This prompted us to further examine potential defects either in MN development and axonal outgrowth. Capitalizing once again on the advantages of the zebrafish for the modelling of human neurodegenerative disorders and further considering the evolutionary conservation of both VACHT and the D147 residue across species, the effect of WT and VACHT-D147N OE on CaP-MN outgrowth was analysed in detail. Although our findings were not conclusive at discerning the pathogenicity of the VACHT-D147N *in vivo*, we observed an axonal migration phenotype that could potentially underlie impairments at the NMJ level. In the light of the novel association of VACHT mutations as causative of myasthenia syndromes, follow-up studies will be performed in order to conclusively confirm the pathogenicity of the VACHT-D147N in a CaP-MN-independent context.

The biological function of CHP1 was of further relevance within the scope of this doctoral project, since CHP1 is currently subject of study as potential modifier of Spinal Muscular Atrophy (SMA). Pre-existing evidence from our research group indicates that Chp1 downregulation –within a certain threshold- restores neurite outgrowth and impaired endocytosis (a key pathway disturbed in SMA) in *Smn1*-depleted NSC-34 cells. Thereupon, this thesis further aimed to validate reduction of Chp1 as potential SMA protective modifier in a zebrafish model of SMA, as a first *in vivo* approach. Here, we demonstrate that Chp1 downregulation ameliorates the CaP-MN axonal outgrowth defects of *Smn*-deficient fish larvae. These findings are in concordance with prior validation studies of two other human SMA modifiers –PLS3 and NCALD- in zebrafish, which despite their different function and mode of action (upregulation or downregulation, respectively) exert similar effects on CaP-MN morphology whereby restoring the CaP-MN phenotype of *smn* morphants in a highly comparable range. Altogether, our findings together with the preliminary findings aforementioned, strongly support CHP1 reduction as a promising therapeutic target for a combinatorial treatment, *i.e.* together with SMN restoration, counteracting SMA pathology.

ZUSAMMENFASSUNG

Neuromuskuläre Erbkrankheiten (NMDs) sind ein Überbegriff für eine Vielzahl von Krankheiten, die die Funktionsfähigkeit der Muskeln und / oder der ihnen zugrunde liegenden Kontrolle des Nervensystems beeinflussen. Obwohl einzelne NMD Erkrankungen sehr selten auftreten, werden NMDs in ihrer Gesamtheit nicht als seltene Krankheit angesehen. Alleine in Europa werden jährlich ungefähr 300.000 Menschen mit einer NMD diagnostiziert. Die Diagnose einer neuromuskulären Erkrankung, die in weniger als 50% der Fälle erfolgreich ist, ist oft verheerend für die Patienten und ihre Angehörigen. Es gibt keine Heilung für die meisten dieser Erkrankungen und die wenigen verfügbaren Behandlungen können bestenfalls nur das Fortschreiten der Krankheit verzögern. Die Entwicklung von Methoden zur Früherkennung von NMDs und deren Behandlung ist deshalb ein Ziel von größter Wichtigkeit. Die jüngsten Fortschritte der NGS Technologie bieten die besten Voraussetzungen, um dieses Ziel zu erreichen. Insbesondere die Anwendung von *whole exome sequencing* (WES) hat nicht nur die Zeit und die Kosten der genetischen Diagnostik minimiert, sondern auch einzigartige Möglichkeiten für die Erforschung der Genfunktion bei der NMD-Pathogenese eröffnet.

Das wichtigste Ziel dieser PhD-Arbeit war die Identifikation und Charakterisierung neuartiger NMD-verursachender Gene, wovon zwei in dieser Arbeit untersucht worden sind. Als Erstes wurde CHP1 (Calcineurin Homologous Protein 1) als ein neues Gen identifiziert, das die autosomal-rezessive zerebelläre Ataxie (ARCA) verursacht. Ebenso wurde VACHT (Vesicular Acetylcholine Transporter, kodiert von *SLC18A3*) im Kontext der distalen hereditären motorischen Neuropathie (dHMN) analysiert.

In einer Kombination aus WES und Kopplungsanalyse wurde eine biallelische 3-bp Deletion (p.K19del) in *CHP1* entdeckt, die mit einer komplexen ARCA bei zwei Geschwistern einer blutsverwandten Familie ko-segregiert. Diese Individuen weisen eine motorische Neuropathie, zerebelläre Atrophie und spastische Paraparese auf.

CHP1 wurde aus den folgenden Gründen als krankheitsverursachendes Gen ausgewählt: (I) Die Mutation war in keiner öffentlichen Datenbank gelistet und betrifft eine Aminosäure, die in vielen Spezies hochgradig konserviert ist, (II) eine Punktmutation im murinen Chp1 verursacht anormales Spleißen und Reduktion des vollständigen Chp1 Transkripts, welches zu einem Verlust der Purkinjezellen und Ataxie führt, (III) CHP1 unterstützt die posttranskriptionale Glykolisierung und Membranlokalisierung von NHE1, einem wichtigen neuronalen Na⁺/H⁺-Austauscher, und (IV) *Nhe1*-Knockout im Mausmodell führt zu Ataxie und eine Funktionsverlustmutation in NHE1 (codiert von *SLC19A1*) verursacht das Ataxie-Taubheits-Syndrom und Lichtenstein-Knorr-Syndrom (LINKS). Aus diesen Gründen vermuteten wir, dass eine Mutation in CHP1, als entscheidender Regulator von NHE1, die Expression und Lokalisation von NHE1 beeinträchtigen würde und dies der Pathogenese in Mäusen und Menschen entsprechen würde. Um weitere Familien aufzudecken, die die CHP1-Mutation tragen, wurde ein breites Screening durchgeführt, das sich auf 2 große ARCA und NMD Kohorten fokussierte (insgesamt ungefähr 1000 Exome). Dabei wurden keine zusätzlichen Träger der Mutation gefunden, was die Seltenheit von CHP1 Varianten und die reduzierte Verträglichkeit von CHP1 Mutationen untermauert.

Mit dem Ziel die funktionellen Konsequenzen der CHP1-K19del Mutation in der Proteinfunktion einzuschätzen, wurden Größenausschlusschromatographie, Proteinfractionierung, 3D-Proteinmodellierung, Fluoreszenzmikroskopie und *in vivo*

Zebrafisch Experimente durchgeführt. Wir zeigten, dass das mutierte CHP1 nicht in funktionelle Proteinkomplexe integriert werden kann. Ebenso neigt es zur Aggregationsbildung, was zu verminderten Konzentrationen an löslichem CHP1 und reduziertem Membran-Lokalisierung von NHE1 in neuronalen, sowie auch in nicht-neuronalen Zellen führt. Um die pathogenen Konsequenzen der hypomorphen CHP1-K19del Mutation *in vivo* zu analysieren, verwendeten wir Morpholinos, die die *chp1* Translation im Zebrafisch herunterregulierten. Ähnlich wie bei den klinischen Merkmalen der von ARCA betroffenen Geschwister, führte die *chp1* Herunterregulation im Zebrafisch zu zerebellärer Hypoplasie, Störungen in den Caudalen Primären Motoneuronen (CaP-MN), sowie zu spastischen Rumpfbewegungen. Alle Defekte wurden durch eine Injektion mit wildtypischer, nicht jedoch der mutierten humaner *CHP1* mRNA verbessert. Folglich zeigte dies die Spezifität des *chp1*-MO-induzierten Phänotyps, sowie den Effekt der CHP1-K19del Mutation auf die Proteinexpression und/ oder -funktion *in vivo*. Zusammengefasst lässt sich sagen, dass unsere Ergebnisse CHP1 als ein neues Ataxie-verursachendes Gen beim Menschen identifizierten. Ferner erweitern diese Ergebnisse auch das Spektrum der ARCA-verursachenden Loci und hebt die entscheidende Rolle von NHE1 in der Pathogenese dieser Erkrankung hervor.

Darüber hinaus führten wir eine Analyse durch, um die funktionale Basis einer dHMN zu ermitteln, die eine Familie mit Gehirnnervenlähmung und Stimmbandparese als Ausgangsmerkmal einer nicht-progressiven infantilen dominanten dHMN zeigte. Die WES-Analyse dieser Familie führte zu der Identifizierung einer *de novo* dominanten Missense-Mutation (c.439 G>A, p.D147N) im VACHT, die bei der erkrankten Mutter erstmalig auftrat, und an ihre betroffene Tochter weiter vererbt wurde. VACHT kontrolliert die Speicherung des Neurotransmitters Acetylcholin durch synaptische Vesikel und spielt daher eine grundlegende Rolle bei der cholinergen Neurotransmission und vielen anderen verwandten Prozessen, wie unter anderem bei der neuronalen Entwicklung und Reifung, der synaptischen Übertragung und Plastizität und bei der Strukturierung der neuronalen Endplatte (NMJ). Die mögliche Wirkung der D147N-Mutation auf die subzelluläre VACHT-Verteilung wurde in der neuronenhähnlichen Zelllinie NSC-34 analysiert, die transiente WT oder mutierte VACHT-GFP-markierte Proteine überexpressierte. Es wurde kein signifikanter Unterschied in der Proteinexpression und Lokalisation beobachtet, sodass ein nachteiliger Effekt der VACHT-D147N-Mutation auf dieser Ebene nicht nachgewiesen werden konnte. Dies veranlasste uns, mögliche Defekte in der Motoneuron Entwicklung und im axonalen Auswuchs weiter zu untersuchen. Wir nutzten dafür wieder die Vorteile des Zebrafischs als Modell für humane neurodegenerative Erkrankungen und da VACHT und D147 Spezies übergreifend evolutionär konserviert sind, wurde die Wirkung von VACHT-D147N Überexpression im Vergleich von WT auf die CaP-MN-Auswüchse im Detail analysiert. Obwohl unsere Ergebnisse bei der Erkennung der Pathogenität der VACHT-D147N-Mutation *in vivo* nicht schlüssig gewesen sind, konnten wir in Bezug auf die neuronale Migration einen Phänotyp beobachten, der am NMJ potenziellen Beeinträchtigungen unterliegt. Im Hinblick auf die kürzlich beschriebene VACHT-Mutationen als Ursache für das Myasthene Syndrom, werden zur Zeit noch Studien durchgeführt, um die Pathogenität der VACHT-D147N-Mutation in einem CaP-MN-unabhängigen Kontext endgültig zu bestätigen.

Die biologische Funktion von CHP1 war in dieser PhD-Arbeit von weiterer Relevanz, da CHP1 in einer anderen Studie derzeit als potenzielles Modifizieren der Spinalen Muskelatrophie (SMA) untersucht wird. Ergebnisse unserer Forschungsgruppe zeigen, dass eine Herunterregulation von CHP1 - in einem bestimmten Rahmen - das neuronale Wachstum und die beeinträchtigte Endozytose (ein Schlüsselmechanismus, der in SMA

gestört ist) in *Smn1*-verminderten NSC-34 Zellen wiederherstellt. Aus diesem Grund war ein weiteres Ziel dieser Doktorarbeit, die Reduktion von CHP1 als potenzielle SMA-Protektion im Zebrafisch-Modell als ersten *in vivo* Ansatz zu validieren. Hier zeigten wir, dass die Chp1 Herunterregulation den axonalen Auswuchs der CaP-MN von Zebrafischen mit *Smn*-Mangel verbesserte. Diese Ergebnisse stimmen mit früheren Studien von zwei weiteren humanen SMA-Modifizierenden - PLS3 und NCALD - im Zebrafischmodell überein, welche trotz ihrer unterschiedlichen Funktion und Wirkungsweise (z.B. Hochregulation für PLS3 neu aufgekommene Assoziation einer und Herunterregulation für *Ncald*), ähnliche Effekte auf die CaP-MN-Morphologie ausüben und den CaP-MN-Phänotyp von *smn*-Morpholino behandelten Zebrafischen wiederherstellten. Insgesamt weisen unsere Ergebnisse zusammen mit weiteren vorläufigen Resultaten darauf hin, dass CHP1-Herunterregulation ein vielversprechendes therapeutisches Ziel für eine kombinatorische Behandlung zusammen mit einer SMN-Hochregulation darstellt, um der SMA-Pathologie entgegen zu wirken.

1. PREAMBLE AND THESIS OUTLINE

Neuromuscular disorders (NMDs) is a broad term that encompasses more than 800 different diseases that impair the function of muscles and/or their underlying nervous system control. The majority of these diseases are rare, complex and in most cases, incurable. Some of them, such as Amyotrophic Lateral Sclerosis (ALS) and Spinal Muscular Atrophy (SMA), are among the most devastating disorders afflicting humans. To date, more than 500 genes have been causatively related to NMDs but, paradoxically, only half of the patients with a suspected NMD receive an accurate genetic diagnostic. This imply that many NMD-causative genes, genetic disease modifiers and/or unknown phenotype-genotype associations remain to be discovered.

The uppermost goal of this PhD project was to identify and characterize novel NMDs-causative genes. Thereby, two NMD-causative genes were investigated in this thesis: *CHP1* (Calcineurin Homologous Protein-1), which was identified as a novel causing gene of Autosomal Recessive Cerebellar Ataxia (ARCA) and *VACHT* (Vesicular Acetylcholine Transporter, encoded by *SLC18A3*), which was analyzed in the context of distal Hereditary Motor Neuropathy (dHMN). These findings are presented along this PhD thesis in a subsection entitled: Part I. Identification and functional characterization of novel NMD-causative genes.

The biological function of *CHP1* was of further relevance within the scope of this doctoral project. Pre-existing evidence from our group indicate that *CHP1* reduction is beneficial in the context of SMA. Indeed, the first functional analyses showed that *CHP1* downregulation restores neurite outgrowth and impaired endocytosis –a key pathway disturbed in SMA- in *Smn1*-depleted neuron-like cells. Thereupon, the second subsection of this thesis aimed to validate that reduction of *CHP1* is SMA-protective *in vivo*. The findings derived from this subsection are presented in: Part II. *Chp1* reduction ameliorates motor neuron degeneration in a zebrafish model of SMA.

This thesis begins with an Introduction (Section 2), which is accordingly subdivided into Parts I and II. Hence, a literature review pertinent to Part I, including an overview of NMDs and the underpinnings of novel disease-causing genes identification, is provided (2.1–2.3). Further on, emphasis converge into the specific NMD subcategories and disease-causative genes studied in this thesis as follows: ARCA and *CHP1* (2.4) and dHMNs and *VACHT* (2.5). Lastly and pertinent to Part II, a succinct description of SMA with emphasis in SMA genetic modifiers is provided (2.6).

Further elaborated research aims are presented in Section 3. The ground hypotheses and the experimental data obtained in this doctoral thesis are presented in Section 4 (Results).

For better understanding, sections 3 and 4 are also sub-divided into Parts I and II. A compilation of the main findings of this work and their contribution to both genetic diagnostics and the understanding of NMDs pathogenesis is discussed in Section 5. Closing this document a general description of Material and Methods is provided (Section 6).

2. INTRODUCTION

PART I. IDENTIFICATION AND FUNCTIONAL CHARACTERIZATION OF NOVEL NMD-CAUSATIVE GENES

2.1. Neuronal circuitry of movement control, an overview

Muscular contraction, whether voluntary or involuntary, is governed by four highly interactive neural centers. The first of these centers is composed by the spinal cord and the brain stem circuits, whose fundamental working units are the lower motor neurons (LMNs), innervating skeletal muscles of the body and head, and the local circuit neurons (LCNs), which provide synaptic inputs to the LMNs, respectively. The second neural center is integrated by the motor cortex and the brainstem, which harbors the cell bodies of the upper motor neurons (UMN). The descending UMN axons synapse with LCNs and LMNs and are essential for the initiation of voluntary movement, the execution of precise movements under complex spatiotemporal sequences and the control of navigational position and movement (Figure 1).

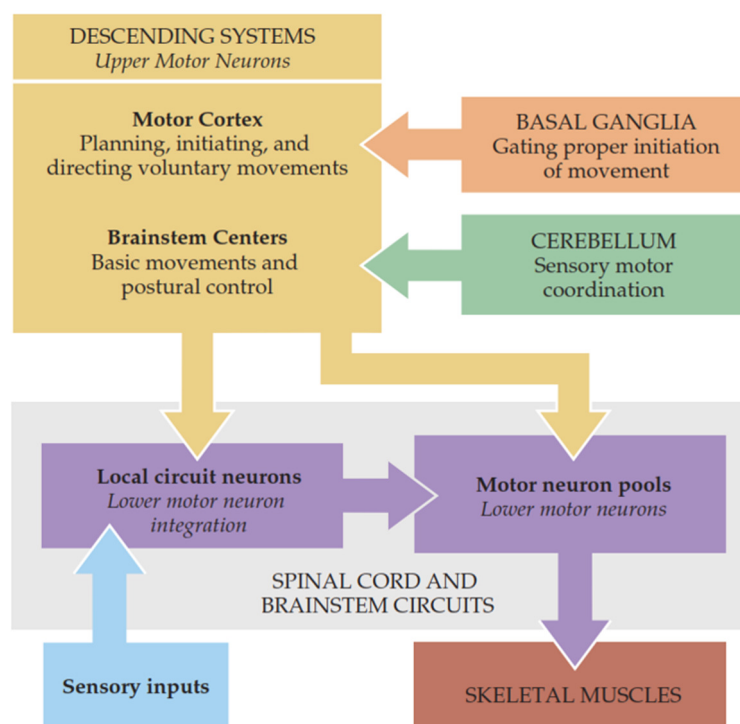


Figure 1. Neural systems for movement control. Figure taken from (Purves, 2004)

The two remaining centers, namely the cerebellum and the basal ganglia, do not “execute” movement, *i.e.* do not synapse with LMNs or LCNs, but rather regulate the activity of UMNs. In detail, the primary function of the cerebellum is to detect, and correct if necessary, the difference between intended and actual movement in real time (during execution). The axons projecting from the basal ganglia prime UMNs for movement initiation and also suppress unwanted responses, hence are fundamental for the proper execution of voluntary movement (Figure 1) (Purves, 2004).

2.2. Inherited neuromuscular disorders

Inherited Neuromuscular disorders (NMDs), is an umbrella term that encompasses a plethora of diseases that impair the proper functioning of muscles, either directly, as pathologies of the voluntary muscles and the neuromuscular junction (dystrophies, myopathies and myasthenias, respectively) or indirectly, by compromising any of the neural centers controlling voluntary movement (Figure 1) (Laing, 2012; McDonald, 2012). Undoubtedly, some of the most devastating NMDs arise from the degeneration, damage or malfunction of a particular neural center. For instance, Spinal Muscular Atrophy (SMA) and the Hereditary Spastic Paraplegias (HSPs) result from the loss of LMNs and UMNs, respectively (reviewed in (Blackstone, 2012; Wirth, 2000)) whereas the vast majority of hereditary ataxias exhibit degeneration of cerebellar and spinocerebellar tracts (Wolf & Koenig, 2013). Moreover, pathological changes of the basal ganglia underlie some of the most studied neurodegenerative disorders: Parkinson’s and Huntington’s disease (DeLong & Wichmann, 2007; McGeer et al, 1987).

2.2.1. Prevalence of NMDs

The first epidemiological study of inherited NMDs was published in 1991 and since then, this “1991 survey” has become of common reference and practice (Emery, 1991a; Emery, 1991b). This study, complemented by others (MacDonald et al, 2000; Merlini et al, 1992), established the incidence of NMDs as one in 2500. One decade after the innovation of the Next Generation Sequencing (NGS) technologies, the epidemiology of NMDs was revisited. Indeed, a thorough review of the scientific literature established that NMDs as a group, have an incidence rate comparable with the prevalence of Parkinson’s disease, that is: 1-3 in 1500 (Bhatt, 2016; Deenen et al, 2015). Thus, nowadays NMDs represent a significant cause of neurological disability worldwide and, as a whole, they are no longer considered as rare diseases.

2.2.2. General classification of NMDs

Although, from the diagnostics point of view, NMDs share some general features such as muscle weakness, cramps, fatigue, torpidity, stiffness and focal wasting (McDonald, 2012), their individual clinico-pathological presentation is extremely heterogeneous. Indeed, NMDs variability in age of onset, mode of inheritance, symptomatology and molecular pathophysiology has led to a rather complex sub-disease categorization, which includes more than 800 described entities associated to more than 500 genetic loci (Laing, 2012; McDonald, 2012). The latter number has been, and still is, constantly changing; thanks to the implementation of NGS technologies in routine genetic diagnostic. This massive access to genome/exome sequencing (see section 2.3) has permitted not only the discovery of novel disease-associated genes but also the validation of novel genotype-phenotype correlations; thus broadening the complex clinical landscape of NMDs.

Table 1 summarizes a very general classification of NMDs, and the number of genes/loci associated to each NMD category. The information included in this table is compiled and updated yearly by the “Neuromuscular disorders” journal (August, 2016).

Table 1. General classification of neuromuscular disorders and known causative genes

Category	Number of genes / loci
Congenital muscular dystrophies	29
Congenital myasthenic syndromes	20
Congenital myopathies	25
Distal myopathies	15
Hereditary ataxias*	46
Hereditary cardiomyopathies	86
Hereditary motor and sensory neuropathies	64
Hereditary paraplegias	46
Ion channel muscle diseases	13
Malignant hyperthermias	2
Metabolic myopathies	26
Motor neuron diseases	51
Muscular dystrophies	40
Myotonic syndromes	6
Other myopathies	22
Other neuromuscular disorders	27
Total	518

Data source: <http://www.musclegenetable.org>. Year of last update: 2016. The NMDs subcategories investigated in this thesis are depicted in bold. * The hereditary ataxias category includes mainly disorders presenting with predominant cerebellar involvement and reported in more than one family.

2.2.3. Diagnosis of NMDs

In clinical practice, the diagnosis of NMDs is sustained on three main pillars namely: (1) evaluation of the family history, (2) thorough musculoskeletal, neurological and physical examination and (3) complementary specialized tests, which include the standard electrodiagnostics studies (e.g. EMG and nerve conduction evaluation), pathological analysis of muscle or nerve biopsies, and magnetic resonance imaging (MRI). Nevertheless, a differential, hence conclusive, diagnostic requires additional molecular or genetic approaches; such as the sequential Sanger sequencing of the most likely disease candidate gene(s) or the mass sequencing of a selection of genes (gene panels), the exome (protein-coding sequences) or the whole genome (Laing, 2012; McDonald, 2012).

Since the discovery of the first muscular dystrophy gene (the Dystrophin gene, causing Duchene Muscular Dystrophy) 25 years ago (Koenig et al, 1987), the NMD field has witnessed an outburst of novel genes discovery, of course facilitated by the aforementioned NGS technologies. The current ease of genetic testing and the growing number of identified pathogenic mutations has definitely impacted diagnostic precision but broadened the complexity of the process. Indeed, new disease genes have shed light upon relevant molecular pathways and expanded the understanding of NMDs pathobiology, which is then translated into development of effective therapies and assessment of factors controlling disease penetrance, onset and severity (Laing, 2012). Nonetheless, novel genes -518 and counting- have also expanded the genetic heterogeneity of NMDs. To exemplify the latter, three examples are given:

- Complex genetic landscape. More than 80 genes have been identified as causative of the peripheral neuropathy Charcot-Marie-Tooth (CMT). Diagnosis requires an algorithm-based approach to discriminate between the different subclinical presentations of the disease. Successful CMT genetic diagnostic is achieved only in less than half of the patients (Fridman & Reilly, 2015; Murphy et al, 2012; Saporta et al, 2011).
- NMDs sub-categories overlapping. Mutations in Hereditary Spastic Paraplegia (HSP) genes overlap with Spinocerebellar Ataxias (SCAs) and both upper and lower MN disorders, namely Primary Lateral Sclerosis (PLS), Amyotrophic Lateral Sclerosis (ALS), SMA and other inherited neuropathies (Coutelier et al, 2015; Tesson et al, 2015).
- Extreme phenotypic variability. Heterozygous mutations in *BICD2* cause SMALED (autosomal dominant SMA, lower extremity-predominant 2). Disease phenotypes vary, on one extreme, from slowly progressive muscle weakness and atrophy –the usual disease presentation, to severe arthrogryposis multiplex congenital (AMC) and early

lethality. On the other extreme, individuals harboring pathogenic *BICD2* mutation can be fully asymptomatic (Storbeck et al, 2017).

Paradoxically, the successful identification of NMD genes do not translate into conclusive diagnostics. For at least 40% of the patients, and families, with suspected NMD the precise disease-causing mutation has not been identified, which implies that many genes remain to be found. The current access to NGS technologies plays, and will play, a pivotal role in the elucidation of more, if not all, NMD-causing genes (Laing, 2012).

2.3. Identification of novel disease-causing genes

Past identification of monogenic disease-genes largely depended on finding large families, with traceable Mendelian inheritance in multiple generations. Candidate genes were selected either because the predicted protein function was relevant to the pathology of interest– the so called functional cloning- or because a positional mapping approach pointed to a gene in a certain genomic region (Botstein & Risch, 2003). The latter, also termed positional cloning, was considered more reliable as it can be applied in an unbiased fashion whereas it does not depend on prior gene function nor clinical knowledge. Among the most important approaches for genetic mapping are karyotyping, linkage analysis, homozygosity mapping, copy number variation (CNVs) analysis and single nucleotide polymorphism (SNPs)-association studies (Gilissen et al, 2012).

Recent advances in NGS technologies have revolutionized the process of disease-genes identification, by making high throughput sequencing of DNA and RNA available, fast and affordable (Schofield et al, 2017; Warr et al, 2015). In contrast to the classical two-step gene identification process of the last decade, *i.e.* positional mapping and sequencing, today's workflow consists of a one-step approach: whole genome sequencing. The majority of genome studies so far, have focused on the exome (the protein-coding part of the genome), since approximately 85% of the mutations associated to Mendelian disorders lay in protein-coding regions (Botstein & Risch, 2003). This strategy is known as Whole Exome Sequencing (WES).

2.3.1. Whole Exome Sequencing

As the number of variants identified per sequenced exome varies from 20 to 50000, a crucial step in a WES run is to prioritize them, in order to reduce the number of false-positive calls (Gilissen et al, 2012). Initially, variants can be filtered based on quality criteria parameters, such as the number of independent reads showing a given variant. Subsequently, variants

with no translational impact, or in other words synonymous or intronic changes, can be also excluded. Nevertheless, caution must be exerted; as synonymous changes affecting critical splicing sites in intron-exon boundaries might result mistakenly excluded. Most importantly, WES-identified variants are dramatically narrowed-down after excluding all known polymorphisms (this step is usually done through variation/SNPs databases) (Abecasis et al, 2010). After prioritization, the remaining variants (around 100), can be considered as potentially pathogenic and therefore further strategies are needed in order to conclusively pinpoint the disease-causative mutation. For this latter step, the traditional mapping strategies, as well as other methodologies, become of great advantage in the frame of WES analyses. Two of these strategies were of significant importance in this thesis and will be shortly explained. The others, no less advantageous, are summarized in Table 2.

2.3.1.1. Linkage analysis

Genetic linkage defines the co-segregation of a given genetic locus together with the disease within a family. Whole Genome Linkage Analyses (WGLA) are based on a panel of polymorphic markers (Restriction Fragment Length Polymorphisms (RFLPs), microsatellites or SNPs) which are genotyped in a family. WGLA, and classic linkage studies, are based on the premise that markers in the vicinity of the disease-causing mutation will co-segregate, generationally together with the mutation, since the probability of meiotic recombination (or separation) between these regions is reduced (reviewed in (Pulst, 1999)). By combining WGLA and WES not only the amount of shared (private) variants is kept to a minimum but also the search area of candidate gene(s) in the exome can be limited to positive linked regions. This approach is a very effective strategy to eliminate a large proportion of WES variants (Gilissen et al, 2012; Smith et al, 2011).

2.3.1.2. *De novo* inheritance assumption

In the absence of family history, either because it is negative or not accessible, *i.e.* there is a single sporadic affected individual, the *de novo* approach has proven to be successful in the process of WES variant prioritization. Following a family-based WES strategy, also known as trio/quartet WES, the exome variants of the affected proband as well as his/her parents will be filtered out in order to exclude all inherited variants. The remaining yield, will include a very limited number of potentially pathogenic *de novo* variants, considering that the average number of *de novo* mutation in the exome is approximately 0-3 mutations (Abecasis et al, 2010; Vissers et al, 2010). The positive identification of a *de novo* disease-

causative mutation does not constitute a direct proof its *de novo* occurrence, therefore further studies are needed in order to confirm pathogenicity (Gilissen et al, 2012).

Table 2. Assumptions for WES variants filtering

Strategy	Scenario	Assumptions	To consider
Linkage analysis	Multiple affected probands within a single family	Fully penetrant mutation segregating with the disorder	
Homozygosity mapping	Single affected proband with consanguineous parents	Homozygous mutation within a homozygous stretch	The disorder might not necessarily be caused by a mutation in a homozygous region
Double-hit	Single affected proband with a recessive disorder	A single rare homozygous or two rare compound heterozygous mutations	Depends on population (expected) carrier frequency
<i>De novo</i>	Single proband sporadically affected	The mutation occurs <i>de novo</i> in the patient	
Candidate gene	Single affected proband with a dominant disorder. No additional family members required.	The causative gene or mutation shares features with known genes / mutations	Biased approach, relying on current biological knowledge

Table adapted from (Gilissen et al, 2012)

2.4. Calcineurin Homologous Protein-1 (CHP1) is a novel causative gene of Autosomal Recessive Cerebellar Ataxia (ARCA)

In this doctoral thesis, a biallelic *CHP1* mutation was identified and validated as a novel cause of ARCA in a consanguineous family with two affected siblings presenting a complex cerebellar ataxia with UMN and LMN involvement (see section 4.1). Therefore, and pertaining to this part of the project, the following introduction subsections (2.4.1 and 2.4.2) describe the most relevant aspects regarding hereditary ataxias with emphasis on ARCAs and the functional roles of CHP1.

2.4.1. Inherited cerebellar ataxias

The hereditary cerebellar ataxias (HCAs) are a diverse group of neurodegenerative disorders in which the predominant feature is progressive cerebellar, brainstem and/or spinocerebellar tracts degeneration with concomitant balance impairment, uncoordinated limb movements and dysarthria. Although ataxic symptoms can originate from isolated cerebellar syndromes, in most cases other neurological manifestations including sensory, pyramidal, extrapyramidal and cognitive dysfunction underpin the clinical spectrum of HCAs (Harding, 1983; Wolf & Koenig, 2013). The worldwide prevalence of HCAs has been reported as 1.2 – 41:100.000, however it is believed that this number is rather

underestimated as prevalence rates tend to be higher than those reported in earlier studies and are subjected to founder effect (Klockgether, 2011; Manto & Marmolino, 2009).

The classification of inherited ataxias has been a difficult task. Nowadays, the most “accepted” classification (followed in this thesis) is based on the mode of inheritance, with further subdivisions based on the causative gene or, in some instances, the underlying molecular pathway(s) (Di Donato, 1998; Di Donato et al, 2001; Jayadev & Bird, 2013). Nevertheless, others have attempted detailed phenotypical/clinical categorizations, which despite their complexity, are the best reflect of the vast genetic heterogeneity underlying these disorders (Barbeau et al, 1984; Harding, 1983; Harding, 1993).

From the diagnostic point of view, ataxias are rather challenging, as degeneration of the cerebellum, or spinocerebellar tracts, have been associated not only with HCAs but also with several acquired infectious, vascular or immune disorders (Klockgether, 2010). Therefore, pertaining this literature review, the acquired ataxias will not be further considered. Genetically, autosomal dominant, autosomal recessive, X-linked and mitochondrial inheritance patterns have been described for HCAs. Since in this doctoral thesis a novel ARCA causative gene was successfully identified, more emphasis is placed on this subsection (see 2.4.1.4). Nevertheless, an overview of all modes of inheritance will be provided in the following pages.

2.4.1.1. Autosomal dominant ataxias

In autosomal dominant cerebellar ataxias (ADCAs), also called spinocerebellar ataxias (SCAs), cerebellar or olivopontocerebellar atrophy is a cardinal, but not definitive, diagnostic sign; since other symptoms such as bulbar signs, neuropathy, retinitis pigmentosa and eye movement disorders are frequently presented along with cerebellar degeneration (Wolf & Koenig, 2013). The precise number of genes/loci associated with ADCAs is rather variable among published reports, most likely due to the misuse or the miss-association of the term SCA to unrelated syndromes (Hersheson et al, 2012). Nevertheless, recent publications have reported more than 35 loci and 20 genes as ADCAs-causative.

ADCAs have a rather late onset, as they appear at approximately 35 years of age, usually with a multigenerational pattern (Durr, 2010). In these disorders, tri-, penta- and hexa-nucleotide expansions are the most common causative mutations, along with conventional point mutations or rearrangements, to a minor extent. Polyglutamin (CAG_n) repeats in protein-coding regions underlie the pathogenesis of 6 different SCA types, namely SCA1, 2, 3, 6, 7, 17 and dentatorubral-pallidoluysian atrophy (DRPLA), whereas non-coding expansions are associated with SCA8 (CTG_n), SCA10 ($ATTCT_n$), SCA12 (CAG_n), SCA31

(TGGAAn) and SCA36 (GGCCTGn). The age of onset and phenotype severity of SCAs correlates with a certain repeat threshold, thus estimation of the expansion length is crucial for accurate genetic diagnostic (Hersheson et al, 2012). As commonly described for polyglutamine and other repeat expansion diseases, mutant proteins adopt aberrant structural conformations leading to toxic aggregations. Since in SCAs, the neurons of the cerebellum are especially vulnerable, the insoluble accumulation of misfolded proteins lead to neuronal dysfunction and ultimately, death (Manto & Marmolino, 2009). The Hereditary Episodic Ataxias (EA) are also included into the category of AD ataxias and represent a group of channel disorders characterized by early onset and periodic (from minutes to days) episodes of ataxia and vertigo, accompanied in some cases with progressive ataxia, migraine, seizures or chorea (Jen, 2008).

2.4.1.2. X-linked ataxia

Patients with Fragile-X syndrome harbor a trinucleotide mutation (CGG) that expands over 200 times, leading to hypermethylation and silencing of the *FMR1* gene, and null FMRP (Fragile X Mental Retardation Protein) expression in neurons. The latter event is the cause of the characteristic intellectual disability observed in Fragile-X patients. Interestingly, *FRM1* trinucleotide expansions between 55 to 199 repeats, *i.e.* allele premutations, are associated with Fragile X-associated tremor/ataxia syndrome (FXTAS). This unique phenotype starts usually after the age of 50 and is characterized by a combination of ataxic gait, kinetic tremor, autonomic dysfunction, Parkinsonism and cognitive defects (Berry-Kravis et al, 2007). FXTAS neuropathological changes include atrophy in the middle cerebellar peduncles, Purkinje cell loss, and neuronal protein inclusions (Greco et al, 2006). In addition, mutations of a putative mitochondrial iron transporter gene *ABC7* have been associated with X-linked sideroblastic anemia and ataxia (XLSA/A), a rare recessive disorder characterized by early onset non-progressive cerebellar ataxia, dysmetria and mild anemia (Allikmets et al, 1999; D'Hooghe et al, 2012).

2.4.1.3. Mitochondrial ataxias

Ataxia is a common clinical manifestation in several mitochondrial disorders underlying oxidative phosphorylation (OXPHOS) defects, hence causative mutations are either in nuclear (nDNA) or mitochondrial (mtDNA) genes and can be transmitted by all modes of inheritance. The number of genes associated with mitochondrial ataxias varies greatly among reports, as in the majority of these disorders the ataxic symptoms are just a piece of a rather complex phenotypic puzzle. Nevertheless, considering that: (1) so far, more than

250 pathogenic mutations have been identified as causative for mitochondrial disorders (Kohda et al, 2016), (2) cerebellar atrophy is the primary neuroradiological finding in patients with mtDNA defects and (3) approximately 65% of patients with mitochondrial diseases show symptoms consistent with ataxia; the number of genes associated to mitochondrial ataxias should be in a similar order of magnitude, and further expanding, as mutations in novel nuclear genes implicated in mitochondrial function are constantly reported (Lax et al, 2012; Vedanarayanan, 2003; Zeviani et al, 2012).

The ataxia observed in patients with mitochondrial diseases can be cerebellar or spinocerebellar and rarely present in isolation. Other neurological and non-neurological symptoms such as, nystagmus, dysarthria, seizures, deafness, cardiomyopathy, retinopathy and diabetes mellitus co-present with cerebellar signs (Jayadev & Bird, 2013). The clinical disability underlying mitochondrial ataxias is largely variable. In some disorders, ataxia is the main cause of functional limitation, whereas in others, neurologic or systemic symptoms eclipse the cerebellar ataxia (Vedanarayanan, 2003). Among the various mitochondrial ataxias caused by mutation or deletions in mtDNA genes, four are relatively frequent: Kearns–Sayre syndrome, neurogenic weakness, ataxia, and retinitis pigmentosa (NARP), mitochondrial encephalopathy, lactic acidosis, and stroke-like episodes (MELAS) and myoclonus epilepsy with ragged-red fibers (MERFF). Moreover, mutations in nDNA genes that encode mitochondrial proteins, are responsible for Mitochondrial Recessive Ataxic Syndrome (MIRAS) and Infantile-Onset Spinocerebellar Ataxia (IOSCA), among others (Zeviani et al, 2012).

2.4.1.4. Autosomal Recessive Cerebellar Ataxias (ARCAs)

ARCAs comprise probably the most heterogeneous group of all hereditary ataxias. Although the salient feature of these disorders is progressive cerebellar degeneration, a plethora of neurological and non-neurological manifestations can accompany positive cerebellar signs. Due to their clinical and genetic complexity, ARCA phenotypes are rather challenging to categorize and therefore to accurately diagnose. In the following pages the most relevant information regarding ARCAs clinical features, epidemiology, diagnostic and molecular pathomechanisms is outlined. To complement this information, Table 4 summarizes the more than 40 ARCA clinical entities –with predominant cerebellar involvement- described to date. (Beaudin et al, 2017; Embirucu et al, 2009)

2.4.1.4.1. Clinical features of recessive cerebellar ataxias

Clinical examination of ARCA patients often reveals gait disorder with imbalance, upper and lower limb dysmetria, dysdiadochokinesia (difficulty to perform alternate movements), hypotonia, dysarthria and saccadic ocular pursuit (Anheim et al, 2010; Fogel & Perlman, 2007). Nevertheless, the acute onset of all these symptoms may have numerous unrelated or non-ARCA causes, such as vascular malformations, meningitis, ischemic cerebellar strokes, toxic agents/drugs (e.g. alcohol, mercury, phenobarbital) or vitamin B₁ deficiency. Thus, a crucial step in ARCA diagnosis is to exclude all secondary pathogenic causes, via magnetic resonance imaging (MRI), neurophysiological examination and ARCA-biomarkers analysis (Anheim et al, 2012). Particularly suggestive of ARCA is the familial history *i.e.* the presence of similar cases in the kindred as well as parental consanguinity. An important feature of these disorders is their early onset, which according to traditional classification systems is before the age of 20 (Harding, 1983). Typical ARCA signs are summarized in Table 3.

Although cerebellar degeneration is frequently present, it is not a conclusive diagnostic ARCA feature, as the predominance of specific ataxic symptoms might underlie the affection of one or more CNS regions such as the brain stem, the cervical spinal cord and/or the cerebellar vermis (Fogel & Perlman, 2007) (see Figure 2). Other neurological signs associated with ARCA might include dystonia, spasticity, pyramidal tract dysfunction, chorea, oculomotor abnormalities, hearing loss, pes cavus, scoliosis, epilepsy, mental retardation and cognitive impairment (De Michele & Filla, 2012; Di Donato et al, 2001; Filla & De Michele, 2012). Moreover, a plethora of non-neurological signs such as, cardiomyopathy, hypogonadism, and scoliosis, among others, can co-manifest with ARCA (see also Table 4). These are of further diagnostic aid, as they define specific ARCA subtypes of more complex etiologies.

Table 3. Typical signs and symptoms of ARCAs

Symptoms
Clumsiness, swerving
Walking difficulties
Balance problems, swaying and falling (leading to or manifested as trauma)
Difficulty in dressing, handling utensils, and writing
Slurred speech
Hypotonia
Delayed motor development (onset of walking after 18 months)
Hand tremors
Dizziness (patient is usual referred to otorhinolaryngologist)
Visual disturbances (patient is usual referred to ophthalmologist)
Incidental finding of cerebellar atrophy on magnetic resonance imaging

Table adapted from (Anheim et al, 2012)

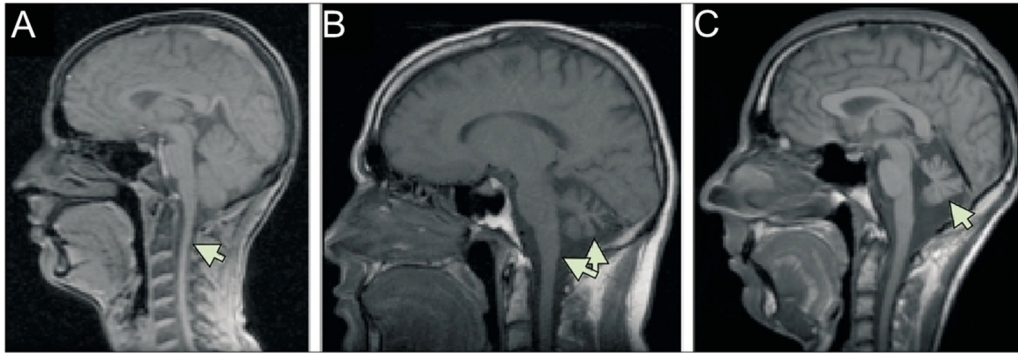


Figure 2. Neuroimaging features of three ARCA types. Panel **A** shows mild atrophy of the cervical spinal cord (arrow) and a normal cerebellum in a 14-year-old boy with Friedreich's ataxia. Panel **B** shows moderate cerebellar atrophy and mild volume loss in the brainstem (arrows) in a 35-year-old man with ataxia telangiectasia. Panel **C** shows marked atrophy of the cerebellar vermis (arrow) in a 21-year-old man with ataxia with oculomotor apraxia type 2. Figure adapted from (Fogel & Perlman, 2007).

2.4.1.4.2. Common ARCA syndromes

The reported prevalence(s) of ARCAs, and hence of the most common syndromes, varies between studies and geographic regions, due to population genetic heterogeneity and methodological design of the studies. More importantly, large areas of the world remain hitherto without prevalence studies. In 2014, a systemic review of various prevalence studies worldwide established an average ARCA prevalence of 1.65:50000 (Ruano et al, 2014). In the following sections, the most frequent ARCA syndromes are shortly outlined. More than 40 ARCA disorders with predominant cerebellar involvement are summarized in Table 4.

2.4.1.4.2.1. Friedreich's ataxia

FRDA is the most frequent ARCA and the most common hereditary ataxia. The estimated prevalence is approximately 1:29000 with a carrier frequency of about 1:85 (Cossee et al, 1997; Ruano et al, 2014). In Europe, FRDA accounts for at least 75% of all ataxias with onset before 25 years (Schulz et al, 2009). Clinically, FRDA is characterized by early-onset (between the ages of 5-25) progressive limb and gait ataxia, dysarthria, loss of vibration and proprioceptive sense, areflexia, abnormal eye movements and pyramidal weakness. Other non-neurological complications are cardiomyopathy, diabetes, scoliosis and pes cavus (Delatycki et al, 2000; Pandolfo, 2009). FRDA neuropathological changes include early atrophy and/or loss of large sensory neurons in the dorsal root ganglia and subsequent deterioration of spinocerebellar and pyramidal tracts (Voncken et al, 2004).

In 98% of patients, FRDA is caused by a trinucleotide GAA expansion within the first intron of the *FXN* (Frataxin) gene (see section 2.4.1.3) which leads to both hypermethylation and formation of a supercoiled DNA structure that impedes gene transcription. In consequence, FRDA patients lack the Frataxin protein (Bidichandani et al, 1998; Campuzano et al, 1996; Grabczyk & Usdin, 2000). The size of the trinucleotide expansion inversely correlates with age at onset, disease severity and manifestation of associated systemic symptoms. More specifically, up to 38 trinucleotide repeats are considered normal in a *FXN* allele; whereas 66 to over 1500 repeats constitute a pathogenic allele; with variable residual, or no Frataxin expression whatsoever (Mateo et al, 2003; Puccio & Koenig, 2000; Sacca et al, 2011). In rare cases (2-5%), FRDA is caused by a combination of heterozygous point mutations in one allele and a GAA expansion in the other allele (Pandolfo, 2008). Frataxin controls the iron-dependent redox chemistry of the mitochondria and therefore the cellular iron homeostasis. Depletion of Frataxin leads to respiratory chain dysfunction, oxidative stress, cellular damage and eventually cell death (Bradley et al, 2000; Pastore & Puccio, 2013). The current understanding of FRDA pathogenesis has directed the development of treatment options towards antioxidant protection (Elinx-Benizri et al, 2016), however potential strategies aiming to increasing Frataxin expression via treatment with histone deacetylase inhibitors are currently under clinical trial validation (Jacoby et al, 2014).

2.4.1.4.2.1. Ataxia telangiectasia (AT)

AT is the second most frequent ARCA, with an estimated worldwide incidence of about 1-75:100,000. Interestingly, this incidence has been estimated to be as high as 1:40,000 in the USA (Anheim et al, 2012; Ball & Xiao, 2005; Woods et al, 1990). Classical AT is characterized by progressive cerebellar ataxia with onset at age 2-3 years. Most patients become wheelchair-bound in the first decade and manifest severe cerebellar atrophy. Other symptoms of frequent co-presentation with ataxia are oculocutaneous telangiectasias, oculomotor apraxia and dysarthria. Systemic manifestations such as immunodeficiency, endocrine disturbances or lymphoid tissues cancer (in one third of the cases) complicate the overall clinical picture of AT patients (Chun & Gatti, 2004).

The AT-causative gene is *ATM* (Ataxia Telangiectasia Mutated). It encodes a member of the phosphatidylinositol-3 kinase family of proteins which in response to DNA damage, phosphorylates key substrates involved in DNA repair and/or cell cycle control (McKinnon, 2004; Savitsky et al, 1995). More specifically, the ATM protein kinase is involved in the signal transduction cascade triggered by DNA double-stranded breaks (DSBs). Loss of ATM disrupts the tight regulation of mitotic progression checkpoints and apoptosis induction, leading to genomic instability (McKinnon, 2004; Shiloh, 2006). The latter is the

most plausible explanation for the severe neurodegeneration and the clinical complexity observed in AT patients. (Fogel & Perlman, 2007). More than 200 different mutations have been described for the *ATM* gene. The majority of AT patients harbor compound heterozygous or missense mutations that give truncated proteins or dramatically alter protein expression; hence, phenotype-genotype correlations also pertain to *ATM* variants and AT. Patients showing milder phenotypes retain residual ATM expression and have a longer lifespan (Becker-Catania et al, 2000; Gilad et al, 1998; Palau & Espinos, 2006; Willems et al, 1993). Treatment for AT, and AT-related disorders remains to date mainly symptomatic. Infections and cancer are the primary cause of pharmacological intervention (Anheim et al, 2012).

Table 4. List of ARCAs with predominant cerebellar involvement

DISORDER	GENE	OMIM	MAIN CLINICAL FEATURES AND NEUROIMAGING FINDINGS
CTX	<i>CYP27A1</i>	213700	Dementia, paresis, tendon xanthomas, atherosclerosis, cataracts, elevated cholesterol level, childhood onset, variable cerebellar atrophy, cerebellar or cerebral leukodystrophy
AVED	<i>TTPA</i>	277460	Retinitis pigmentosa, head titubation, low serum vitamin E, teenage onset, spinal cord atrophy, absence of cerebellar atrophy
AT	<i>ATM</i>	208900	Telangiectasias, oculomotor apraxia, photosensitivity, immunodeficiency, predisposition for cancer, elevation of α -foetoprotein, infantile onset, cerebellar atrophy
FRDA	<i>FXN</i>	229300	Bilateral Babinski sign, square-wave jerks, scoliosis, hypertrophic cardiomyopathy, sensory involvement, teenage onset, spinal cord atrophy, absence of cerebellar atrophy
ATLD	<i>MRE11</i>	604391	Oculomotor apraxia, childhood onset, cerebellar atrophy
ARSACS	<i>SACS</i>	270550	Spastic paraparesis, retinal striation, pes cavus, infantile or childhood onset, anterior superior cerebellar atrophy, occasional T2-weighted linear hypointensities in pons
AOA1/EAOH	<i>APTX</i>	208920	Oculomotor apraxia, cognitive impairment, hypoalbuminemia, hypercholesterolemia, childhood onset, cerebellar atrophy
SCAN1	<i>TDP1</i>	607250	Peripheral axonal sensorimotor neuropathy, distal muscular atrophy, hypercholesterolemia, teenage onset, cerebellar atrophy
CAYMAN ATAXIA	<i>ATCAY</i>	601238	Psychomotor retardation, hypotonia, strabism, neonatal onset, cerebellar hypoplasia
SANDO or MIRAS/SCAE	<i>POLG1</i>	607459	SANDO: sensory ataxia, ophthalmoparesis, myoclonus, ptosis, adult onset, variable cerebellar atrophy, cerebellar white matter lesions, stroke-like lesions. MIRAS: cerebellar and sensitive ataxia, epilepsy, migraine, myoclonus, childhood or teenage onset, signal abnormalities in cerebellum and thalamus
AOA2	<i>SETX</i>	606002	Polyneuropathy, pyramidal signs, oculomotor apraxia, head tremor, chorea, dystonia, elevation of α -foetoprotein, teenage onset, cerebellar atrophy
CAMRQ1, DES	<i>VLDR</i>	224050	Non-progressive cerebellar ataxia, mental retardation, hypotonia, strabismus, occasional quadrupedal gait, congenital onset, inferior cerebellar hypoplasia, cortical gyral simplification
IOSCA/MTDPS7	<i>C10orf2</i>	271245	Athetosis, hypotonia, optic atrophy, ophthalmoplegia, hearing loss, epilepsy, hypogonadism, liver involvement, infantile onset, moderate atrophy of brainstem and cerebellum.
MSS	<i>SIL1</i>	248800	Cataracts, mental retardation, myopathy, short stature, childhood onset, cerebellar atrophy
DCMA/MGCA5	<i>DNAJC19</i>	610198	Dilated cardiomyopathy, non-progressive cerebellar ataxia, mental retardation, testicular dysgenesis, anemia, increased urinary 3-methylglutaconic acid, infantile onset
ARCA1	<i>SYNE1</i>	610743	Pure cerebellar ataxia, cognitive impairment, occasional pyramidal signs, late onset, cerebellar atrophy
ARCA2	<i>ADCK3</i>	612016	Exercise intolerance, epilepsy, myoclonus, cognitive impairment, childhood onset, cerebellar atrophy, occasional stroke-like cerebral lesions
SESAME SYNDROME	<i>KCNJ10</i>	612780	Epilepsy, sensorineural deafness, mental retardation, tubulopathy and electrolyte imbalance, infantile onset, absence of cerebellar atrophy
CAMRQ3	<i>CA8</i>	613227	Mild mental retardation, occasional quadrupedal gait, congenital onset, cerebellar atrophy, white matter abnormalities
Salih ataxia/ SCAR15	<i>KIAA0226*</i>	615705	Epilepsy, mental retardation, childhood onset, absence of cerebellar atrophy
PHARC	<i>ABHD12</i>	612674	Sensorimotor neuropathy, cataract, hearing loss, retinitis pigmentosa, teenage onset, variable cerebellar atrophy
SPAX4*	<i>MTPAP*</i>	613672	Spastic paraparesis, optic atrophy, cognitive involvement, infantile onset
ARCA3	<i>ANO10</i>	613728	Cognitive impairment, downbeat nystagmus, teenage or adult onset, cerebellar atrophy
SCAR11*	<i>SYT14*</i>	614229	Psychomotor retardation, late onset, cerebellar atrophy
CAMRQ2	<i>WDR81</i>	610185	Occasional quadrupedal gait, cognitive impairment, congenital onset, hypoplasia of cerebellum and corpus callosum
AOA3*	<i>PIK3R5</i>	615217	Oculomotor apraxia, sensorimotor involvement, teenage onset, cerebellar atrophy
SCAR13	<i>GRM1</i>	614831	Cognitive impairment, mild pyramidal signs, short stature, seizures, congenital onset, cerebellar atrophy
CAMRQ4	<i>ATP8A2*</i>	615268	Cognitive impairment, occasional quadrupedal gait, congenital onset, cerebellar and cerebral atrophy
SCAR7	<i>TPP1</i>	609270	Pyramidal signs, posterior column involvement, tremor, childhood onset, atrophy of the cerebellum and pons
ATAXIA AND HYPOGONADISM	<i>RNF216</i>	212840	Hypogonadotropic hypogonadism, dementia, occasional chorea, childhood to young adult onset, cerebellar and cerebral atrophy
SCAR18	<i>GRID2</i>	616204	Tonic upgaze, psychomotor retardation, retinal dystrophy, infantile onset, cerebellar atrophy
SCAR16	<i>STUB1</i>	615768	Pyramidal signs, neuropathy, occasional hypogonadism, variable age at onset, cerebellar atrophy
SCAR12	<i>WVOX</i>	614322	Tonic-clonic epilepsy, mental retardation, spasticity, neonatal to childhood onset, variable cerebellar or cerebral atrophy
ATLD2	<i>PCNA*</i>	615919	Telangiectasias, sensorineural hearing loss, photosensitivity, cognitive impairment, short stature, childhood onset, cerebellar atrophy
SCAR20	<i>SNX14</i>	616354	Mental retardation, sensorineural hearing loss, macrocephaly, dysmorphism, infantile onset, cerebellar atrophy
SCAR17	<i>CWF19L1</i>	616127	Mental retardation, congenital onset, cerebellar hypoplasia
ACPHD	<i>DNAJC3*</i>	616192	Diabetes mellitus, upper-MN signs, demyelinating neuropathy, sensorineural hearing loss, childhood to adult onset, generalized supra- and infratentorial atrophy
LIKNS/SCAR19	<i>SLC9A1*</i>	616291	Sensorineural hearing loss, childhood onset, variable vermian atrophy
AOA4	<i>PNKP</i>	616267	Dystonia, oculomotor apraxia, polyneuropathy, cognitive impairment, childhood onset, cerebellar atrophy
SCAR2	<i>PMPCA</i>	213200	Non-progressive cerebellar ataxia, cognitive impairment, pyramidal signs, short stature, congenital or infantile onset, cerebellar atrophy
SCAR21	<i>SCYL1</i>	616719	Liver failure, peripheral neuropathy, mild cognitive impairment, childhood onset, cerebellar vermian atrophy, thinning of optic nerve
SCAR22	<i>VWA3B*</i>	616948	Cognitive impairment, pyramidal signs, adult onset, cerebellar atrophy and thin corpus callosum
SCAR23	<i>TDP2*</i>	616949	Tonic seizures, cognitive impairment, dysmorphism, childhood onset
SCAR24	<i>UBA5*</i>	617133	Cataracts, peripheral neuropathy, childhood onset, cerebellar atrophy

CPHD Ataxia, combined cerebellar and peripheral, with hearing loss and diabetes mellitus, AOA ataxia with oculomotor apraxia, ARCA autosomal recessive cerebellar ataxia, ARSACS autosomal recessive spastic ataxia of Charlevoix-Saguenay, AT ataxia-telangiectasia, ATLD ataxia-telangiectasia-like disorder, AVED ataxia with vitamin E deficiency, CA Cayman ataxia, CAMOS cerebellar ataxia mental retardation optic atrophy and skin abnormalities, CAMRQ cerebellar ataxia mental retardation with or without quadrupedal locomotion, DCMA Dilated cardiomyopathy with ataxia, DES Desequilibrium syndrome, EAOH early-onset ataxia with oculomotor apraxia and hypoalbuminemia, FRDA Friedreich ataxia, IOSCA infantile onset spinocerebellar ataxia, LIKNS Lichtenstein-Knorr syndrome, MGCA5 3-methylglutaconic aciduria type 5, MIRAS mitochondrial recessive ataxia syndrome, MCSZ Microcephaly seizures developmental delay, MSS Marinesco-Sjogren syndrome, MTDPS7 mitochondrial DNA depletion syndrome 7, PEOA3 progressive external ophthalmoplegia with mitochondrial DNA deletions, autosomal dominant 3, PHARC polyneuropathy hearing loss ataxia retinitis pigmentosa and cataract. SANDO sensory ataxic neuropathy with dysarthria and ophthalmoparesis, SCAE spinocerebellar ataxia with epilepsy, SCAN1 spinocerebellar ataxia with axonal neuropathy 1, SCAR Spinocerebellar ataxia, autosomal recessive, SeSAME Seizures sensorineural deafness ataxia mental retardation and electrolyte imbalance, SPAX spastic ataxia. * indicates one family register. Table adapted from (Beaudin et al, 2017).

2.4.1.4.2.2. Molecular pathogenesis of ARCAs

During the last years, the ARCA field experienced an exponential identification of novel genes and mutations which have not only revealed unknown phenotype-genotype correlations but most importantly, molecular pathways we were unaware of. Some pathophysiological pathways are common to several ARCAs and hence, useful for the classification of some ARCA entities. According to the molecular mechanisms underlying disease phenotype, ARCAs are classified in four groups: defective DNA repair, mitochondrial, metabolic (or defects in lipoprotein assembly) and abnormal protein folding and aggregation (De Michele et al, 2004; Filla & De Michele, 2012). A graphic summary of these pathways is given in Figure 3.

First of all, the ARCAs associated with DNA repair defects, comprise disorders caused by mutations in genes involved in sensing, excising and repairing DNA breaks. Within this category, two major sub-groups can be recognized: ataxias caused by defects of DSBs or SSBs DNA repair. The aforementioned AT and the AT-like disorder (ATLD) fall into the first sub-category; whereas the Ataxia with Oculomotor Apraxia Type 1 (AOA1) and the Spinocerebellar Ataxia with Neuropathy 1 (SCAN1), among other types, belong to the second sub-category (Paulson & Miller, 2005). As exemplified by FRDA, mitochondrial ARCAs are caused by defects in mitochondrial proteins, encoded either by the mitochondrial or nuclear genomes (see also section 2.4.1.3). The metabolic ataxias are caused by disorders of the urea cycle or the metabolism of pyruvate, vitamin E, lipids and amino acids. The symptomatology of this group of ataxias overlaps with the clinical presentation of FRDA. Lastly, chaperone dysfunction, abnormal protein folding and degradation have been associated to a subgroup of spastic ataxias comprised by the autosomal recessive spastic ataxia of Charlevoix–Saguenay (ARSACS) and the Marinesco–Sjögren syndrome (MSS) (De Michele et al, 2004; Filla & De Michele, 2012). Other molecular pathways, of more recent identification and/or reported in single families, include defective vesicular trafficking, synaptic transmission, calcium homeostasis and intracellular pH regulation (Guissart et al, 2015; Hills et al, 2013; Sudhof, 2004; Thomas et al, 2014; Utine et al, 2013).

All together, these pathways and the numerous cell types involved, are hard to reconcile with a specific mechanism leading to cerebellar and/or spinocerebellar atrophy and more specifically, with the particular susceptibility of Purkinje neurons to degeneration. Hence, the description of novel genes and the functional characterization of the emerging pathways is fundamental to understand the complex molecular pathogenesis of ARCAs and to develop effective treatment strategies for these devastating disorders.

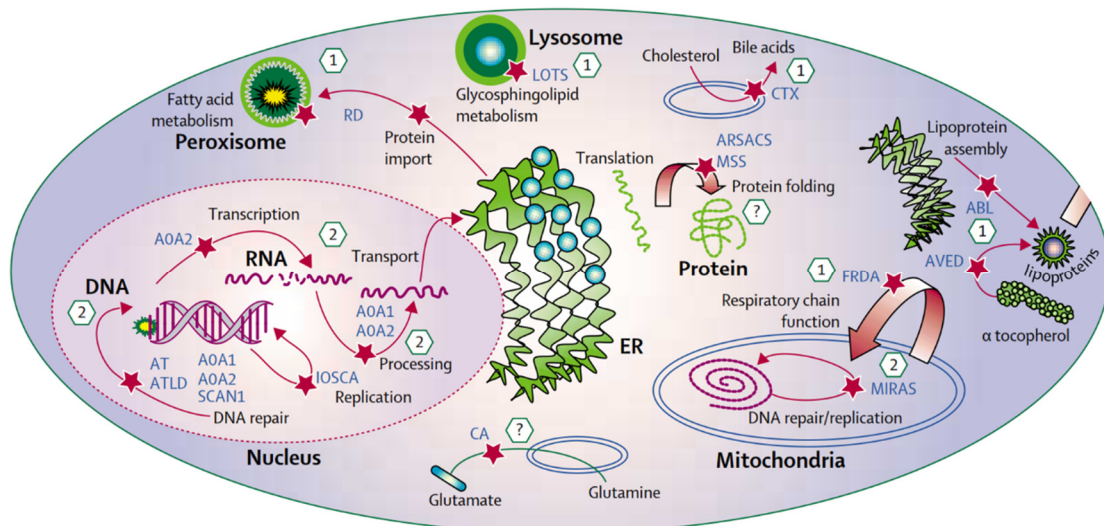


Figure 3. Molecular pathogenesis of the autosomal recessive ataxias. Major organelles within the cell are labelled in bold. The pathways or sites affected by the various mutations in ARCA-causative genes are indicated by a red star. Disease mechanisms/processes are presented with numbers. **(1)** Increased oxidative stress and other metabolic abnormalities leading to premature cell death. **(2)** Genetic instability. Processes occurring within and/or in association with a subcellular structure are depicted near the respective organelle. Abbreviations: ER, endoplasmic reticulum; FRDA, Friedreich's ataxia; AVED, ataxia with vitamin E deficiency; ABL, Abetalipoproteinaemia; RD, Refsum's disease; LOTS, late-onset Tay-Sachs disease; CTX, cerebrotendinous xanthomatosis; MIRAS, mitochondrial recessive ataxia syndrome; SCAN1, spinocerebellar ataxia with axonal neuropathy; AT, ataxia telangiectasia; AOA1, ataxia with oculomotor apraxia, type 1; AOA2, ataxia with oculomotor apraxia, type 2; ARSACS, autosomal recessive ataxia of Charlevoix-Saguenay; IOSCA, infantile-onset spinocerebellar ataxia; CA, Cayman ataxia; MSS=Marinesco-Sjögren syndrome. Figure taken from (Fogel & Perlman, 2007).

2.4.2. Calcineurin Homologous Protein-1 (CHP1)

CHP1, also termed p22, is a member of the CHP family; a group of evolutionary conserved proteins involved in calcium signaling. Calcium, as a second messenger molecule, influences a plethora of cellular processes and is particularly important for the fine modulation of the neuronal biochemical machinery of neurotransmission (Bading, 2013). The properties and molecular roles of CHP1 and the other CHP family members, CHP2 and CHP3, are very diverse and therefore still a matter of debate. Nevertheless all CHP proteins seem to be functionally reunited around one central role: the regulation of plasma membrane proteins (Di Sole et al, 2012). In contrast to CHP2 and CHP3, whose expression is mostly restricted to intestinal epithelia and developing testes, respectively; CHP1 is ubiquitously expressed across tissues and highly abundant in the brain (Barroso et al, 1996; Inoue et al, 2003; Lin & Barber, 1996; Perera et al, 2001).

Structurally, CHP1 consists of two globular domains - the N and C lobes - containing four EF-hand motifs, from which only two can bind to calcium. Furthermore, CHP1 possesses two conserved nuclear export signals and a N-terminal myristoylation site which seems to

be required to induce protein conformational changes upon calcium binding (Naoe et al, 2005; Pang et al, 2004). Because CHP1 can bind calcium with an affinity constant of approximately 90nM, an intermediate affinity value between CHP2 (~800nM) and CHP3 (~1nM), it has been suggested that CHP1 may act as both calcium sensor and calcium buffering protein (Di Sole et al, 2012).

2.4.2.1. CHP1 molecular functions

The established biological roles of CHP1 can be better understood by exploring its molecular targets of regulation, which can be classified into three major categories: gene transcription, intracellular and vesicular trafficking and membrane ion transport (Figure 4).

2.4.2.1.1. Regulation of gene transcription

When localized in the nucleus, CHP1 can block the synthesis of ribosomal RNA via association with Upstream Binding Factors (UBF); a group of transcription factors that participate in the assembly of the preinitiation complex integrated by the Polymerase I and the ribosomal RNA, among other proteins (Jimenez-Vidal et al, 2010). Furthermore, CHP1 binds and inhibits the kinase activity of DRAK2 (encoded by *STK17B*, Serine/Threonine Kinase 17bv gene), an apoptosis-inducing protein (Kuwahara et al, 2003).

Remarkably, the role of CHP1 on gene expression regulation can be also independent of the nuclear localization of the protein. CHP1 modulates Calcineurin (CaN) activity, a calcium/calmodulin-dependent phosphatase (see also next section 2.4.2.1.2). The activation of CaN has been implicated in the dephosphorylation and nuclear translocation of NFAT (Nuclear Factor of activated T cells), a transcription factor important for the triggering of immune response processes, since it promotes the transcription of the cytokines IL-2 and IL-4, which in turn control the proliferation of T-cells (Chow et al, 1999; Clipstone & Crabtree, 1992).

2.4.2.1.2. Regulation of intracellular trafficking

Since CHP1 is required for the targeting and fusion of transcytotic vesicles with the plasma membrane through a process reliant on both CHP1 N-terminal myristoylation and calcium binding (Barroso et al, 1996); it was speculated that CHP1 might serve as a calcium sensor for constitutive exocytosis (Di Sole et al, 2012; Pang & Sudhof, 2012). Further strengthening this notion, it has been reported that CHP1 also modulates the endocytosis of glutamate

AMPA receptors via regulation of Calcineurin (CaN) activity (Baumgartel & Mansuy, 2012; Lin et al, 1999). Moreover, because of CHP1 self-distribution along microtubules and interaction with the motor protein KIF1B β 2 (kinesin-related protein) and the actin-bundling protein GAPDH (Andrade et al, 2004a), other intracellular transport functions have been linked to the calcium-sensing properties of CHP1. Precisely, CHP1 participates in the interactions between the ER and Golgi membranes with microtubules, thereby modulating organelle assembly, transport and microsomal vesicle trafficking (Andrade et al, 2004b; Barroso et al, 1996; Nakamura et al, 2002; Timm et al, 1999).

2.4.2.1.3. CHP1 as regulator of integral membrane proteins. The CHP1-NHE1 interaction.

The CHP family of proteins regulates a family of ubiquitous membrane proteins known as NHE (Solute Carrier Family *SLC9A*, isoforms 1-9). These proteins catalyze the electroneutral exchange of Na⁺ for H⁺ ions (hence the designation NHE) and are involved in numerous essential cellular functions such as pH regulation, cell volume and shape maintenance, cellular proliferation, adhesion and migration, and cell cycle progression (Cardone et al, 2005; Casey et al, 2010; Putney et al, 2002).

CHP1 was originally identified as a binding partner of the Na⁺/H⁺ exchanger NHE1 (encoded by *SLC9A1*), an integral membrane protein that catalyze the efflux of intracellular protons and the influx of intracellular sodium ions (Lin & Barber, 1996), thus playing a vital role in intracellular pH (pHi) homeostasis maintenance (Grinstein et al, 1992; Pedersen et al, 2013; Pouyssegur et al, 1984; Putney et al, 2002). Further studies demonstrated that CHP1 is an essential cofactor of NHE1, since it controls the physiological pHi sensitivity, the membrane localization and the stimuli-triggered activation of NHE1 (Lin & Barber, 1996; Liu et al, 2013; Pang et al, 2004; Pang et al, 2001). It is pertinent to highlight that pHi homeostasis is crucial for neurotransmission and neuronal excitability, as intracellular acidification and fast acid-base changes arise permanently upon neuronal firing (Chesler, 2003; Chesler & Kaila, 1992) and subtle pH changes strongly influence neurotransmitter release and neuronal excitability (Chen & Chesler, 1992; Dietrich & Morad, 2010).

To date, no human pathogenic *CHP1* mutations have been reported. Nevertheless, a missense loss-of-function mutation in *SLC9A1* (NHE1) was reported to cause an autosomal recessive disorder (Lichtenstein-Knorr syndrome (LINKS) OMIM: 616291) that involves cerebellar ataxia and sensorineural hearing loss. More precisely, the G305R mutation in *SLC9A1* introduces a positive charge in the eighth transmembrane domain of NHE1, leading to membrane mistargeting, reduced glycosylation -a process where CHP1 also

intervenes- and loss of ion-pumping activity. Loss of NHE1 activity and the concomitant collapse of pHi homeostasis was causatively associated to LINKS syndrome (Guissart et al, 2015).

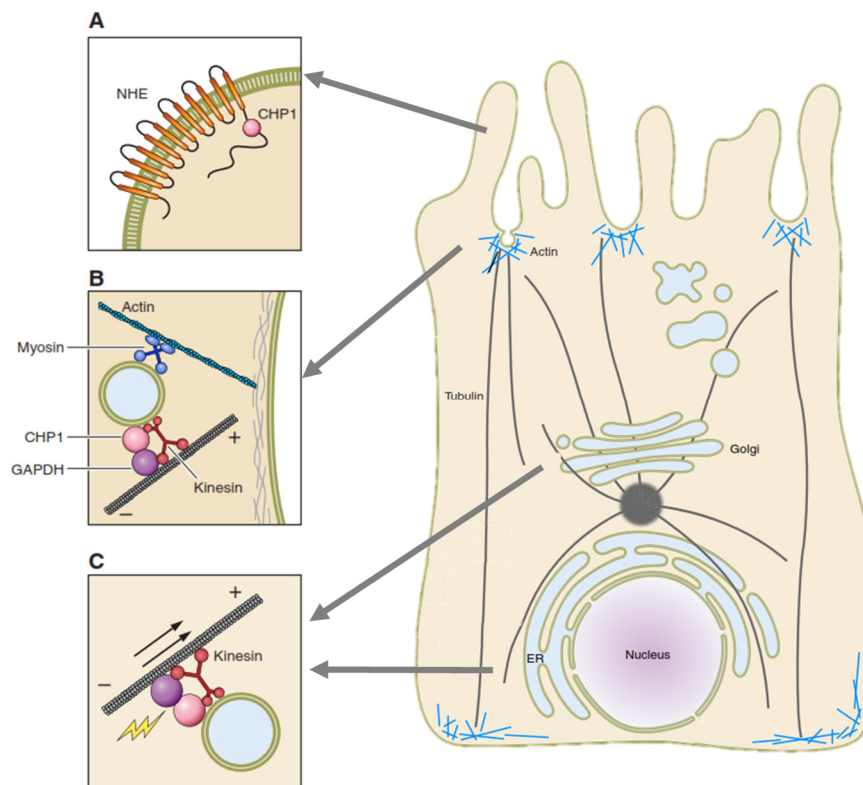


Figure 4. Main cellular processes regulated by CHP1. (A) Na^+/H^+ exchanger 1 (NHE1) in lamellipodia and membrane ruffles of polarized cells. Depicted is the CHP1-NHE1 complex at the inner cell membrane (B) Fusion of transcytotic vesicles with the plasma membrane and possible molecular model of CHP1-mediated microtubule and actin transport, based on CHP1 interaction partners GAPDH and Kinesin. (C) A similar transport mechanism could facilitate CHP1-mediated microsomal trafficking. Figure adapted from (Di Sole et al, 2012).

2.4.2.2. CHP1 animal models

The effect of *CHP1* depletion has been addressed in two animal models. Loss-of-function *pbo-1* mutations (*pbo-1*, posterior body contraction mutant), the *CHP1* orthologue in *C. elegans* (64% similarity to human *CHP1*), cause drastic impairment of posterior body contraction and severely reduce proton movement across apical and basolateral intestinal membranes (Wagner et al, 2011). These phenotypes resemble the dysfunctional pHi regulation observed in *pbo-4/nhx-7* and *nhx-2* mutants; the nematode NHE exchangers (Beg et al, 2008; Nehrke, 2003; Pfeiffer et al, 2008; Wagner et al, 2011).

By positional cloning, *vac* was identified as a point mutation in the mouse *Chp1* gene (*Vacillator -vac-* mutation: c.657 A>G, p.D168G) (Liu et al, 2013). This hypomorphic mutation resulted in aberrant *Chp1* splicing and translation of two truncated products unable

to promote full glycosylation and membrane expression of NHE1 in axon terminals. Mistargeting of NHE1 in *vacillator* mice led to early onset degeneration, progressive loss of Purkinje cells and ataxia (Liu et al, 2013). Interestingly, knockout (KO) of mouse *Nhe1*, also cause neuronal loss in the cerebellum and brainstem, severe locomotor ataxia, behavioral arrest and epilepsy (Bell et al, 1999; Cox et al, 1997).

2.5. Functional characterization of a *de novo* mutation in *SLC18A3* in a family with distal motor neuropathy (dHMN)

A *de novo* dominant mutation in *SLC18A3*, the gene encoding the Vesicular Acetylcholine Transporter (VACHT), was found in a family manifesting cranial nerve palsies and vocal cord paresis as initial features of a non-progressive dominant dHMN. The consequences of this VACHT mutation on MN pathogenesis were analyzed within the scope of this PhD thesis (see section 4.2). In the next subsections (2.5.1 and 2.5.2) the different dHMN forms as well as the cellular functions of VACHT are described.

2.5.1. Inherited distal motor neuropathies (dHMNs)

dHMNs are a group of disorders characterized by distal LMN weakness resembling the Charcot-Marie-Tooth (CMT) neuropathy, in which MNs are also primarily affected. In contrast to SMA, dHMNs initially and predominantly affect the distal limb muscles *i.e.* the longest motor axons. Therefore, dHMNs are also termed as the spinal form of CMT (spinal-CMT), axonal CMT (CMT2) or distal SMA (dSMA) (Landrieu et al, 2013; Murphy et al, 2013; Rossor et al, 2012). The prevalence of dHMNs has been estimated as 1:50000 approximately, (Bansagi et al, 2017), representing 10% of all inherited neuropathies (Irobi et al, 2006).

Patients with classic dHMN, manifest slow-progressive weakness and wasting of the extensor muscles of the toes and feet. Subsequently, weakness and wasting also affect the distal upper limb muscles. Foot deformity is a common observation. Additional features including progressive weakness with hands predominance, vocal cord paralysis, diaphragm paralysis and pyramidal signs can co-present with distal neuropathy in complicated dHMNs forms. From the nosology point of view, dHMNs can be very hard to distinguish from the CMT neuropathy, when the latter presents without unequivocal sensory signs. Hence, electrophysiological examinations are crucial to make a differential diagnosis between these disorders (Harding, 2005; Harding & Thomas, 1980; Klein et al, 2013).

Notwithstanding that more than 30 causative genes have been described for dHMNs, a successful dHMN diagnosis is possible only in half of the patients (Bansagi et al, 2017). More strikingly, another study published shortly after the massive NGS advent, reported that in approximately 80% of the dHMN patients, the genetic diagnosis was negative (Dierick et al, 2008). These facts highlight the crucial impact that NGS technologies have had in the clinical diagnosis of these complex disorders.

2.5.1.1. Classification of dHMNs

Based on the mode of inheritance, age of onset and phenotype, dHMNs are classically categorized into seven subtypes, from dHMN type I to VII, where types I, II, V and VII represent the disorders with autosomal dominant inheritance and types III, IV and VI are autosomal recessive (Harding, 2005). The integration of NGS technologies into routine genetic diagnostic and the concomitant harvest of novel disease genes has further delineated the classical Harding classification of dHMNs. Moreover, the dHMN entities of more recent identification have expanded the phenotypic overlap that exists among dHMNs themselves and with other neuropathies. Consequently, and against the Harding classification, it has recently been suggested that dHMNs should not be considered a group apart from the motor CMTs, whereas both entities are not only clinically similar but also share various pathogenic mutations in the same genes (Bansagi et al, 2017). In the following subsections, the dHMN entities associated with each inheritance mode (*i.e.* dominant, recessive and X-linked) are succinctly commented. Complementing this information, Table 5 summarizes the dHMNs classification based on the system of current use (Harding, 2005), and includes dHMN-causative genes of recent identification and their associated dHMNs phenotypes. It is important to highlight that these novel genes confront the general conceptualization of dHMNs as length-dependent neuropathies of only motor axons, whereas sensory and cerebellar involvement have been reported for a small subset of these disorders.

2.5.1.1.1. Autosomal dominant distal HMN

Dominant inheritance is the most common inheritance mode among dHMNs. From the seven subtypes described by Harding, four types are autosomal dominant (Harding, 2005). The dHMNs types I and II (also termed CMT2F and CMT2L) are typical dHMNs of the lower limbs with onset in childhood or adulthood, respectively (Harding, 2005; Irobi et al, 2004). Type V dHMN (also termed CMT2D) is characterized by early onset muscle weakness and wasting that predominantly affects the upper-limbs (Harding, 2005). Type VII dHMN is

defined by predominant upper limb weakness with adult onset accompanied of vocal cord paresis (McEntagart et al, 2002; Puls et al, 2003). In this category it is important to include the most recently described forms of autosomal dominant SMA (SMALED), characterized by predominant lower limb weakness with slow progression (Harms et al, 2012; Neveling et al, 2013).

2.5.1.1.2. Autosomal recessive distal HMN

In general, recessive dHMNs are associated with more severe phenotypes. The dHMNs types III, IV and VI are associated with “pure MN” presentations with moderate to severe symptoms. Types III and IV are considered chronic dHMN forms and have been linked to the same genetic locus (11q13.3), however only Type IV present with diaphragmatic palsy (Irobi et al, 2006; Viollet et al, 2002; Viollet et al, 2004). dHMN type VI (also termed SMARD1) is a severe neuropathy characterized by early onset distal weakness and respiratory distress (Grohmann et al, 2001). Other recessive dHMN forms of recent description include two SMA-related entities presenting either early onset epileptic seizures (SMAPME Spinal Muscular Atrophy with Progressive Myoclonic Epilepsy) or bone/joint fractures (SMABF, Spinal Muscular Atrophy with Congenital Bone Fractures (Knierim et al, 2016; Zhou et al, 2012).

2.5.1.1.3. X-linked distal HMN

X-linked dHMN (dSMAX) was reported in one family with 17 affected individuals exhibiting predominant weakness and atrophy of the lower limbs. Disease progression is slow with onset in the first decade of life (Kennerson et al, 2009; Takata et al, 2004).

Table 5. Classification of dHMNs and recently described causative genes

	Disorder	Gene	OMIM	Clinical Features
dHMN-I	dHMN1	Unknown Locus: 7q34-q36	182960	Autosomal dominant. Juvenile onset lower limb predominant distal weakness and wasting.
dHMN-II	dHMN2A	<i>HSPB8</i>	158590	Autosomal dominant. Adult onset lower limb predominant distal weakness and wasting. 2D subtype is calf predominant.
	dHMN2B	<i>HSPB1</i>	608634	
	dHMN2C	<i>HSPB3</i>	613376	
	dHMN2D	<i>FBXO38</i>	608533	
dHMN-III	dHMN3	Unknown Locus: 11q13.3	607088	Autosomal recessive. Adult onset distal weakness and wasting.
dHMN-IV	dHMN4	Unknown Locus: 11q13.3	607088	Autosomal recessive. Juvenile onset severe muscle weakness and wasting and paralysis of the diaphragm.
dHMN-V	dHMN5	<i>GARS BSCL2</i>	600794	Autosomal dominant. Upper limb predominant distal muscle weakness and wasting.
dHMN-VI	dHMN6 dSMA1	<i>IGHMBP2</i>	604320	Autosomal recessive. Infantile onset with respiratory distress.
dHMN-VII	dHMN7A	<i>SLC5A7*</i>	158580	Autosomal dominant with vocal cord paralysis.
	dHMN7B	<i>DCTN1</i>	607641	Autosomal dominant. Adult onset breathing difficulties due to vocal cord paralysis, facial weakness and hand muscle atrophy.
	dHMN8	<i>TRPV4</i>	600175	Autosomal dominant. Congenital Spinal muscular atrophy, distal, nonprogressive.
	X-Linked dHMN dSMAX	<i>ATP7A</i>	300489	X-linked. Juvenile onset distal weakness and wasting.
	dSMA4	<i>PLEKHG5*</i>	611067	Autosomal dominant congenital. Non-progressive lower limb weakness and paralysis with contractures.
	dSMA5	<i>DNAJB2</i>	614881	Autosomal recessive. Adult onset spinal muscular atrophy, distal.
	dHMN-ALS4	<i>SETX</i>	602433	Autosomal dominant. Juvenile onset distal weakness and wasting with positive pyramidal signs.
	dHMN-dSMA2	<i>SIGMAR1*</i>	605726	Autosomal recessive. Juvenile onset distal weakness and wasting with pyramidal tract signs.
	SMAJ	<i>CHCHD10</i>	615048	Autosomal dominant. Adult onset distal weakness and muscle cramps.
	SMALED1	<i>DYNC1H1</i>	158600	Autosomal dominant. Juvenile onset SMA. Distal weakness and wasting with pyramidal tract signs.
	SMALED2	<i>BICD2</i>	615290	Lower extremity-predominant.
	SMAPME	<i>ASAH1</i>	159950	Autosomal recessive. Infantile onset proximal muscle weakness and seizures.
	SMABF	<i>ASCC1*</i>	616867	Autosomal recessive. Congenital. Spinal muscular atrophy with joint contractures and respiratory distress.
	HMN2D	<i>FBXO38</i>	615575	Autosomal dominant. Adult onset progressive distal hereditary motor neuropathy.
	HMN5B	<i>REEP1*</i>	614751	Autosomal dominant. Juvenile onset distal hereditary motor neuropathy.
	HMSNO	<i>TFG</i>	604484	Autosomal dominant. Adult onset hereditary motor and sensory neuropathy (Okinawa type)
	HNARMD	<i>FBLN5</i>	608895	Autosomal dominant. Juvenile onset predominantly distal motor neuropathy with or without macular degeneration
	PEBAT	<i>TBCD</i>	617193	Autosomal recessive. Early onset severe hypotonia and muscle weakness. Progressive encephalopathy with brain atrophy and thin corpus callosum.
	PNMHH	<i>MYH14*</i>	614369	Autosomal recessive. Juvenile onset distal weakness and wasting with pyramidal tract signs.

Abbreviations: ALS, amyotrophic lateral sclerosis; SMAJ, Spinal Muscular Atrophy, Jokela type; SMALED, spinal muscular atrophy, lower extremity-predominant; SMAPME, Spinal Muscular Atrophy With Progressive Myoclonic Epilepsy, SMABF, Spinal Muscular Atrophy with Congenital Bone Fractures 2; HMN, Hereditary Motor Neuropathy; HMSNO, Hereditary Motor and Sensory, Okinawa Type; HNARMD, Hereditary Neuropathy with or without Age-Related Macular Degeneration; PEBAT, Encephalopathy, Progressive, Early-Onset, with Brain Atrophy and Thin Corpus Callosum; PNMHH, Peripheral Neuropathy, Myopathy, hoarseness, and hearing loss. * Indicates one family register. Data source: <http://neuromuscular.wustl.edu> (in category dHMN). Year of last update: 2017.

2.5.1.2. Molecular pathogenesis of dHMNs

Although the genes associated to dHMNs are functionally heterogeneous, some common molecular pathomechanisms can be recognized. Mutations in the RNA-processing genes *GARS* (Glycyl-tRNA Synthetase), *SETX* (Senataxin) and *IGHMBP2* (Immunoglobulin Mu Binding Protein 2) causing dHMN5, ALS4 (a juvenile form of ALS) and dHMN6, respectively, have a detrimental impact on RNA transcription and pre-mRNA splicing, editing, translation and degradation (Antonellis et al, 2003; Chen et al, 2004; Grohmann et al, 2001; van Blitterswijk & Landers, 2010). Hence, RNA metabolism disturbance is a significant contributor to dHMNs pathogenesis.

Protein aggregation is a disease mechanism underlying neurodegeneration in several disorders (Ross & Poirier, 2004; Taylor et al, 2002) and dHMNs are not the exception. Mutations in the small chaperones *HSPB8* (Heat Shock Protein Family B (Small) Member 8) and *HSPB1* (Heat Shock Protein Family B (Small) Member 1), causative of dHMN2A and dHMN2B respectively (see Table 5), have been associated with formation of insoluble neuronal aggregates *in vitro* (Ackerley et al, 2006; Evgrafov et al, 2004; Irobi et al, 2004). Moreover, in dHMN5 with mutation in *BSCL2* (Bernardinelli-Seip Congenital Lipodystrophy Type 2 Protein), accumulation of misfolded protein in aggresome-like structures were observed in the endoplasmic reticulum (ER) of cultured cells, leading to ER stress and concomitant cell death (Ito & Suzuki, 2009).

Lastly, disrupted axonal transport is a pathogenic mechanism observed in dHMN2B, dHMN2A and dHMN7B, caused by mutations in *HSPB1*, *HSPB8* and *DCTN1* (Dynactin Subunit 1) respectively. On one hand, HSPB1 aggregates have been linked with disrupted assembly and accumulation of neurofilaments (NF) (Ackerley et al, 2006); whereas mutant HSPB8 alters axonal transport in primary MNs (Irobi et al, 2010). Moreover, disruption of the motor function of DCTN1, a core component of the microtubule-dependent transport machinery, results in defective microtubule binding and impaired axonal transport (Levy et al, 2006; Puls et al, 2003). A graphic summary of known dHMN-causative genes and further molecular pathomechanisms underlying these disorders, e.g. synaptic transmission defects and disturbed mitochondrial function is provided in (Figure 5).

It is still unknown, how mutations in ubiquitously expressed genes lead to specific LMN phenotypes. Probably the reliance of LMNs on active transport mechanisms, through very long axons, and on high energetic consumption, underlie their susceptibility to alterations in general cellular processes governed by ubiquitous proteins. Future discovery and characterization of novel dHMNs genes will be pivotal to pinpoint common disease mechanisms and pathways and to uncover potential targets for pharmacological intervention and/or prevention of these complex disorders.

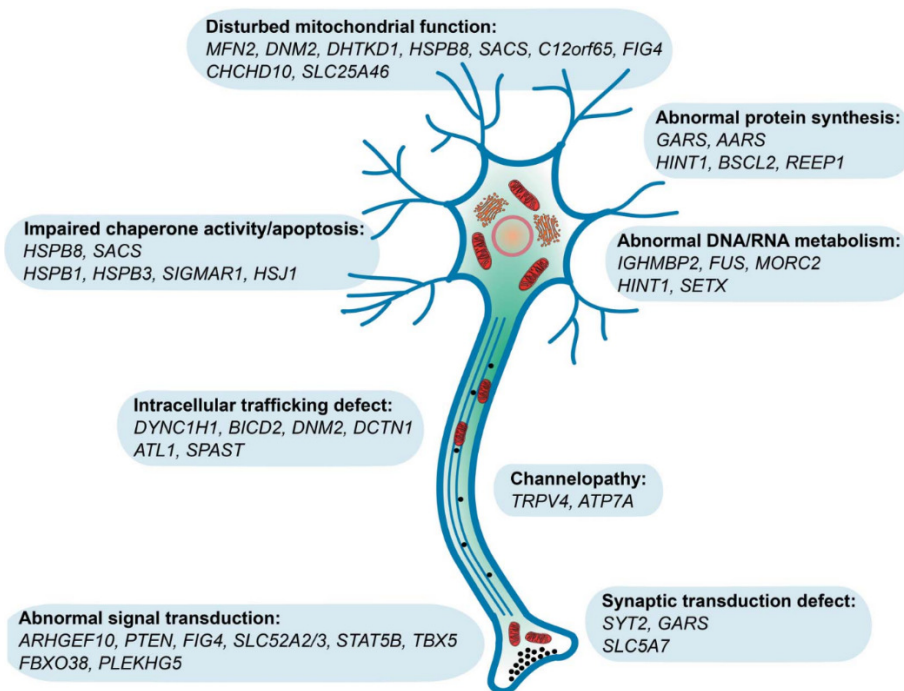


Figure 5. Molecular pathomechanisms in dHMNs. The main cellular processes and/or mechanisms behind neuronal degeneration in dHMNs are depicted. Genes and mutations of recent identification have revealed novel mechanisms underlying MN pathogenesis in dHMNs. Figure taken from (Bansagi et al, 2017).

2.5.2. Vesicular Acetylcholine Transporter (VACHT)

2.5.2.1. The cholinergic neurotransmission

Cholinergic neurotransmission regulates several central and peripheral nervous system outputs, being therefore indispensable for general physiological functions, such as the formation, wiring and proper nerve-muscle patterning of the neuromuscular junction (NMJ) (Brandon et al, 2003; Misgeld et al, 2002). In cholinergic neurons, the synthesis of the neurotransmitter acetylcholine (ACh) begins with the uptake of the choline precursor by the High Affinity Choline Transporter (CHT1). In the cytoplasm, the ACh precursor is used as a substrate to synthesize acetylcholine (ACh) in a reaction catalyzed by the enzyme Choline Acetyl Transferase (ChAT). Because of the cationic nature of the ACh, a transport mechanism is required for the secretion/release of this neurotransmitter. Hence, ACh is loaded into synaptic vesicles by VACHT (encoded by *SLC18A3*, Solute Carrier Family 18 Member 3). Upon arrival of the nerve impulse, cholinergic vesicles fuse with the plasma membrane and release the ACh. On the postsynaptic side, the released neurotransmitter will trigger the activation of Nicotinic and Muscarinic receptors (Figure 6) (Purves, 2004). Although the mechanisms regulating ACh storage are not fully understood, it is well known that the amount of stored neurotransmitter depends on the amount of expressed VACHT.

Consequently, ACh release is rate-limited by VACHT expression and function (Lima R de et al, 2010).

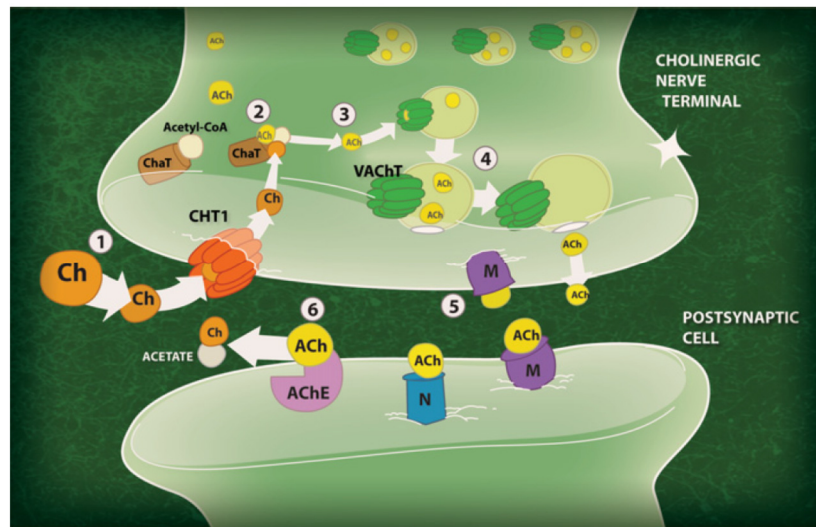


Figure 6. ACh synthesis, packaging and release in cholinergic neuron. (1) Uptake of the ACh precursor (Choline) by CHT1. (2) ACh is synthesized by the enzyme ChAT (reaction includes Choline and Acetyl-CoA). (3) ACh is loaded into synaptic vesicles by VACHT. (4) After depolarization (nerve impulse), vesicles fuse to plasma membrane and release ACh. (5) In the post synapse (e.g. muscle), ACh signals nicotinic (N) and muscarinic (M) receptors. (6). ACh is degraded into acetate and Choline by the enzyme AChE. Abbreviations: ChAT, Choline acetyltransferase; VACHT Vesicular Acetylcholine Transporter; AChE, Acetylcholinesterase. Figure taken from (Prado et al, 2013)

2.5.2.2. Animal models of VACHT

The consequences of altered expression/activity of VACHT have been widely analyzed in different animal models demonstrating its crucial implication in neurotransmitter release and post-synaptic signaling. The first evidence of the essential function of VACHT *in vivo* came from experiments with *C. elegans*. Mutations in the VACHT orthologue *unc-17* cause miscoordination and severe neuromuscular function deficits whereas complete *unc-17* KO is lethal (Alfonso et al, 1993). Similarly, ablation of the VACHT function in *Drosophila* results in delayed development and slow locomotion or embryonic lethality, depending on the extent of VACHT reduction, *i.e* strong or weak *dVACHT* alleles (Kitamoto et al, 2000).

Homozygous *Slc18a3* KO in mouse (*VACHT^{del/del}*) is incompatible with life. *VACHT^{del/del}* embryos die shortly after birth due to severely undeveloped NMJs, abnormal nerve sprouting, muscle necrosis and profound cardiac remodeling (de Castro et al, 2009; Lara et al, 2010). Nonetheless, VACHT knockdown within a safety threshold (approximately 50% reduction) is better tolerated, as mice survive after birth but show neuromuscular and neurotransmission defects, disrupted long-term habituation of the startle response (unresponsiveness to repetitive stimuli) and social/object recognition deficits (de Castro et

al, 2009; Prado et al, 2006; Schmid et al, 2011). Contrastingly, mice overexpressing VACHT with concomitant increased cholinergic transmission, exhibit cognitive defects, accelerated degeneration of the NMJs and motor deficits (Sugita et al, 2016). Restricted VACHT OE in striatal cholinergic neurons alters VACHT localization and leads to cellular morphological remodeling and impaired axonal trafficking (Janickova et al, 2017).

2.5.2.3. Mutations in VACHT underlie congenital myasthenic syndromes

The Congenital Myasthenic Syndromes (CMS) are a group of inherited disorders of the neuromuscular junction (NMJ) function. Typical CMS symptoms include early onset muscle fatigable weakness of skeletal muscles (e.g. facial, bulbar and limb muscles), ptosis (drooping of the upper eyelid) and ophtalmoplegia (Engel et al, 2015; Hantai et al, 2013). CMS are traditionally classified into 3 major categories depending on the location of the affected protein within the NMJ namely, presynaptic, synaptic (or basal lamina associated) or postsynaptic CMS. 50% of CMS cases underlie mutations in postsynaptic proteins and the majority of them affect the function of the muscle nicotinic ACh receptor (AChR). Synaptic and presynaptic mutations account for 10% and 5% of the CMS cases, respectively and affect the synthesis, anchoring (to the basal lamina) and release of ACh from nerve terminals (Engel et al, 2015; Hantai et al, 2013). More precisely, mutations in *CHAT* that is essential for ACh synthesis as well as in *MUNC13*, *SYT2* and *SNAP25* which are necessary for ACh vesicles priming and exocytosis, have been associated to presynaptic CMS (Engel et al, 2016; Engel et al, 2015; Shen et al, 2014; Whittaker et al, 2015).

Very recently, pathogenic VACHT mutations were reported in two unrelated families with affected individuals presenting symptoms compatible with presynaptic CMS type 21 (OMIM 617239). More specifically, the patients exhibited ptosis, ophtalmoplegia, fatigable weakness and apneic crisis, among other complicating systemic features in one proband (O'Grady et al, 2016). The unrelated probands carried either a biallelic *SLC18A3* missense mutation (D398H) or compound heterozygous mutation, with one homozygous missense mutation (G186A) and a large heterozygous deletion (10q11.22-q11.23, 4,83Mb) encompassing several genes, including both VACHT and CHAT, which are transcribed from the same regulatory locus (Erickson et al, 1994). A second study reported a *SLC18A3* loss-of function mutation (G360R) in two siblings presenting a very severe CMS (Aran et al, 2017). Functional studies for all novel VACHT mutations were not performed.

PART II. CHP1 REDUCTION AMELIORATES MOTOR NEURON DEGENERATION IN A ZEBRAFISH MODEL OF SMA

Beyond CHP1 role in the pathogenesis of ARCA, another feature of CHP1 function which is of relevance in our research group is that it also interacts with the actin-binding and bundling protein Plastin-3 (PLS3) a human protective genetic modifier of SMA. Preliminary functional analysis strongly indicate that CHP1 may be a novel SMA protective modifier (see section 4.3). Within this frame, this thesis provides experimental evidence that confirms the beneficial effect of Chp1 downregulation in a zebrafish model of SMA. The following subsections include information about SMA and SMA genetic modifiers validated in human and across species.

2.6. Modifier genes of Spinal Muscular Atrophy

Genetic modifiers, understood as a genetic locus that enhances or suppresses *-i.e.* modifies- the outcome of the primary disease-causing mutation are of crucial importance in the pathogenesis of complex and monogenic disorders, as they modulate important disease features such as onset, severity and progression (Lamar & McNally, 2014; Nadeau, 2001; Nadeau, 2003). The genetic variability observed among individuals carrying pathogenic mutations in *SMN1*, the causative gene of SMA, is a perfect example of the modifier concept introduced above.

SMA is a devastating neuromuscular disorder caused by homozygous deletions, or rarely point mutations, of the ubiquitously expressed *SMN1* gene, which results in the functional loss of the SMN1 protein and concomitant degeneration of alpha motor neurons (LMNs, see section 2.1), defective NMJs development and maturation and impaired neurotransmission (Harding et al, 2015; Kariya et al, 2008; Kong et al, 2009; Lefebvre et al, 1995; Ling et al, 2012). Hence, SMA patients exhibit progressive and symmetrical atrophy of the proximal voluntary muscles and paralysis. Approximately 60% of the affected individuals die within the first two years of life (Dubowitz, 2009; Markowitz et al, 2004). Based on disease onset and motor function, SMA is classified into four different subtypes namely:

- Type I (Werning Hoffman disorder, OMIM), the most severe and early lethal form of the disorder and the most common genetic cause of infant death (Melki et al, 1994). The main disease symptoms are generalized muscular weakness, hypotonia and areflexia with onset in the first months of life (Finkel et al, 2014).

- Type II or intermediate SMA, is characterized by disabling muscle weakness with onset between 6 and 18 months of age. These patients cannot stand or walk and, although they can reach adulthood, their life expectancy is reduced (Dubowitz, 1964).
- Type III, a milder SMA form with onset after 18 months. Type III patients learn to walk independently but as disease worsens, they become wheelchair-dependent. Life expectancy in this patients is normal (Kugelberg & Welander, 1956).
- Type IV SMA is of rare frequency. With onset in late adulthood and, is considered the mildest of all SMA forms. Type IV patients manifest progressive muscle weakness, which might result incapacitating. Life expectancy is normal (Zerres et al, 1995).

SMN levels, and thus SMA severity, are mainly influenced by *SMN2*, a paralog gene almost identical to *SMN1* except for five nucleotide exchanges, all translationally silent (Burglen et al, 1995) (Feldkotter et al, 2002) (Lunn & Wang, 2008). Remarkably, a C to T transition in *SMN2*, disrupting an exonic splice enhancer (ESS), results in the exclusion of exon 7 in approximately 90% of the transcripts. The remaining 10%, are full-length transcripts which encode a protein identical to the one produced by the *SMN1* gene (Lorson & Androphy, 2000; Lorson et al, 1999). As the number of *SMN2* copies varies from zero to eight in the general population, the residual protein expression of this paralog strongly correlates with disease severity (Figure 7) (Feldkotter et al, 2002; Wirth et al, 2006). Therefore, *SMN2* is not only the main modifier of SMA but also the central target for pharmacological intervention of this disorder (Kaczmarek et al, 2015).

In rare instances, individuals with homozygous deletion of *SMN1* and 3 to 4 copies of *SMN2*, the genetic combination found in type III SMA patients (see Figure 7), are completely asymptomatic. These individuals, belonging to the so called discordant families, have revealed the existence of protective genetic SMA modifiers in humans and further unmasked endocytosis as the main molecular process underlying disease pathogenesis. These modifiers namely, Plastin 3 (PLS3) and Neurocalcin delta (NCALD) were identified in our research group and are currently matter of investigation (Hosseinibarkooie et al, 2016; Oprea et al, 2008; Riessland et al, 2017).

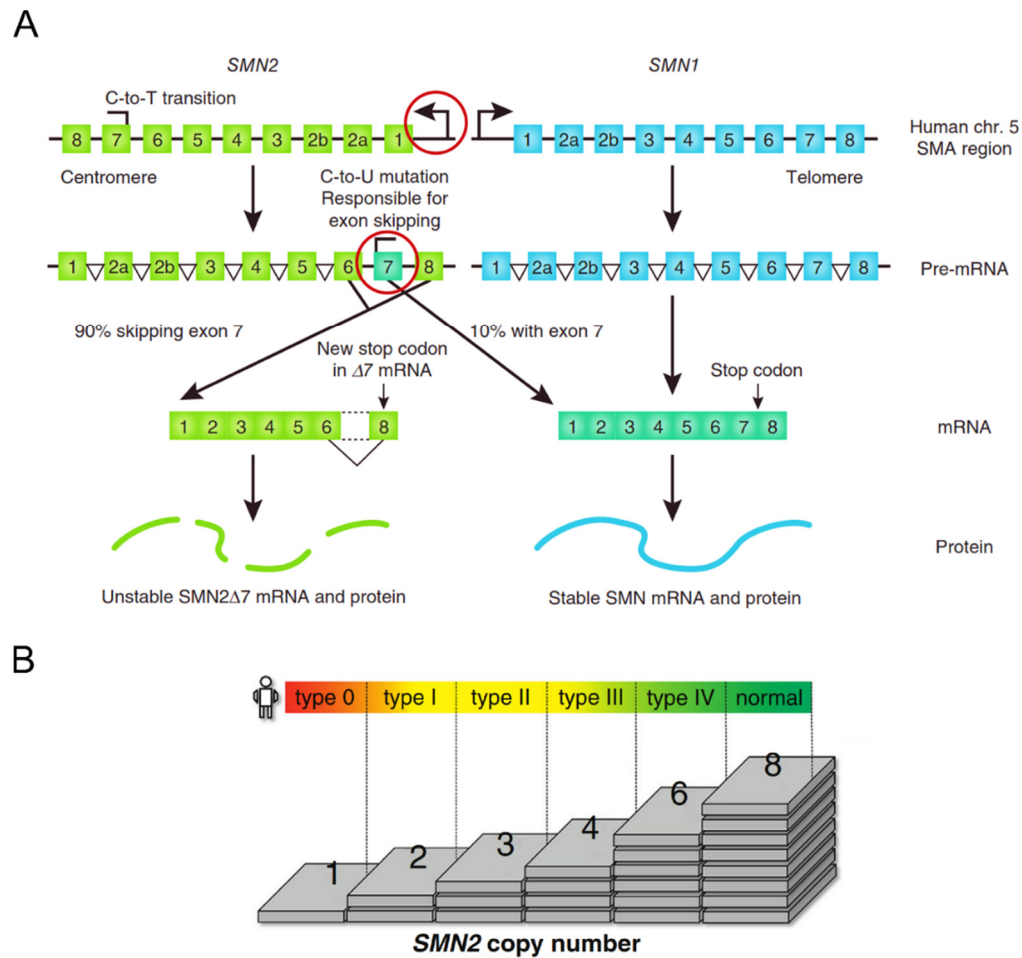


Figure 7. The genetic determinants of SMA. (A) Schematic diagram of the *SMN1* and *SMN2* genes on human chromosome 5. In SMA, both allelic copies of the *SMN1* gene are deleted or mutated. The *SMN2* gene is also transcribed, but most of the resulting gene products give rise to a truncated SMN protein lacking the exon 7. This is caused by a C-to-T transition at position 6 of exon 7, which disrupts a splice enhancer site and generates a cryptic splice silencer site. SMA therapies (in red circles) include increase activity of the *SMN2* promoter and enhanced production of *SMN2* full-length transcripts. **(B)** *SMN2* copies determine SMA severity in humans. Image depicts the correlation of the *SMN2* copy number and the phenotype of SMA patients. Since each *SMN2* copy produces about 10% of full length (FL) *FL-SMN2* transcripts, the amount of FL-SMN protein increases accordingly. Milder SMA phenotypes result from SMN protein produced by each *SMN2* allele. In humans only eight copies lead to a normal phenotype in the absence of *SMN1*. Image modified from (Sendtner, 2010) and (Wirth et al, 2013).

2.6.1. Plastin 3

Plastin 3 (PLS3), the first human modifier of SMA ever identified, was found to be 40-fold overexpressed in SMA protected (vs affected) siblings from different discordant families, resulting in full protection against the disease (Oprea et al, 2008). PLS3 is an F-actin-binding and bundling protein that influences the globular/filamentous (G/F) actin ratio and consequently, the molecular processes reliant on this fine balance; such as axon development, cell polarity, endocytosis, cell migration and vesicle trafficking (Engqvist-Goldstein & Drubin, 2003; Hosseinibarkooie et al, 2017; Pollard & Borisy, 2003). It is

important to highlight that functionally, SMN might have an important, yet not fully accepted, role in axonal generation, since reduced SMN levels impact F-actin dynamics (reviewed in (Wirth et al, 2017) and (Hosseinibarkooie et al, 2017)).

PLS3 overexpression (OE) restores the SMA pathology in invertebrate and vertebrate models of the disease. Precisely, increased PLS3 levels ameliorate the axonal outgrowth defects of cultured MN derived from SMA mice and the defective CaP-MN axonal projections of *Smn*-depleted zebrafish larvae (Oprea et al, 2008). More importantly, PLS3 OE dramatically extends survival and restores the motoric abilities of an intermediate SMA mouse model, which closely resembles the human pathology of a Type III SMA affected individual (Hosseinibarkooie et al, 2016).

2.6.2. Neurocalcin delta

Neurocalcin delta (NCALD) was recently identified as protective of the SMA pathology in a three-generation SMA discordant family with five asymptomatic and two type I SMA-affected individuals. NCALD is a neuronal calcium sensor which, contrary to PLS3, is SMA-protective when downregulated. Indeed, reduced expression of NCALD restores axonal outgrowth in MNs derived from SMA mice *in vitro*, whereas *in vivo* it rescues defective CaP-MN axonal projections, NMJ functionality and swimming speed of *smn* zebrafish morphants, and the reduced pharyngeal pumping of a *C. elegans* SMA model (Riessland et al, 2017).

Most conclusively, NCALD knockdown (KD) in severely affected SMA mice, significantly restores the main pathological SMA hallmarks including defective NMJ size and maturation and reduced MN outgrowth and proprioceptive inputs. Complementing these results, NCALD reduction in mildly affected SMA mice, resembling the pathogenesis of SMA-protected individuals, also restores NMJ architecture as well as motoric abilities (Riessland et al, 2017). Mechanistically, and similar to PLS3 (Hosseinibarkooie et al, 2016) reduction of NCALD also improves disturbed endocytosis in SMA, however NCALD is a negative regulator of the process, whereas PLS3 is positive.

3. STUDY AIMS

PART I. IDENTIFICATION AND FUNCTIONAL CHARACTERIZATION OF NOVEL NMD-CAUSATIVE GENES

With a combined prevalence of about one in 1500, neuromuscular disorders (NMDs), as a whole, are among the most common inherited neurological diseases in humans and represent not only a significant cause of chronic neurological disability but also a social and economic burden for the patients, families and health care providers. Despite the fact that the genetic basis of some NMDs –perhaps the most prevalent ones-, is partly known; 50% of the patients with a suspected NMD will not receive an accurate genetic diagnosis. A better understanding of the underlying molecular mechanisms of NMDs is of utmost importance to uncover novel disease determinants and, hopefully, novel targets to develop disease therapies and preventive strategies.

This study aims at the identification and characterization of novel gene mutations causing NMDs in order to elucidate the molecular consequences of the altered gene products as well as the mechanisms by which the candidate genes contribute to disease pathogenesis. For this purpose the following objectives were developed:

- I. Implementation of state-of-the-art gene identification and sequencing strategies to identify potential disease-causative genes.
- II. Functional characterization of the identified disease-candidate mutations and their effect on protein function *in vitro*, using relevant cellular models and through both biochemistry and fluorescence microscopy approaches.
- III. Confirmation of the pathogenicity of the novel identified mutations *in vivo* in an animal model that permits the quantification of suitable phenotype readouts via downregulation and/or overexpression of the candidate genes. This thesis will capitalize on the advantages of zebrafish for the modeling of neuromuscular disorders.

PART II. CHP1 REDUCTION AMELIORATES MOTOR NEURON DEGENERATION IN A ZEBRAFISH MODEL OF SMA

Functional absence of *SMN1* causes one of the most devastating neurodegenerative disorders afflicting humans, SMA. The paralog gene *SMN2* is considered the main SMA modifier and the main target for SMA therapy. Nevertheless, elevation of SMN levels via *SMN2* manipulation seems to be insufficient to counteract the severe systemic SMA

phenotype. In rare instances, individuals harboring *SMN1* mutations are completely asymptomatic. Underlying this protection are PLS3 and NCALD, two genetic modifiers validated across numerous SMA animal models. The discovery of these modifiers by our group have unraveled endocytosis as a crucial process impaired in SMA, thus revealing a potential therapeutic target independent of SMN.

Since the precise mechanism by which PLS3 modulates the SMA phenotype is not yet fully understood, the PLS3 interactome has been explored in order to pinpoint novel interacting partners and novel potential SMA modifiers. CHP1 was identified as the only yeast-two-hybrid PLS3 interacting partner and therefore, further analyzed in the context of SMA. Preliminary results from our group demonstrate that CHP1 downregulation restores impaired endocytosis and axonal outgrowth of *Smn1*-depleted NSC-34 cells.

The second part of this thesis, aims at the validation of CHP1 as a potential SMA protective modifier *in vivo*. In order to do so, the effect of Chp1 depletion on MN development –the most affected cells in SMA- will be tested in a disease-relevant model. A well-characterized zebrafish model of SMA, already established in our group, will be used for this purpose.

4. RESULTS

The data presented in this section has been either accepted for publication in the Neurology Genetics Journal of the American Academy of Neurology (Mendoza-Ferreira et al, 2018) and/or presented in several scientific meetings (see section 9. Publications and Abstracts).

PART I. IDENTIFICATION AND FUNCTIONAL CHARACTERIZATION OF NOVEL NMD-CAUSATIVE GENES

Working under the umbrella of the NeurOmics consortium (<http://rd-neuromics.eu>) and through the establishment of research partnerships with numerous European universities and research institutes, our group gained access to sizable ARCA and NMD patient cohorts, which was pivotal for the uncovering of the disease-causative candidate genes studied within the scope of this PhD project. In this chapter, focus is placed on the identification and characterization studies that led to the uncovering of *CHP1* as a novel causative gene of ARCA. Subsequently, the functional studies of *SLC18A3*; a candidate gene of distal hereditary motor neuropathy will be developed in detail as well.

4.1. Calcineurin Homologous Protein-1 (CHP1) is a novel causative gene of autosomal recessive cerebellar ataxia

The starting point of this project was a consanguineous marriage of Moroccan origin with two, out of six, siblings presenting a complex and undiagnosed neuropathy with upper and lower motor neuron involvement and moderate cerebellar atrophy, intellectual disability, slow ocular saccades and ovarian failure in the female proband. A combinatorial strategy of next-generation sequencing (NGS) and linkage analysis was undertaken in an effort to ascertain the genetic defect underlying the complex neuropathy of the affected probands. The family pedigree is presented in (Figure 8).

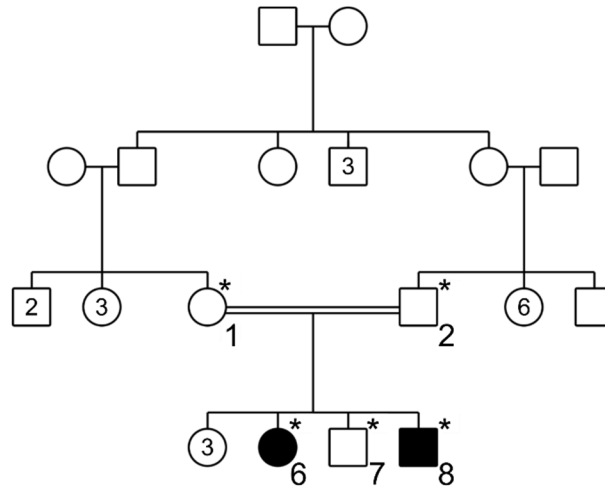


Figure 8. Kindred structure of the index family. Parents are consanguineous (1 and 2). Two out of six siblings are affected (6 and 8). DNA was obtained from individuals marked with an asterisk.

4.1.1. Detailed clinical features of the index family

Patients and relatives from the index family were recruited as part of the Spastic Paraplegia and Ataxia (SPATAX) network cohort by our NeurOmics collaborators: Drs. Alexandra Durr and Alexis Brice, affiliated to INSERM (Institut du Cerveau et de la Moelle épinière) and APHP (Hôpital de la Pitié-Salpêtrière, Neurogenetic reference center) in Paris, France.

More precisely, the female proband presented with severe growth retardation (-4SD) at age 10, exhibiting a bone age of 6 years. At age 14, primary ovarian failure, presumably of hypogonadism origin, was diagnosed. Immunological causes and Turner syndrome were excluded. She also had intellectual difficulties and was not able to read and write despite adapted schooling. Gait instability existed since she started walking at 12 months of age, but she came to medical attention for growth retardation only at age 10. Neurological examination at age 26 revealed spastic ataxia, with unsupported gait. Axial hypotonus and ligamentous laxity were also observed. Pyramidal syndrome was diffuse, with increased reflexes in all four limbs, bilateral extensor plantar reflex and positive Hoffman's reflex. Distal weakness was evident and associated with distal wasting. Vibration and pain sensation were unremarkable. She had surgical correction of pes cavus at age 20 and hammer toes were noticeable. Cerebellar unsteadiness and irregular finger-nose and knee-heel maneuvers were also recognized, but no cerebellar dysarthria. Ocular motility revealed slow saccades and latencies, with limited upward and horizontal gaze. Ophthalmological examination showed normal fundus but decreased visual acuity. Hearing ability and sense of smell were normal. Echocardiography was normal as well as brain MRI.

The male proband (younger brother) presented with progressive gait difficulties including frequent falls at age 5. He showed moderate intellectual disability and a mild growth deficit at age 10, less severe than his sister (-2SD). Neurological examination at age 20 showed spastic paraparesis with cerebellar hypotonia. Increased reflexes, bilateral extensor plantar reflexes and unilaterally positive Hoffman's reflex were present. Vibrating sensation at the ankles was decreased and distal wasting with moderate weakness in feet and hands were also registered. Pes cavus with hammer toes were diagnosed. Electromyography and nerve conduction studies revealed pure motor neuropathy. Ocular movements were slow, and gaze was limited upwards and horizontal with diplopia. The brain MRI showed isolated atrophy of the cerebellar vermis (Figure 9). The clinical features of the affected probands are summarized in (Table 6).

Table 6. Clinical features and neurophysiological findings of the affected probands

	♀ Patient 6	♂ Patient 8
Age at examination	26 years	20 years
Age of onset	12 months	5 years
Growth retardation	-4 SD	-2 SD
Pyramidal signs (Motor Neuron)		
Spastic paraplegia (gait difficulties)	+	+
Increased deep tendon reflexes	+	+
Distal muscle atrophy and weakness	+	+
Cerebellar signs		
Gait instability	+	+
Ocular dysmetria	+	+
Motor dysmetria	+	Not available
Hypotonia	Not available	+
Others		
Pes cavus, hammer toes	+	+
Sensory involvement	-	+
Mild intellectual disability	+	+
Hypergonadotropic hypogonadism	+	Not available
Brain MRI	Normal	Cerebellar vermis atrophy

(+) and (-) symbols denote presence and absence, respectively. SD indicates standard deviation.

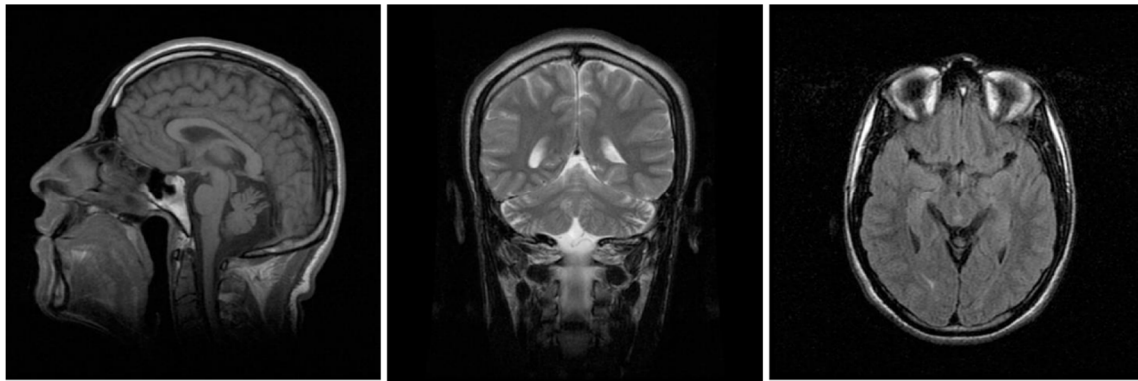


Figure 9. Brain MRI of male proband at 22 years of age. Sagittal (left panel), coronal (middle panel) and axial (right panel) sections of T1-weighted images are shown. Hypoplasia of the posterior and nodular regions of the cerebellar vermis, but not of the hemispheres, are evident. Axial FLAIR section shows no evident abnormalities of the white matter.

4.1.2. Linkage analysis and WES in the index family

Linkage studies and WES were performed in collaboration with Drs. Giovanni Stevanin and Marie Coutelier, affiliated to INSERM (*Institut du Cerveau et de la Moelle épinière*). Paris, France.

4.1.2.1. Whole genome linkage analysis (WGLA)

To localize ARCA-associated genes, WGLA was performed in five individuals of the index family, including the affected subjects, one unaffected sibling and the unaffected parents (6, 8 and relatives 1, 2 and 7 in pedigree, see Figure 11A) using the Illumina Infinium HumanLinkage-12 Genotyping BeadChip (6090SNP). Due to pedigree structure and size limitations, linkage mapping did not lead to identification of a unique, well-defined-associated locus. Instead, multiple putatively linked or unexcluded loci, with LOD scores above -2 were found in the family (Figure 10A).

The largest linkage region, with multipoint LOD scores reaching the maximal expected values (+1.917), was located on chromosome 15 and flanked by SNP markers rs2732029 (LODscore 1.546, hg18 coordinate 22786809) and rs8027424 (LODscore 1.379, hg18 coordinate 58990929) (Figure 10B). Autosomal recessive transmission under a 0.90 penetrance model, similar recombination fractions between males and females and a disease allele frequency of 0.00001 were assumed.

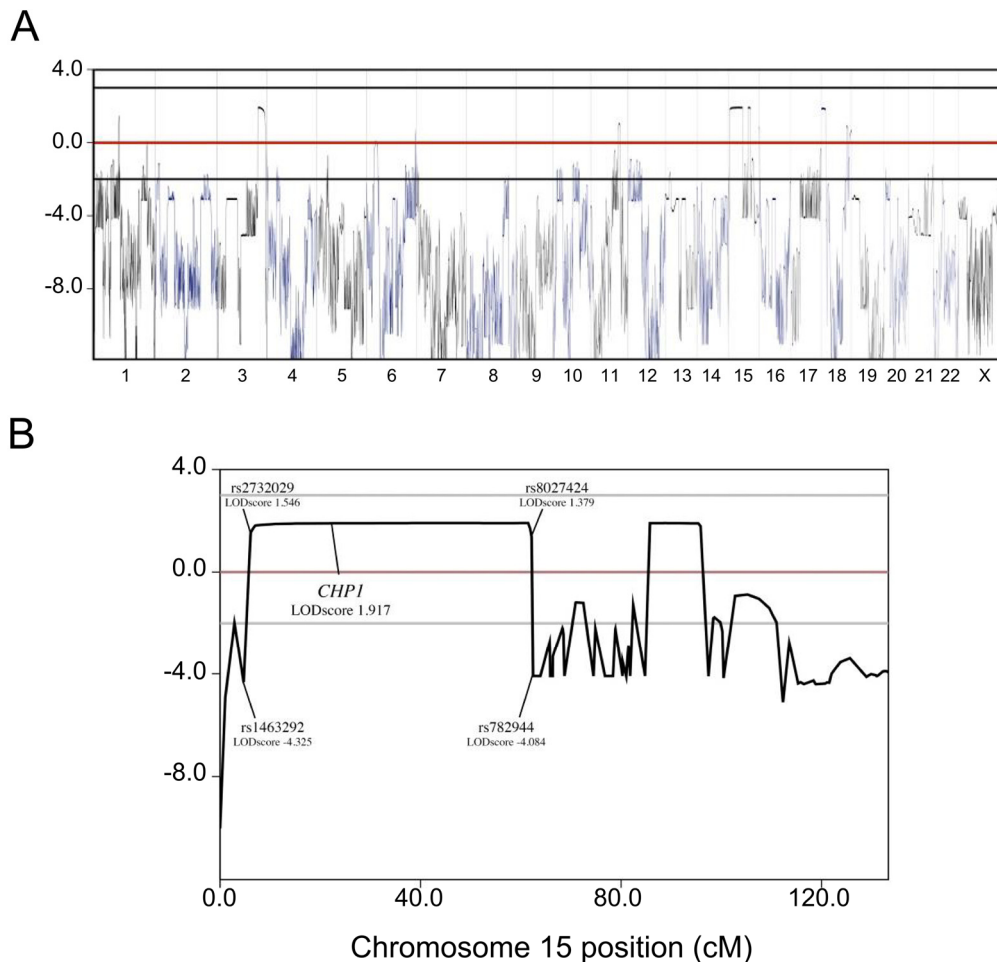


Figure 10. Multipoint linkage analysis. (A) Genotypes of the affected subjects, one unaffected sibling and the parents (see pedigree in Figure 11A) were available. Similar recombination fractions between males and females, a disease frequency of 0.00001 and an autosomal recessive transmission under 0.90 penetrance model with equal allele frequencies were assumed. Due to pedigree structure and size limitations, WGLA did not lead to the identification of a unique well-defined associated locus, instead various putatively linked or unexcluded (LOD scores above -2) loci were found in the family. **(B)** WGLA detail in chromosome 15 region. LODscores and coordinates for linked regions are depicted (rs2732029 – rs8027424).

4.1.2.2. WES identifies *CHP1* as the causative gene of autosomal recessive cerebellar ataxia

After exclusion of mutations in conventional ARCA genes, WES of individuals 1, 2, 6 and 8 was performed (Figure 11A and B), obtaining an average of 84.556.652 sequence reads per sample, of which more than 98.5% could be aligned to the reference sequence. Mean coverage was 77-fold, with 78.9% of targeted sequence covered more than 20x. Variants were analyzed according to the following conventional criteria:

- I. The homozygous state in the affected individuals, heterozygous in both parents and either heterozygous or homozygous wild-type in the unaffected sibling (because of consanguinity).

- II. A frequency inferior to 0.1% in public databases (dbSNP137, NHLBI Exome Sequencing Project Exome Variant Server [EVS], and the Exome Aggregation Consortium [ExAC] Browser).
- III. The effect on the coding sequence of an annotated protein-coding gene.
- IV. The location within genomic regions not excluded by linkage analysis (multipoint LOD score >-2).

Twelve variants fulfilled the established criteria (Table 7). Further strict filtering based on alternate allele homozygosity status (GnomAD) and weak effect prediction (at least four out of five different scores) excluded five variants. Out of these, a biallelic 3-bp deletion (NM_007236.4:c.54_56del:p.Lys19del) in the Calcineurin Homologous Protein-1 gene (*CHP1*), hereafter defined as K19del, was further selected as a top disease candidate since:

- I. It is located in the largest non-excluded region on chromosome 15, where the maximum LOD score was reached.
- II. It is absent from all public databases.
- III. The mutation affects a residue highly conserved across species and one of the most conserved amino acids among the identified variants (see conservation scores GERP++_RS and phyloP100way in (Table 7).
- IV. A point mutation in murine *Chp1* causing aberrant splicing and reduced full-length transcripts, leads to Purkinje cells degeneration and ataxia (Liu et al, 2013).
- V. *CHP1* assists the posttranscriptional glycosylation and membrane localization of NHE1; a major Na^+/H^+ exchanger listed in the ataxia-ome (Lim et al, 2006).
- VI. KO of murine *Nhe1* also cause ataxia (Bell et al, 1999; Cox et al, 1997).
- VII. Loss-of-function mutation in *NHE1* cause ataxia-deafness Lichtenstein-Knorr syndrome (LINKS) (Guissart et al, 2015).

The remaining exome variants were located within genes functionally unrelated to cerebellar or motor neuron pathogenesis, not expressed in Purkinje or motor neurons and/or absent in other vertebrate species (Table 7). Segregation of the *CHP1* c.54_56 deletion in the index family was validated by standard PCR and Sanger sequencing (Figure 11B). ClustalW2 alignment of *CHP1* protein sequences from various organisms demonstrates a high conservation degree of the mutated residue and, in general, among orthologues (Figure 11C).

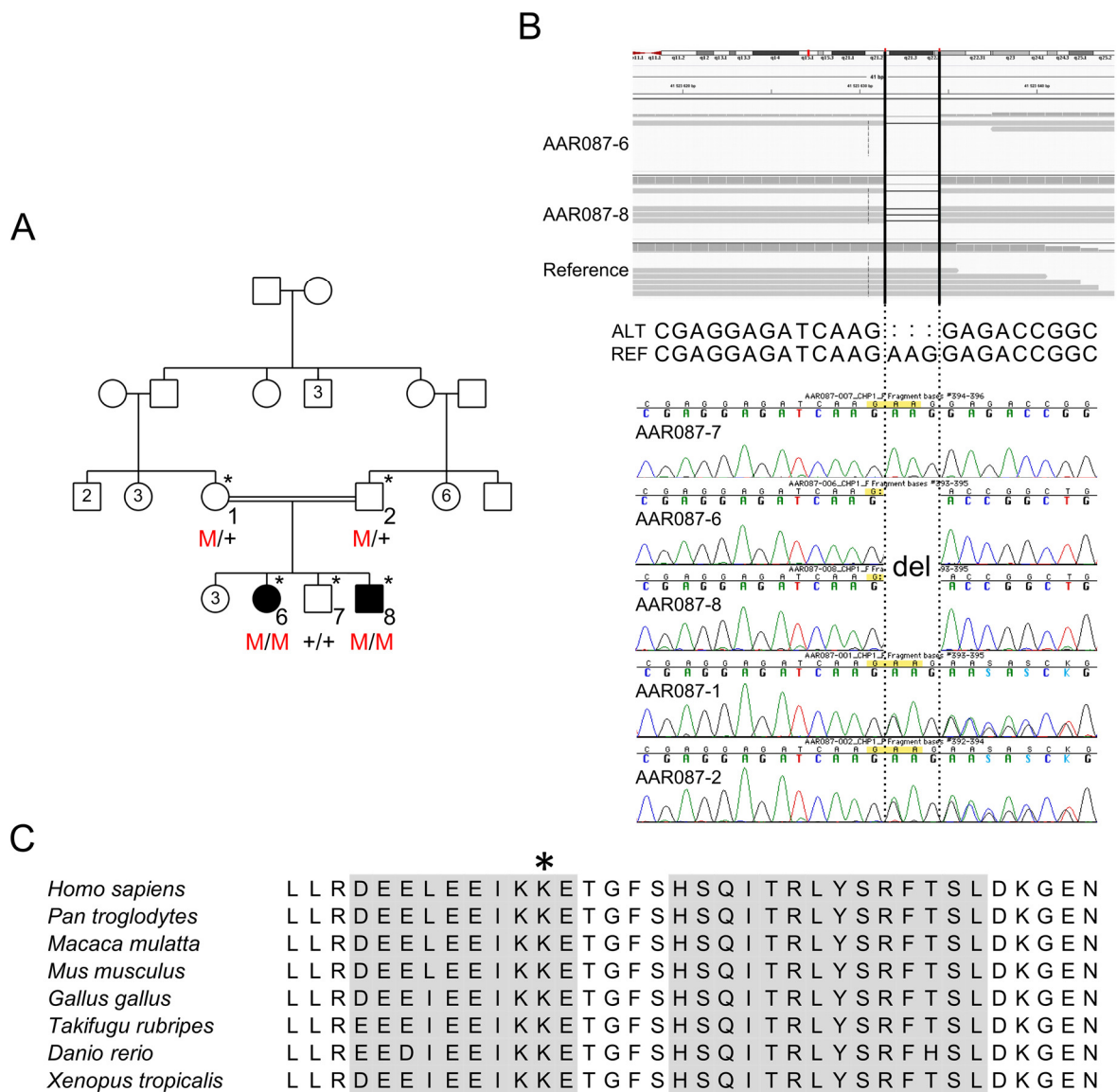


Figure 11. Pedigree of the index family and Sanger confirmation of the CHP1 p.K19del mutation in affected probands. (A) Pedigree of the family showing the segregation of the CHP1 p.K19del mutation (red M; + denotes the reference allele). (B) CHP1 NGS sequencing reads show the homozygous NM_007236:c.54_56del: p.K19del variant for individuals AAR087-6 and AAR087-8. Sanger sequencing chromatograms show homozygosity for the 3-bp deletion in both patients (AAR087-6 and 8) and heterozygosity in both parents (AAR087-1 and 2); the unaffected sibling (AAR087-7) matches homozygous reference sequence. NGS was performed on individuals marked with * in pedigree. (C) Protein sequence alignment of CHP1 orthologues shows high conservation in the region including the K19del mutation (marked with asterisk). Grey color indicates α -helical protein structure.

Table 7. Characteristics of variants segregating in index family

Mutation Characteristics												Mutation effect prediction					Conservation	
Chr	Start	End	Ref	Alt	Gene	Aminoacid change in longest transcript	1000 Genomes Frequency	ExAC Frequency	ESP6500 Frequency	dbSNP ID	Gnom AD	Sift Score	Polyphen 2 HDIV Score	Polyphen 2 HVAR Score	LRT score	Mutation Taster score	GERP ++_RS	phyloP 100way
3	184009964	184009964	C	T	ECE2 *	NM_014693:c.C2590 T:p.R864W	0.0002	0.0001	.	rs201775833	1	0 (D)	0.998 (D)	0.764 (P)	N	N (0.994)	2.62	0.144
3	193032845	193032848	GAG	-	ATP13A5	NM_198505:c.2071_2073 del:p.691_691del	.	0.0002	0.0001	5.56	7.651
11	119045378	119045378	C	T	NLRX1	NM_001282144:c.C1066T:p.R356W	0.0004	0.0003	0.0003	rs142087333	0	0.07 (T)	0.999 (D)	0.96 (D)	N	D (0.994)	4.2	4.737
15	40764353	40764353	G	A	CHST14 **	NM_130468:c.G941A p.R314Q	0.0002	8.24E-06	.	rs556002453	0	0.31 (T)	0.004 (B)	0.006 (B)	N	N (0.939)	1.84	0.769
15	41523634	41523637	AAG	-	CHP1	NM_007236:c.54_56 del:p.19_19del	5.79	6.329
15	42652235	42652235	C	A	CAPN3	NM_000070:c.C232A p.P78T	0.0004	0.0004	0.0004	rs138867099	0	0.01 (D)	0.614 (P)	0.524 (P)	U	D (1)	5.98	5.043
15	44127266	44127266	C	T	WDR76	NM_024908:c.C470T p.S157L	.	0.0001	0.0004	rs139119504	0	0.05 (D)	0.968 (D)	0.192 (B)	N	N (0.841)	2.73	2.702
15	45412435	45412435	G	A	DUOXA1 *	NM_144565:c.C638T p.T213M	0.0036	0.0039	0.0024	rs149960164	11	0 (D)	1 (D)	0.995 (D)	D	D (1)	5.12	6.445
15	57999082	57999082	G	C	POLR2M	NM_015532:c.G42C:p.E14D	0.0006	0.0015	0.0015	rs150413697	0	0.39 (T)	0.998 (D)	0.941 (D)	.	N (1)	3.84	3.204
15	83933230	83933230	C	T	BNC1	NM_001717:c.G773 A:p.G258E	0.004	0.0008	0.0023	rs116464429	2	0.01 (D)	1 (D)	0.986 (D)	D	D (1)	5.75	5.842
15	86312927	86312927	G	A	KLHL25 **	NM_022480:c.C115T p.L39F	0.21 (T)	0.669 (P)	0.512 (P)	N	D (0.992)	3.93	3.297
18	2769780	2769780	C	T	SMCHD1 **	NM_015295:c.C4808 T:p.T1603I	0.004	0.0012	0.0026	rs147034750	2	0.2 (T)	0 (B)	0 (B)	N	N (1)	0.292	-0.226

Annovar (www.openbioinformatics.org/annovar/) was used for variant annotation. Variant frequencies were obtained from 1000 Genomes database (<http://www.1000genomes.org/>), Exome Aggregation Consortium (ExAC, <http://exac.broadinstitute.org/>), Exome Variant Server (EVS, <http://evs.gs.washington.edu/EVS/>), and identifiers were researched in dbSNP (<http://www.ncbi.nlm.nih.gov/SNP/>). Scores of pathogenicity prediction were estimated as follows: SIFT (<http://sift.jcvi.org/>) predicts deleteriousness (D) under 0.05, otherwise the variant is assumed to be tolerated (T); Polyphen2 (<http://genetics.bwh.harvard.edu/pph2/>) classifies SNPs as probably damaging (D; HDIV \geq 0.957, HVAR \geq 0.909), possibly damaging (P; 0.453 \leq HDIV \leq 0.956, 0.447 \leq pp2_hdiv \leq 0.908), or benign (B; HDIV \leq 0.452, HVAR \leq 0.446); LRT differentiates variants with deleterious (D), neutral (N) or unknown (U) effect; MutationTaster (<http://www.mutationtaster.org/>) classifies variants as "disease-causing-automatic" (A), "disease-causing" (D), "polymorphism" (N) or "polymorphism-automatic" (P) with a given probability value, 1 being the most probable. For both GERP++ (<http://mendel.stanford.edu/SidowLab/downloads/gerp/>) and PhyloP (<http://compgen.bscb.cornell.edu/phast/help-pages/phyloP.txt>), higher scores indicate better residue conservation.

* indicates: variant excluded for homozygosity in alternate allele (GnomAD). ** indicates: variant excluded for weak predicted effect (4/5 or 5/5 scores)

4.1.3. Focused screening for *CHP1* variants in two large neurodegenerative disease cohorts

After selection of *CHP1* as the most promising disease candidate, we continuously searched for a second family. In order to do so, we not only improved *CHP1* exon coverage from our first exome data, but also searched for *CHP1* variants in other neuromuscular disease cohorts. WES of 319 Autosomal Recessive Cerebellar Ataxia ARCA index patients (N=319) yielded a *CHP1* average coverage of 44x. Excellent coverage levels were reached upon exons 2 and 6 re-sequencing, with 100% 30x coverage in 99.1% (n=316) and 91.8% (n=293) of the patients respectively, and a mean coverage of 4943x and 305x, respectively (Table 8). No additional *CHP1* variants were detected.

Table 8. Focused screening of *CHP1* mutations in ARCA cohort.

Gene	Exon in transcript NM_007236	Length	Target (hg19)	Average coverage by WES	Average percentage above 10 by WES	Average percentage above 30 by WES	Average coverage by panel	Average percentage above 10 by panel	Average percentage above 30 by panel
<i>CHP1</i>	1	66	chr15:41523582-41523647	58.8	98.2	89.8			
<i>CHP1</i>	2	73	chr15:41535865-41535937	14.6	73.8	6.0	4943	99.5	99.1
<i>CHP1</i>	3	81	chr15:41549108-41549188	74.5	98.0	89.3			
<i>CHP1</i>	4	128	chr15:41554954-41555081	46.0	98.9	75.3			
<i>CHP1</i>	5	62	chr15:41562755-41562816	57.3	99.6	93.3			
<i>CHP1</i>	6	123	chr15:41570965-41571087	25.2	94.2	25.4	305	98.1	94.6
<i>CHP1</i>	7	54	chr15:41571534-41571587	42.2	99.2	81.3			
	All exons			44.0	94.7	62.2			
Total with both methods								98.7	88.3

In a second screening effort, we also searched for *CHP1* variants in a large WES/WGS (whole genome sequencing) cohort (N=657), which includes the data of patients with neuromuscular and neurodegenerative disorders (our own NeurOmics cohort). Moreover, we interrogated GeneMatcher, a freely accessible web service created to enable data sharing between clinicians and researchers from around the world who share an interest in the same gene(s). No further *CHP1* mutations were found.

The ExAC browser (The Exome Aggregation Consortium) integrates exome information of more than 60,000 control individuals, sequenced as part of various disease-specific and population genetics studies in humans, and constitutes an excellent and powerful tool for variant interpretation nowadays. Interestingly, *CHP1* interrogation in ExAC revealed constraint metrics (a given Z score) compatible with reduced gene tolerability for missense mutation (z-score 2.64).

4.1.4. Generation and validation of V5-tagged CHP1-WT and CHP1-K19 constructs for protein expression analyses

To investigate the effect of the K19 deletion in the CHP1 protein, the mutation was introduced by site-directed mutagenesis using the human full-length *CHP1* cDNA as template (NCBI: 11261). *CHP1* cDNA was previously cloned into a pcDNA3.1-CT-GFP expression vector by Eva Janzen, who kindly provided this plasmid for further experiments. CHP1-WT and mutant cDNAs were subcloned into a pcDNA3.1-CT-HisV5-TOPO vector to generate C-terminal V5-tagged CHP1 proteins. All clones were verified by Sanger sequencing, including regions upstream and downstream of the open reading frame. To validate the generated vectors, expression of CHP1-WT-V5 and CHP1-K19del-V5 was analyzed on protein and mRNA level. Transiently transfected HEK293T cells were used to isolate proteins and total mRNA within different time points (24, 48 and 72 hours). An empty-vector was included as negative control. Total protein lysates were analyzed by Western blot (Figure 12A).

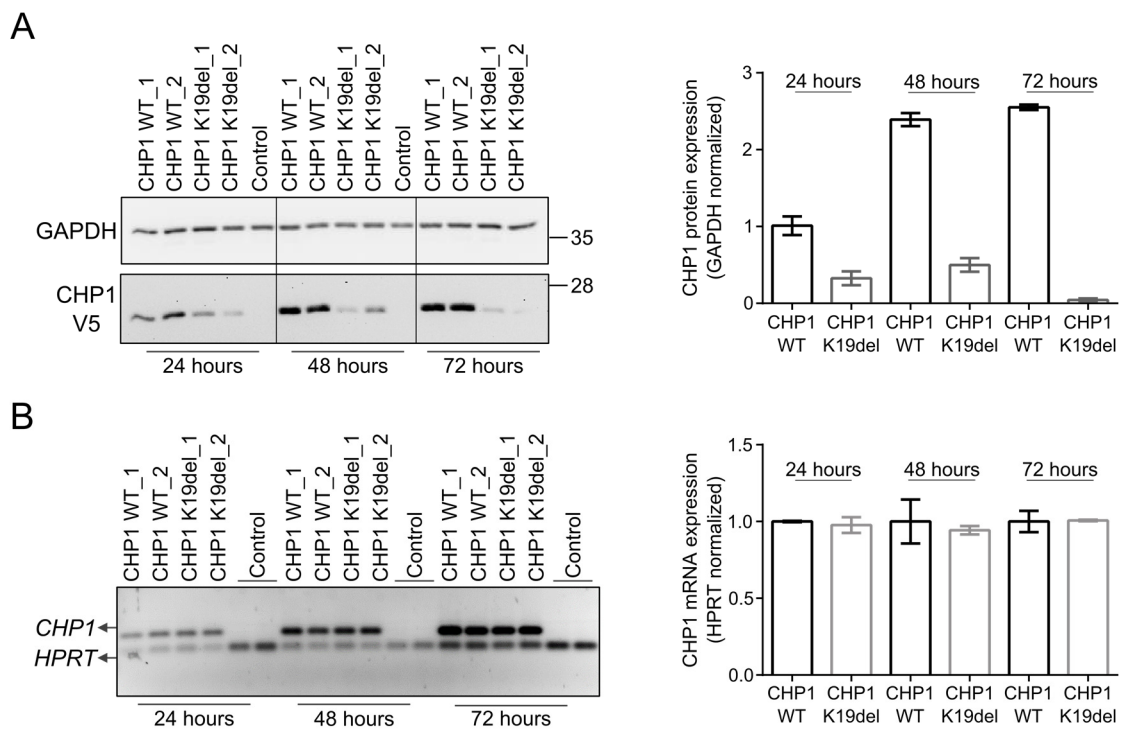


Figure 12. Time-course protein and mRNA expression analyses from HEK293T cells transiently expressing CHP1-WT-V5 and CHP1-K19del-V5. (A) WB of protein lysates of HEK293T transiently expressing CHP1-WT-V5, CHP1-K19del-V5 or control V5-vector (empty) collected 24, 48 and 72h upon transfection. WB membrane was probed with antibodies against V5, to detect CHP1 WT and mutant proteins, and GAPDH as loading control. Expression of CHP1-K19del-V5 is almost undetectable after 72 hours. Graph represents quantification of CHP1 relative expression over different time points. Bars show the mean \pm SEM. **(B)** Determination of *CHP1-WT-V5* and *K19del-V5* transcripts by semi-quantitative RT-PCR. Graph represents quantification of *CHP1-V5* transcripts normalized to *HPRT* expression. Bars show the mean \pm SEM. No differences were observed between WT and *CHP1-K19del* transcripts.

In agreement with the molecular weight expected for the active monomeric form of CHP1 (Naoe et al, 2005; Timm et al, 1999); a unique band of ~25KDa was detected for both CHP1-WT and CHP1-K19del using an anti-V5 antibody. No immunoreactivity was detected in protein lysates from the transfection control. Moreover, time-course expression analysis revealed dramatic reduction in CHP1-K19del-V5, whereas CHP1-WT-V5 exhibited higher and increasing protein levels over 72 hours of OE (Figure 12A). To exclude a transcriptional impairment of the mutant CHP1 construct, semi-quantitative RT-PCR was carried out to specifically detect *CHP1* transcripts in total mRNA. No evident difference was observed between *WT* and mutant *CHP1* transcripts, therefore a transcriptional impairment, potentially explaining CHP1-K19del-V5 reduced levels, was ruled out (Figure 12B). As 48h transfection showed optimal/maximal CHP1-K19del expression, further transfections for protein analyses were performed accordingly. Triplicate sample processing for statistical analyses were performed only for this time-point (Figure 13).

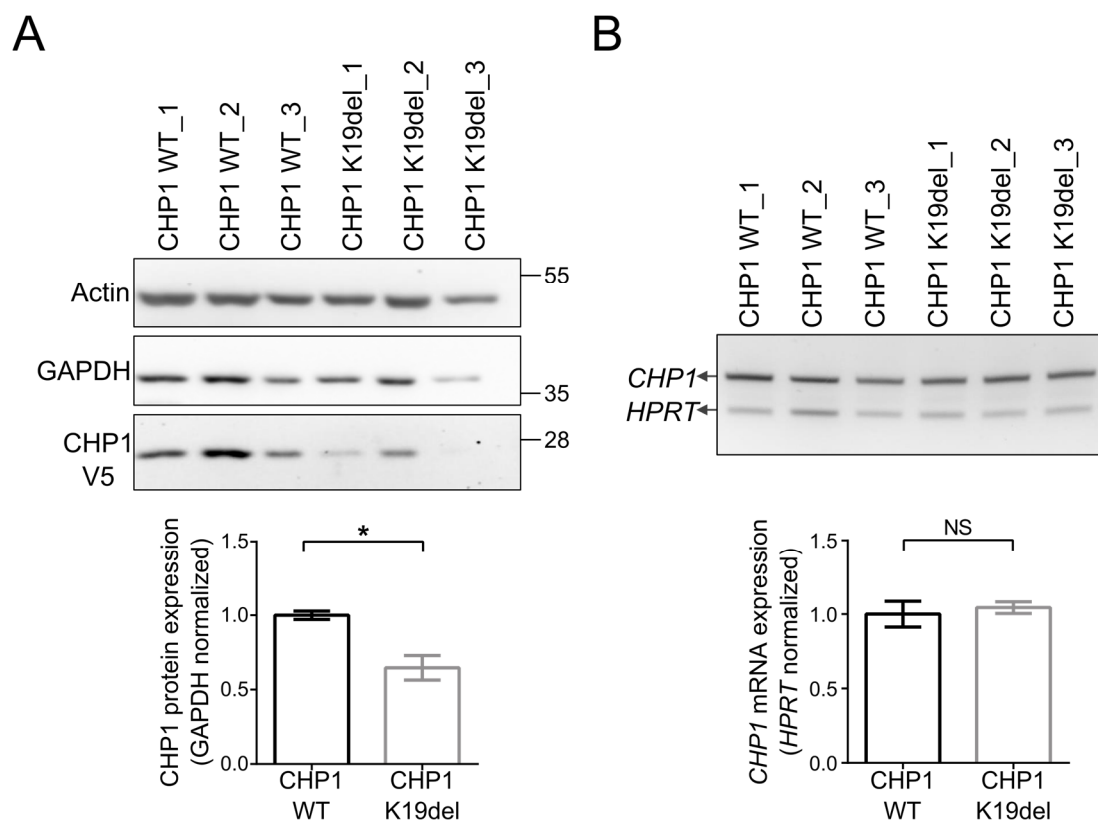


Figure 13. Time-course protein and mRNA expression analyses after 48h transfection. (A) WB from protein lysates of HEK293T transiently expressing CHP1-WT-V5, CHP1-K19del-V5 or control V5-vector collected after 48h transfection. WB membrane was probed with antibodies against V5, to detect CHP1 WT and mutant proteins, and GAPDH as loading control. Graph represents quantification of CHP1 relative expression. Bars show the mean \pm SEM. * denotes statistical significance ($p \leq 0.05$ two-tailed Student's t-test) between CHP1-WT and CHP1-K19del expression. **(B)** Determination of *CHP1-WT-V5* and *K19del-V5* transcripts by semi-quantitative RT-PCR. RNA samples were collected after 48h transfection. Graph represents quantification of *CHP1-V5* transcripts normalized to *HPRT* expression. Bars show the mean \pm SEM. NS denotes no significant difference ($p > 0.05$ two-tailed Student's t-test) between *CHP1-WT* and *CHP1-K19del* transcripts.

4.1.5. The K19del mutation alters CHP1 expression and solubility

The validation of CHP1 vectors expression revealed that mutant CHP1 dramatically affects total protein amount. This fact not only pointed towards the hypomorphic condition of the CHP1-K19del mutation but also uncovered a potential underlying pathogenic mechanism. Therefore, further experiments aimed to confirm the effect of the K19del mutation on CHP1 expression were undertaken. The expression of CHP1-WT-V5 and CHP1-K19del-V5 in soluble and insoluble fractions was assessed via protein fractionation and Western blot. Cell lysates from transiently transfected HEK293T cells were separated into soluble (cytoplasmic) and insoluble (cytoskeletal) fractions and relative enrichment of HSP90 and Vimentin were used to assess both efficiency and specificity of each subcellular fraction, respectively. In congruence with CHP1 functional roles and known cellular localization (Matsushita et al, 2011; Timm et al, 1999) protein expression was detected in both fractions. CHP1-K19del-V5 was reduced by at least 60% in the soluble fraction whereas it increased in the insoluble fraction by ~65% (Figure 14). Since the functional monomeric form of CHP1 is predominantly cytosolic (Naoe et al, 2005), reduction of soluble CHP1-K19del indicates that active CHP1 is depleted.

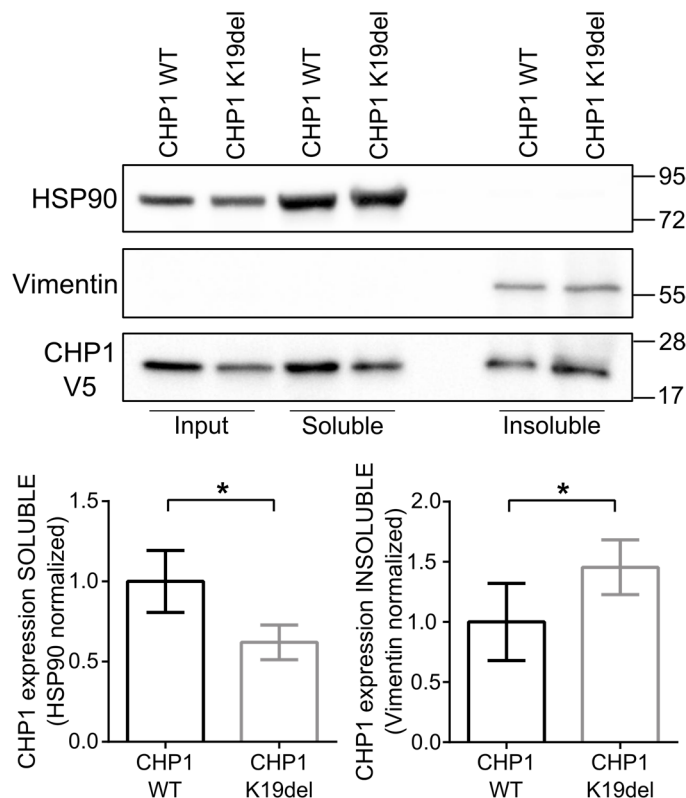


Figure 14. The K19del mutation affects the expression and solubility of CHP1 in HEK293T cells. (See figure legend on the next page)

Figure 14. Subcellular fractionation of protein lysates from HEK293T transiently overexpressing CHP1-WT-V5 or CHP1-K19del-V5. Total protein lysates were purified after 48h transfection and separated into soluble (cytoplasmic) and insoluble (cytoskeletal) fractions by differential lysis and centrifugation. Representative WB from total lysates (input) and fractions were probed with V5 antibodies to detect CHP1 WT and mutant proteins. HSP90 and Vimentin were used as enrichment markers for soluble and insoluble fractions, respectively. Graphs represents quantification of relative expression of CHP1 in the soluble and insoluble fractions. Bars show the mean \pm SEM from 3 independent blots, carried out and processed in parallel. * denotes statistical significance ($p \leq 0.05$ two-tailed Student's t-test) between WT-CHP1 and K19del-CHP1 expression.

To corroborate that reduced CHP1-K19del-V5 expression also takes place in a cellular model relevant for the pathogenesis of ARCA; the neuroblastoma cell line Neuro2A (N2A) was used for transfection and transient OE of CHP1 constructs (see also section 4.1.7.1). Likewise, expression of CHP1-WT-V5 and CHP1-K19del-V5 in soluble and insoluble N2A cellular fractions was assessed by protein fractionation and Western blot, yielding very similar results (Figure 15).

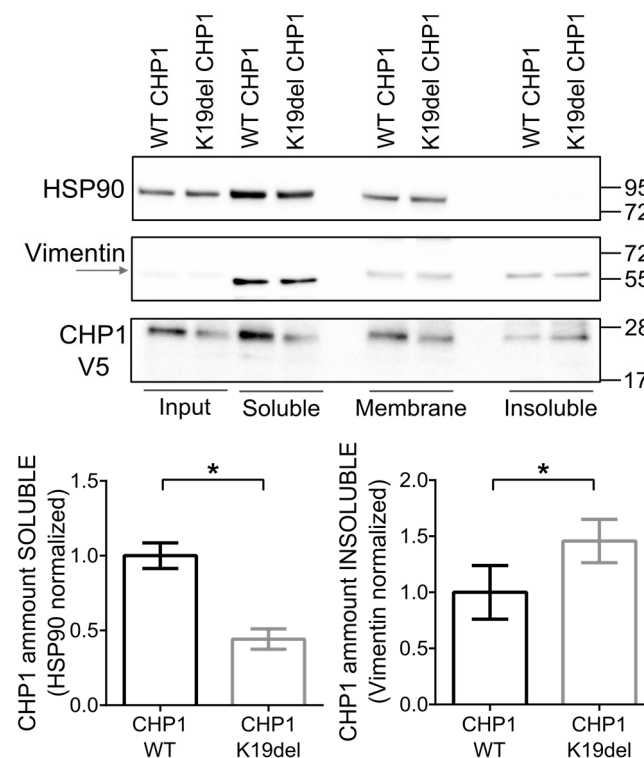


Figure 15. The K19del mutation affects the expression and solubility of CHP1 in N2A cells. Subcellular fractionation of protein lysates from N2A transiently overexpressing CHP1-WT-V5 or CHP1-K19del-V5. Total protein lysates were separated into soluble (cytoplasmic) and insoluble (cytoskeletal) fractions by differential lysis and centrifugation. Representative WB from total lysates (input) and fractions probed with V5 antibodies for WT and mutant CHP1 detection. HSP90 and vimentin were used as enrichment markers for soluble and insoluble fractions, respectively. Membrane probing with anti-Vimentin revealed an unspecific band only in the cytoplasmic fraction. Arrow indicates the specific vimentin band (upper and faint). Graphs represents quantification of CHP1 relative expression in soluble and insoluble fractions. Bars show the mean \pm SEM from 3 independent blots, carried out and processed in parallel. * denotes statistical significance ($p \leq 0.05$ two-tailed Student's t-test) between CHP1-WT and CHP1-K19del expression.

Altogether, these findings hint towards defects in protein localization, folding or stability of the CHP1 mutant form which, alone or in combination, might explain the reduced levels of the soluble form of the protein.

4.1.6. CHP1-K19del adopts larger protein conformations

To analyze the consequence of CHP1-K19del mutation on protein folding and protein-complexes formation, size exclusion chromatography experiments were performed. Total protein lysates from HEK293T cells expressing CHP1-WT-V5 and CHP1-K19del-V5 were fractionated by a Size Exclusion Chromatography (SEC) assay, which was calibrated by elution of purified proteins standards of known molecular masses (aldolase, aprotinin, carbonic anhydrase, canalbumin, ferritin, ovalbumin and ribonuclease). Elution chromatograms of CHP1 protein lysates exhibited similar separation and column loading (not shown). A total of 80 fractions were collected (40 for each CHP1 protein) and resolved by SDS-page, using acrylamide gels of 24 wells. The elution profiles of WT and mutant CHP1 were determined by anti-V5 immunoblotting (Figure 16) and the molecular weight of CHP1 fractions was estimated from the SEC calibration curve (logarithmic representation of MW against fraction coefficients of protein standards).

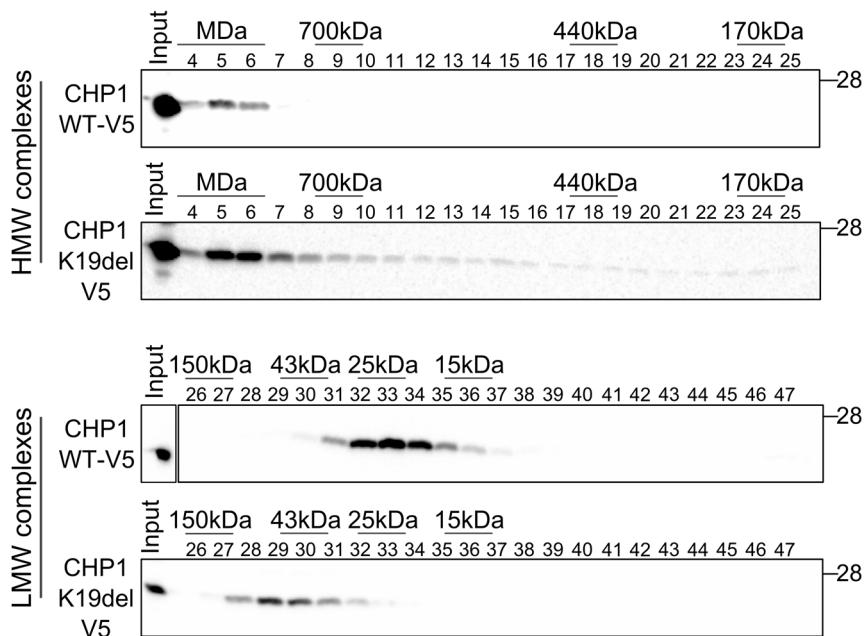


Figure 16. K19del mutation alters CHP1 protein conformations and folding. (A) SEC of total protein lysates from HEK293T cells expressing CHP1-WT-V5 and CHP1-K19del-V5. 21 fractions in the HMW range and 21 in the LMW range, were analyzed by WB. Blots were probed with anti V5 antibodies to detect CHP1-V5-tagged proteins. Elution differences between WT and mutant CHP1 in HMW fractions (7-25) are markedly visible. CHP1-K19del-V5 elution in LMW fractions shifted to higher MW (29-30), away from the most abundant monomeric range (32-34). Depicted molecular weights were calculated upon calibration and standard curve representation (not shown).

The peak elution for CHP1-WT-V5 in the low molecular weight complexes (LMW) was in fractions 32-34, consistent with the active monomeric form of CHP1 (~25KDa) (Naoe et al, 2005; Timm et al, 1999). Furthermore, CHP1-WT reactivity was also detected in fractions 4-6, indicating that CHP1-WT forms high molecular weight (HMW) complexes (~1MDa) in HEK293T cells (Figure 16). In contrast, the elution profile of CHP1-K19del-V5 in the LMW shifted away from the monomeric range (towards fractions 29-30). More strikingly, in the HMW complexes, CHP1-K19del-V5 reactivity was detected in almost all the analyzed fractions. The latter indicates that mutant CHP1, in contrast to the WT protein, adopts larger structural conformations.

Complementarily, SEC-V5-positive fractions were resolved in standard SDS-page gels for detailed analysis of CHP1 and its interacting partners. Firstly, immunoblotting of PLS3 and GAPDH, two known CHP1 interactors ((Andrade et al, 2004a) and Janzen, Mendoza-Ferreira et al, manuscript in preparation) only showed reactivity in the LMW fractions and did not display any difference between WT and mutant CHP1 elution patterns (Figure 17), suggesting that the formation of protein complexes among these proteins is unaltered. In contrast, the analysis of HMW complexes remarkably revealed different elution patterns of NHE1, one of CHP1's most studied interacting partners (Naoe et al, 2005; Pang et al, 2004). Indeed, upon CHP1-K19del-V5 expression, NHE1 reactivity was observed in more than one HMW fraction, contrasting with the CHP1-WT situation, where only one NHE1 band was detected (Figure 17). These results demonstrate that high molecular forms of mutant CHP1 affect the association of endogenous NHE1 into functional protein complexes.

Altogether, SEC analyses strongly indicate that mutant CHP1 adopt abnormal folding patterns and forms protein complexes of high molecular size. Regarding the latter, it is plausible to conjecture that reduced mutant CHP1 solubility underlies these large structural defects.

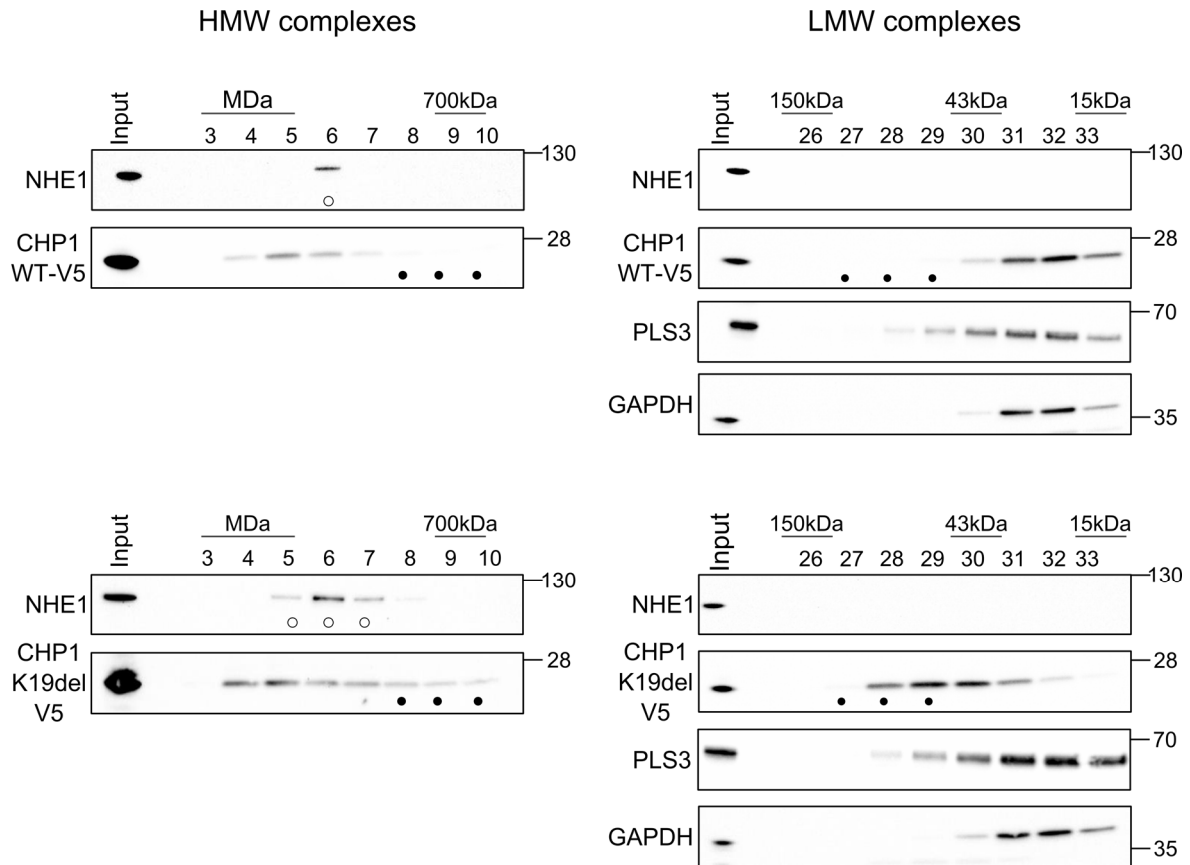


Figure 17. The K19del mutation alters NHE1 elution in HMW complexes. (A) Representative SEC fractions from High Molecular Weight (HMW) and Low Molecular Weight (LMW) complexes were analyzed by WB. Depicted molecular weights were calculated upon calibration and standard curve representation (not shown). Blots were probed with antibodies against V5 to detect CHP1-V5-tagged proteins, NHE1, GAPDH and PLS3. Open circles denote differential NHE1 elution and bold circles denote CHP1 differential elution between WT and K19del protein lysates.

4.1.7. Mutant CHP1 is prone to aggregation

The propensity of a protein to aggregate is governed by its conformational stability and proper folded state. Therefore, misfolded proteins are more prone to accumulate and aggregate with each other. Aberrant protein accumulation not only limits the availability of soluble protein but leads to functionally inactive conformations, which is later translated into hypo- or loss-of-function (Chiti & Dobson, 2006; Hipp et al, 2014). To further strengthen the results obtained from SEC and fractionation experiments and to assess possible aggregation events underlying mutant CHP1 expression, protein subcellular localization analyses were undertaken.

4.1.7.1. Optimization of Neuro2A culture and differentiation

Expression plasmids encoding CHP1-WT-GFP and CHP1-K19del-GFP were transiently transfected in various cell lines in order to visualize the exogenous expressed proteins by immunofluorescence microscopy. Three cell lines were selected for transfection and protein localization analysis, namely: Human cervical carcinoma (HeLa) and the neuron-like cell lines murine pheochromocytoma PC12, and murine neuroblastoma Neuro2A (N2A) (see 6.1.7.1)

Because of their ability to differentiate into neurons within a few days, N2A and PC12 cells have been extensively used to understand neuronal function and signaling pathways (LePage et al, 2005; Schlachetzki et al, 2013; Shafer & Atchison, 1991). In this project, both cell lines were utilized to assess CHP1 subcellular distribution. Since the in-culture growth of N2A cells is faster than other neuron-like cells (Kim et al, 2013) and the transfection/differentiation efficiency was considerably higher than in PC12 cells; CHP1 expression and colocalization analyses were undertaken exclusively in N2A cells. In addition to the latter, N2A cells were considered more relevant for this study as they are an excellent and validated system for the study of neuronal disorders underlying motor neuron degeneration, such ALS and SMA (Hornburg et al, 2014) or cerebellar degeneration, as observed in SCAs, paraneoplastic cerebellar degeneration (PCD) and transmissible spongiform encephalopathy (prion disease) (Okano et al, 1999; Qin et al, 2006; Venkatraman et al, 2014).

Transient N2A transfection was performed following standard procedures (described in 6.2.5.4), however, as no consensus N2A differentiation protocol was found in the literature, different concentrations of Retinoic Acid (RA), alone or in combination with variable FCS amounts were used in order to select the best differentiation and starvation conditions. A final combination of 20 μ M and 2% FCS was selected to induce N2A differentiation over 72 hours (Figure 18).

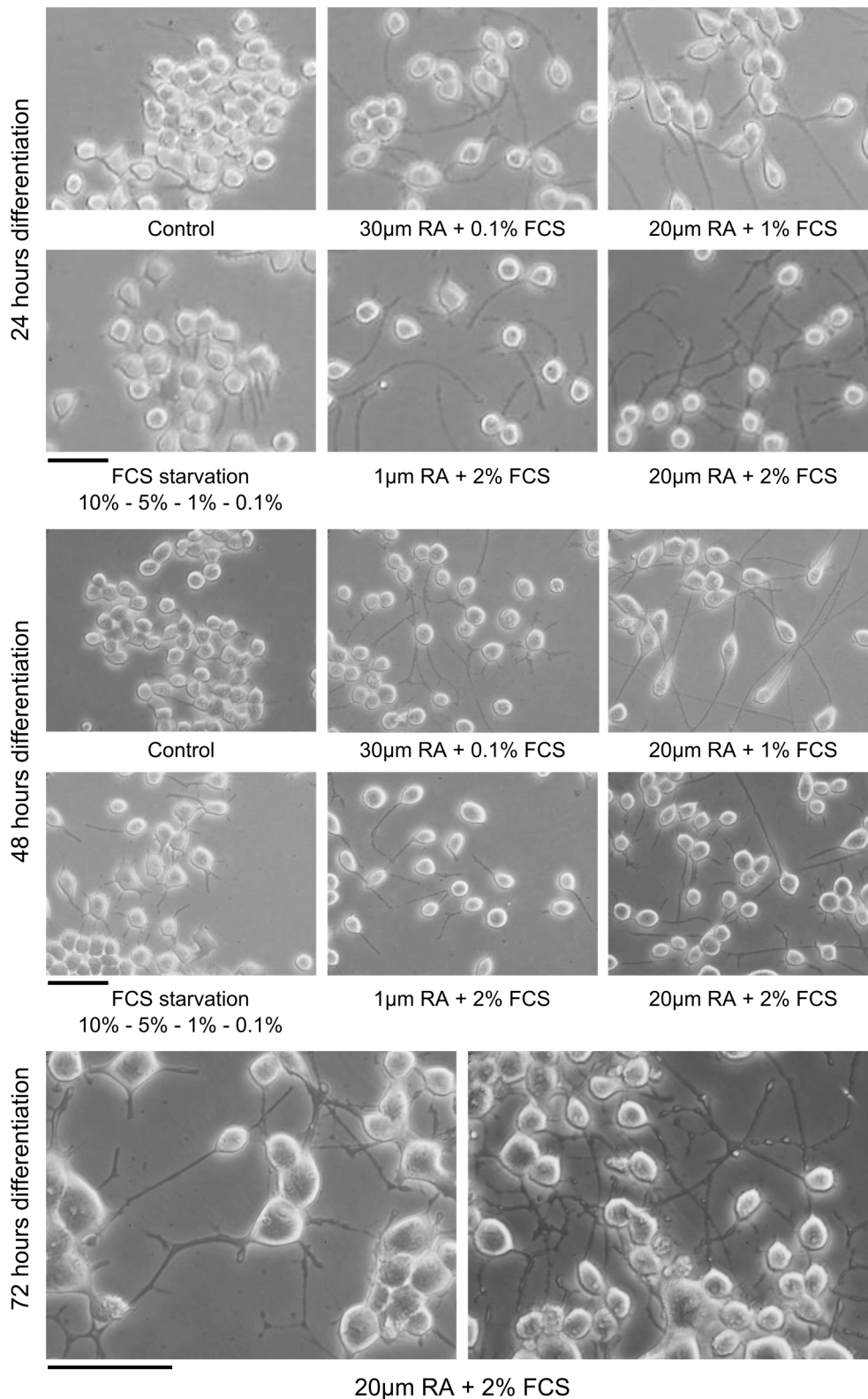


Figure 18. Optimization of N2A differentiation. Several combinations of starvation media, indicated by FCS%, alone or in combination with different RA concentrations were used to induce N2A differentiation. After 24h of transfection, cells were differentiated for 72h and imaged every 24h. The best differentiation condition is depicted in the bottom panels together with representative pictures of this time point. FCS: Fetal Calf Serum. RA: Retinoic Acid. Scale bar: 50 μ m.

4.1.7.2. Expression and cellular localization of GFP-tagged CHP1 proteins

All cell lines, namely: N2A, HeLa and PC12, transiently expressing CHP1-WT-GFP exhibited a uniform protein distribution throughout the cell, including neurite-like structures in the case of N2A and PC12 cells (Figure 19). In HeLa cells particularly, CHP1 enrichment around the nucleus was more distinctly observed (Figure 19B). These observations are in congruence with previous studies and therefore, validate the correct expression of the CHP1-WT-GFP construct. Indeed, CHP1 localizes predominantly in the cytoplasm, as it possesses two functional nuclear export signals (Nagita et al, 2003). Nevertheless, protein enrichment in perinuclear areas arises from CHP1 association to membranes of the early secretory pathway (Andrade et al, 2004b; Jimenez-Vidal et al, 2010). Immunostaining with the *cis* Golgi marker GM130 corroborated CHP1-WT-GFP localization in this compartment (Figure 19B).

Expression of CHP1-K19del-GFP led to massive protein aggregates in all cell lines, which upon detailed observation revealed two distinct patterns: small puncta-like structures and large amorphous accumulations with a very strong fluorescent signal (Figure 19). Aggregate localization did not show any compartment-specific pattern, as they were found throughout the cytoplasm and neurite-like structures (Figure 19C). Total accumulation/aggregation events in GFP-positive cells were quantified for all three cell lines. With regard to N2A cells, ~50% of the CHP1-K19del-GFP transfected cells presented accumulations in contrast to ~18% in the CHP1-WT-GFP cells. Although few puncta-like aggregates were also observed in CHP1-WT-GFP cells (15% of the cells vs 30% in the CHP1-K19del-GFP), severe protein accumulations were detected nearly exclusively in CHP1-K19del-GFP cells (22.5% vs 5% in the WT; $p < 0.0001$) (Figure 19C). Similar aggregation events were calculated for GFP-positive PC12 and HeLa cells, with quantification percentages comparable to those calculated for N2A cells and highly significant differences between CHP1-WT-GFP and CHP1-K19del-GFP ($p < 0,0001$) (Figure 19A and B). During the imaging process, microscope settings for shorter GFP exposure times were implemented in order to obtain adequate pictures of large protein accumulations. Therefore, when necessary, cells otherwise visible with longer exposure times were co-stained with Phalloidine in order to define cell contour.

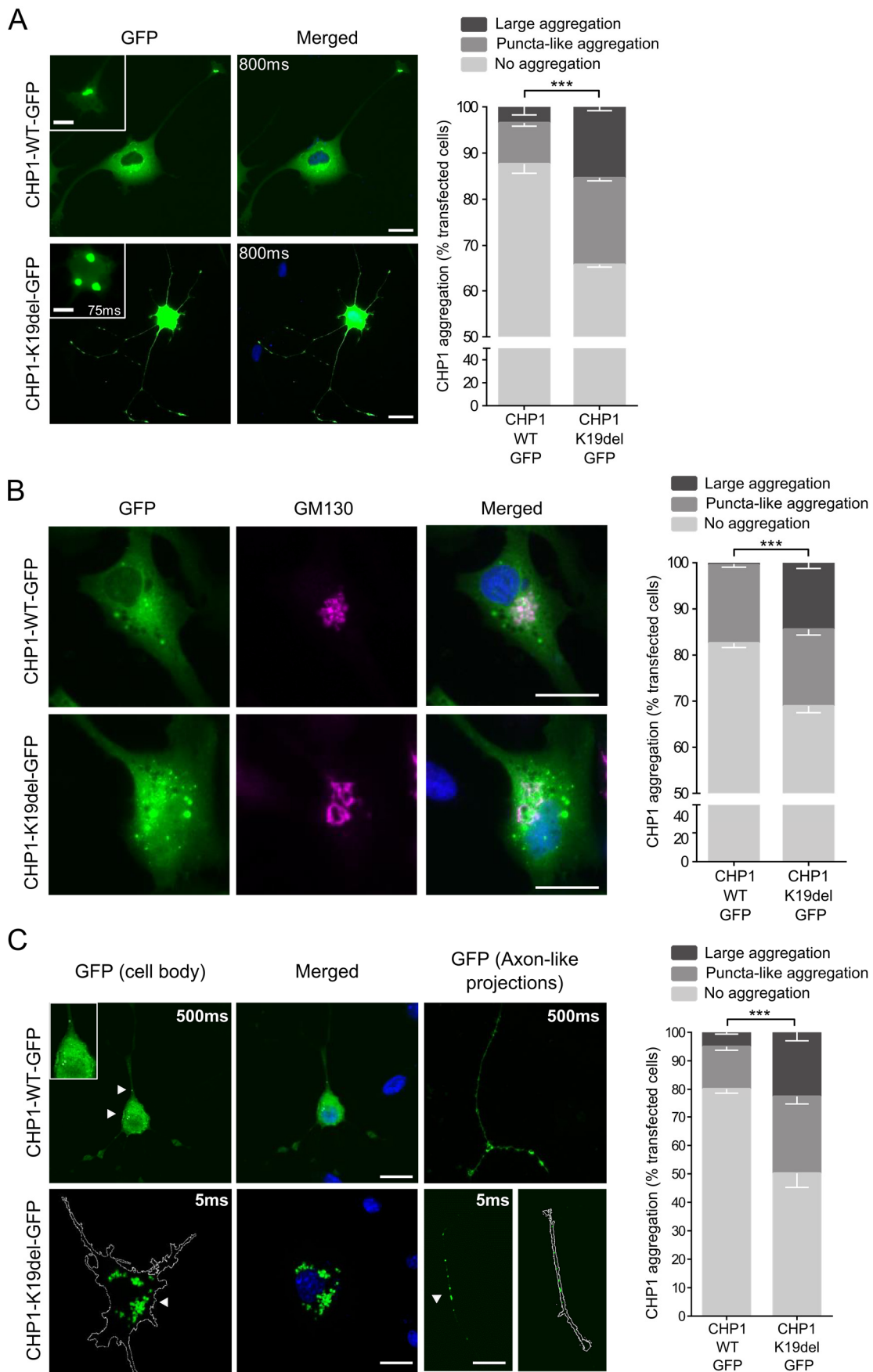


Figure 19. Protein aggregation in cell lines transiently expressing WT and mutant CHP1-GFP.
(See figure legend on the following page).

Figure 19. (A) Representative images of differentiated PC12 cells expressing CHP1-GFP WT and mutant constructs. CHP1-WT-GFP is expressed in the cell body and neurite-like structures of PC12 cells. Small puncta-like aggregates in neurite projections are magnified in the inset. CHP1-K19del-GFP expression led to massive protein aggregation in the cell body. The inset depicts aggregate magnification with reduced exposure time. Green fluorescence exposure time is indicated in milliseconds (ms) inside the panels. Scale bar of main images: 20 μ m and scale bar of magnified insets: 10 μ m. The graph represent aggregation quantification in GFP-positive cells. Bars show the mean \pm SEM (error bars) from 3 independent experiments ($n \geq 130$). *** denotes statistical significance ($p < 0.001$ Chi-square test). **(B)** Representative images of HeLa cells expressing WT or mutant CHP1-GFP constructs. Few puncta-like aggregates and protein perinuclear expression can be observed in cells expressing CHP1-WT-GFP. Expression of CHP1-K19del-GFP led to formation of large protein aggregates distributed throughout the cell. Perinuclear expression of mutant CHP1 is evident. Immunostaining with the *cis* Golgi marker GM130, in magenta, colocalize with CHP1 reactivity in merged image. Scale bar: 20 μ m. Graph represents aggregation quantification in GFP-positive cells. Bars show mean \pm SEM (error bars) from 3 independent experiments ($n \geq 300$). *** denotes statistical significance ($p < 0.001$ Chi-square test). **(C)** Representative images of differentiated N2A cells expressing CHP1-WT-GFP or CHP1-K19del-GFP proteins. CHP1-WT-GFP appears uniformly distributed in the cell body and neurite-like structures. Small puncta-like aggregates are visible. CHP1-K19del-GFP expression led to large protein aggregations, both in the cell body and throughout neurite-like structures. Puncta-like and large aggregations are indicated with white arrowheads. Exposure time in ms is indicated inside the panels. Scale bar: 20 μ m. Graph represents aggregation quantification in GFP-positive cells. Bars show the mean \pm SEM from 6 independent experiments ($n \geq 250$). *** denotes statistical significance ($p < 0.001$ Chi-square test).

4.1.7.2.1. CHP1 aggregates colocalize with protein homeostasis markers

To safeguard proteome integrity and cellular viability, protein synthesis and turnover must be finely balanced and misfolded proteins effectively cleared. Hence, the presence of aggregates is a clear indication of protein homeostasis (proteostasis) imbalance. The removal of misfolded proteins is mainly performed by proteasome complexes (ubiquitin proteasome system UPS) localized in cytosol and nucleus, whereas large protein aggregates and insoluble inclusions, resistant to dissociation, can be removed by selective autophagy; the other major pathway of proteostasis maintenance (Kopito, 2000; Rideout et al, 2004; Varshavsky, 2012). Diseases associated with protein aggregation –mainly neurodegenerative disorders- are characterized by the formation of intracellular inclusions or aggregates, which are ubiquitin and P62 (autophagy ubiquitin adaptor) positive (Iwata et al, 2005; Taylor et al, 2002; Zatloukal et al, 2002). Therefore, we examined whether these proteostasis markers colocalize with mutant CHP1 aggregates by immunostaining.

N2A cells expressing CHP1-K19del-GFP were stained for ubiquitin and P62 (Figure 20) and Costes-adjusted Pearson colocalization coefficients were calculated for green (GFP) and red probes (proteostasis markers) superimposition areas. Both puncta-like and large aggregates displayed positive colocalization and extensive accumulation of the two markers (Pearson coefficients: Ubiquitin 0.9 and P62 0.85), indicating that these structures are cleared by neuronal proteostasis control systems and explaining CHP1-K19del reduced expression (Figure 20A and B).

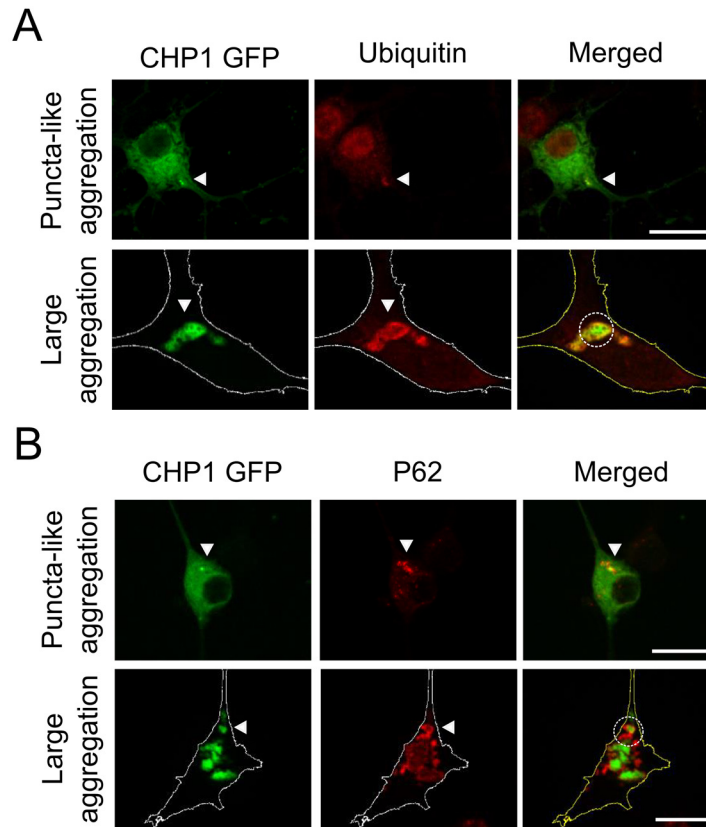


Figure 20. CHP1-K19del-GFP aggregates colocalize with proteostasis markers. N2A cells transiently expressing CHP1-WT-GFP or CHP1-K19del-GFP proteins were immunostained with anti-ubiquitin and P62 antibodies. Representative images of puncta-like and large aggregations are depicted. Costes-adjusted Pearson colocalization coefficients (P) were calculated for aggregate areas depicted in open circles. **(A)** Ubiquitin P=0.9 and **(B)** P62 P=0.85. Positive coefficients indicate that aggregates colocalize with ubiquitin and P62. White cell contour indicates Phalloidine staining. Scale bar: 20 μ m.

Altogether, these subcellular localization analyses strongly suggest that CHP1-K19del altered conformation and soluble expression deficits result in protein aggregation proneness and instability.

4.1.8. The K19del mutation potentially alters CHP1 conformational changes

One of the main factors influencing protein aggregation propensity is the loss of conformational flexibility in the soluble state (Valerio et al, 2005). To gain further insight into potential folding alterations caused by the K19del mutation, the CHP1 crystal structure was analyzed in detail using 3D-protein modelling tools. These analyses were performed in collaboration with Christian Pichlo affiliated to the Institute of Biochemistry, University of Cologne. Cologne, Germany.

Two structural models have been generated for CHP1, corresponding to the unbound (free) CHP1 crystal from *Rattus norvegicus* (Naoe et al, 2005) and the NMR-generated CHP1-NHE1-Cter segment complex from *Homo sapiens* (Mishima et al, 2007). Superimposed models of both free and bound CHP1 were generated in an effort to identify potential conformational changes, associated to NHE1 binding. *H. sapiens* and *R. norvegicus* are 99% identical in CHP1 aminoacid identity (Figure 21), hence protein folding properties are comparable.

The K19 residue is localized on the first N-terminal α helix of the CHP1 protein (Figure 22). Closer examination of this feature in both CHP1 structures revealed that CHP1- α helix undergoes large conformational changes upon NHE1 binding, forming a clamp fixating NHE1-C-terminal segment. Indeed, in the free CHP1 structure, the α helix has an open conformation, distant from the NHE1 binding cleft (Figure 22). Although the structure-function relationship of the α feature is not understood, these observations are in accordance with previous NHE1-CHP1 binding studies which hypothesize that CHP1, similar to other related proteins, might undergo conformational changes in order to form a bigger ligand-binding pocket to host four NHE1 α -helical turns (Naoe et al, 2005; Zhou et al, 2004). This structural analysis suggest that K19del could interfere with a fully functional CHP1-NHE1 complex formation, which in turn could impair NHE1 targeting to the membrane and compromise the function of this complex.

```

                                *
Homo sapiens   MGSRASTLLRDEELEEEIKKETGFSHSQITRLYSRFTSLDKGENGTLSRED
Rattus norvegicus MGSRASTLLRDEELEEEIKKETGFSHSQITRLYSRFTSLDKGENGTLSRED
                *
Homo sapiens   FQRIPELAINPLGDRINAFFPEGEDQVNFRGFMRTLAFHRPIEDNEKSK
Rattus norvegicus FQRIPELAINPLGDRINAFFSEGEDQVNFRGFMRTLAFHRPIEDNEKSK
                *
Homo sapiens   DVNGPEPLNSRSNKLHFAFRLYDLKDEKISRDELLQVLRMMVGVNISDE
Rattus norvegicus DVNGPEPLNSRSNKLHFAFRLYDLKDDKISRDELLQVLRMMVGVNISDE
                *
Homo sapiens   QLGS IADRTIQEADQDGD SAISFTEFVKVLEKVDVEQKMSIRFLH
Rattus norvegicus QLGS IADRTIQEADQDGD SAISFTEFVKVLEKVDVEQKMSIRFLH
                *

```

Figure 21. CLUSTALW2 alignment of CHP1 from *H. sapiens* and *R. norvegicus*. Lower * indicate identical residues. Only one aminoacid indicated with lower dot differs between both species (P/S). Indicated with a bold asterisk is the mutated residue K19.

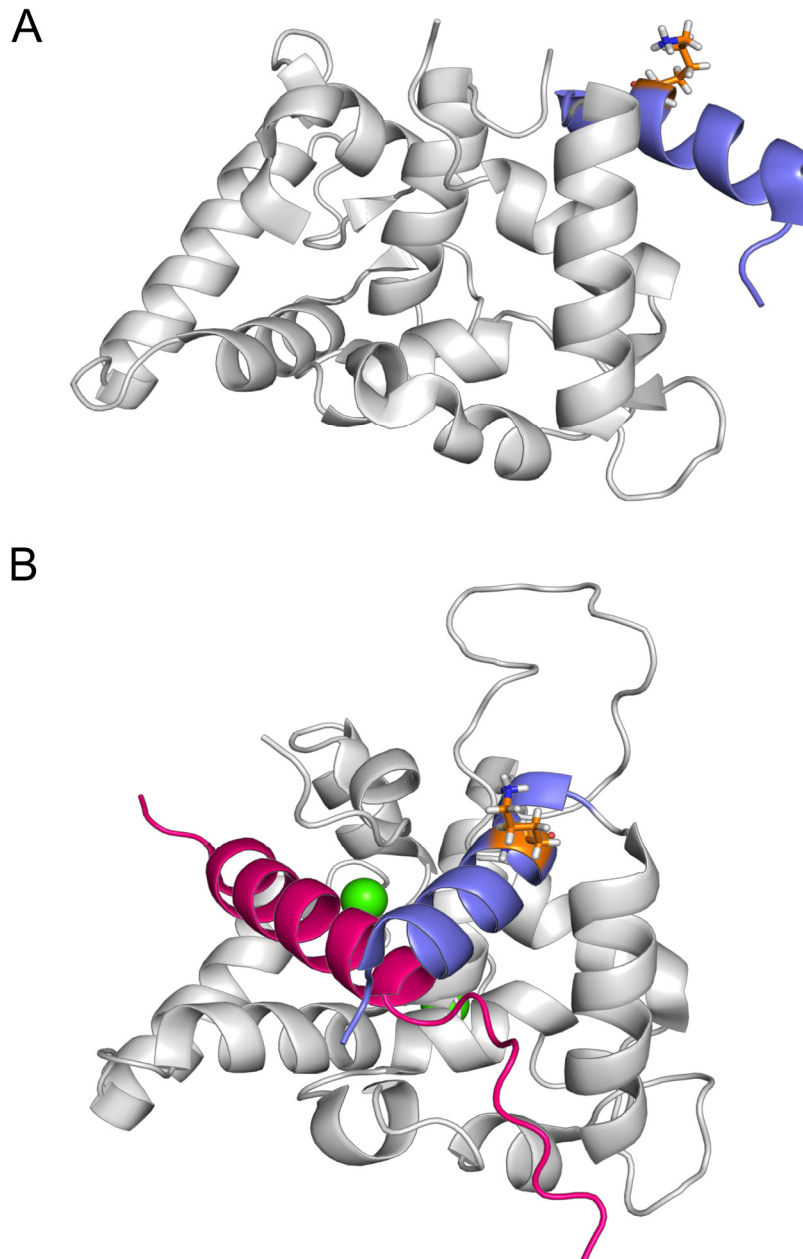


Figure 22. K19del mutation potentially compromises CHP1 conformational changes. Cartoon representation of (A) *R. norvegicus* free CHP1 crystal structure (PDB accession 2CT9) and (B) *H. sapiens* NMR complex structure of NHE1-bound CHP1 (PDB accession 2E30). CHP1 is colored in grey, the NHE1 segment in magenta and Ca²⁺ ions in green. The CHP1 Aα helix (amino acids 1 to 23) is presented in blue and the K19 residue is shown in orange sticks. Observe the open conformation of CHP1 Aα helix in the free-CHP1 structure and its closed-to-NHE1 hydrophobic pocket in the CHP1 bound structure.

4.1.9. Membrane-bound NHE1 is reduced upon overexpression of CHP1 K19del

Characterization studies of the CHP1-NHE1 complex demonstrate that this calcium-dependent interaction exclusively involves eight residues of the Jα helix of the C-terminal region of CHP1 (Naoe et al, 2005; Pang et al, 2004). These findings excluded the possibility

of a direct implication of K19 in the interaction between the two proteins, however, in the light of the aforementioned conformational analyses, a detrimental impact of CHP1-K19del on NHE1 targeting could not be ruled out. To investigate the effect of mutant CHP1 on membrane expression/targeting of NHE1, cell lysates from HEK293T cells transiently expressing CHP1-WT-V5 and CHP1-K19del-V5 were separated into soluble (cytoplasmic) and membrane fractions. Relative enrichment of HSP90 and EGFR were used to assess specificity of each subcellular fraction, respectively (Figure 23).

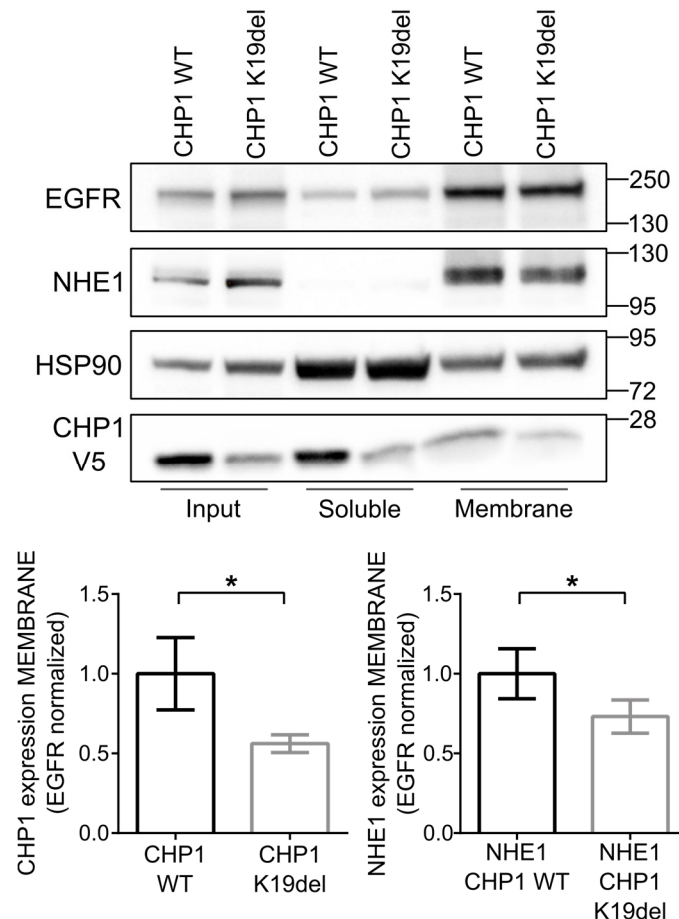


Figure 23. CHP1-K19del impairs NHE1 membrane targeting in HEK293T cells. Subcellular fractionation of total protein lysates from HEK293T overexpressing CHP1-WT-V5 and CHP1-K19del-V5. Lysates were separated into cytoplasmic and membrane fractions by differential lysis and centrifugation. Representative WB of total lysates (input) and fractions. Blots were probed with anti-V5, for CHP1-V5 tagged proteins detection, and anti-NHE1 antibodies. HSP90 and EGFR were used as enrichment markers for cytoplasmic (soluble) and membrane fractions, respectively. Graphs represent quantification of CHP1 and NHE1 relative expression in the membrane fraction. Bars show the mean \pm SEM (error bars) from 3 independent blots. * denotes statistical significance ($p \leq 0.05$ Student's t-test).

In line with reduced soluble (cytoplasmic) levels (Figure 14), CHP1-K19del membrane levels were also markedly diminished. More important, significant NHE1 reduction in membrane fractions was observed upon expression of mutant CHP1, indicating that CHP1-K19del misexpression interferes with NHE1 membrane targeting (Figure 23). These

observations are in agreement with previous studies which demonstrate that membrane, but not cytoplasmic, localization of CHP1 is reliant on NHE1 (Liu et al, 2013) but also, cell-surface expression and posttranscriptional glycosylation of NHE1 is largely dependent on CHP1 (Matsushita et al, 2011). Taking into account that reduced NHE1 membrane expression correlates with loss in exchanger activity (Matsushita et al, 2007), these results indicate that CHP1-K19del expression reduces NHE1 targeting to membrane compartments and compromises as well protein function. Similar results were observed in membrane fractions obtained from transiently transfected N2A cells (Figure 24).

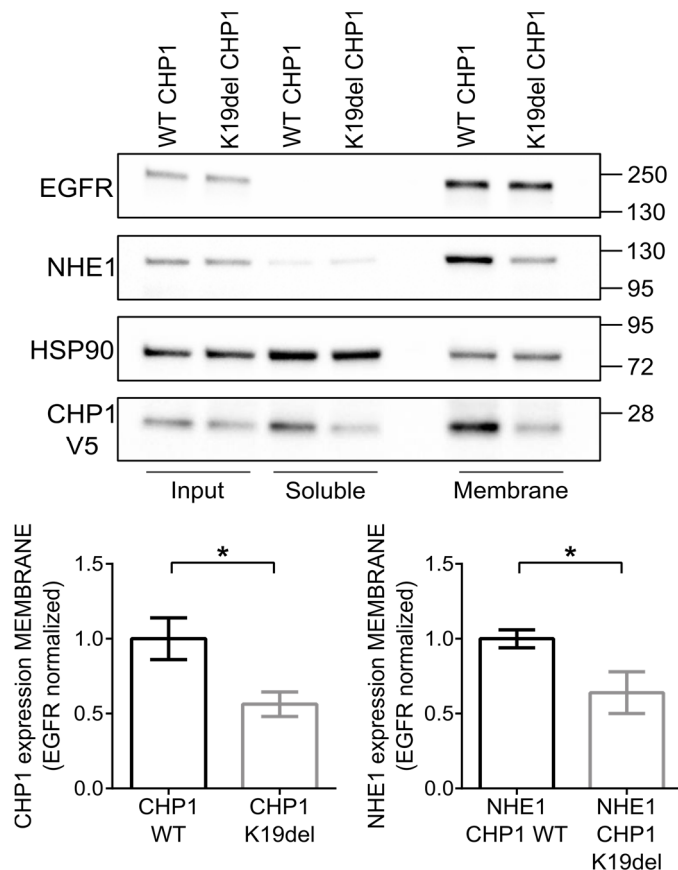


Figure 24. CHP1-K19del impairs NHE1 membrane targeting in N2A cells. Subcellular fractionation of protein total lysates from N2A transiently overexpressing CHP1-WT-V5 and CHP1-K19del-V5 proteins. Lysates were separated into cytoplasmic and membrane fractions by differential lysis and centrifugation. Representative WB of total lysate (input) and fractions. Blots were probed with anti-V5, for CHP1-V5 tagged proteins detection, and anti-NHE1 antibodies. HSP90 and EGFR were used as enrichment markers for cytoplasmic (soluble) and membrane fractions, respectively. Graphs represent quantification of relative CHP1 and NHE1 expression in membrane fractions. Bars show the mean \pm SEM from 3 independent blots. * denotes statistical significance ($p \leq 0.05$ two-tailed Student's t-test).

In summary, the *in vitro* studies described so far demonstrate that the K19del mutation alters CHP1 solubility, folding, subcellular localization, stability and, very likely, conformational 3D structure; thereby impairing NHE1 membrane expression and consequently function. These protein defects underlie the pathogenicity of mutant CHP1,

ratify K19del as a hypomorphic mutation and strongly indicate that CHP1 mutation cause ataxia in a NHE1-dependent manner.

4.1.10. Generation of a zebrafish model for *chp1*-deficiency analyses

Evolutionary conservation of human disease genetic mechanisms in zebrafish underpin the power of this organism for the modelling of human inherited ataxias (Akizu et al, 2015; Burns et al, 2014; Kabashi et al, 2011; Kawahara & Hayashi, 2016; Margolin et al, 2013). Therefore, to functionally test the consequences of a hypomorphic *CHP1* allele *in vivo*, a zebrafish model was generated using antisense morpholino (MO) oligonucleotides (Nasevicius & Ekker, 2000) to inhibit translation and downregulate the expression of the orthologous zebrafish *chp1*. As *Homo sapiens* and *Danio rerio* share a CHP1 aminoacid identity of almost 90%, *chp1* MO-associated phenotypes were expected to recapitulate to a great extent the pathogenesis of CHP1 depletion in human.

The zebrafish work was performed in collaboration with Dr. Mathias Hammerschmidt and Dr. Heiko Löhr from The Institute for Zoology / Developmental Biology of the University of Cologne (Germany).

4.1.10.1. Description of selected neurological readouts. Why and how to assess motor neuron and cerebellar defects underlying *chp1* depletion?

First and foremost, *chp1* MO injections were performed in one-to-four cell stage embryos, which were allowed to grow for ~34 or ~72hpf (hours post fertilization) for subsequent Caudal Primary Motor Neuron (CaP-MN), cerebellar and motoric analyses, respectively. These two phenotypic readouts were selected for quantification since fairly parallel the main pathogenic features of the CHP1 patients, namely neuropathy with UMN and LMN involvement, cerebellar atrophy and spastic ataxia (see Table 6).

On one hand, the morphology of CaP-MNs in zebrafish, was analyzed in terms of truncations (shortened axonal projection), atrophies (absence of axonal projection) and increased terminal branching. These features constitute an excellent surrogate system to assess motor neuron development and have been widely used to assess MN damage in the context of inherited motor neuropathies (reviewed in (Babin et al, 2014) and (Kabashi et al, 2010)) and complex spastic ataxia phenotypes with MN involvement (Issa et al, 2012; Lin et al, 2008; Martin et al, 2012; Valdmanis et al, 2007). More specifically, CaP-MN defects were classified as follows: with regard to their axonal length; CaP-MN were defined as:

normal, short (truncated axonal projection) or absent (total axonal atrophy), whereas based on terminal branching, CaP-MN axons were classified as normal, mild (one branching ventral from midline), medium (2-3 or more branches at ventral or midline) or severe (>3 branches ventral or dorsal from midline).

On the other hand, the effect of *chp1* depletion effect on cerebellar morphology was interpreted in the context of cerebellar hypoplasia (also known as cerebellar disorganization), a reliable phenotypic surrogate of developmental loss of cerebellar axonal tracts (Bae et al, 2009; Bernier et al, 2014; Golzio et al, 2012). This readout has been previously modelled in zebrafish for functional analyses of neurodegenerative ataxias with underlying cerebellar atrophy (Borck et al, 2015; Kawahara & Hayashi, 2016; Margolin et al, 2013). In particular, when the cerebellar area of observation was clearly reduced, *chp1* morphants were catalogued as “exhibiting cerebellar defects”.

Since individuals carrying *CHP1* mutation exhibit spastic paraparesis with gait instability and ataxia (see results section 4.1.1), the movement of *chp1*-depleted ~34hpf larvae was analysed in detail. Hence, a third motoric/movement readout was assessed via the estimation of the frequency of spontaneous contractions of ~34hpf larvae in a time-lapse of 30 seconds. Alterations of this motoric parameter have been observed and characterized previously in the frame of recessive ataxia and are included in the zebrafish behavioral catalogue as pathological readouts of ataxia and epilepsy (Kalueff et al, 2013; Mahmood et al, 2013). In addition, fin and trunk movements of older larvae (~72hpf) were video-recorded in order to observe swimming or trashing alterations. Extended details pertinent to the quantification of these phenotypic readouts are provided in section 6.2.7.2.

4.1.10.2. Selection of a suitable MO-dosage for phenotypic analyses

Zebrafish embryos generated from the crosses between transgenic males TL/EK-*hb9-GFP* (Flanagan-Steet et al, 2005) and wild-type TL/EK females were used for *chp1* MO injections and subsequent visualization of GFP-positive CaP-MNs axons. By contrast, cerebellar analyses were performed in embryos derived from wild-type TL/EK matings after ~72hpf. Antibodies against zebrafish Znp1 (Synaptotagmin) and acetylated Tubulin were used for immunostaining and visualization of CaP-MN and cerebellar axonal tracts, respectively. In order to select a *chp1* MO dosage with little effect on fish development but quantifiable neurologic readout, three different MO concentrations (*i.e.* 1, 2 and 3ng) were injected in the embryos. Body axis bending as an indicator of severe spine malformation underlying non-specific MO toxicity was observed and quantified after ~34hpf (Bedell et al, 2011; Zoupa & Machera, 2017).

Injection of 1ng *chp1* led to ~18% of embryos with evident morphological defects whereas injection of 2 and 3ng resulted, in a dose-dependent manner, in morphological defects in ~50% and almost 100% of the analysed embryos, respectively (Figure 25). Because the analysis of neurological readouts was limited to fish larvae with normal appearance, the 3ng MO dosage was thereby excluded.

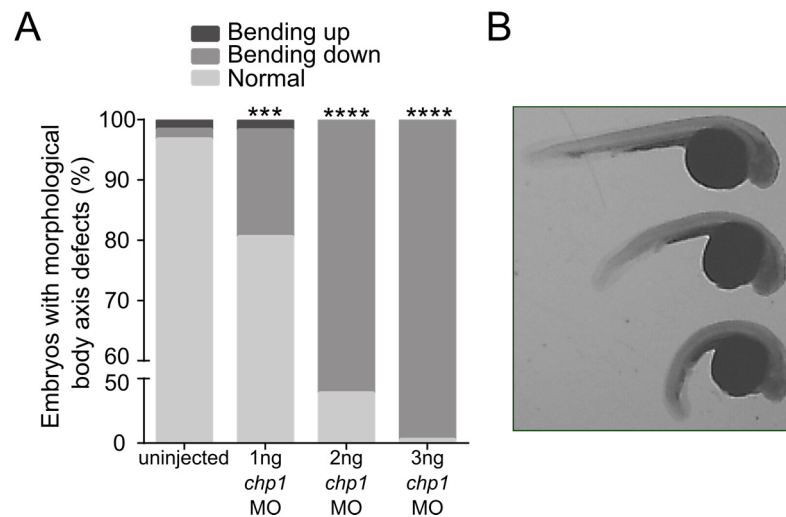


Figure 25. Quantitative analysis of body axis phenotype upon injection of increasing concentrations of *chp1* MO. (A). Embryos with body axis defects were grouped in 3 categories: bending up, bending down and normal axis. Injection of 2 and 3ng of MO resulted in severe body axis bending downwards. Results are presented in percentages from $n = \geq 60$ analyzed morphants representing 3 independent experiments. *** and **** denote statistical significance ($p < 0.001$ and $p < 0.0001$ Fisher exact test). **(B)** Representative picture of 36hpf zebrafish larvae. The upper fish larva in the picture exhibits a normal appearance whereas the middle and below larvae depict different degrees of downwards bending. As the upwards axis bending was barely observed, no pictures were acquired from these larvae.

Subsequent analysis of CaP-MN and cerebellar readouts upon *chp1*-MO injection unveiled 1ng MO as the best concentration for subsequent experiments. Indeed, injection of this dosage led to a clear MN phenotype, with axonal projection defects in 15-30% of the analyzed motor axons (Figure 26A-C) as well as cerebellar defects in almost 70% of the quantified morphants (Figure 26D-E). The latter observation excluded further analysis of cerebellar morphology with higher than 1ng *chp1* MO concentrations. Given the extent of the cerebellar phenotype, additional injections with a control (non-targeting) MO were performed, aiming to discard potential toxic events associated either with the manual injection process or with the MO preparation. No cerebellar defects were observed in this control group (Figure 26D-E). The knock-down (KD) efficacy of 1ng *chp1* MO was confirmed by Western blot analysis of protein lysates obtained from MO-injected and uninjected fish larvae after ~36hpf (Figure 26F).

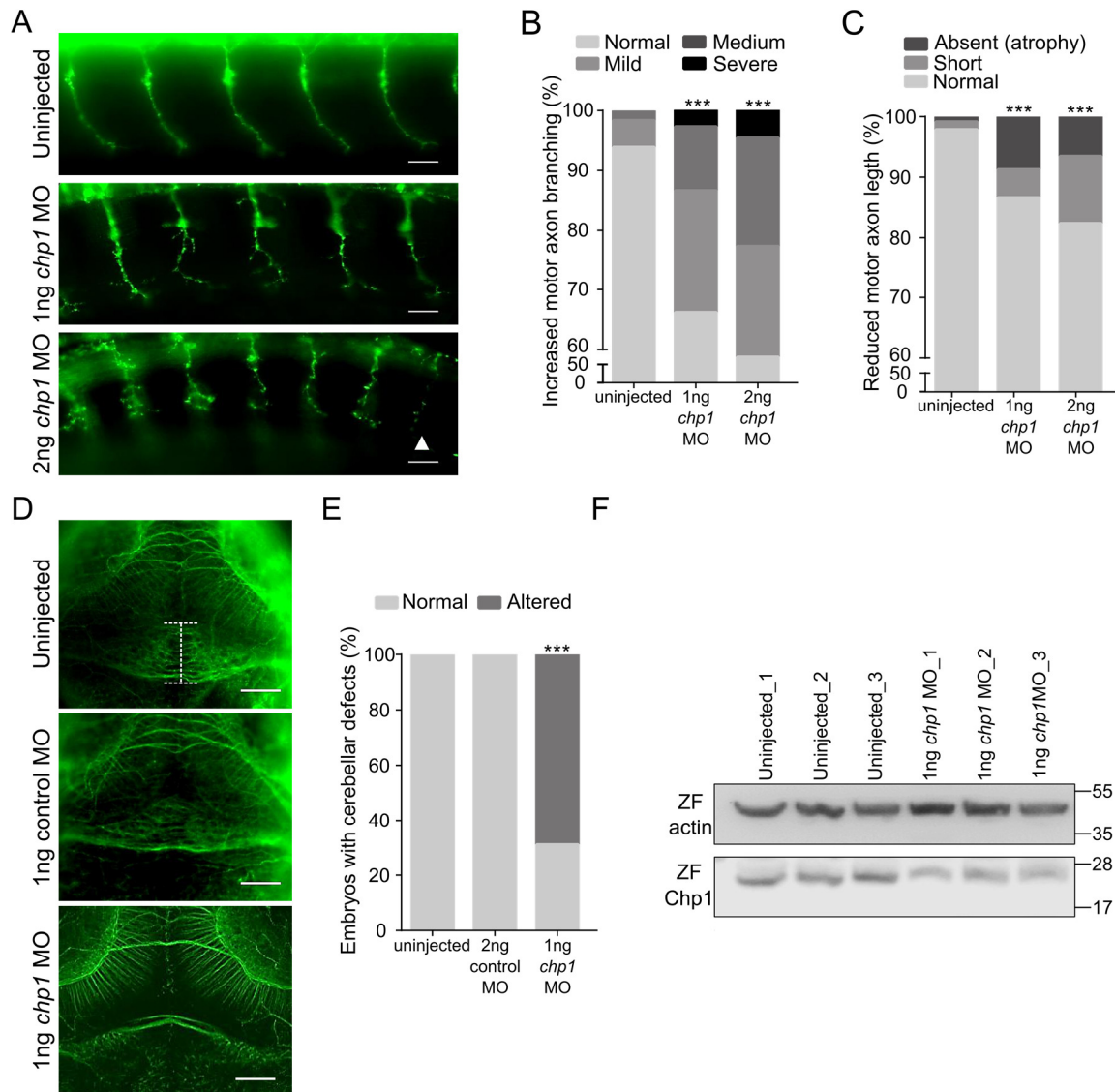


Figure 26. *chp1* MO dosage optimization. **(A)** Lateral views of ~34hpf embryos stained with synaptotagmin antibody (Znp1). Representative images of *chp1* injections show terminally branched motor axons and one axon truncation (white filled arrowhead) in *chp1*-MO injections (see also Figure 29A, C and D), Scale bar: 25 μ m. **(B)** and **(C)** Quantitative analysis of CaP-MN defects demonstrates that two different *chp1* MO concentrations lead, in a dose-dependent manner, to increased CaP-MN terminal branching and shorter axonal projections (truncations) in comparison to uninjected zebrafish. Graphs are presented in percentage from $n \geq 150$ analysed axons representing 3 independent experiments. NS denotes no significant difference and * and *** denote statistical significance ($p \leq 0.05$ and $p < 0.001$ Fisher exact test). **(D)** Dorsal views of ~72hpf embryos labelled with acetylated tubulin. In representative image of the uninjected, the structure depicted between white horizontal lines indicates cerebellar region of interest (see also Figure 29B-E), Scale bar: 25 μ m. **(E)** Quantitative analysis of cerebellar phenotype indicates that injection of 1ng *chp1* MO cause cerebellar defects in ~70% of the morphants. Injection of 2ng non-targeting MO has no effect on the cerebellar morphology. Results are presented in percentages from $n \geq 40$ observed zebrafish morphants representing 3 independent experiments. NS denotes no significant difference. * and *** denote statistical significance ($p \leq 0.05$ and $p < 0.001$ Fisher exact test). **(F)** WB analysis of protein lysates isolated from uninjected and 1ng *chp1* MO-injected zebrafish embryos demonstrates KD efficiency. Blots were probed with antibodies against zebrafish Chp1 and β -actin as loading control.

4.1.10.3. Generation of *CHP1* WT and mutant mRNAs for rescue experiments

Specificity of the MO or KD phenotype, can -and must- be addressed in zebrafish experiments. A very common strategy is to reverse the MO effects by an approach known as RNA rescue, which entails the simultaneous injection of synthetic mRNAs encoding the protein from the targeted locus (Bill et al, 2009; Ekker & Larson, 2001). Given the high homology and conservation among human and zebrafish genes, phenotype rescues further allow for the comparison between WT and mutation-bearing human mRNAs. Hence, pathogenic variants can be additionally validated in MO-injected larvae according to their “complementation” extent (Kabashi et al, 2011).

To perform rescue experiments, human *CHP1-WT* (NCBI: 11261) and *CHP1-K19del* cDNAs were inserted into PCS2+ expression vectors, to generate *in vitro* transcribed mRNAs. Since *CHP1* cDNA templates were subcloned from the *CHP1-GFP* constructs used for protein overexpression analyses (see 4.1.4), site directed mutagenesis was not performed in PCS2+ vectors. After concentration determination, mRNAs quality was assessed in non-denaturing agarose gels (see 6.2.2.9). Band smearing, an indication of mRNA degradation, was not observed in the analyzed samples (Figure 27A) thereby validating the excellent quality of the *CHP1* mRNAs used for zebrafish experiments.

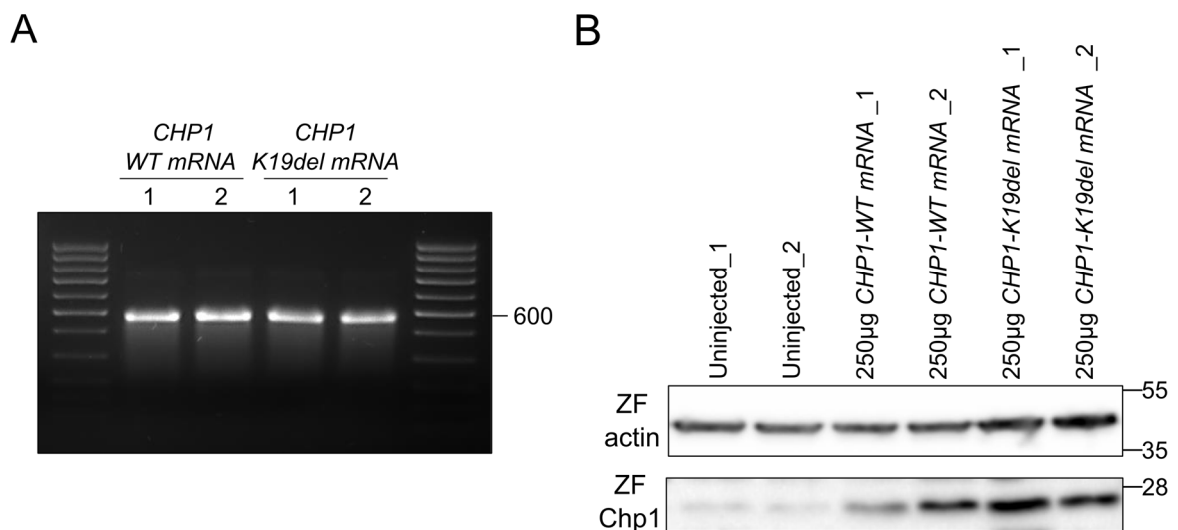


Figure 27. mRNA quality assessment and WB confirmation of *CHP1* mRNAs overexpression. (A) Non-denaturing agarose gel for mRNA quality assessment. 2µl of *in vitro*-transcribed *CHP1-WT* and *CHP1-K19del* mRNAs were loaded into agarose gels to visualize mRNA integrity. Neither band smearing nor residual linearized template are observed. Band molecular size (~600bp) corresponds to what is expected for single-stranded *CHP1* mRNA products. (B) WB confirmation of *CHP1-WT* and *CHP1-K19del* OE. Total protein lysates from ~34hpf larvae injected with WT and mutant *CHP1* mRNAs demonstrate efficient protein overexpression. Blots were probed with antibodies against human/zebrafish *CHP1* and zebrafish β-actin. Endogenous *Chp1* signal appears weak as exposure time was reduced to avoid saturation in *CHP1* OE lanes.

250pg of *CHP1-WT* and *CHP1-K19del* mRNAs were injected to evaluate protein overexpression (OE), exclusively. Western blot of protein lysates obtained from mRNA-injected and uninjected fish larvae confirmed protein OE after ~34hpf (Figure 27B), therefore subsequent rescue experiments were performed using this amount of mRNA. Neither gross morphological changes nor developmental spine bending were observed upon *CHP1* proteins OE in zebrafish (data not quantified). Likewise, neither significant CaP-MN nor cerebellar defects were observed upon sole injection of 250pg *CHP1-WT* or *CHP1-K19del* mRNAs in comparison with uninjected larvae (Figure 28). Nevertheless a slight increment in CaP-MN defects was observed upon mutant *CHP1* OE (Figure 28B-C).

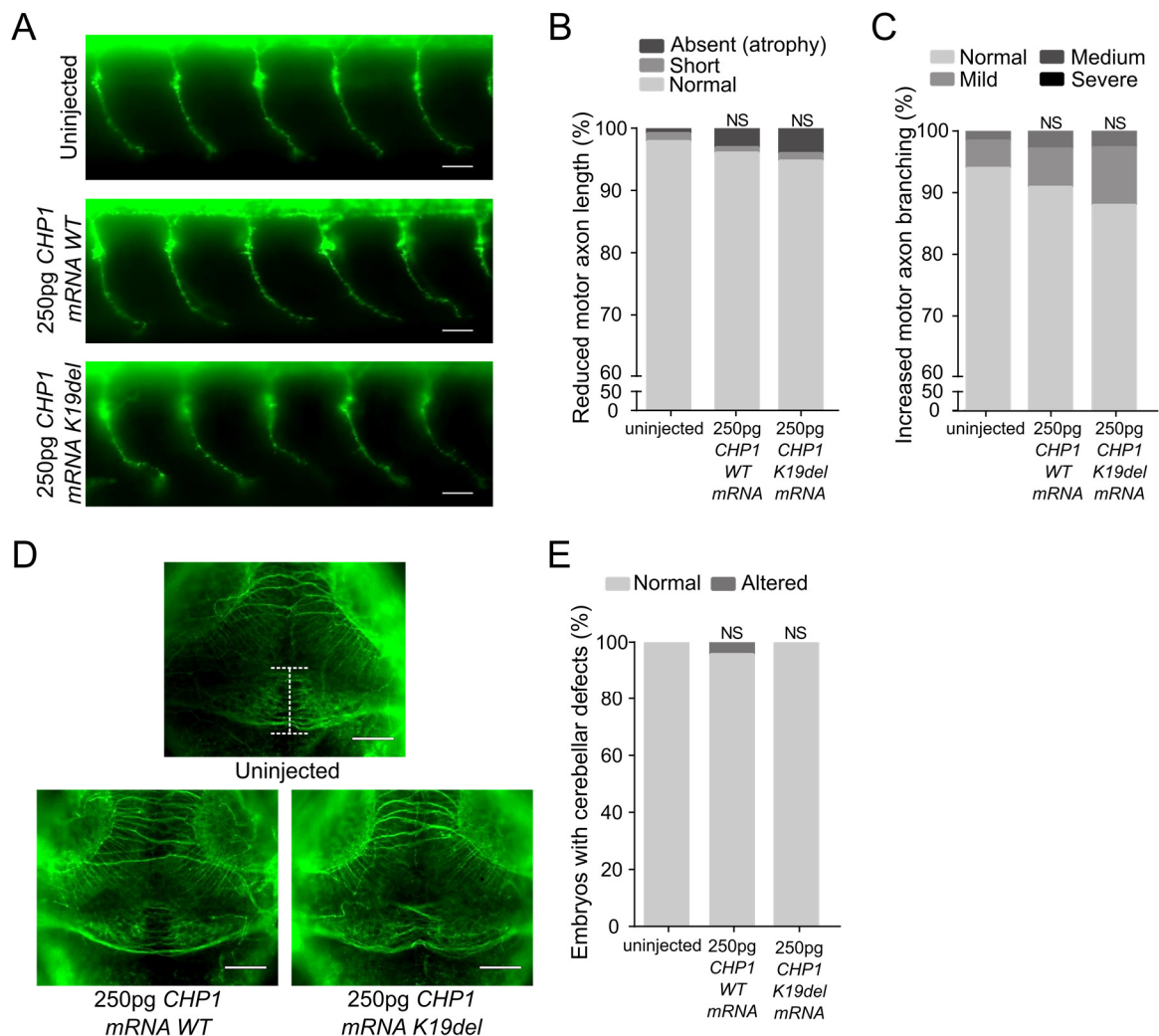


Figure 28. Overexpression of sole *CHP1-WT* and *CHP1-K19del* mutant mRNAs has no effect on CaP-MN or cerebellar morphology. (See figure legend on the following page)

Figure 28. (A) Lateral views of ~34hpf embryos stained with Synaptotagmin antibody (Znp1). Representative images of *chp1* injections show normal-projecting motor axons in mRNA-injected and uninjected fish larvae. Scale bar: 25µm. **(B)** and **(C)** Quantitative analysis of CaP-MN demonstrates that injection of 250pg of human *CHP1-WT* or *CHP1-K19del* mRNAs cause negligible CaP-MN defects (see also Figure 29 A, C and D) in comparison to uninjected zebrafish. Results are presented in percentages from $n \geq 150$ analysed axons representing 3 independent experiments. NS denotes no significant difference. * and *** denote statistical significance ($p \leq 0.05$ and $p < 0.001$ Fisher exact test). **(D)** Dorsal views of ~72hpf embryos labelled with acetylated tubulin. In the representative image of the uninjected, the structure depicted between white horizontal lines indicates cerebellar region of interest (see also Figure 29B and E). Scale bar: 25µm **(E)** Quantitative analysis of cerebellar defects indicates that injection of 250pg of human *CHP1-WT* or *CHP1-K19del* human mRNAs do not affect cerebellar morphology. Results are presented in percentages from $n \geq 40$ observed zebrafish morphants representing 3 independent experiments. NS denotes no significant difference. * and *** denote statistical significance ($p \leq 0.05$ and $p < 0.001$ Fisher exact test).

4.1.10.4. *chp1* downregulation in zebrafish causes motor axon, cerebellar and movement defects, which are rescued by WT but not mutant CHP1 mRNA

Once the 1ng *chp1*-MO dosage was established as the best working-concentration, several injection rounds were performed with the purpose of characterizing the phenotype of *chp1*-morphants. Hence, the data presented hereafter, although highly comparable with the results presented in (Figure 26), was analysed independently from these experiments.

As anticipated from previous results, *chp1* downregulation led to CaP-MN defects, namely axonal truncations and increased terminal branching. In detail, ~23% of the analysed CaP-MNs exhibited defects in axonal projections and ~35% showed increased terminal branching (Figure 29A, C and D). Likewise, *chp1* downregulation led to cerebellar hypoplasia in ~70% of the analysed morphants. Intriguingly, only in morphants with pronounced cerebellar hypoplasia, a second group of axonal tracts corresponding to the trochlear decussation was observed (Norton et al, 2005), probably as a consequence of the large axonal loss in the cerebellum (Figure 29B and E). Reduced size of the optic tecta, an additional surrogate of zebrafish neurogenesis defects (Borck et al, 2015; Seminara et al, 2002), was also observed (Figure 29B) but not included for quantification analyses due to methodological limitations regarding the dorsal embedding of ~72hpf fish larvae. Moreover, Chp1 reduction led to significantly increased frequency of spontaneous contractions in ~34hpf larvae (Figure 29F) and provoked abnormal spastic-like trunk contractions and fin movements, unaccompanied by locomotion, in ~72hpf morphants. The latter phenotypes were recorded but not included for quantification analyses.

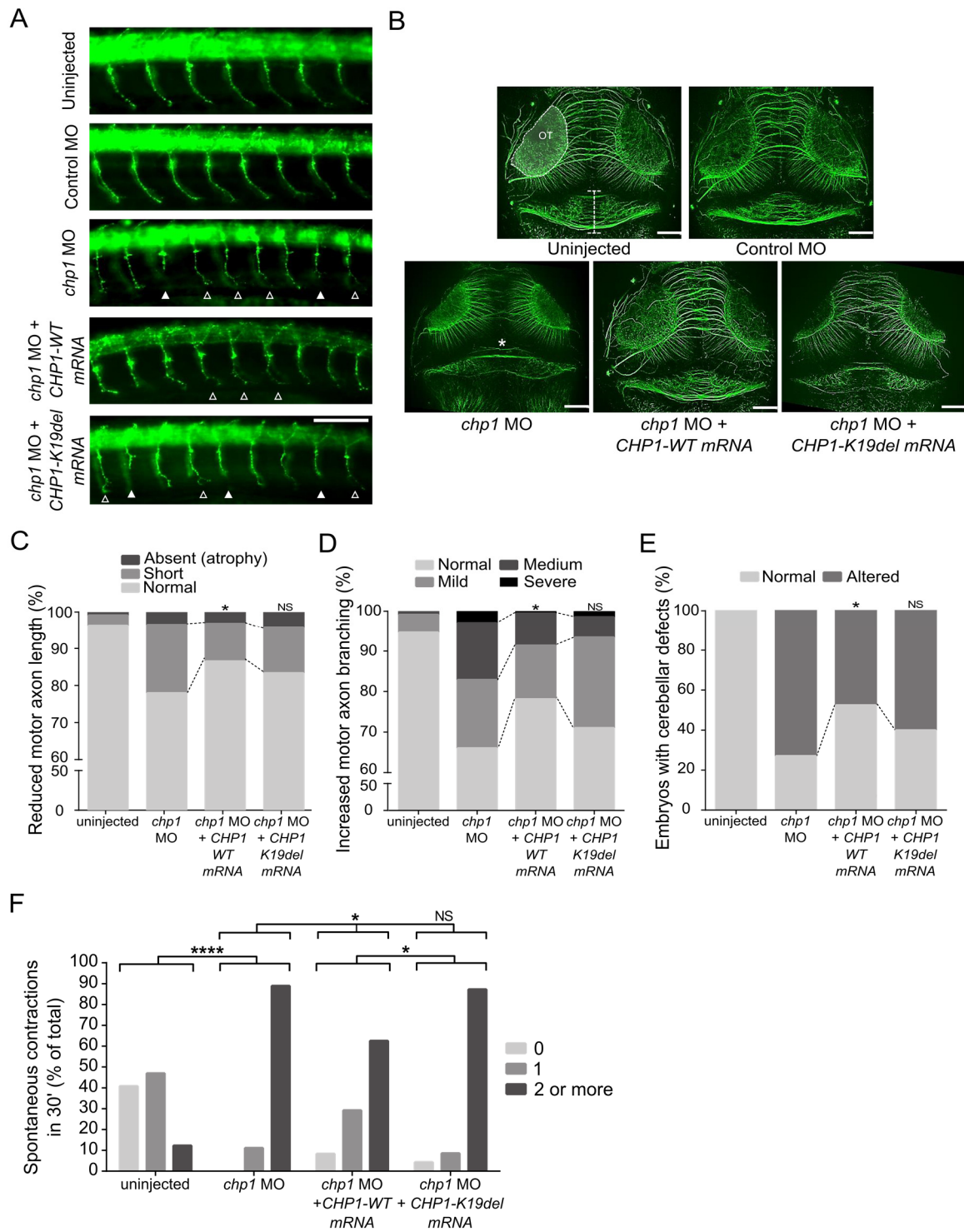


Figure 29. CHP1 downregulation in zebrafish causes CaP-MN, cerebellar and movement defects which are rescued with WT, but not mutant *CHP1* mRNA. (See figure legend on the following page).

Figure 29. (A) Lateral views of whole-mount embryos immunostained with Znp1 (synaptotagmin). Truncated and absent motor axons are indicated with solid arrowheads and terminally-branched axons with open arrowheads. Scale bar: 25 μ m. **(B)** Dorsal views of whole-mount ~72hpf embryos immunostained with anti-acetylated tubulin. The structure depicted between white horizontal lines in the uninjected fish indicates cerebellar area of observation. Optic tectum (OT) is outlined. Severe cerebellar hypoplasia is observed in *chp1*-depleted zebrafish in comparison to control MO and uninjected fish. * in *chp1* MO image show trochlear decussation. Scale bar: 25 μ m. **(C)** and **(D)** *chp1* morphants exhibit CaP-MN truncations and increased terminal branching in comparison to control MO and uninjected fish. Quantitative analysis of CaP-MN demonstrates that co-injection of *chp1* MO and *CHP1-WT* mRNA significantly improves axonal defects. Co-injection of *chp1* MO and *CHP1-K19del* mRNA fails to ameliorate CaP-MN defects in comparison to *CHP1-WT* mRNA. Results are presented in percentages from $n \geq 150$ analysed axons representing 3 independent experiments. NS denotes no significant difference and * denotes statistical significance in comparison with *chp1* MO group ($p \leq 0.05$ Chi-square test). **(E)** Quantitative analysis of cerebellar defects demonstrates that co-injection of *chp1* MO and *CHP1-WT* mRNA significantly ameliorates this phenotype. Co-injection of *chp1* MO and *CHP1-K19del* mRNA fails to improve cerebellar defects to WT levels. Results are presented in percentages from $n \geq 40$ observed zebrafish morphants from 3 independent experiments. NS denotes no significant difference. * and *** denote statistical significance ($p \leq 0.05$ and $p < 0.001$ Fisher exact test). **(F)** *chp1*-depleted morphants show an increased frequency of spontaneous contractions. Larvae contractions inside the chorion (~34hpf) were calculated manually from recorded videos. For graphic representation, spontaneous contractions were categorized as follows: 0 (no contraction), 1 (one contraction in 30 sec), 2 or more (2 or more contractions in 30 sec). Results are presented as percentage of the total, from $n \geq 50$ observed zebrafish larvae representing independent experiments. Co-injection of *chp1* MO and *CHP1-WT* mRNA, but not *CHP1-K19del* mRNA, significantly reduced spontaneous contractions in 30 sec. NS denotes no significant difference and *** denotes statistical significance ($p < 0.001$ Fisher exact test).

To corroborate the specificity of the *chp1* MO phenotype and further confirm the pathogenicity of mutant CHP1 *in vivo*, rescue experiments were performed by co-injection of the *chp1* MO along with synthetic WT and mutant human *CHP1* mRNAs (see section 4.1.10.3). As expected, co-injection of the *chp1* MO with *CHP1-WT* mRNA, but not *CHP1-K19del* mRNA, significantly ameliorated all neurological and movement defects associated to *chp1*-deficiency. More precisely, *CHP1-WT* mRNA improved axonal truncations, terminal branching and cerebellar disorganization by ~13% ~20% and 25%, respectively, compared to *chp1* MO alone, and spontaneous contractions were partially restored towards control (uninjected) values (Figure 29). A probable explanation for the incompletely or –not fully rescued- *chp1*-MO phenotypes will be addressed in discussion section 5.1.4.

Altogether, the CaP-MN and cerebellar defects observed upon *chp1* depletion not only recapitulate the main clinical features of the siblings harboring the *CHP1-K19del* mutation but also validate the pathogenic reduction of CHP1 as the underlying cause of the UMN/LMN and cerebellar signs observed in these patients. Most certainly, these data ratify cerebellar hypoplasia as the central pathogenic feature underpinning the pathogenesis of *CHP1-K19del* mutation *in vivo*.

4.1.10.5. Chp1 downregulation do not affect axonal projections of other neuronal populations

To verify the particular sensitivity of CaP-MN and cerebellum to *chp1* depletion or, in other words, to discard that *chp1* MO injection has a detrimental effect on other neuronal populations, two additional axonal projections namely the posterior lateral line nerve (PLL) and the cranial nerve were examined in *chp1* morphants upon immunostaining with anti-acetylated Tubulin.

On one hand, the PLL axons originate from the bilateral posterior lateral line ganglion and project horizontally along the trunk and tail of the zebrafish larvae. This group of sensory axons innervate organs involved in motion and vibration detection and can be observed, fully projected, in ~48hpf or older larvae (Ghysen & Dambly-Chaudiere, 2004). Deviations of the sensory lateral line from the normal path and aberrant or absent neuronal projections are indicators of PLL axon outgrowth and guidance defects (Brosamle & Halpern, 2009). On the other hand, the complex axonal arbors of the hindbrain cranial nerves and, more specifically, the ventral extension of the facial nerve can be efficiently detected upon acetylated tubulin immunostaining in ~56hpf or older larvae (Brosamle & Halpern, 2009). When properly extended, the facial nerve (VII facial nerve) can be easily identified as it projects ventrally in a forked-branched-like structure (Higashijima et al, 2000). Mildly abnormal outgrowth of the facial nerve fork has been analysed in a zebrafish model of SMA and thus validated as a surrogate of MN loss underlying denervation of the facial muscles (Beattie et al, 2007).

Examination of PLL and facial nerve neuronal tracts in ~72hpf zebrafish larvae injected with 1ng *chp1* MO did not reveal any defects in length and morphology of the axonal projections (Figure 30). These analyses, although performed in a small number of *chp1* morphants, indicate that MN and cerebellar axons are particularly sensitive to reduced Chp1 levels.

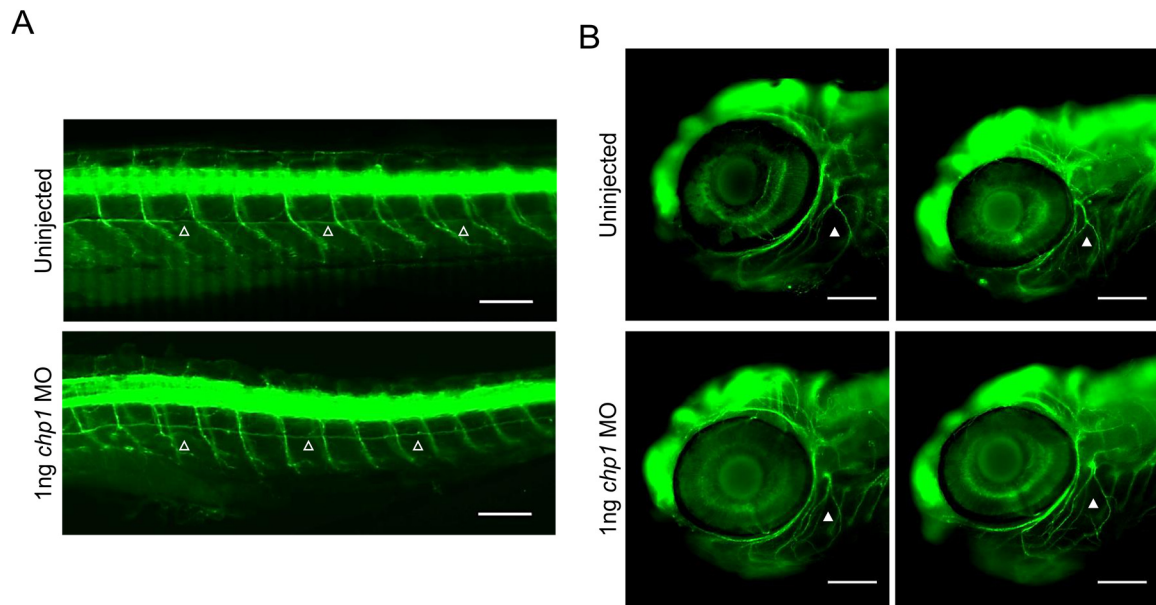


Figure 30. Injection of 1ng *chp1* MO do not affect other neuronal populations. Lateral views of ~72hpf larvae stained with anti-acetylated tubulin. **(A)** Representative pictures of the lateral line sensory neurons. Horizontal axonal projections are intact in MO-injected (n=12) and uninjected larvae (n=9). Open arrowheads indicate horizontal sensory line. **(B)** Representative pictures of the VII facial nerve. The forked-branched-like axonal projection is unaltered in both MO-injected (n=5) and uninjected (n=7) larvae. Solid arrowheads indicate fork-branch structure. Scale bar: 100 μ m.

4.1.10.6. Endocrine dysfunction is independent of CHP1 expression

The syndromic presentation of ataxia with endocrine dysfunction, e.g. hypergonadotropic hypogonadism, was first described in 1908 (Abs et al, 1990; Holmes, 1908). Nonetheless the genetic basis of this combination, except for a few successful studies (Margolin et al, 2013; Pierce et al, 2010), remains hitherto elusive. The female proband of this study presented with ovarian failure, however neither *Chp1 vacillator* nor *Nhe1*-depleted mouse females were reported as infertile/subfertile (Bell et al, 1999; Cox et al, 1997; Liu et al, 2013). Since the *Chp1 vacillator* mouse has been characterized and used for investigation purposes (independent to this project) in our research group, histological analysis of ovaries from *vacillator* females were undertaken in order to conclusively demonstrate that CHP1 depletion does not underlie ovarian failure.

Uteri were dissected from 12-week old *Chp1^{vac/vac}* females and general morphology was macroscopically examined. Since mice were processed at different periods in the estrous cycle, two *Chp1^{wt/wt}* control uteri at proestrus (before ovulation) and metestrus/diestrus (after ovulation) phases were used as reference to assess potential uterus hypoplasia in *Chp1^{vac/vac}* females. As expected, uteri examination did not reveal ovarian or uterus impairments (Figure 31). The latter observation summed to the fact that *chp1*-depleted mice are fertile, refute a potential role of CHP1 in female reproductive organs development or

function. The potential underpinnings for the association of ataxia and hypogonadism in the CHP1 family will be commented on the discussion section 5.1.6.

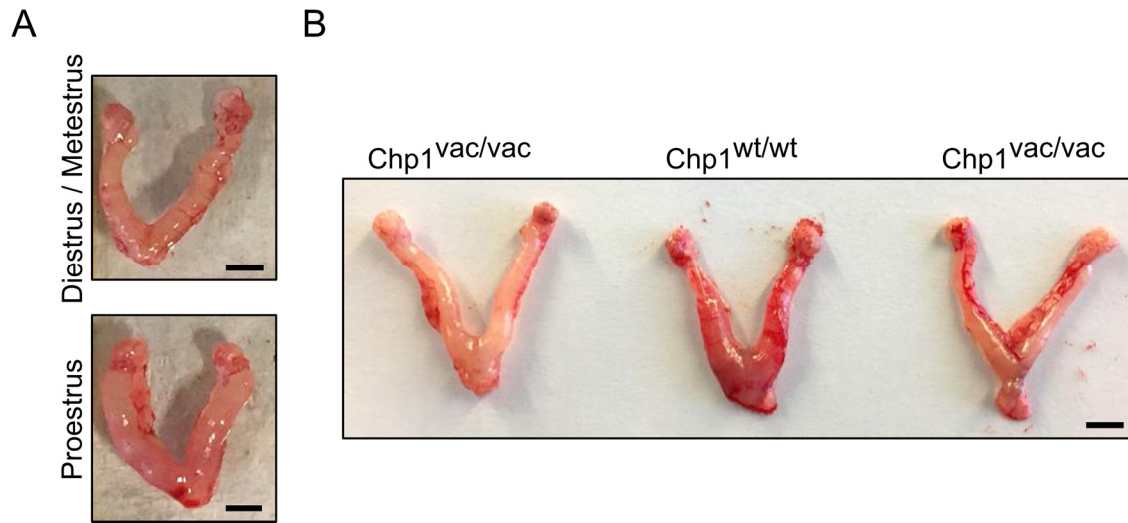


Figure 31. Macroscopic examination of uteri and ovaries from *Chp1^{vac/vac}* females. Ovaries and uteri were collected from 12-week-old females. **(A)** Representative pictures of uteri at different estrous phases. **(B)** Dissected uteri from *Chp1^{vac/vac}* (n=2) and *Chp1^{wt/wt}* (n=1) show no difference in overall uterine horns morphology or size. Scale bar, 2 mm. Uteri dissections were performed by PhD student Eva Janzen.

4.2. Functional characterization of a *de novo* mutation in *SLC18A3* in a family with distal motor neuropathy

In collaboration with Dr. Pavel Seeman (Department of Child Neurology, Charles University Prague, Czech Republic) and Dr. Konny Neveling (Department of Human Genetics, Radboud University Medical Centre, The Netherlands) we conducted functional analysis to address the pathogenic effects of a mutation in *SLC18A3*, a candidate causative gene of distal hereditary motor neuropathy (dHMN).

4.2.1. Clinical features of the index family and candidate gene identification

The starting point of this project was a family of Czech origin presenting with multiple cranial nerve palsies as an initial feature of a novel infantile-onset dHMN subtype. The family was thoroughly described and published as a case report by our collaborators (Haberlova et al, 2009), since the clinical presentation of the disease did not match any previously known dHMN entity.

The affected probands, a 28-year old woman and her 6-month old daughter, were similarly affected since childhood. At the age of 4 months, the mother manifested facial weakness, horizontal nystagmus, quadruhyperreflexia and dysphagia. By 8 months, a life-threatening vocal cord paresis was diagnosed and surgically intervened by age 10. Muscular weakness, predominately in the hands and face, appeared during infancy and progressed slowly during adolescence and adulthood. Her 6-month-old daughter was never able to suck and presented horizontal nystagmus, bilateral facial weakness and legs hyperreflexia. Nerve conduction studies and brain MRI were unremarkable. Clinical features of the affected probands are summarized in (Table 9).

WES trio analysis, performed on DNA isolated from the affected mother and daughter and the unaffected father, led to the identification of a *de novo* missense mutation (c.439 G>A, p.D147N) in the Vesicular Acetylcholine (ACh) Transporter (VACHT) encoded by the *SLC18A3* gene. Sanger sequencing confirmed heterozygosity of the mutation and its segregation from the affected mother to the affected daughter. *SMN1* deletion and mutations in *BSCL2*, *DCTN1*, *GARS*, *HSP22*, *HSP27*, *SETX* and *VAPB*, known dHMN-causative genes, were excluded after direct sequencing of all genes (Haberlova et al, 2009). Exome analysis, variant filtering and candidate gene/mutation selection were conducted by Dr. Pavel Seeman, who contacted us for further functional studies. At the time of WES (2011) and mutation characterization analyses (2013), no pathogenic variants had been reported for *SLC18A3*.

Table 9. Clinical features and neurophysiological findings of the affected probands

	♀ Patient 1 Mother	♀ Patient 2 Daughter
Age of onset	4 months	4 months
Clinical examination		
Age of examination	6-8 months	4 months
Horizontal nystagmus	+	+
Facial weakness	+	+
Bilateral eye closing weakness	+	+
Hyperreflexia	+	+
	Quadruple	Legs
Stridor	+	+
Dyspnea	+	NR
Vocal cord paresis	+	NR
Electrophysiological examination		
Age of examination	17 years	7 months
MNCV	Normal	Normal
SNAP	Normal	Normal
CMAP	Decreased	Decreased
EMG	Abnormal IP	Abnormal IP
Brain MRI	Normal	Normal

Table legend: (+) symbol denotes presence. NR indicates not reported in (Haberlova et al 2009). Abbreviations: MNCV (Motor Nerve Conduction Velocity), SNAP (Sensory Nerve Action Potential), CMAP (Compound Muscle Action Potential), EMG (Electromyography), IP (Interference Pattern).

The vesicular acetylcholine (ACh) transporter, hereafter termed VACHT, controls the storage of the neurotransmitter ACh by synaptic vesicles, hence it plays a fundamental role in cholinergic neurotransmission. The latter process governs a plethora of essential life functions, including the formation, wiring and proper nerve-muscle patterning of the neuromuscular junction (NMJ) (Brandon et al, 2003; Misgeld et al, 2002). Consistently, *SLC18A3* knockout is incompatible with life as homozygous *VACHT^{del/del}* mice develop severe NMJ dysfunction and die shortly after birth (de Castro et al, 2009). Notwithstanding, VACHT reduction within a safety threshold, above 50%, is well tolerated; since mice survive after birth but exhibit impaired neuromuscular transmission and function, decreased capacity to sustain physical activity and social/object recognition deficits (de Castro et al, 2009; Prado et al, 2006).

At the presynaptic level, *VACHT* depletion underlies neuronal impairment. Indeed, MNs and nerve terminals from *VACHT^{del/del}* mice exhibit increased axonal sprouting and abnormal branching, and are therefore unable to establish proper contacts with ACh receptors clusters (de Castro et al, 2009). In contrast, mice overexpressing VACHT exhibit increased cholinergic transmission which results in cognitive defects, accelerated degeneration of the

NMJ, without an apparent loss of MNs, and motor deficits of adult mice (Sugita et al, 2016). In addition, VACHT OE in striatal cholinergic neurons led to dramatic morphological remodeling and severely altered VACHT localization and axonal trafficking (Janickova et al, 2017).

Taking all these facts into consideration (in short: the dominant segregation of the VACHT-D147N mutation and the crucial function of the transporter in neurotransmission), the focal point of further characterization experiments was the analysis of VACHT-WT and VACHT-D147N OE consequences *in vitro* and *in vivo*. Throughout the time of *SLC18A3* validation studies were conducted, we kept in constant search of a second family. The VACHT-D147N mutation and all relevant patients' information were introduced into GeneMatcher in 2015, nevertheless no additional mutations in *SLC18A3* were found.

4.2.2. The D147N mutation has no effect in VACHT subcellular distribution

A pCMV-GFP plasmid with the human *SLC18A3* (*VACHT*) cDNA ORF insert was purchased from OriGene®. To investigate the effect of the D147N mutation on VACHT subcellular localization, the missense c.439 G>A transition was introduced by site-directed mutagenesis using the pCMV-VACHT-GFP construct as a template. All clones were verified by Sanger sequencing, including regions upstream and downstream of the open reading frame.

Expression plasmids encoding C-terminally GFP-tagged VACHT proteins were transiently transfected into NSC-34 cells; a murine neuroblastoma/spinal cord hybrid cell line which can be differentiated *in vitro* via addition of retinoic acid (Cashman et al, 1992). These cells were chosen for experimental analysis due to their significant morphological and physiological resemblance to primary MNs and their suitability for cholinergic neurotransmission studies, as they express various cholinergic markers, including the VACHT (Maier et al, 2013; Matusica et al, 2008). More importantly, a plethora of human mutations underlying hereditary motor neuropathies have been characterized utilizing NSC-34 cells as *in vitro* model (*e.g.* (Kwok et al, 2011; Magrane et al, 2009; Yi et al, 2012)).

After 48h of transfection, NSC-34 cells were differentiated with retinoic acid (RA) to promote neurite-like structures outgrowth. Analysis of GFP-positive cells indicated that expression of both VACHT-WT and VACHT-D147N is predominantly cytoplasmic, in accordance with previous reports referring VACHT OE and cytoplasmic/perinuclear localization in neuron-like cell lines (Barbosa et al, 1999; Kim & Hersh, 2004). Nonetheless, comparison between WT and mutant VACHT-GFP cells revealed no apparent differences in protein expression, localization or distribution (Figure 32). In consequence, a detrimental effect of the D147N

mutation on VACHT expression or localization was excluded. Nevertheless, an implication of the mutant protein in other neuronal processes, such as axonal outgrowth, was an intriguing possibility that could not be ruled out.

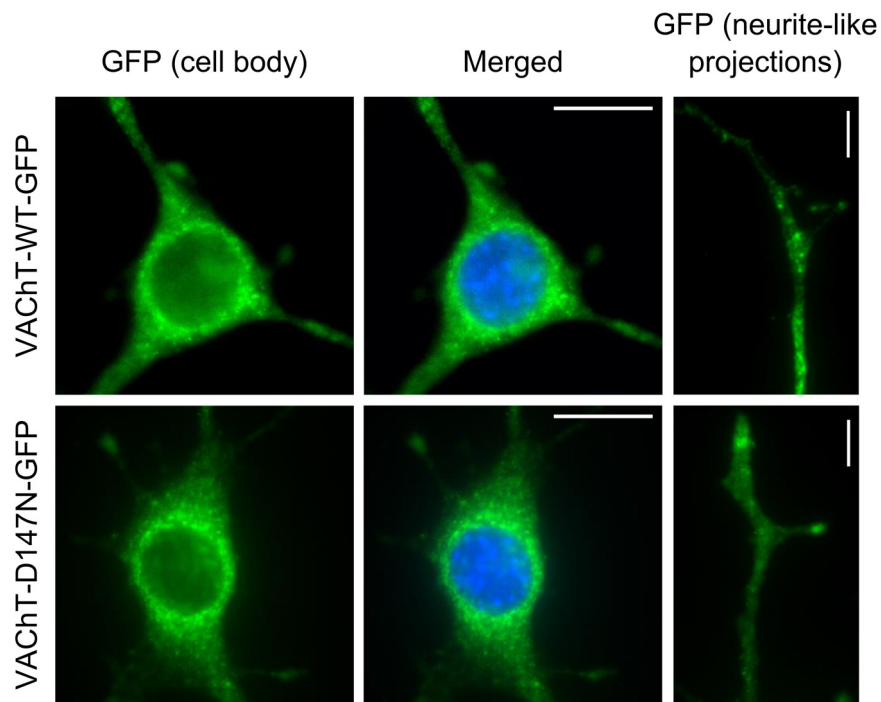


Figure 32. Mutant VACHT overexpression has no effect on protein subcellular distribution. Representative images of differentiated NSC-34 cells transiently expressing VACHT-WT-GFP and VACHT-D147N-GFP constructs. Observation of GFP-positive cells revealed that mutant VACHT reactivity as well as VACHT-WT, is distributed in the cytoplasm and neurite-like structures of NSC-34 cells. Scale bar: 12 μ M.

4.2.3. Generation of *VACHT-WT* and *VACHT-D147N* human mRNAs for protein OE analysis in zebrafish

Taking into account that: (1) OE of mutant VACHT had no apparent effects on protein expression or localization, (2) affected patients carrying *de novo* VACHT mutation manifest positive pyramidal signs *i.e.* axonal neuropathy (Haberlova et al, 2009) and (3) misexpression of *VACHT* underlies both neuronal outgrowth and muscular defects; a potential pathogenic effect of mutant VACHT on MN outgrowth and/or development was subsequently investigated.

Capitalizing once again in the advantages of the zebrafish for the modelling of human motor neuropathies (reviewed in (Kabashi et al, 2011) and (Babin et al, 2014)) and further considering the vast evolutionary conservation of both *SLC18A3* and the D147 residue across species, the effect of WT and VACHT-D147N OE on zebrafish CaP-MN was analysed in detail (see CaP-MN defects as neurologic readout in section 4.1.10.1). The

zebrafish work was performed in collaboration with Dr. Mathias Hammerschmidt and Dr. Heiko Löhr from The Institute for Zoology / Developmental Biology of the University of Cologne (Germany).

Autosomal dominant mutations in human genes leading to pathogenic gain-of-function can be tested in zebrafish by overexpressing the WT or mutant human mRNAs without MO downregulation of the corresponding zebrafish orthologous (Kabashi et al, 2010). Consequently, to generate an *in vivo* model of motor axonal abnormalities underlying the mutated VACHT potential gain-of-function, both *VACHT-WT* and *VACHT-D147N* human mRNAs were injected in one-to-four cell stage embryos in order to achieve ubiquitous protein expression at developmental stages. As described before, (see section 4.1.10.3) cDNAs encoding human *VACHT-WT* and *VACHT-D147N* were subcloned into PCS2+ expression vectors, in order to generate *in vitro* transcribed mRNAs. The quality and integrity of *VACHT* mRNAs was assessed in non-denaturing agarose gels prior to injection experiments (Figure 33A).

On a first attempt, 100pg of the *VACHT-WT* mRNA were injected in zebrafish embryos in order to confirm VACHT OE efficiency. Protein lysates from injected and uninjected larvae were processed via Western blot and probed with a murine/human-reactive VACHT antibody. No band, matching the expected MW of VACHT (~60KDa), was detected thus indicating that the amount of mRNA delivered in the embryos was not sufficient to induce protein OE (data not shown). Fish injections were repeated with double the mRNA amount, thereby 200pg of *VACHT-WT* and *VACHT-D147N* mRNA were injected in the embryos. Total protein lysates were isolated from ~34hpf fish larvae and efficient protein OE was confirmed by Western blot (Figure 33B).

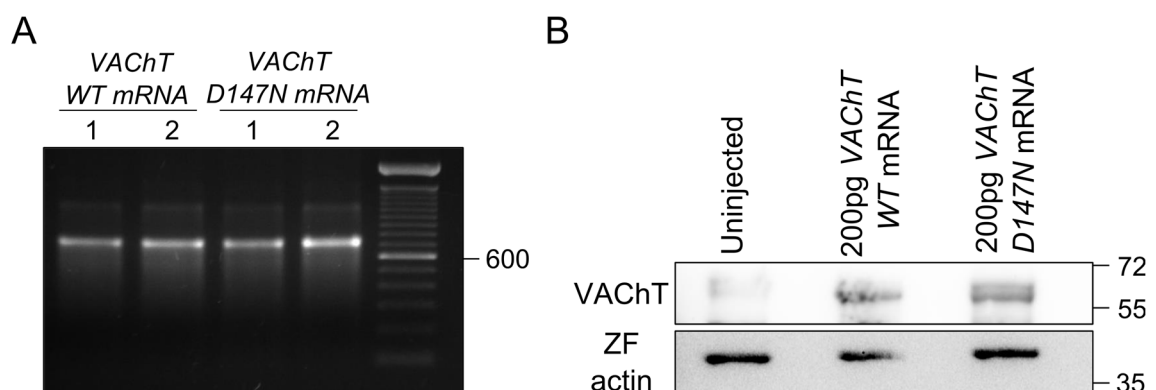


Figure 33. mRNA quality assessment and WB confirmation of *VACHT* mRNAs overexpression. (A) Non-denaturing agarose gel for mRNA quality assessment. 2 μ l of *in vitro*-transcribed *VACHT-WT* and *VACHT-D147N* mRNAs were loaded into agarose gels to visualize mRNA integrity. Neither band smearing nor residual linearized template are observed. Band molecular size (700bp) corresponds to what is expected for single-stranded *VACHT* RNA products. (B) WB confirmation of *VACHT-WT* and *VACHT-D147N* OE. Total protein lysates from ~34hpf larvae injected with 200pg WT and mutant *VACHT* mRNAs demonstrates efficient protein overexpression. Blots were probed with antibodies against human VACHT and zebrafish-specific β -actin.

4.2.3.1. OE of VACHT-WT, as well as VACHT-D147N, increase CaP-MN axonal outgrowth

Zebrafish embryos, generated from the crosses between transgenic males TL/EK-*hb9-GFP* (Flanagan-Steet et al, 2005) and wild-type TL/EK females, injected with 200pg *VACHT-WT* and *VACHT-D147N* mRNAs were processed for visualization of motor axons after ~34hpf. Fish larvae overexpressing VACHT-D147N were morphologically indistinguishable from VACHT-WT larvae. Likewise, no differences were observed between uninjected and injected groups. Znp1 immunostaining of fish larvae did not reveal CaP-MN axonal outgrowth defects, namely abnormal branching or truncations (Figure 34A and B. See also 4.1.10.1). In an effort to corroborate that insufficient VACHT OE do not underlie the absence of MN phenotype, 400pg of *VACHT-WT* and *VACHT-D147N* mRNAs were delivered into the zebrafish embryos in a second set of injections. Similarly, no CaP-MN defects were observed in Znp1-labelled ~34hpf fish larvae (Figure 34C). On this matter, it is important to mention that the absence of evident/gross MN defects was somehow expected, as the rather mild phenotype of the affected patient's progresses slowly during adolescence and adulthood and is not underpinned by neuronal/axonal degeneration at early developmental stages.

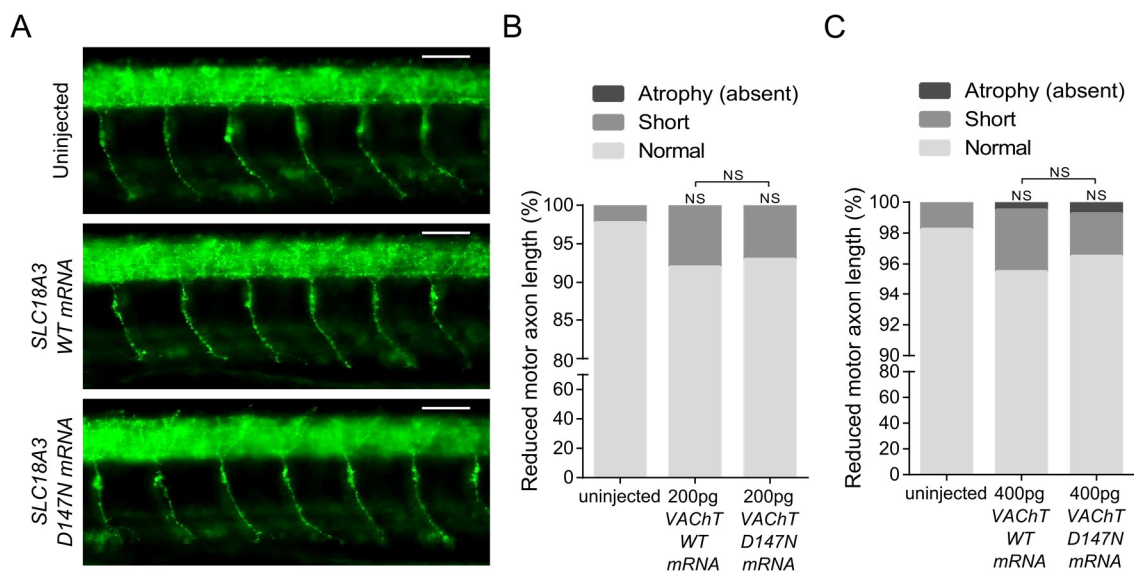


Figure 34. OE of VACHT-WT and VACHT-D147N has no effect on CaP-MN morphology. (A) Lateral views of ~34hpf whole-mount immunostained with Znp1 (synaptotagmin). Representative images of fish larvae injected with 200pg *VACHT* mRNAs. Truncated and/or terminally branched axons were not observed. CaP-MN axons from injected larvae exhibit a straighter ventral trajectory. Notice the uninjected CaP-MN axons arch (more evident in axon 3-6, from left to right). Scale bar: 25 μ m. **(B)** Quantitative analysis of CaP-MN defects demonstrate that injection of 200pg of *VACHT-WT* or *VACHT-D147N* mRNAs is not significantly different from control/uninjected group. Results are presented in percentages of $n \geq 50$ analysed axons representing independent experiments. NS denotes no significant difference ($p > 0.05$ Fisher exact test) **(C)** Quantitative analysis of CaP-MN defects demonstrate that injection of 400pg of *VACHT* WT or mutant mRNA is not significantly different from control/uninjected group. Results are presented in percentages of $n \geq 400$ analysed axons representing independent experiments. NS denotes not significant ($p \geq 0.05$ Chi-square test).

Subsequently, a more detailed analysis of the CaP-MN axonal projections was performed in an effort to detect possible moderate pathogenic effects underlying VAcHt-D147N OE and conclusively confirm/exclude a pathogenic role of the mutation on MN outgrowth. The length of individual axonal projections was calculated for the first five CaP-MN anterior to the end of the yolk extension and measured from the exit point of the spinal cord to the ventral tip of the outgrowing axon (Figure 35B). CaP-MN axons from zebrafish injected with WT and mutant *VAcHt* mRNAs were significantly longer than in the uninjected larvae, a phenomenon not yet documented for VAcHt OE *in vivo*. Nevertheless no statistical differences were observed between WT and mutant injections (Figure 35C). Axon length measurements were further analysed in stratified groups according to their position after the yolk sac, in order to better compare the size of CaP-MN axons, which tend to be shorter towards the posterior end of the spinal cord. Similarly, the average motor axon length of the fourth and fifth CaP-MN after the yolk was significantly longer in fish larvae overexpressing VAcHt, independently of the WT or mutant mRNA injection, in comparison with uninjected animals (Figure 35D). It is important to highlight that in contrast to uninjected CaP-MN axons, VAcHt-WT and mutant axons follow a straighter ventral and dorsal trajectory and, in some cases, the deep arch that characterizes normal axons is less pronounced in VAcHt OE axons. This phenomenon potentially explains the differences in average axon length between uninjected and VAcHt axons.

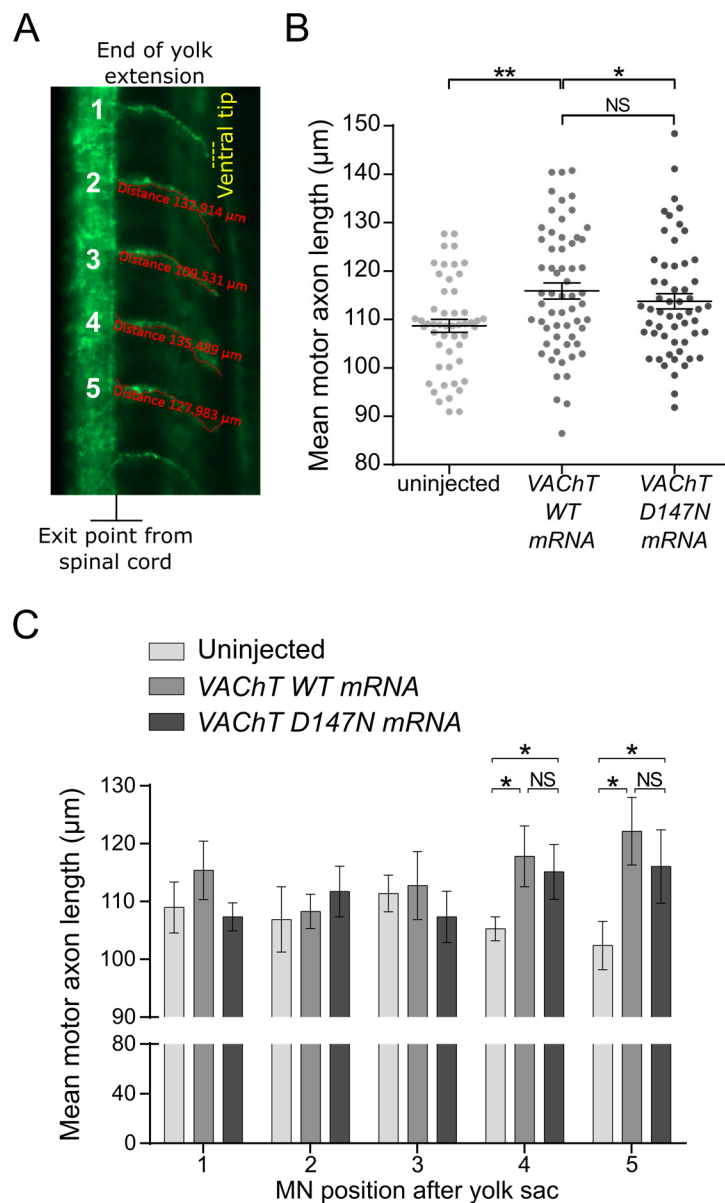


Figure 35. CaP-MN axonal length upon VACHT-WT and VACHT-D147N OE. (A) Scheme shows the first five CaP-MN axonal projections (labelled 1-5) anterior to the end of the yolk extension. Axon length was manually calculated from the exit point of the spinal cord to the ventral tip (indicated in yellow-dotted line). **(B)** Cumulative axonal length measurements. VACHT-WT and mutant axonal projections are longer than uninjected CaP-MN axons. Graph represents individual measurements of $n \geq 35$ axons from $n=8$ embryos. Bars show the mean \pm SEM (error bars). * and ** denotes statistical significance ($p \leq 0.05$ and $p < 0.01$, Student's t-test, respectively). **(C)** Axon measurement are stratified accordingly to their position anterior to the end of the yolk extension. Differences in axonal length between VACHT-injected and uninjected embryos are significant only for the 4th and 5th CaP-MN. Graph represents stratified CaP-MN axon length measurements from $n=8$ embryos. Bars show the mean \pm SEM (error bars). * denotes statistical significance ($p \leq 0.05$, student's t-test).

In summary, the absence of evident morphological MN alterations and the mildly increased CaP-MN axonal length underlying VACHT-WT and VACHT-D147N OE indistinctly indicate that excessive ACh vesicular packing and/or release might result in moderate MN migration defects; which could have an impact at other functional levels, such as the NMJ. In addition,

these results demonstrate that the hypothesized toxic gain-of-function of the *SLC18A3* D147N mutation neither impacts protein expression and subcellular localization nor does it exerts a detrimental MN phenotype at early developmental stages. Nevertheless, the pathogenicity of this mutation cannot be ruled out with base in the experimental evidence provided here. To shed light upon the molecular mechanism underlying VAcHT-D147N expression *in vivo* it is necessary to perform phenotypic analyses at later developmental time points, in accordance with the slow disease progression observed in patients harboring the *SLC18A3 de novo* mutation.

PART II. CHP1 REDUCTION AMELIORATES MOTOR NEURON DEGENERATION IN A ZEBRAFISH MODEL OF SMA

Beyond the novel validated role of *CHP1* in the pathogenesis of ARCA in humans, another feature of CHP1 function which is of relevance in our research group is that it also interacts with the actin-binding and bundling protein Plastin-3 (PLS3) a human protective genetic modifier of SMA (Oprea et al, 2008). Indeed, increased PLS3 levels counteract *SMN1* deficiency in females carrying homozygous deletion of *SMN1* and identical *SMN2* copy numbers as their affected siblings. The protective effect of PLS3 OE has been confirmed *in vitro* and in several SMN-depleted animal models, *i.e.* mouse, zebrafish, nematode and fly, reinforcing the notion that PLS3 is a cross-species modifier of SMA (reviewed in (Wirth et al, 2017)). Recently, a comprehensive study of the protective role of PLS3 in mouse and fish SMA models uncovered endocytosis as a cardinal mechanism disturbed in SMA, hence shedding light onto a novel cellular process underlying disease pathogenesis and opening attractive avenues for pharmacological intervention of this devastating disorder (Hosseinibarkooie et al, 2016).

Despite the significant body of evidence supporting PLS3 as a powerful SMA modifier, the precise molecular mechanism behind its protective role remains hitherto elusive. As a strategy to understand the function of PLS3 in SMA, yeast-two-hybrid (Y2H) analyses were undertaken in order to uncover PLS3 direct-interactome and pinpoint novel interacting proteins and/or potential SMA modifiers (Hosseinibarkooie, 2016 - Thesis). CHP1 was identified as the only direct interacting partner of PLS3 and selected for further analyses since:

- I. CHP1 is involved in molecular processes disturbed in SMA, such as regulation of endocytosis and synaptic transmission proteins (Baumgartel & Mansuy, 2012), microtubule dynamics (Andrade et al, 2004b; Timm et al, 1999) and membrane trafficking (Barroso et al, 1996; Di Sole et al, 2012).
- II. Similar to the SMA modifier NCALD, CHP1 is a calcium sensing protein (Di Sole et al, 2012; Riessland et al, 2017).
- III. Our preliminary functional analyses showed that CHP1 expression is elevated in spinal cord and brain of severely affected SMA mice. Moreover, CHP1 downregulation restores neurite outgrowth and impaired endocytosis in *Smn1*-depleted NSC-34 cells. (Janzen, Mendoza-Ferreira et al, manuscript in preparation).

4.3. MO-mediated downregulation of *chp1* restores CaP-MN axonal outgrowth in *smn* zebrafish morphants

As an initial strategy to test the beneficial effect of CHP1 reduction on the SMA phenotype *in vivo*, MO-mediated downregulation of *chp1* and *smn*, alone or in combination, was performed in zebrafish. Conveniently, the consequences of *Smn* depletion on motor CaP-MN, *i.e.* axonal truncations and increased branching, were known beforehand since a SMA zebrafish model based on the MO-mediated model published by (Oprea et al, 2008) was previously established in our laboratory (Riessland et al, 2017). As described before, MO injections were performed in one-to-four cell stage embryos, which were allowed to grow for ~34hpf for subsequent CaP-MN morphological analyses. To better visualize motor axons, zebrafish embryos generated from the crosses between transgenic males TL/EK-*hb9*-GFP (Flanagan-Steet et al, 2005) and wild-type TL/EK females were used for injections. In complement, immunostaining with zebrafish Znp1 antibody was performed for visualization of axonal tracts.

An optimal *smn* MO dosage of 2ng was identified to mimic the SMA pathogenesis in zebrafish, without compromising larvae survival (HosseiniBarkooie et al, 2016; Riessland et al, 2017). Regarding the *chp1* MO, it is important to clarify that the MO used for these experiments differs from the *chp1* MO used for the characterization studies of the CHP1 as ARCA-causative, as they were purchased in different years and they come from a different batch.

Prior to CaP-MN analyses, the KD efficiency of both MOs, alone or in combination, was determined via Western blot. Notably, injection of 1ng *chp1*-MO did not lead to detectable protein downregulation (data not shown), in contrast with injections of the same MO dosage from a different batch (see Figure 26). Nevertheless, a dosage of 2ng *chp1* MO efficiently reduced Chp1 expression alone or in combination with the *smn* MO. As expected, injection of 2ng *smn* MO led to efficient *Smn* downregulation *per se* or when co-injected with 2ng *chp1* MO (Figure 36). Protein immunodetection was performed in separate rounds, as the incubation with the Chp1 antibody caused unspecific immunoreactivity and interfered with *Smn* detection. For this reason, ~34hpf zebrafish protein lysates were loaded into different gels, although ran and processed in parallel, to detect Chp1 and *Smn* separately. The CHP1 antibody used to probe this blots was specific for human and mouse (rabbit α -CHP1 from Thermo Scientific, see section 6.1.5), although the antibody epitope is highly complementary to the zebrafish protein. Interestingly, Chp1 immunodetection with this antibody revealed a double-band pattern, most likely equivalent to the myristoylated form of the protein (Andrade et al, 2004b).

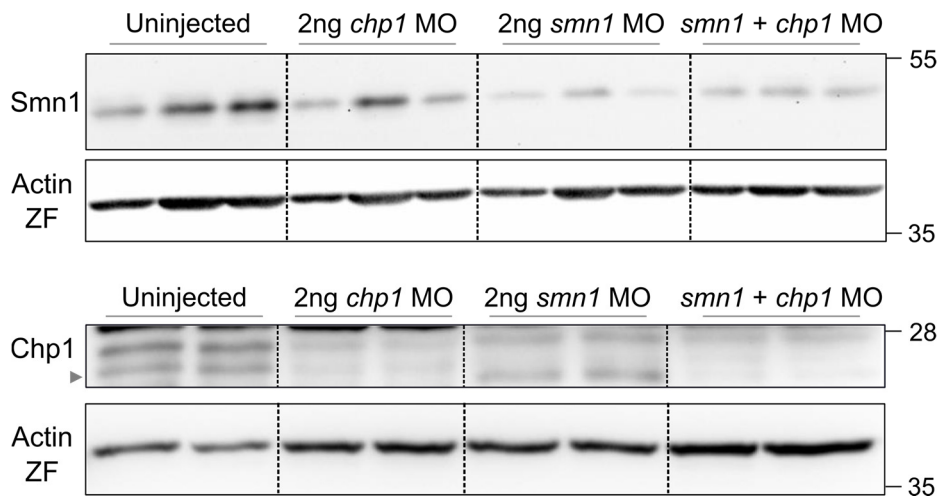


Figure 36. Injection of *smn* and *chp1* MOs, alone or in combination, efficiently reduce protein expression. Western blots from total protein lysates from ~34hpf uninjected or MO-injected larvae. Proteins were isolated in a final volume of 50 μ L from which ~10 μ L were necessary to load 15 μ g of protein, therefore protein samples for Chp1 detection were not processed in triplicates. WB probing with antibodies against Smn (upper panel) and Chp1 (lower panel) demonstrate efficient protein downregulation upon MO or double MO injection. Double Chp1 band corresponds to myristoylated Chp1 form. ZF actin was used as loading control.

As expected, and in line with other studies (HosseiniBarkoie et al, 2016; McWhorter et al, 2003; Riessland et al, 2017), injection of 2ng *smn*-MO led to severe CaP-MN axon defects. More exactly, ~30% of the analyzed motor axons did not fully project into the ventral muscle (truncated axons) whilst ~10% were completely absent (atrophy). Moreover, increased terminal branching was observed in ~50% of all observed axonal projections (Figure 37). Recapitulating prior results, injection of 2ng *chp1*-MO resulted in a moderate CaP-MN phenotype in comparison with *smn* morphants. In detail, ~15% of CaP-MN axons were truncated and ~20% exhibited increased, but not severe, terminal branching (Figure 37. See also Figure 29). Downregulation of *chp1* in the context of *smn*-depletion, *i.e.* co-injection of *chp1* and *smn* MOs, improved axonal truncations by ~23% compared to *smn* MO alone. Most likely as a secondary effect of the improvement of axonal truncations, CaP-MN terminal branching was also ameliorated by ~20% upon double MO co-injection (Figure 37).

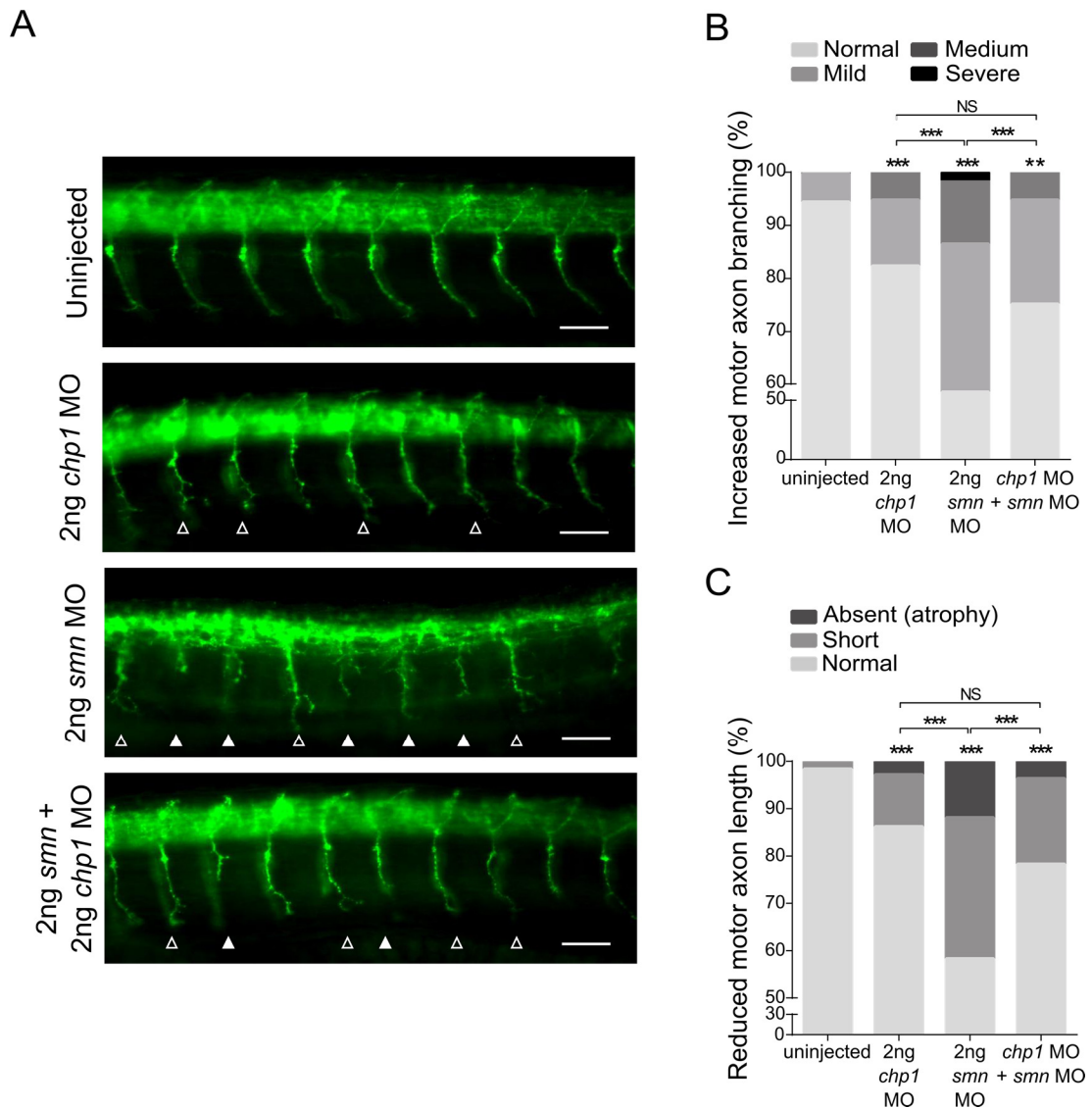


Figure 37. Chp1 downregulation ameliorates CaP-MN defects in *Smn*-depleted zebrafish. (A) Lateral views of whole-mount embryos immunostained with Znp1 (synaptotagmin). Truncated and absent motor axons are indicated with solid arrowheads and terminally-branched axons with open arrowheads. *smn*-MO motor axons show increased terminal branching and severe truncations. *chp1*-MO motor axons show mild terminal branching (see also **Figure 29**). Scale bar: 25 μ m. **(B)** Quantitative analyses of CaP-MN demonstrates that co-injection of *smn* and *chp1* MOs ameliorate increased motor axon branching of *smn*-morphants. Results are presented in percentages from $n \geq 150$ analysed axons representing 3 independent experiments. ** and *** denote statistical significance ($p < 0.01$, $p < 0.001$, respectively. Chi-square test). **(C)** Quantitative analyses of CaP-MN demonstrate that co-injection of *smn* and *chp1* MOs ameliorate motor axon truncations of *smn*-morphants. Results are presented in percentages from $n \geq 150$ analysed axons representing 3 independent experiments. *** denotes statistical significance ($p < 0.001$ Chi-square test).

4.4. Chp1 is expressed in zebrafish MNs

In addition to the foregoing results, immunostainings of ~34hpf larvae with a specific zebrafish Chp1 antibody were performed aiming to corroborate the expression of

endogenous Chp1 in primary MNs. This subset of MNs not only include the aforementioned CaP-MNs, which innervate the ventral trunk musculature, but also the MiP-MNs (Middle Primary Motor Neurons, innervating the dorsal trunk musculature) and the RoP-MNs (Rostral Primary Motor Neurons that innervate muscles fibers in between) (Lewis & Eisen, 2003). As shown in (Figure 38) Chp1 immunoreactivity was detected in the cell bodies of spinal cord MNs, confirming that Chp1 is expressed in MNs at early developmental zebrafish stages. Although Chp1 reactivity for each specific population was not assessed in combination with antibodies against MNs-subsets markers, the expression of Chp1 in primary MNs further strength the results obtained upon co-injection of both *smn* and *chp1* MOs. This finding demonstrate that, similar to Smn (McWhorter et al, 2003), Chp1 is expressed in MNs and is thus highly relevant to SMA pathogenesis.

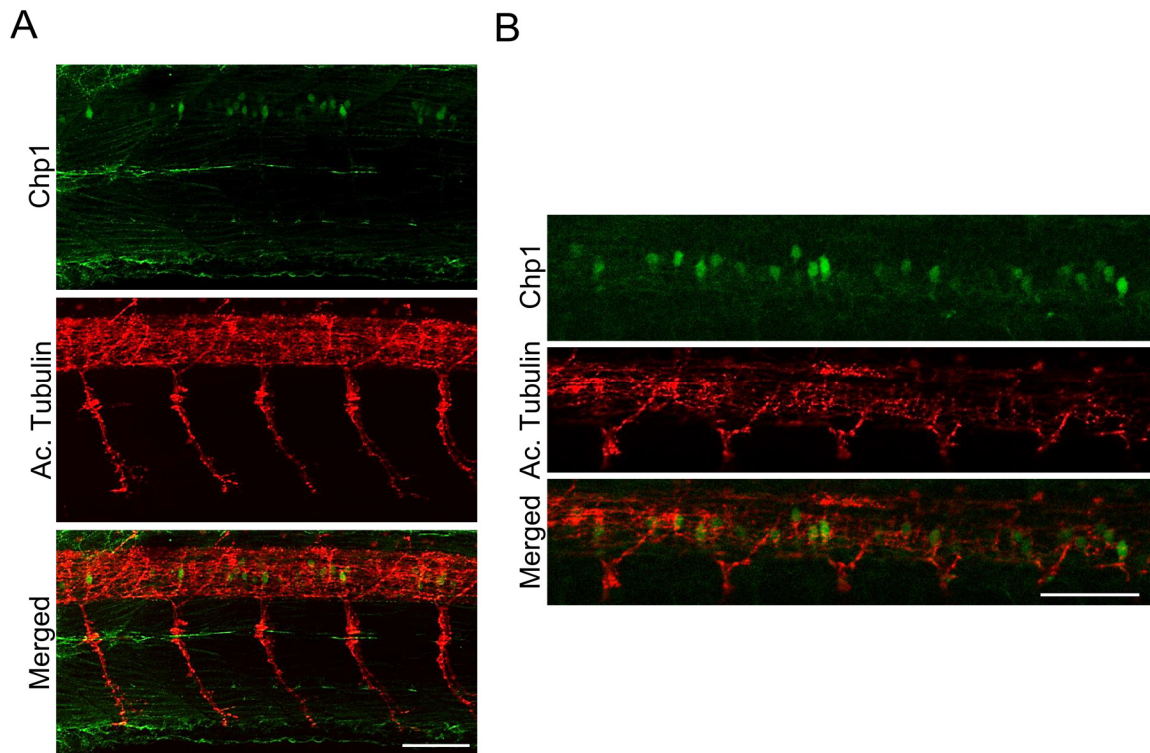


Figure 38. Chp1 is expressed in zebrafish spinal cord MNs at larvae-developmental stage. Lateral views of whole-mount ~34hpf embryos immunostained with Chp1 (in green) and acetylated tubulin (in red). **(A)** Representative images show Chp1 reactivity in MNs cell bodies in the spinal cord. **(B)** Spinal cord zoom-in for better appreciation of Chp1 staining. Scale bar of images: 50 μ m.

Altogether, these results demonstrate that Chp1 reduction ameliorates the SMA phenotype (axonal outgrowth defects) in zebrafish and strongly suggest that CHP1, similar to the other modifiers PLS3 and NCALD (Hosseini-barkoobie et al, 2016; Riessland et al, 2017), is a cross-species modulator of the SMA pathogenesis.

5. DISCUSSION

The genetic studies undertaken in this thesis have led to the identification and validation of novel disease-causative mutations, genotype-phenotype associations and potential genetic modifiers for inherited NMDs. In the following pages, the most important findings of this project and their contribution to both genetic diagnostics and the better understanding of disease pathomechanisms will be outlined.

5.1. Biallelic mutation of *CHP1* expands the number of genes causing ARCA

Following a combination of WES and linkage analysis in a consanguineous family, we identified the first biallelic mutation in *CHP1* in two patients with ARCA. The various functional analyses conducted to assess the consequences of the *CHP1*-K19del mutation have provided conclusive evidence supporting biallelic *CHP1* mutation as ARCA-causative as follows:

- I. The hypomorphic *CHP1*-K19del mutation severely affects protein solubility, subcellular localization and conformational folding. Together, these defects underpin mutant *CHP1* proneness to aggregation and concomitant protein instability.
- II. *CHP1* deficiency causes ataxia across species. Resembling the ataxia pathogenesis in mice and humans (this thesis and (Liu et al, 2013)), MO-mediated *chp1* reduction in zebrafish causes CaP-MN defects, cerebellar hypoplasia and marked ataxic trunk movements. These defects were ameliorated by MO co-injection with WT but not mutant *CHP1* RNA, confirming both the specificity of the *chp1*-depletion phenotype and the pathogenicity of the *CHP1*-K19del mutation *in vivo*.
- III. Expression of mutant *CHP1* impairs NHE1 membrane expression. Given that Nhe1 mistargeting and reduction underlie cerebellar degeneration and ataxia in humans and mouse models of *Chp1* downregulation and *Nhe1* KO (Bell et al, 1999; Cox et al, 1997; Guissart et al, 2015; Liu et al, 2013), we postulate that *CHP1* mutation causes ataxia in humans in a NHE1-dependent mechanism (see 5.1.5).

Altogether, our findings have indeed uncovered *CHP1* as a novel ARCA gene, expanding the number of genetic loci causative of ARCA. Moreover, *CHP1* functional studies and the novel implication of *NHE1* in ARCA pathogenesis have shed light onto a molecular mechanism poorly explored in the field of recessive ataxias: pH homeostasis deregulation as cause of axonal degeneration. The following sub-sections will emphasize in the most impactful insights of this project, their correlation with the state-of-the-art knowledge, and the potential molecular mechanism behind *CHP1* and its implication in ataxia pathogenesis.

5.1.1. *CHP1* variants are scarce

Despite the fact that *CHP1* exome coverage was further improved by re-sequencing of exons 2 and 6, no other *CHP1* mutations -including splice site variants- were found. Moreover, neither focused screening for *CHP1* mutations in two large ARCA and NMD cohorts, equivalent to almost 1000 patients, nor GeneMatcher interrogation yielded any positive findings. The scarcity of *CHP1* mutations –even heterozygous- is in line with the rather reduced tolerability of the gene for missense variation, as found in the ExAC database, a compendium of more than 60,000 reference exomes (Lek et al, 2016). Particularly, *CHP1* has a positive ExAC Z-score of 2.66 which, according to ExAC constraints, indicates that the gene has fewer variants than expected in the reference population (negative Z scores are given to genes that had more variants than expected). This intolerability is not particularly surprising considering that *CHP1* is highly conserved across evolution (99% amino acid identity in mouse, 92% in zebrafish) and that the *CHP1*-K19del mutation was scored as one of the most conserved residues among all the WES variants identified in the *CHP1* family.

It must be also taken into consideration that during the course of this project, the search for *CHP1* variants concentrated on coding sequences and intronic splice site intervals (exon-intron boundaries) and therefore other types of genetic variation such as copy number variations (CNVs), large indels (insertions-deletions) and mutations in regulatory untranslated regions (UTRs and core promoter) were automatically excluded. To surpass these limitations it is necessary to expand the search of *CHP1* variants towards these unexplored genomic regions, or the whole genome, in order to potentially uncover additional mutations in *CHP1*.

5.1.2. Is *CHP1*-K19del aggregation proneness a disease mechanism?

SEC experiments confirmed that *CHP1*-K19del adopts abnormal protein conformations, which have a direct impact on protein solubility and therefore protein availability. Moreover, subcellular fractionation experiments demonstrated that approximately 50% of the mutant *CHP1* protein is re-localized to the insoluble fractions. These impairments critically influence the regulatory role of *CHP1* on NHE1, which relies on functional protein availability and more importantly, on precise cytoplasmic *CHP1* localization (Liu et al, 2013; Matsushita et al, 2007; Matsushita et al, 2011).

From this perspective, it was conjectured that altered expression of mutant *CHP1* could have an effect on protein subcellular localization. Consistently, it was observed that OE of *CHP1*-K19del-GFP led to massive protein aggregation in both neuron and non-neuron-like

cells. This finding was not entirely surprising considering that protein aggregation propensity is governed by three main determinants: the chemical properties of the amino acid sequence, conformational stability (given by solubility) and cellular concentration (Ciryam et al, 2013; Hipp et al, 2014). In our experimental set-up for CHP1 subcellular localization analyses, most, if not all, the conditions for aggregation took place: altered solubility and conformation as well as supersaturation. Thus, in this particular context, aggregation must be considered as a reliable readout of abnormal protein folding rather than a pathogenic disease mechanism. Additional analyses of patients-derived fibroblasts or other families carrying *CHP1* mutations would be necessary to clarify the potential contribution of toxic CHP1 aggregates to ARCA neuropathogenesis.

Nevertheless, it is important to consider that abnormal folding and aggregation are inherent to numerous neurodegenerative disorders (Ross & Poirier, 2004; Taylor et al, 2002), including HCAs (see section 2.4.1). Although, the vast majority of HCAs underlying toxic aggregation result from dominant gain-of-function mutations (see section 2.4.1.1), recessive mutations leading to inefficient folding and aggregation underlie the pathogenesis of the ARCA entity Marinesco-Sjögren Syndrome (MSS). Splice site or missense mutations in *SIL1* (SIL1-Like Protein Endoplasmic Reticulum Chaperone) the causative gene of MSS, have been reported to cause either protein misfolding or absence of important functional domains (Anttonen et al, 2005; Senderek et al, 2005). Particularly, OE of the *SIL1* mutation L457P causes aggregation in transiently transfected COS-1 cells (Anttonen et al, 2008). Moreover, disruption of mouse *Sil1* causes Purkinje ER stress, accumulation of misfolded proteins and neuronal loss (Zhao et al, 2005).

5.1.3. Zebrafish model of *chp1* downregulation closely recapitulates the phenotype of ARCA-affected patients

The affected siblings of this study manifest a complex spastic ataxia phenotype, underpinned by both cerebellar and motor neuron defects. These defects were recapitulated to a great extent in the zebrafish *chp1* downregulation model generated in this study.

Firstly, *chp1* morphants exhibited alterations in CaP-MNs axonal outgrowth, namely truncations and terminal branching. This finding not only validates CHP1 reduction as the cause of motor neuropathy in ARCA-affected siblings but also confirms that MNs are susceptible to CHP1 downregulation *in vivo*. The latter is in fact, the first report of MN susceptibility to CHP1, and potentially NHE1, misbalance.

Secondly, *chp1* downregulation in zebrafish led to cerebellar hypoplasia, confirming that CHP1 depletion causes ataxia in humans and across species. Interestingly, throughout cerebellar morphology analyses of *chp1* morphants, the trochlear decussation, a subgroup of cranial motor axons which innervate extraocular muscles in zebrafish (Ingold et al, 2015), appeared visible only in severe cases of cerebellar hypoplasia. A plausible explanation for this phenomenon is that severe loss of cerebellar structure, referred by others as mid hindbrain compression (Kasher et al, 2011), facilitates the observation of axonal tracts, hidden otherwise in normal conditions. Although these axons were not considered for further analysis, the functional implication of trochlear tracts in disease pathogenesis cannot be categorically excluded, considering that some ARCA patients, including the probands of this study, manifest slow ocular movements (Table 6). Moreover, the staining of cerebellar axons with the α -acetylated tubulin antibody revealed an additional neuronal population; the optic tecta. Reduction of the optic tecta is considered a complementary readout of neuronal loss in zebrafish and has been described in combination with cerebellar atrophy in other ARCA zebrafish models (Borck et al, 2015; Margolin et al, 2013). Even though this phenotype was not further quantified, the fact that it was observed in combination with other surrogates of neuronal damage strengthens a more general -not cerebellar specific- role of CHP1 in axonal integrity.

Thirdly, *chp1*-depleted fish larvae exhibited increased spontaneous contractions and spastic-like trunk movements, confirming that CHP1 deficiency causes movement defects compatible with the motoric phenotype of the affected siblings. In this context it is important to highlight that this type of involuntary and fast body movements, can be observed in larval zebrafish stages as surrogates of epilepsy and ataxia phenotypes (Kalueff et al, 2013) and, interestingly, depletion of *Nhe1* also results in ataxia and epileptic-like episodes in mice (Bell et al, 1999; Gu et al, 2001). Therefore, the observed defects in movement strongly suggest that *Nhe1* could be concomitantly perturbed in *chp1* morphants; although protein reduction of *Nhe1* was not confirmed by Western blot.

The specificity of the *chp1* downregulation phenotype in zebrafish was confirmed by co-injection of *CHP1-WT* mRNA with *chp1* MO and the subsequent amelioration of CaP-MN, cerebellar and movement defects, however rescue levels did not reached control levels. One explanation for this is the mosaicism of MO and synthetic capped mRNAs co-injection (Beattie et al, 2007; Bill et al, 2009) and the very limited time of mRNA expression (Pyati et al, 2007) which compromise the analysis of late severe phenotypes; such as the cerebellar hypoplasia. Furthermore, phenotypic rescues, in most cases, do not lead to complete developmental rescue, as mRNA injections can produce phenotypes like those expected from mis/overexpression due to elevated, untimed or ectopic protein synthesis (Angerer & Angerer, 2004). In our zebrafish experiments, the effect of sole mRNA *CHP1-WT* and

CHP1-K19del OE and their effect on the selected neurological readouts was observed and found to be rather negligible. Nevertheless, misexpression of *CHP1* RNAs at critical embryo developmental time points (the first 24 hours), potentially masking the extent of phenotype reversion, is a possibility that cannot be ruled out. Despite incomplete rescue levels, the fact that mutant *CHP1 mRNA* co-injection failed to ameliorate all analyzed readouts in the zebrafish, validates the negative effect of K19del on *CHP1* expression and/or function and further support the specificity of *chp1* MO-associated phenotypes.

The cerebellar and motoric phenotypes observed in this study, are in congruence with other ARCA genes/mutations modelled in zebrafish (Akizu et al, 2015; Borck et al, 2015; Burns et al, 2014; Kawahara & Hayashi, 2016; Mahmood et al, 2013; Margolin et al, 2013) which have correlated cerebellar abnormalities in humans with abnormal cerebellar development and/or motoric impairments in fish larvae. These studies, in addition to ours, suggest conservation of crucial genes for the development of the cerebellum of zebrafish, which regardless of their different cellular roles, might converge into similar functional pathways. In this respect, the easily tractable phenotypes of the ataxia model generated in this study, represent a promising system for high-throughput screenings of ataxia modifiers and drug targets.

5.1.4. Incomplete phenotypic translation from fish and mouse to human

The neuropathogenesis of *chp1*-depleted zebrafish, *Chp1* KO and *Nhe1*-deficient mouse models and patients carrying either *CHP1* or *NHE1* mutations is interconnected through one common denominator: cerebellar degeneration (Bell et al, 1999; Cox et al, 1997; Guissart et al, 2015; Liu et al, 2013). Altogether, the phenotypes of fish, mouse and humans ratify Purkinje neurons degeneration and concomitant ataxia as the central pathogenic feature underpinning the malfunction of *CHP1* and/or *NHE1* and strongly suggest that Purkinje cells are extremely sensitive to functional defects of these proteins.

Interestingly, the pathogenesis of *CHP1* and *NHE1* depletion seems to associate with additional neuropathological features of variable presentation across species, which seem to underlie the involvement of other neuronal populations, besides Purkinje cells, in disease pathogenesis. For instance, patients harboring *CHP1* mutation exhibit motor neuropathy signs, which were recapitulated in the zebrafish model of *Chp1*-depletion. Similarly, LINKS patients carrying *NHE1* loss-of-function mutation present lower and upper limb areflexia, suggestive of peripheral motor neuropathy (Guissart et al, 2015). On the contrary, the mouse models of *Chp1* KD and *Nhe1* KO do not exhibit motor neuropathy signs, or these were not reported/analyzed in the publications (Bell et al, 1999; Cox et al, 1997; Guissart et

al, 2015; Liu et al, 2013). We conjecture, in agreement with others, that other neuronal populations (e.g. MNs) are variably sensitive to CHP1/NHE1 dysfunction and that this differential proneness underpin the different pathogenic outcomes across species. These phenotypic discrepancies and potential compensatory mechanisms of CHP1-NHE1 imbalance are discussed hereafter.

In contrast with the clinical picture of patients harboring the *CHP1* mutation, *NHE1* loss-of-function mutation was presumptively associated with hearing loss, despite that neither *Nhe1* nor *Chp1* (*vacillator*) mouse models presented deafness (Bell et al, 1999; Cox et al, 1997; Guissart et al, 2015; Liu et al, 2013). The authors who first reported *NHE1* mutations as LINKS-causative, correlated patient's deafness with the fact that NHE1 is highly expressed and important for pH homeostasis maintenance in the endolymphatic sac, which is essential for the normal hearing function (Guissart et al, 2015; Son et al, 2009). Most intriguingly, depletion of mouse *Nhe1* results in ataxia and epilepsy (Bell et al, 1999; Gu et al, 2001), however neither the *vacillator* mouse nor patients carrying *CHP1* or *NHE1* mutations manifested convulsive seizures.

Tissue-specific expression of other CHP or NHE proteins could underlie phenotypic compensations, further explaining the incomplete translation from animal models to humans and the variability among human symptoms. In this respect, balancing mechanisms among CHP proteins were hypothesized in the work from Liu and collaborators (Liu et al, 2013) to explain the phenotypic differences between *Chp1* and *Nhe1* mouse models; that is, the absence of epileptic episodes in the *Chp1 vacillator* animals. Liu and collaborators suggested that the expression of CHP3 (Tescalcin) in non-Purkinje cells, contrariwise to CHP1, could compensate for NHE1 deficiency in a subset of neurons in the adult brain. Interestingly, *Chp3* transcripts are present in the granular layer of the cerebellum (www.brain-map.org), a population of cells relevant for the pathology of syndromic ataxia-epilepsy (Ivanov et al, 2004; Liu et al, 2013; Signorini et al, 1997). Other phenotypic compensatory possibilities could stem from the fact that both CHP1 and CHP2 can bind and target NHE1 to membrane compartments, however CHP2 expression is mostly restricted to the intestine and tumor cells (Ben Ammar et al, 2006; Pang et al, 2002). Vice versa, CHP1 also assists NHE3 targeting to the membrane, yet the latter alternates between cellular and organelle membranes and it is almost exclusively found in absorptive cells of the intestine and, to a lesser extent, in the colon, gall bladder, renal proximal tubules, epididymis, ovary and prostate, among others tissues (Brett et al, 2005; Donowitz et al, 2013; Hoogerwerf et al, 1996). *Nhe3* transcripts were reported in rat Purkinje cells, nonetheless no functional role for this transporter has been delineated in this or other neuronal populations (Ma & Haddad, 1997).

In consideration of the foregoing, we postulate that differential NHE1 dosages might tune different syndromic ataxia presentations in humans. In other words, reduced NHE1 will certainly lead to ataxia, but remaining levels might be sufficient to prevent epilepsy in LINKS patients or epilepsy and deafness in CHP1 patients. Notably, the CHP1-K19del mutation reduces, but does not abolish CHP1 expression, thereby NHE1 membrane targeting is diminished, but not fully compromised.

5.1.5. Intracellular pH (pHi) imbalance and neuronal degeneration. A potential molecular mechanism underlying CHP1-related ARCA pathogenesis

A unifying mechanism for disease pathogenesis that is common to all the ARCAs likely does not exist. The reasons for how perturbations of a plethora of different proteins, involved in very different pathways, compromise cerebellar integrity is hitherto unknown. Nevertheless, our own results and the findings of others, strongly suggest that Purkinje cells are particularly sensitive to CHP1-NHE1 misbalance and therefore to pH homeostasis deregulation (Bell et al, 1999; Guissart et al, 2015; Liu et al, 2013). In spite of some studies linking NHE1 disruption with axonal and neurite degeneration (Guissart et al, 2015; Sin et al, 2009), the precise mechanism by which NHE1 causes such impairment is not yet understood. It has been suggested that modulation of intra and extracellular pH by the NHE transporters could play an important role in synaptic activity and axonal homeostasis (Diering et al, 2011; Dietrich & Morad, 2010). We agree on this vision, and thus the potential interconnection between CHP1, NHE1 and ARCA pathogenesis will be discussed within this frame in the following paragraphs.

Due to the pH-sensitivity of various neuronal membrane proteins, such as channels, receptors and ATP-dependent pumps, the excitability of neurons is especially sensitive to slight changes in both intracellular and extracellular pH (Sinning & Hubner, 2013). Altogether these proteins modulate essential neuronal processes such as: (1) loading of synaptic vesicles with neurotransmitters and neuronal responsiveness to neurotransmitters, (2) threshold setting for firing action potentials and resting membrane potential and, (3) duration of the action potential and length of the refractory period (membrane repolarization for a subsequent stimulus) (Ruffin et al, 2014). The activity of NHE1 –and hence of its modulator CHP1- in the restoring of pHi after an acidic load (e.g. after firing an action potential) is crucial for all the aforementioned neuronal activities. Evidence of the latter has come from the observation of hippocampal pyramidal (CA1) neurons from *Nhe1*-null mice, which exhibit a significantly lower steady-state pHi (acidification) than wild-type neurons and a slower recovery from induced acid loads. In this neurons, complete NHE1 depletion results in a complex neuronal phenotype with increased Na⁺-current density *i.e* neuron

hyperexcitability (explaining seizures in this mouse model) as well as neuronal degeneration and loss (Gu et al, 2001; Xia et al, 2003; Yao et al, 1999). Nevertheless, the link between pH and neuronal excitability is not that simple, as in other neuronal populations inhibition of NHE1 leads to alkalization and hypoexcitability. These differences are modulated by differential expression of transporters, receptors, and channels which govern neuron excitability in different cell populations (Ruffin et al, 2014).

An example of differential responsiveness to acidic imbalance are the GABAergic cerebellar granule cells (CGCs). Indeed, inhibition of NHE activity with amiloride in CGCs, alters pH buffering at the presynaptic cleft, consistent with reduced acidification, causing decreased spontaneous release of GABAergic vesicles. Moreover, at the postsynaptic level, NHE inhibition reduces GABA_A receptor responses via alkalization of the extracellular pH (Dietrich & Morad, 2010). This study strongly suggest that NHE1 activity, the most abundant neuronal NHE isoform, may affect not only presynaptic GABAergic vesicle release by increasing pHi but also GABAergic neurotransmission by modulating extracellular pH (Dietrich & Morad, 2010; Sinning & Hubner, 2013). The cerebellar Purkinje cells are also GABAergic neurons, and therefore potentially sensitive to NHE1 misregulation.

A hallmark of the physiology of Purkinje neurons, is that they are highly active at the resting state. In other words, they sustain a remarkably regular firing, which does not require any excitatory input as it arises from a unique group of ion channels expressed by these cells (Khaliq et al, 2003; Raman & Bean, 1999). Electrophysiological reduction of this firing pace has been observed in various mouse models that exhibit behavioral ataxia, and most importantly, it appears to precede Purkinje neurons loss (Hansen et al, 2013; Mark et al, 2015; Sekerkova et al, 2013; Tsai et al, 2012; Walter et al, 2006). Furthermore, it has been shown that reduced pacemaking affects inhibitory Purkinje outputs to the deep cerebellar nuclei and the vestibular nucleus, which ultimately establish excitatory synapses with the premotor cortex (UMNs) (Heiney et al, 2014; Meera et al, 2016; Scoles et al, 2017). As NHE1 inhibition potentially alters GABAergic neurotransmission, it is very plausible to speculate that CHP1 mutations altering the membrane targeting and hence function of NHE1, could result in ataxia phenotypes in human and across species through a mechanism of Purkinje degeneration similar to the one described here (Figure 39).

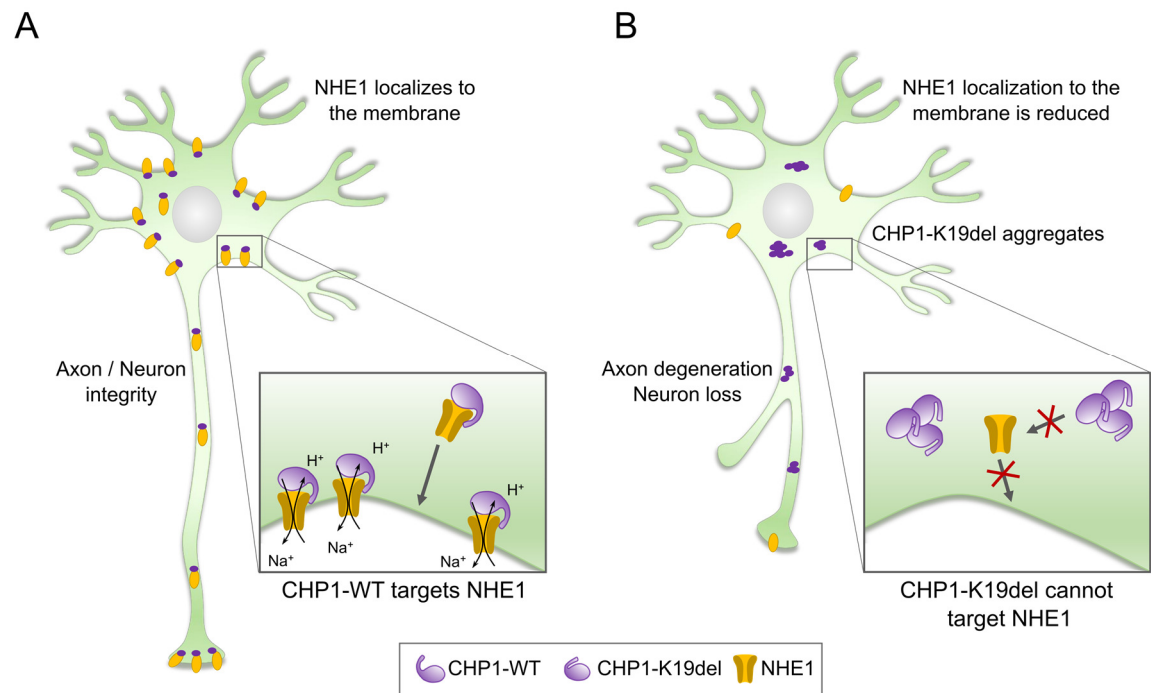


Figure 39. CHP1-mediated NHE1 deregulation causes ataxia. Diagrammatic representation of the molecular pathogenic mechanism for the CHP1-K19del mutation. **(A)** NHE1 is properly targeted to the membrane by CHP1, thus maintaining axonal pH homeostasis and preserving axonal integrity. **(B)** Mutant CHP1 is misfolded and aggregate. Diminished CHP1 levels are insufficient to target NHE1 to the cellular membrane. NHE1 deficiency in axonal membranes alters pH homeostasis thus leading to altered neurotransmission and concomitant axonal degeneration and loss.

5.1.6. A second WES variant potentially explains endocrine dysfunction in female proband of the CHP1 family

The presentation of ataxic syndromes together with reproductive endocrine dysfunction has been described in numerous studies (Abs et al, 1990; De Michele et al, 1993; Holmes, 1908; Lowenthal et al, 1979; Synofzik et al, 1993; Tarnutzer et al, 2015), nonetheless the genetic cause of this combination remains unclear; while there is very little or no association between causative-ARCA genes and hypogonadotropic conditions. The female proband we describe in this study presented with ovarian failure, yet neither *Chp1 vacillator* nor *Nhe1*-depleted mouse females have been reported as infertile.

In this regard, we hypothesize that a second independent mutation might account for this defect. Indeed, WES revealed a pathogenic variant (c.859 C>T, p.G258E) in the Basonuclin 1 gene (*BNC1*) which encodes a protein, presumably a transcription factor, with a very restricted expression in reproductive germ cells (Vanhoutteghem et al, 2016) and an essential function in oogenesis and spermatogenesis (Ma et al, 2006; Zhang et al, 2012). *Bnc-1* null mice are differentially affected by gender; with females presenting complete infertility due to egg misdevelopment and pre-implantation failure while the subfertile males

exhibit smaller testes, loss of germ cells and reduced sperm motility (Ma et al, 2006; Zhang et al, 2012). Interestingly, a pathogenic copy number variation (CNV) (15q25.2 Position: chr15: 83213963–84811815) including the *BNC1* gene, was recently detected in a large retrospective study of spontaneous premature ovarian failure (POF) and associated to POF susceptibility (Tsuiko et al, 2016). Overall, *BNC1* role in the ovary potentially explains the combination of hypergonadotropic hypogonadism with ataxia further clarifying the pathogenic landscape with regards to the *CHP1* family.

5.2. Functional characterization of a *de novo* mutation in *SLC18A3* (VAcHT) in a family with distal motor neuropathy

5.2.1. Is the VAcHT-D147N mutation causative of dHMN?

Within the scope of this project we conducted functional analyses to address the consequences of the VAcHT-D147N mutation in MN development, since the clinical presentation of the affected individuals was consistent with dHMN (Haberlova et al, 2009). Both *in vitro* and *in vivo* analyses performed to characterize the pathogenicity of this VAcHT mutation did not reveal significant differences between the OE phenotypes of WT and mutant VAcHT. Nevertheless, these findings are not sufficient to exclude the pathogenicity of this mutation. Complementary analyses of other zebrafish readouts, discussed in the following section, might be necessary in order to conclusively confirm the detrimental effect of the VAcHT mutation, either in the context of MN development or independently of MN pathology.

The CaP-MN defects (curved axonal projections) observed upon VAcHT-WT and VAcHT-D147N OE experiments are very similar to the CaP-MN axonal impairments underpinning the neuropathogenesis of a zebrafish model of *Ache* (Acetylcholine esterase) depletion (Behra et al, 2002; Downes & Granato, 2004). This finding could be related to the fact that both VAcHT upregulation and AChE downregulation lead to accumulation of ACh in the synaptic cleft (Behra et al, 2002; Downes & Granato, 2004; Janickova et al, 2017; Li et al, 2003; Nagy & Aubert, 2012; Sugita et al, 2016). More precisely, loss-of-function mutation in *Ache* leads to progressive increase of ACh and causes abnormal motor axon navigation – similar to what we observed upon VAcHT OE-, aberrant nicotinic receptors clustering, muscle fibers defects and impaired NMJ development (Behra et al, 2002; Downes & Granato, 2004). These findings demonstrate that excessive ACh accumulation can lead to CaP-MN defects which, although mild, underlie severe disturbances at the muscle and/or NMJ levels. Contrasting these findings with our results, it seems feasible that the CaP-MN

analyses undertaken in this work were not robust enough to ascertain slight differences between VACHT-WT and VACHT-D147N OE in the zebrafish larvae. Most importantly, we did not observe other phenotypic surrogates, such as myofibres organization or motor endplate arrangement, which could have been important to finely dissect the differences between VACHT WT and mutant OE and to further uncover the mechanism underlying disease pathogenesis in individuals with *SLC18A3* mutation.

The autosomal dominant inheritance and the *de novo* nature of the VACHT-D147N mutation are suggestive of gain-of-function of the mutated product, nonetheless, a haploinsufficiency cannot be unequivocally excluded. Site-directed mutagenesis studies have had not only refined the VACHT structure but also uncovered crucial residues involved in ACh recognition and translocation, proton exchange and vesicle trafficking. Aspartate (D) residues within transmembrane domains and cytoplasmic loops of the VACHT transporter have been extensively studied in this context and proved to be necessary for ACh binding and transport (Kim et al, 1999). Interestingly, the D147N mutation was analyzed within this framework and proven to slightly reduce ACh uptake *in vitro* in approximately 5%, compared to WT reference values (100% of the activity). Although almost negligible, a deficient ACh uptake caused by VACHT-D147N mutation, could potentially led to cholinergic transmission defects which in circumstances such as slow progression of disease (as in the patients harboring *SLC18A3* mutation), could account for a mild motor neuropathy phenotype. In this scenario, generation of transgenic zebrafish lines carrying the *SLC18A3* mutation would be an important tool to analyze long-term phenotypic outcomes resulting from a longer exposure to the altered gene products.

Very recently, missense mutations and deletions in *SLC18A3* were causatively associated to myasthenic syndromes –NMJ disorders- in two unrelated families (Aran et al, 2017; O'Grady et al, 2016). These studies raised the question whether the neuropathological symptoms of the affected individuals carrying the *SLC18A3* mutation were myasthenia-associated rather than dHMN. It is important to emphasize that even if the clinical symptoms of the patients do not entirely recapitulate the typical myasthenia presentation; the severity of myasthenia syndromes varies greatly as some individuals experience minor weakness (predominantly in the facial muscles) and others are unable to walk (Haberlova et al, 2009). Thus, in a potential VACHT-D147N haploinsufficiency context, the possibility of a mild myasthenic phenotype is a possibility that cannot be entirely ruled out.

5.3. Chp1 reduction ameliorates axonal outgrowth defects in a zebrafish model of SMA

The indication that CHP1 could be a novel SMA modifier originated from three main observations: (I) CHP1 was identified as a direct interacting partner of PLS3 (HosseiniBarkoobe, 2016 - Thesis), the first fully protective SMA modifier identified, (II) similar to NCALD, the most recently described human SMA modifier, CHP1 is a calcium binding and sensing protein (Di Sole et al, 2012; Riessland et al, 2017), and (III) preliminary evidence indicates that CHP1 expression is increased in spinal cord and brain of severely affected SMA mice (Janzen, Mendoza-Ferreira et al, manuscript in preparation). As an initial *in vivo* approach to demonstrate the potential beneficial role of CHP1 in SMA, the effect of Chp1 downregulation on MN outgrowth and development was analyzed in a zebrafish model of SMA. Particularly, the zebrafish CaP-MNs were chosen as a phenotypic readout because MNs are the main cell type affected by SMN depletion, and therefore the main drivers of the SMA pathology (Harding et al, 2015; Kariya et al, 2008; Kong et al, 2009; Ling et al, 2012).

The work of this thesis demonstrated that firstly, Chp1 is expressed in zebrafish MNs cell bodies. This is in agreement with our own unpublished results, as Chp1 localizes to the soma and growth cones of mouse-derived MNs (Janzen, Mendoza-Ferreira et al. Manuscript in preparation) and secondly, Chp1 downregulation in zebrafish ameliorates the CaP-MN axonal outgrowth defects of Smn-deficient fish larvae. Together, these results strongly suggest that CHP1 might perform an important role(s) in the cell type of utmost relevance in SMA, the MN.

Calcium signaling influences a broad range of biological events in neurons, including axon development, synaptic strength, survival and death. Most importantly, calcium-mediated cues are essential for two additional processes of critical relevance in the SMA pathology namely, the development and extension of terminal growth cones and developing dendrites as well as synaptic vesicle release and recycling *i.e.* endo and exocytosis (Burgoyne, 2007; Gomez & Zheng, 2006). As calcium homeostasis is disturbed in SMA (Ruiz et al, 2010), the aforementioned processes are most likely also compromised. In this context, the role of CHP1 as a calcium buffering protein is highly relevant. Indeed, CHP1 binds calcium and transduces local calcium concentration changes to a variety of signaling processes or downstream effectors (Di Sole et al, 2012). Therefore, modulation of this protein in SMA conditions could have a direct effect on calcium-dependent processes, including MN development and outgrowth. It is important to highlight that, similar to CHP1, the protective modifiers PLS3 and NCALD also contain EF-hands which enable them to bind to and sense calcium, and both ameliorate the SMA phenotype in a calcium dependent-manner across

species (Ackermann et al, 2013; Chang et al, 2008; Dimitriadi et al, 2010; Hosseinibarkooie et al, 2016; Lyon et al, 2014; Oprea et al, 2008; Riessland et al, 2017).

Furthermore, CHP1 could modulate calcium homeostasis in an NHE1-dependent mechanism. It has been shown that intracellular acidification modifies the activity of neuronal Ca^{2+} ATPase pumps (calcium extruders), Ca^{2+} channels as well as the internal concentration of intracellular calcium (Ouyang et al, 1994; Pick & Karlsh, 1982; Willoughby et al, 2001; Wolosker et al, 1997). As NHE1 depletion leads to acidosis in specific neuronal populations (Ruffin et al, 2014; Yao et al, 1999), the CHP1-NHE1 balance might play an important role also in the context of SMA. In this regard, it is important to highlight that key processes of vesicular neurotransmitter release, such as calcium influx, vesicle loading, release (exocytosis) and membrane recycling (endocytosis), are governed by cytosolic pH gradients (Blakely & Edwards, 2012; Sinning & Hubner, 2013; Zhang et al, 2010). For instance, the Clathrin-mediated endocytosis has been shown to be enhanced/favored in alkaline cytosolic pH and, contrarily, acidification can inhibit one or more components of this particular endocytic pathway (Coleman et al, 2008; Tabares & Betz, 2010; Zhang et al, 2010). Further considering that the Clathrin-mediated endocytosis is impaired in SMA and that the modifiers PLS3 and NCALD rescue this impairment (Hosseinibarkooie et al, 2017; Riessland et al, 2017), it is very plausible to conjecture that CHP1-mediated modulation of pH_i could restore impaired Clathrin –or other types- of endocytosis in a pH-dependent manner, while the neuropathogenesis of SMA could underlie an imbalance on pH homeostasis and the processes reliant on it.

Interestingly, our preliminary evidence strongly suggests that CHP1 reduction restores impaired endocytosis in SMN-deficient cells in a mechanism dependent on CHP1 inhibition of Calcineurin phosphatase activity ((Lin et al, 1999), Janzen, Mendoza-Ferreira et al. Manuscript in preparation)). Interestingly, Calcineurin has been implicated in NGF-activated signaling pathways controlling axonal growth, as it is required for the endocytic internalization and intracellular trafficking of the TrkA receptor (Tropomyosin receptor kinase A) responsive to NGF (Bodmer et al, 2011). TrkA internalization supports local axonal growth, extension, branching, guidance and retrograde signaling from distal axons to cell bodies to promote neuronal survival (Gallo et al, 1997; Gallo & Letourneau, 1998).

The fact that CHP1 directly interacts with PLS3, and that the latter is a calcium-dependent F-actin-binding and -bundling protein that influences the G/F-actin ratio, opens up the possibility of a potential implication of CHP1 in actin-related processes; which are pivotal in the context of SMA. Tight regulation of actin filaments assembly, *i.e.* actin dynamics, at neuronal growth cones generates and transmits the mechanical forces necessary for growth cone advancement and axonal pathfinding (Schaefer et al, 2008; Stiess & Bradke, 2011).

Most importantly, the functional integration of actin and other cytoskeleton components such as, microtubules, microfilaments and intermediate filaments –among a plethora of specific regulatory proteins- governs crucial processes for MNs such as cellular shape, migration, RNA metabolism, vesicular trafficking and endocytosis, among others (Engqvist-Goldstein & Drubin, 2003; Pollard & Borisy, 2003). SMN-deficient cells exhibit reduced F-actin levels, most likely due to disturbed axonal transport of β -actin mRNA to the growth cones (Ackermann et al, 2013; Hosseinibarkooie et al, 2016; Rossoll et al, 2003). The modifier PLS3 rescues various F-actin dependent-processes such as: axonal outgrowth, NMJ innervation, neurotransmission, proprioceptive input at MN soma, synaptic vesicle recycling and endocytosis, thus further validating the critical role of actin dynamics in SMA (Ackermann et al, 2013; Hao et al, 2012; Hosseinibarkooie et al, 2016; Oprea et al, 2008).

CHP1 downregulation may have a potential effect on actin dynamics both in a PLS3-dependent or independent manner. As an interacting partner of PLS3, CHP1 could directly modulate the availability or the function of PLS3 at relevant MN sites, such as the growth cone or the presynapse. Besides PLS3, other CHP1 interacting partners also play relevant roles in actin-related pathways. On one hand, CHP1 interacts with Ezrin, an Actin-binding and bundling protein (Babich & Di Sole, 2015; Di Sole et al, 2009). Ezrin, connects cortical actin with the plasma membrane, thereby modulating various cell surface-related processes such as endocytosis, migration and signal transduction from the surface to the interior of the cells (Bretscher et al, 1997; Maniti et al, 2013). CHP1 not only binds Ezrin but also regulates its phosphorylation at threonine T567 which is essential for the activation of Ezrin's F-actin-binding capacity at apical membranes (Janke et al, 2008; Zh et al, 2007). Moreover, Ezrin activity is linked with the signaling pathways triggered by the small GTPases of the Rho family, and can therefore exert a direct modulatory effect on axonal growth, guidance and branching (Hall & Lalli, 2010). Most importantly, Ezrin is required for the formation of focal adhesions and actin stress fibers in response to active RhoA, which is aberrantly activated in SMN deficient cells (Bowerman et al, 2007; Mackay et al, 1997). Additionally, the further interaction of CHP1 with GAPDH facilitates both binding and distribution of CHP1 along microtubules and also interactions with other motor proteins. The role of CHP1 in the regulation of microtubule dynamics and stability might also influence neurite outgrowth, thereby influencing cytoskeletal rearrangements at growth cones (Andrade et al, 2004a; Andrade et al, 2004b; Timm et al, 1999).

5.3.1. CHP1 reduction is ARCA-causative and SMA protective. A matter of protein dosage

It is indeed very intriguing that reduced CHP1 expression can have both pathogenic and beneficial effects as it causes ARCA in humans and ameliorates the SMA phenotype of *smn*-depleted zebrafish larvae. The underpinnings of this duality may lie in the unique neurophysiology, morphology and function of Purkinje and motor neurons. The results of this work and the findings of others demonstrate that Purkinje cells are extremely sensitive to CHP1 and/or NHE1 depletion, whereas other neuronal populations, such as MNs, seem to show variable vulnerability to this deficiency (see section 5.1.4). It is important to stress that, independently of the neuronal type, CHP1 is differentially disturbed in ARCA and SMA as follows (Figure 40):

- CHP1 balance in ARCA

Time-course OE and protein fractionation analyses undertaken in this study demonstrate that the CHP1-K19del dramatically alters but not abolishes protein expression. These findings are congruent with the expression of mutant Chp1 in the *vacillator* mouse. Indeed, the biallelic splice mutation in *Chp1* (*Chp1^{vac/vac}*) leads to reduced protein levels, however residual Chp1 can be detected in homozygous animals (Liu et al, 2013). These facts demonstrate that mutations in CHP1 are pathogenic only when protein expression falls under a certain level, and that residual CHP1 levels (as well as expression/compensation of other CHP proteins) could counteract phenotype severity or lethality. In the ARCA context, reduced CHP1 expression alters NHE1 targeting and function. As discussed in 5.1.5, Purkinje degeneration and concomitant ataxic symptoms likely arise from an NHE1-dependent collapse of pH homeostasis which hinders GABA neurotransmission.

- CHP1 balance in SMA

In SMA, Calcium-, actin dynamics- and, very likely, pH-reliant processes are impaired (see section 1.3). In addition, the expression of CHP1 has been shown to be elevated in spinal cord and brain of severely affected SMA mice (Janzen, Mendoza-Ferreira et al, manuscript in preparation). Downregulation of CHP1 in the SMA scenario, ameliorates the neuropathogenesis of the disease by restoring the aforementioned processes (see section 5.3), either individually or collectively.

Facing a potential therapeutic intervention of CHP1 in the context of SMA it is important to highlight that heterozygous carriers of *CHP1* mutation (*i.e.* parents of the affected ARCA siblings) and heterozygous *vacillator* animals (*Chp1^{vac/wt}*) are fully asymptomatic. Therefore,

moderate reduction of CHP1, mimicking heterozygous loss of *CHP1*, might be well tolerated (Figure 40). The cumulative evidence that demonstrates the beneficial effect of CHP1 reduction *in vitro* as well as *in vivo* in zebrafish, strongly support the potential of a combinatorial therapy using *SMN2* and *CHP1* antisense oligonucleotides (ASOs) to protect against SMA. The latter, is currently an ongoing project in our research group. Further considering that CHP1 may potentially act on calcium, pH and actin-related processes; modulation of CHP1 expression could constitute a therapeutic target for other neurodegenerative disorders such as ALS and HSP which also exhibit misregulation or defects in processes reliant on calcium homeostasis and/or actin dynamics (Hadano et al, 2001; Schreij et al, 2016; Wu et al, 2012).

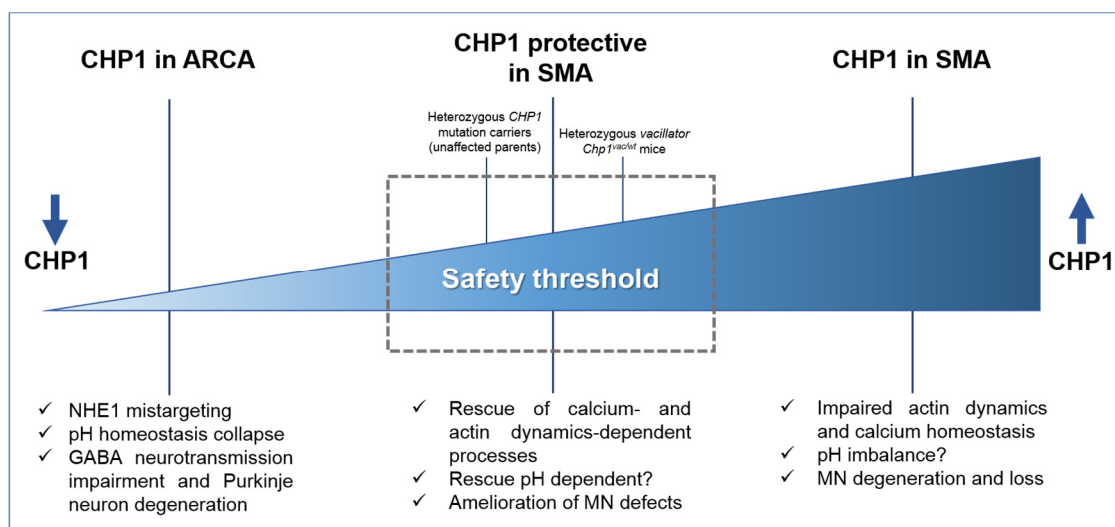


Figure 40. A model of CHP1 balance in ARCA and SMA. Mutation in *CHP1* leading to very reduced protein expression cause ataxia in a NHE1-dependent manner. CHP1 reduction within a safety threshold or tolerability, rescues impaired processes/mechanisms disturbed in SMA.

5.4. Concluding remarks and future outlook

Identification of novel gene mutations, disease modifiers and further characterization of gene/phenotype associations is critical to understand the molecular processes underlying NMDs pathogenesis. Capitalizing in the novel NGS technologies, the work of this doctoral thesis aimed to identify and characterize novel NMD-causative candidate genes. The functional studies undertaken herein, led to the successful validation of *CHP1* as a novel causative gene of ARCA and uncovered NHE1 imbalance *i.e* pH_i homeostasis misregulation, as the molecular mechanism most likely underpinning pathogenic axonal degeneration. Nevertheless, some questions remained unanswered and therefore open novel research avenues to follow upon:

- I. To further strengthen the connection between CHP1, NHE1 and pHi homeostasis in the neuropathogenesis of ARCAs, pHi could be measured in cells overexpressing CHP1-K19del and in MNs/Purkinje cells derived from *Chp1*-deficient mice (*vacillator*). Experimental approaches for the latter could include pH-sensitive fluorescent compounds (BCECF) and pH-sensitive genetically encoded sensors (ratiometric pHRed, pHlash or Thy-YFP).
- II. Our protein modeling analysis strongly suggest that CHP1-K19del alters protein conformational changes and potentially, the functionality of the CHP1-NHE1 complex. To confirm this, the affinity of the interaction between CHP1-K19del and NHE1 could be analysed via Surface Plasmon Resonance (SPR-Biacore).
- III. In order to clarify the complete phenotypic landscape of the CHP1 family, the BNC1-G258E mutation could be further characterized in order to demonstrate its causal implication with the hypogonadotropic condition diagnosed in the female proband. Assessment of the consequences of the BNC1-G258 mutation on protein expression and function is necessary to potentially correlate altered protein expression with BNC1 misfunction and ovarian failure.

Furthermore, a *de novo* mutation in *SLC18A3* (VAChT) was functionally characterized in the context of dHMN. The experimental findings obtained in this regard were not conclusive at discerning the pathogenicity of the VAChT-D147N mutation. In the light of the novel VAChT mutations identified as a cause of myasthenia syndromes, we believe that our negative functional study was mainly due to our restricted screening of zebrafish CaP-MNs. Nonetheless, our findings have revealed that increased VAChT expression, WT or mutant indistinctly, cause axonal migration defects which have been previously associated with impairments of the NMJ and muscle fibers. Since our results do not favor but also do not exclude the pathogenicity of the VAChT-D147N mutation, further analyses are necessary to ascertain the pathogenicity of the latter, either in the dHMNs or the myasthenia syndromes context. Supplementary experiments could include:

- I. Analysis of both muscle fibers and NMJ organization in zebrafish embryos overexpressing VAChT-WT and VAChT-D147N proteins. In complement, we could make use of the novel VAChT mutations reported in the literature for these analyses, since no functional studies were performed to ascertain their pathogenicity. An experimental setup of embryo mRNA injection, similar to the one performed in this thesis, can be followed for this purpose.
- II. Taking into account that patients carrying *SLC18A3* mutation exhibit a slow progression of the disease, the generation of transgenic zebrafish lines carrying the *slc18a3* mutations, using the CRISPR-Cas9 method, would be an important tool to analyze long-term phenotypic outcomes.

Within the scope of this project, Chp1 reduction was confirmed to rescue the CaP-MN outgrowth defects in Smn-depleted zebrafish. These findings are quite congruent with previous characterization studies of other human SMA modifiers –PLS3 and NCALD- in zebrafish, which serves as indication of convergence into similar functional pathways for all modifiers, despite variable function and modes of action (e.g. upregulation or downregulation). Additionally, this novel evidence summed to our preliminary findings in Smn-depleted neuron-like cells, indicate that reduced CHP1 exerts a positive effect both *in vitro* and *in vivo*. Thus, targeted intervention of CHP1 constitute a promising therapeutic strategy to treat SMA. Even though these findings, on the whole, have shed light onto the potential role(s) of CHP1 in SMA pathogenesis, further experiments are crucial to understand how CHP1 ameliorates axonal outgrowth defects in SMA.

- I. Up to now, our analysis of Chp1 reduction in Smn-depleted zebrafish larvae was restricted to the analysis of CaP-MN axonal outgrowth. Further analyses of the neuromuscular system, *i.e* NMJ organization and muscle fiber structure, can be conducted to better understand the consequences of Chp1 depletion.
- II. CHP1, PLS3 and NCALD are calcium sensor proteins. Moreover, CHP1 is also considered to have calcium buffering function. As calcium homeostasis is disturbed in SMA and CHP1 modulation could have an effect on calcium-dependent signaling; further analysis, including calcium imaging, are necessary to gain further insights onto this process. A genetically encoded calcium indicator (GCaMP) has been successfully used for this purpose in zebrafish.
- III. Since CHP1 and PLS3 directly interact and both CHP1 KD and PLS3 OE rescue the axonal outgrowth defects of Smn-depleted zebrafish, it is possible that the SMA-rescuing function of CHP1 could rely on its interaction with PLS3. Combinatorial injection of MOs and mRNAs in zebrafish could be an excellent alternative to address this potential mechanism. Taking advantage of the experimental zebrafish set-up developed in this thesis, a potential synergistic effect of both PLS3 and CHP1 on the SMA phenotype could be additionally addressed in zebrafish via MO and/or mRNAs injections.

6. MATERIALS AND METHODS

6.1. Materials

6.1.1. Laboratory equipment and devices

Item	Reference	Manufacturer
Äkta chromatography system	Äkta pure	GE Healthcare
Analytical balance	AX2202M	Ohaus
Analytical balance (precision)	ARJ 120-4M	Kern
Centrifuges	Allegra X22-R	Beckmann Coulter
	Avanti J-20XPI	Beckmann Coulter
	5415R	Eppendorf
	5415D	Eppendorf
	5804	Eppendorf
Chambers for DNA Electrophoresis	Galaxy Mini	VWR
	MGV-620T	C.B.S & Scientific
Chambers for Proteins SDS-PAGE	SGE-020-02	C.B.S & Scientific
	Mini-Protean 3 cell	BioRad
	Mini-Protean Tetra System	BioRad
Freezer (-80°C)	Protean II XL System	BioRad
	HERA freeze	Heraeus
Gas Bunsen burner	Fireboy Plus	IBS
Gel documentation	ChemiDoc XRS	BioRad
	Gel Doc XR+	BioRad
Heating block	HTMR132	HLC Bio Tech
Heating magnetic stirrer	MR3001	Heidolph
Horizontal shaker	3015	GFL
Homogenizer	Precellys 24	Peqlab
Ice machine	AF 80	Scotsman
	Innova 44	New Brunswick Scientific
	Innova 4230	New Brunswick Scientific
Incubator for cell lines	Heracell™ 150	Heraeus
Laminar airflow hood	Herasafe™ KS 12	Heraeus
Light source (Optic Fiber)	KL 1500 LCD	Leica
Microplate reader	Safire ²	Tecan
Microscope	Bright field / DMiL	Leica
Microscope (Fluorescence)	Axioshop 2 / Imager M2	Zeiss
	S8AP0	Leica
Microscopes (stereo)	VisiScope SBL 350	Leica
Microwave	R-898(AL)-A	Sharp
Neubauer chamber	1100000	LO Laboroptik Ltd.
Orbital Shaker	3015	GFL
pH meter	inoLab pH level 1	WTW
Photometer	BioPhotometer	Eppendorf
Photometer cuvettes	UV-vette	Eppendorf
Photometer	NanoDrop 1000	Peqlab

Item	Reference	Manufacturer
Pipettes	2.5/10/20/100/200/1000/5000 µL	Eppendorf
	Automatic 10/100µL Research Pro	Eppendorf
Pipettor	Repetitive / Multipipette Plus	Eppendorf
	Easypet	Eppendorf
Power supply	PowerPac™ Basic	Bio-Rad
	PowerPac™ HC	Bio-Rad
	PowerPac™ 1000	Bio-Rad
Roll incubator	SRT9	Stuart
	SRT6D	
Superose column	RM5	Hartenstein
	Superose 6 10/300 GL	GE Healthcare
Thermocycler	DNAengine Tetrad2	MJ Research
	DNAengine Dyad	MJ Research
	S1000	BioRad
Transfer WB System	C1000 Touch	BioRad
	Trans-Blot Turbo	BioRad
Ultrasonicator	Bioruptor	Diagenode
Vortex	444-1372	VWR
Water bath	1083	GFL
	FBC 620	Fischer Brand

6.1.1.1. Zebrafish equipment

Item	Reference	Manufacturer
Embryo injector pump	PV820 Pneumatic PicoPump	World Precision Instruments
Fluorescence microscope (stereo)	Sterni2000	Zeiss
Forceps	Dumont #55	Fine Science Tools
Incubator	Heraeus	Thermo Fisher Scientific
Micropipette puller	P-2000	Sutter Instruments Company
Minutien pins	26002-10	Fine science tools

6.1.2. Chemicals

Item	Manufacturer
2-Mercaptoethanol (99%, p.a.)	AppliChem
2-Propanol (≥ 99.5%)	AppliChem
Agarose for routine use	Sigma-Aldrich
Agarose (low melting)	Biozym
Ammonium persulfate (APS)	AppliChem
Ampicillin	AppliChem
BactoAgar	AppliChem
Bovine Serum Albumin (BSA)	Sigma-Aldrich
Bromophenol blue	AppliChem
Chloroform	AppliChem
Coomassie Brilliant Blue R-250	AppliChem

Item	Manufacturer
Dimethyl sulfoxide (DMSO)	Sigma-Aldrich
Ethanol ($\geq 99.5\%$, p.a.)	AppliChem
Ethidium bromide (1% in H ₂ O)	AppliChem
Ethylenediaminetetraacetic acid (EDTA)	AppliChem
Glycerol (86%, p.a.)	AppliChem
Hydrochloric acid (37%)	AppliChem
Hydroxymethylaminoethane (Tris)	AppliChem
Isopropanol	AppliChem
Methanol ($\geq 99.9\%$, p.a.)	AppliChem
Milk powder (low fat)	AppliChem
Mowiol	Roth
NP40	AppliChem
Paraformaldehyde	Fluka
Sodium chloride (p.a.)	AppliChem
Sodium dodecyl sulfate (SDS)	AppliChem
Sodium hydroxide	AppliChem
Tertramethylethylenediamine (TEMED)	AppliChem
Triton X-100	AppliChem
Trizma base	Sigma-Aldrich
Tryptone (microbiology grade)	AppliChem
Tween-20 (Polysorbate 20)	AppliChem
Water (HPLC grade)	Sigma-Aldrich
Yeast extract (microbiology grade)	AppliChem

p.a. indicates pro analysis purity grade

6.1.3. Reagents

6.1.3.1. Molecular biology reagents

Item	Manufacturer
10x PCR master mix	New England Biolabs
6x DNA loading dye	Thermo Fisher Scientific
Quick-Load® Purple 2-Log DNA Ladder	New England Biolabs
AquaPlus Mix 40% (39:1 Acrylamide/Bisacrylamide)	AppliChem
Bradford reagent	AppliChem
Complete Mini Protease Inhibitors Cocktail	Roche
dNTPs	Peqlab
Page Ruler Prestained Protein Ladder	Thermo Fisher Scientific
PBS (10x)	VWR
Ponceau S	Sigma-Aldrich
ProLong mounting media with or without DAPI	Life Technologies
Restore Western Blot Stripping Buffer	Thermo
RIPA buffer	Sigma-Aldrich
Super Signal West Pico ECL Substrate	Thermo

6.1.3.2. Cell culture reagents and media

Item	Manufacturer
1x PBS Dulbecco, w/o Ca ²⁺ , Mg ²⁺	Life Technologies
Amphotericin B	Promocell
DharmaFECT®	Thermo Scientific
DMEM (4.5 g/L D-Glucose, L-Glutamine, Pyruvate)	Life Technologies
Fetal Calf Serum (FCS)	Biochrom AG
Horse Serum	Biochrom
Laminin	Thermo Scientific
Lipofectamine® 2000	Life Technologies
Neurite Growth Factor (NGF)	Life Technologies
OptiMEM®	Life Technologies
Penicillin/Streptomycin	Life Technologies
Trypsin/EDTA	Life Technologies
Retinoic Acid	Sigma-Aldrich

6.1.3.3. Zebrafish work reagents

Item	Manufacturer
1-phenyl 2-thiourea (PTU)	Sigma-Aldrich
Dymethylpolysiloxane	Sigma-Aldrich
Phenol Red	Sigma-Aldrich
Rhodamine dextran	Sigma-Aldrich

6.1.4. Enzymes

Item	Manufacturer
Accu Prime DNA Polymerase	Life Technologies
BamHI (HF) endonuclease	New England Biolabs
EcoRI (HF) endonuclease	New England Biolabs
NotI (HF) endonuclease	New England Biolabs
Platinum Taq DNA Polymerase High Fidelity	Life Technologies
Pfu Ultra HF DNA Polymerase	Agilent
Proteinase K	AppliChem
RNase A	Life Technologies
RNase-free DNase I	QIAGEN
T4 DNA ligase	Promega

6.1.5. Antibodies and staining reagents

Application	Antibody / Dye	Dilution	Manufacturer	Catalogue number
Western blot	mouse α - β -actin HRP conjugated	1:5000 1h / RT	Proteintech	HRP-60008
	rabbit α -EGFR	1:1000 o/n 4°C	Santa Cruz Biotechnology	(1005) sc-03
	mouse α -GAPDH HRP-conjugated	1:5000 1h / RT	Sigma-Aldrich	G9295
	rabbit α -HSP90	1:1000 o/n 4°C	Cell Signaling Technology	C45G45
	mouse α -NHE1 4E9	1:1000 o/n 4°C	Santa Cruz Biotechnology	sc-58635
	mouse α -VAcHT	1:1000 o/n 4°C	Abcam	Ab134298
	mouse α -V5	1:5000 o/n 4°C	Thermo Scientific	R960-25
	mouse α -Vimentin	1:1000 o/n 4°C	Sigma-Aldrich	V6389
	mouse α -SMN	1:3000 o/n 4°C	BD Biosciences	610646
Zebrafish Western blot	rabbit α -CHP1	1:1000 o/n 4°C	Thermo Scientific	PA5 29876
	rabbit α -CHP1 N-terminal	1:1000 o/n 4°C	Aviva Systems Biology	ARP52307P050
	rabbit α -beta-actin (ZF)	1:1000 o/n 4°C	Anaspec Eurogentec	AS-553399
Cells Immunostaining (Primary antibodies)	rabbit α -GM130	1:500 o/n 4°C	Abcam	Ab31561
	mouse α -Ub	1:250 1h / RT	Santa Cruz biotechnology	SC-8017
	mouse α -p62	1:50 1h / RT	Abcam	AB56416
	mouse α -VAcHT	1:150 1h / RT	Abcam	Ab134298
	Phalloidine AlexaFluor 568	1:40 1h / RT	Thermo Scientific	A12380
Zebrafish Immunostaining (Primary antibodies)	mouse α -Znp1 (Synaptotagmin)	1:150 o/n 4°C	Hybridoma Bank	AB2315626
	mouse α -acetylated tubulin	1:150 o/n 4°C	Sigma Aldrich	T7451
	rabbit α -CHP1 N-terminal (ZF)	1:100 o/n 4°C	Aviva Systems Biology	ARP52307P050
General Immunostaining (Secondary antibodies)	goat- α -mouse-HRP	1:2500 1h / RT	Dianova	115-035-146
	goat- α -rabbit-HRP	1:2500 1h / RT	Cell signaling	7074P2
	mouse α -AlexaFluor-488	1:500 1h / RT	Thermo Scientific	A11001
	rabbit α -AlexaFluor-488	1:500 1h / RT	Thermo Scientific	A21206
	mouse α -AlexaFluor-647	1:500 1h / RT	Thermo Scientific	A31571
	rabbit α -AlexaFluor-647	1:500 1h / RT	Thermo Scientific	A32733

6.1.6. Routinely used media and solutions

6.1.6.1. Cell culture and growth media

All cell culture media was kept at 4°C, unless noted otherwise.

Name	Composition
DMEM growth medium for HeLa, HEK293T, NSC-34 and N2A cells	500 ml DMEM; 50 ml FCS; 1% (v/v) Penicillin / Streptomycin (10 U/ml); 250 µg/ml Amphotericin B
DMEM growth medium for PC12 cells	500 ml DMEM GlutaMAX™; 50 ml Horse Serum; 25 ml FCS; 1% (v/v) Penicillin/Streptomycin (10 U/ml); 250 µg/ml Amphotericin B
Freezing medium for HeLa, HEK293T, NSC-34 and N2A	90 % FCS; 10 % DMSO. Filtered
Freezing medium PC12 cells	90 % PC12 growth medium; 10% DMSO. Filtered
E3 Embryo medium zebrafish	5.0 mM NaCl; 0,17 mM KCl; 0,33 mM CaCl; 0,33 mM MgSO; 0,05% Methylene blue (fungicide)

6.1.6.2. Solutions for DNA work

Name	Composition
DNA sample buffer, 10x	100 mM EDTA (pH 8); 1% (w/v) SDS; 50% (v/v) Glycerin; 0.1% (w/v) Bromophenol blue; 0.25% (w/v) Xylene cyanol
dNTPs Mix (1.25 mM per dNTP)	dNTP stocks (100mM). 5 µl dATP; 5 µl dCTP; 5 µl dGTP; 5 µl dTTP; 480 µl H ₂ O

6.1.6.3. Solution for work with bacteria

Name	Composition
Ampicillin stock solution	50 mg/ml in 50% Methanol. Storage at -20°C
LB agar	3.75 g Bacto Agar in 250 ml LB-medium
LB medium	5 g Bacto-Trypton; 2.5 g Bacto-yeast-extract; 2.5 g NaCl (for 500ml ddH ₂ O)

6.1.6.4. Solutions for immunostaining

Name	Composition
Blocking solution for cells immunostaining	5% BSA; 1%FCS in PBST (0,2% Tween20)
Blocking solution for Zebrafish MN immunostaining	1% DMSO; 2% BSA; 5% FCS in PBST (0.1% Tween20)
Blocking solution for Zebrafish cerebellum immunostaining	1% BSA and 10% FCS in PBS.
Dent's fixative for zebrafish	80% methanol; 20% DMSO
Paraformaldehyde (PFA)	4% Paraformaldehyde (PFA) in PBS (pH 7.3)

6.1.6.5. Solutions for protein work

Name	Composition
Ammonium Persulfate (APS)	1% (w/v) in deionized H ₂ O. Storage at -20°C
Blocking solution for Western blot	5% (w/v) milk powder; 1% (w/v) BSA in TBST
Laemmli buffer for SDS page (3x)	2.4 ml Tris (1 M, pH 6.8); 3 ml SDS (20 %); 3 ml Glycerol; 1.6 ml 2-β-Mercaptoethanol; 0.006 g bromophenol blue. ddH ₂ O to 10ml
Ponceau staining solution	1% (w/v) Ponceau S; 2% (v/v) ml acetic acid in ddH ₂ O
Resolving gel (SDS-PAGE) 12%	4.85 ml H ₂ O; 2.55 ml 30% acrylamide mix (AquaPlus 39:1); 2.6 ml 1.5 mM Tris pH 8.8; 100 μl 10% SDS; 100 μl 10% APS; 4 μl TEMED (for 10 ml)
SDS electrophoresis buffer, 10x	30.29 g Tris (Base); 144,13 g Glycin; 10 g SDS; ddH ₂ O to 1000 ml
Stacking gel (SDS-PAGE), 4%	2,96 ml H ₂ O; 520 μl 30% acrylamide mix (AquaPlus 39:1); 520 ml 1.5 mM Tris pH 6.8; 40 μl 10% SDS; 40 μl 10% APS; 4 μl TEMED (for 4ml)
TBS	20 mM Tris; 137 mM NaCl
TBST	0.5% (v/v) Tween-20 in TBS
Transfer buffer for Western Blot	15 mM Tris-base; 150 mM Glycine; 20% (v/v) Methanol

6.1.7. Cell lines and zebrafish strains

6.1.7.1. Cell lines

The cell lines utilized in this study are listed below:

- HEK293T. Specific cell line originally derived from human embryonic kidney cells and transformed with sheared adenovirus 5 DNA (Graham et al, 1977). Given their ease for transfection, this cell line was used in this study for protein overexpression and various downstream applications including: RNA and protein isolation, immunofluorescence and subcellular fractionation.
- HeLa. First human cell line established in culture. Originated from a cervical cancer tumor of a patient. In this study, HeLa cells were used for protein overexpression and immunofluorescence (Gey, 1952).
- PC12. Cell line derived from a pheochromocytoma (neuroendocrine tumor) of the rat adrenal medulla. The neuroblastic origin of PC12 makes them suitable for differentiation into neuron-like cells upon NGF stimulation (Greene & Rein, 1977; Greene & Tischler, 1976). In this project, PC12 cells were utilized for protein overexpression and immunofluorescence.
- NSC-34. Hybrid cell line produced by fusion of murine neuroblastoma cells with embryonic spinal cord cells. These cells resemble many phenotypic features

characteristic of motor neurons (Cashman et al. 1992). In this study, NSC-34 cells were used for protein overexpression and immunofluorescence (Cashman et al, 1992).

- Neuro2A (N2A). Fast growing cell line established from a mouse brain tumor (neuroblastoma). Similarly to PC12, N2A cells can be conveniently differentiated into neuron-like cells upon RA stimulation and/or starvation. Because of their propensity for transfection, fast growth and ease for differentiation, these cells were used in this study for immunofluorescence and subcellular fractionation analyses (Klebe & Ruddle, 1969).

6.1.7.2. Zebrafish strains and lines

Zebrafish experiments were performed in collaboration with Dr. Mathias Hammerschmidt and Dr. Heiko Löhr from The Institute for Zoology / Developmental Biology of the University of Cologne (Germany). The following zebrafish strains/lines were used for embryo injections:

- TL/EK. Wild type zebrafish strain (TL: *Tupfel long fin* / EK: *Ekkwill*).
- *tg(mnx1-GFP)^{ml2TG}*. Transgenic zebrafish line also known as *HB9:GFP*. In this line the expression of GFP is regulated by genomic elements of the zebrafish *hb9* gene. Hb9 is a transcription factor expressed in motor neurons and required for early stages of their development (Flanagan-Steet et al, 2005).

6.1.8. Primers and morpholinos

All primers used in this study were purchased from IDT (Integrated DNA Technologies). The lyophilized primers were diluted in ddH₂O to obtain a stock solution of 100 pmol/μl and working solution of 10 pmol/μl. All primers were designed with SeqBuilder software. Exceptionally, primers for site-directed mutagenesis were designed with the QuikChange® Primer Design Program provided with the QuikChange® II XL mutagenesis kit. Molecular features of all designed primer pairs, such as melting temperature (T_m), self-complementarity (or complementarity between primer pairs) and potential hairpin formation were assessed with the web application OligoCalc. In the following tables, primer sequences are given in direction 5' to 3' and the abbreviations FWD and REV stand for forward and reverse, respectively.

6.1.8.1. Primers for cloning

Application	Description	Sequence (5' to 3')	Tm
<i>CHP1</i> subcloning Topo HIS-V5 vector	CHP1_TOPO_FWD	ACCATGGGTTCTCGGGCCTCC	60.2°C
	CHP1_TOPO_REV	GTGAAGAAATCGGATGCTCATTCTGTTC	58.9°C
<i>CHP1</i> subcloning PCS2+ vector	CHP1_PCS2_FWD	GCAGGATCCACCATGGGTTCTCGG	62.5°C
	CHP1_PCS2_REV	CTTGAATTCTTAGTGAAGAAATCGGATGC	58°C
<i>SLC18A3</i> subcloning PCS2+ vector	SLC18A3 PCS2 FWD	GCAGGATCCACCATGGAATCCGCG	62.5°C
	SLC18A3 PCS2 REV	TTGAATTCCTAGCTGCGGGTGTAGTAGTA	60.1°C

6.1.8.2. Primers for site-directed-mutagenesis

Application	Description	Sequence (5' to 3')	Tm
Site-directed Mutagenesis <i>CHP1</i>	CHP1 K18del FWD	CTCGAGGAGATCAAGGAGACCGGCTTTTC	64.3°C
	CHP1 K18del REV	GGAAAAGCCGGTCTCCTTGATCTCCTCGA	64.3°C
Site-directed Mutagenesis <i>SLC18A3</i>	SLC18A3 D147N FWD	GCGGGCCCTTCATCAACCGCATGAGCTAC	65°C
	SLC18A3 D147N REV	GTAGCTCATGCGGTTGATGAAGGGCCCGC	65°C

6.1.8.3. Primers for Semi-Quantitative RT-PCR

Application	Description	Sequence (5' to 3')	Tm
Semi- quantitative RT-PCR	CHP1_FWD	CTTCTTTCCAGAGGGAGAGACCAG	61°C
	CHP1_REV	CCTTCTCCAAAACCTTAACAAATTCTGTG	57.3 °C
	HPRT_FWD	AAGGAGATGGGAGGCCAT	50.3 °C
	HPRT_REV	GTTGAGAGATCATCTCCACCAAT	53.5 °C

6.1.8.4. Morpholinos for zebrafish experiments

Translational blocking morpholinos (MO) were designed and purchased as lyophilized from GeneTools, LLC in a prequantitated amount 300nmol. Following the company recommendations, MOs were dissolved in 100µl of HPLC-grade water to obtain a 3mM working solution and stored at 4°C. In table, MO sequences are given in direction 5' to 3'.

Application	Description	Sequence (5' to 3')	NCBI RefSeq
Zebrafish functional testing	<i>chp1</i> morpholino	CTGGAGCCCATGACTGCTGAAGATC	NM_199715.1
	<i>smn</i> morpholino	CGACATCTTCTGCACCATTGGC	NM_131191
	Control morpholino (non-targeting)	CCTCTTACCTCAGTTACAATTTATA	

6.1.9. Plasmids

Plasmids purchased or produced in this study are listed in the table below. For amplification, competent *Escherichia coli* DH5α and TOP10 were used for transformation. All vectors were verified by Sanger sequencing and conserved as glycerol stocks (6.2.3.3). All plasmids used in this study were Ampicillin resistant.

Name	Vector backbone	Insert	Original plasmid source	GVO No.
CHP1-GFP-WT	pcDNA 3.1/CT GFP-TOPO	Human <i>CHP1</i> cDNA	Life Technologies	553
CHP1-GFP-K19del	pcDNA 3.1/CT GFP-TOPO	Human <i>CHP1</i> cDNA with mutation K19del	Life Technologies	689
CHP1-WT_PCS2	PCS2+	Human <i>CHP1</i> cDNA	Kind gift. Prof. Sigrun Korsching	690
CHP1-K19del_PCS2	PCS2+	Human <i>CHP1</i> cDNA with mutation K19del	Kind gift. Prof. Sigrun Korsching	691
CHP1-V5-WT	pcDNA3.1/CT V5-HIS-TOPO	Human <i>CHP1</i> cDNA	Life Technologies	692
CHP1-V5-K19del	pcDNA3.1/CT V5-HIS-TOPO	Human <i>CHP1</i> cDNA with mutation K19del	Life Technologies	693
VACHT-GFP-WT	pCMV6-AC-GFP	Human <i>SLC18A3</i> cDNA	Origene	694
VACHT-GFP-D147N	pCMV6-AC-GFP	Human <i>SLC18A3</i> cDNA with mutation D147N	Origene	695
VACHT-WT_PCS2	PCS2+	Human <i>SLC18A3</i> cDNA	Kind gift. Prof. Sigrun Korsching	696
VACHT-D147N_PCS2	PCS2+	Human <i>SLC18A3</i> cDNA with mutation D147N	Kind gift. Prof. Sigrun Korsching	697

6.1.10. Kits

If not stated otherwise, all kit-related protocols were performed according to the manufacturer's instructions.

Item	Manufacturer
QuikChange II XL	Agilent
mMESSAGE mMACHINE SP6 Transcription Kit	Ambion
NucleoSpin Gel and PCR Clean-up	Macherey-Nagel
pcDNA3.1/V5-HisTOPO TA Expression Kit	Life Technologies
Pure Yield Plasmid Midiprep System	Promega
Pure Yield Plasmid Miniprep System	Promega
RNeasy Mini Kit	Qiagen
RNase free DNase Kit	Qiagen
SuperSignal West Pico Chemiluminescent Substrate	Thermo Scientific
QIAshredder Kit	Qiagen
Quantitect Reverse Transcription Kit	Qiagen
Subcellular Protein Fractionation Kit	Thermo Fisher Scientific

6.1.11. Software packages

Software / Package	Application	Distributor
EndNote X7	Bibliography organization	Thomson Reuters
Image J (Fiji)	Image analysis and processing	Open source
GraphPad Prism 7	Graph generation, statistical analysis	GraphPad Software
Inkscape	Figure design	Inkscape Community
Lasergene Package	DNA sequence analysis	DNASTAR Inc.
Image Lab 5.2.1	Image acquisition and analysis	BioRad
ZEN 2	Image acquisition and analysis	Zeiss
Pymol 1.5.0.4	3D Modelling protein	Schrödinger

6.1.12. Internet databases and web applications of routine use

Software / Package	Application
Ensembl	http://www.ensembl.org/index.html
ExonPrimer	http://ihg.gsf.de/ihg/ExonPrimer.html
Genecards	http://www.genecards.org/
NCBI	http://www.ncbi.nlm.nih.gov/
OligoCalc	http://basic.northwestern.edu/biotools/OligoCalc.html
PrimerBLAST	http://www.ncbi.nlm.nih.gov/tools/primer-blast/
Pubmed	http://www.ncbi.nlm.nih.gov/pubmed
Mutagenesis primer design	http://www.genomics.agilent.com/primerDesignProgram.jsp
UCSC	http://genome-euro.ucsc.edu/
UniProt	http://www.uniprot.org/

6.2. Methods

6.2.1. Patient's recruitment and ethics regulations

The patients analysed in this study were recruited by our research collaborators –stated in the following sections 6.2.1.1 and 6.2.1.2- in the frame of the NeurOmics project. NeurOmics is an integrated European Project (FP7 EU funded) which brings together the leading research groups in human molecular genetics in Europe. Since its establishment in 2013, the NeurOmics consortium aimed to understand and revolutionize the diagnostics of ten major neurodegenerative and neuromuscular diseases affecting the cortex, basal ganglia, cerebellum, spinal cord, peripheral nerves, neuromuscular junction, and muscle. As the Human Genetics Institute in Cologne was an active member of this project (NeurOmics has ended in 2017), we gained –and shared- access to sizable NMD cohorts.

6.2.1.1. The *CHP1* family

Patients and relatives from family AAR-087, together with 319 index individuals with assumed autosomal recessive cerebellar ataxia, were recruited as part of the Spastic Paraplegia and Ataxia (SPATAX) network cohort (<https://spatax.wordpress.com/>). Our collaborators: Drs. Giovanni Stevanin and Alexandra Durr are coordinators of this network. Patients from the family AAR-087, were examined using a standardized evaluation form (<https://spatax.files.wordpress.com/2013/09/fichecliniquespatax-eurospa-2011.pdf>). Blood samples were obtained for 5 individuals (1, 2, 6, 7 and 8 in pedigree, Figure 11) after signed informed consent. All procedures were in accordance with French ethics regulations (Paris Necker ethics committee approval (RBM 01-29 and RBM 03-48) granted to Dr. Alexandra Durr). DNA was extracted following standard procedures.

6.2.1.2. The *SLC18A3* family

The patients with suspected dHMN analyzed in this project were recruited by our collaborator, Dr. Pavel Seeman (Department of Child Neurology, Charles University Prague, Czech Republic). The WES in the *SLC18A3* family was performed by Dr. Konny Neveling (Department of Human Genetics, Radboud University Medical Centre, The Netherlands). The clinical features of the affected probands were published as a case report prior to our participation in this research collaboration (Haberlova et al, 2009). Examined patients signed informed consent for DNA testing to clarify the cause of the hereditary neuropathy and the study was approved by the Ethics Committee of University Hospital

Motol (Prague, Czech Republic). DNA was extracted following standard laboratory procedures.

6.2.2. Molecular biology methods

6.2.2.1. Isolation of plasmidic DNA from bacteria

For routine sequencing and verification of cloning products or expression vectors; the Spin Miniprep Kit (Qiagen) was used. For this purpose, small bacteria cultures of 5-10 mL were processed following the kit's instructions. To obtain DNA suitable for transfection, *i.e.* high yield and endotoxin-free, the PureYield Plasmid Midiprep System (Promega) was employed.

A maximum culture volume of 200mL was processed according to manufacturer's instructions. DNA concentration was determined via spectrophotometry using a NanoDrop ND-1000 spectrophotometer (Pqlab). As indicators of DNA quality, the absorbance wavelength ratios 260/280 (~1.8 ratio indicates high DNA purity) and 260/230 (nucleic acid purity – contaminant free), were used. Purified plasmid DNA was stored at -20°C.

6.2.2.2. Isolation of RNA from eukaryotic cells

RNA-handling procedures were performed under RNase-free conditions using sterile tubes and stuffed (filter) pipette tips. The RNeasy Mini Kit (Qiagen) was routinely used for RNA isolation following manufacturer's instructions. RNA was isolated from HEK293T cells seeded in 6-well culture plates. Briefly, cells were washed with PBS, lysed in RLT buffer (Qiagen) and collected with a cell scraper. Cell lysates were homogenized in QiaShredder columns (Qiagen) and processed according to the kit's indications. The on-column DNase digestion step was always performed. RNAs were eluted in RNase free ddH₂O and stored at -80°C.

RNA concentration was firstly determined via spectrophotometry using a NanoDrop ND-1000 spectrophotometer (Pqlab). As indicators of RNA quality, the absorbance wavelength ratios 260/280 (~2.0 ratio indicates high RNA purity) and 260/230 (nucleic acid purity – contaminant free), were used. For quantitative applications *i.e.* semi-quantitative RT-PCR (see 6.2.2.7), RNA concentration was accurately determined using the Quant-IT RiboGreen RNA assay (Life Technologies) following manufacturer's instructions. The RiboGreen method overcomes the major drawback of the absorbance-based RNA concentration determination that is the large relative contribution of proteins and free nucleotides to the

signal. This technique is based on the properties of the RiboGreen dye, which increases its fluorescence only when bound to RNA. As the Quant-IT RiboGreen RNA kit includes a series of ribosomal RNA standards (from 0 to 100 ng/ μ l), the RNA concentration of a given sample can be calculated from the linear regression plotting of the reference values.

6.2.2.3. Polymerase chain reaction (PCR)

In this project, various molecular biology approaches with different purposes, relied on the amplification of DNA sequences by PCR. Particularly, PCR was used for cloning, validation of expression vectors, transcripts quantification and site-directed mutagenesis.

6.2.2.3.1. Standard PCR reaction

The following table (Table 10) summarizes a standard PCR setup on a 25 μ L scale. For all PCR purposes, the Recombinant Taq DNA Polymerase kit (Life Technologies) was used.

Table 10. Standard PCR components

Component	Volume
PCR buffer (10x)	2.5 μ l
MgCl ₂ (50mM)	0.75 μ l (1,5mM final)
FWD Primer (10 μ M)	1 μ l
REV Primer (10 μ M)	1 μ l
Taq DNA polymerase	0.4 μ l
dNTPs mix	4 μ l
Template (DNA-cDNA)*	1 μ l
ddH ₂ O add up to 25 μ l	14,35 μ l
Final volume	25 μ l

*According to downstream applications, template amount varies between 25-300ng.

During a standard PCR program, cycles of denaturation, annealing and extension are repeated in order to achieve exponential amplification of the sequence of interest. The number of cycles as well as the temperatures of annealing (primer binding) can be modified in order to increase PCR efficiency. Table 11 summarizes a standard PCR program.

Table 11. Standard PCR program

Step	Duration	Temperature	
Initial denaturation	5 min	95°C	
Denaturation	30 sec	95°C	
Annealing	30 sec	58-62°C T _m (primer) dependent	35 cycles
Extension	1 min per 1 kb	72°C Polymerase dependent	
Final extension	10 min	72°C	

For cloning purposes, the proof reading polymerases AccuPrime Polymerase and Platinum Taq Polymerase (Life Technologies) were used in order to avoid the insertion of mutations into the amplified sequence. PCR reactions with these polymerases were performed according to manufacturer's instructions. When necessary, PCR conditions were optimized by adjusting $MgCl_2$ concentration, annealing temperature and number of PCR cycles. Optimization was performed to either reduce the amplification of unspecific products or to increase/boost Taq polymerase performance.

6.2.2.3.2. Site directed mutagenesis PCR

Site-directed-mutagenesis was performed using the QuikChange® II XL Site-Directed-Mutagenesis Kit (Agilent Technologies) according to the manufacturer's instructions. Briefly, desired mutations can be inserted in a single PCR reaction using a high fidelity *PfuTurbo* DNA Polymerase and mutant oligonucleotide primers. The PCR reaction used in this study is shown in Table 12. Most importantly, this reaction requires a small amount of template and low number of PCR cycles in order to increase mutation insertion efficiency and decrease the generation of random mutations. The PCR program used for site-directed mutagenesis is similar to the standard program described in Table 11, but for the number of cycles which was always 18, as recommended in the Kit's instructions. Primers used for mutagenesis are provided in section 6.1.8.2.

Table 12. PCR components for site-directed-mutagenesis

Component (provided in kit)	Volume
Reaction buffer (10x)	5 μ l
FWD Primer (10 μ M)	1.5 μ l (125ng)
REV Primer (10 μ M)	1.5 μ l (125ng)
dNTPs mix	1 μ l
Quik Solution	3 μ l
<i>PfuTurbo</i> DNA polymerase	1 μ l
Template (DNA-cDNA)	1 μ l (10ng)
ddH ₂ O add up to 50 μ l	36 μ l
Final volume	50 μ l

After PCR, the amplified product was incubated with the endonuclease *DpnI* in order to digest residual parental DNA template and to select mutation-containing synthesized DNA. The vectors containing the desired mutations –in *CHP1* and *SLC18A3* cDNAs- were transformed into XL1-Blue supercompetent cells, provided with the kit. XL1-Blue cells are endonuclease (*endA*) deficient, which greatly improves the quality of mini/midiprep DNA, and also recombination (*recA*) deficient, to improve insert stability. Plasmidic DNA was purified as described in 6.2.2.1.

6.2.2.4. Clean-up of PCR products

Applications such as enzymatic digestions, sequencing, and DNA fragments ligation are sensitive to remaining buffer, free nucleotides or primers from PCR reactions. Thus, when necessary, PCR products were cleaned using both the QIAquick PCR Purification Kit (Qiagen) and the NucleoSpin Gel and PCR Clean-up Kit (Macherey Nagel). Manufacturer's instructions were followed and PCR products were eluted in ddH₂O.

6.2.2.5. Agarose gel electrophoresis

DNA or RNA molecules/fragments of different sizes were routinely separated by agarose-gel electrophoresis. According to the expected amplicon size, different agarose concentrations (0.8-1.2%) were used. Briefly, powdered standard or low melting agarose (LMA) were melted into 100ml of TBE buffer by warming up in a microwave and ethidium bromide was added to a final concentration 1 µg/ml to allow DNA visualization. The liquid agarose was poured into a chamber with well-combs (of different volume capacities) and left to solidify at RT. DNA samples were mixed with loading buffer, pipetted into the gel and separated at 70-80V for approximately 30 min. As reference, a standard DNA ladder was loaded in order to determine the fragment's relative size. DNA was visualized and analyzed by densitometry using the ChemiDoc XRS and the ImageLab documentation system (BioRAD).

6.2.2.6. Reverse transcription (cDNA synthesis)

The synthesis of DNA from an RNA template via reverse transcription, produces complementary DNA (cDNA). The latter, can be used as PCR template and thereby the transcripts produced by a given gene can be quantified. In this study, cDNA synthesis was performed using the QuantiTect Reverse Transcription kit (Qiagen) according to the manufacturer's instructions. RNAs were isolated as described in 6.2.2.2. For this specific application, the concentration of template RNAs was accurately determined by the RiboGreen method (6.2.2.2). A standard cDNA reaction is provided in Table 13.

Table 13. Reverse transcription set-up for a 20µl reaction

Component	Amount
Template RNA	300ng
7x gDNA wipe-out	2 µl
RNase-free H ₂ O	to the final volume of 14µl
Incubate at 42°C for 2 min. Transfer immediately to ice	
5x Quantiscript RT buffer	4 µl
RT Primer mix	1 µl
Quantitect Reverse transcriptase	1 µl
Incubate at 42°C for 45min	
Final step 75°C for 3min	

6.2.2.7. Semi-quantitative Reverse Transcription PCR

To detect and quantify *CHP1* transcripts in total mRNA isolated from HEK293T cells expressing V5-tagged CHP1 constructs, semi-quantitative Reverse Transcription PCR (semi-quantitative RT-PCR) was utilized. As this technique uses single-stranded cDNA as a template, transcript amounts at a given time can be estimated by densitometry; measuring band intensities on an agarose gel. For accurate transcript amount determination, semi-quantitative PCR was optimized (based on a standard PCR reaction, see 6.2.2.3.1) and performed as multiplex with the housekeeping gene *HPRT* (NCBI 3251). To avoid saturation of amplified products, PCR cycle number was set to 24. Densitometric analysis of normalized *CHP1/HPRT* expression was performed using the ImageLab system (BioRAD).

6.2.2.8. Cloning procedures

6.2.2.8.1. Cloning into TOPO vector

To generate V5-tagged CHP1 constructs, the human *CHP1* cDNA (NCBI 11261) was cloned into the pcDNA3.1/TOPO V5-HIS using the pcDNA3.1 TOPO TA Expression Kit (Life Technologies) and following manufacturer's instructions. Vectors used for cloning as well as all generated pcDNA3.1/TOPO plasmids are listed in section 6.1.9. The TOPO-TA cloning system takes advantage of the ligation activity of the Topoisomerase I (from *Vaccinia virus*) and the terminal transferase activity of the *Taq* polymerase. This enzyme adds a single 3'-A overhang to each end of the PCR product, thus making possible to clone a PCR product directly into a linearized cloning vector with single 3'-T overhangs. The *CHP1* cDNA was amplified from a previously cloned *CHP1* construct (pcDNA3.1-CT-GFP) using the primers listed in 6.1.8.1, which were designed according with the kit's recommendations. The ligation reaction was performed during 5 minutes at RT and included: 4µl of PCR product, 1µl of linearized TOPO vector and 1µl of salt solution (provided) in a final reaction

volume of 5 μ l. TOP10 *E. coli* competent cells were transformed with 1 μ l of the ligation reaction.

6.2.2.8.2. Subcloning into PCS2+ vector

cDNAs from both *CHP1* (NCBI 11261) and *SLC18A3* (NCBI 6572) were subcloned into PCS2+ expression vectors in order to generate *in vitro* transcribed mRNAs for subsequent protein OE experiments in zebrafish. Both *CHP1* and *SLC18A3* cDNAs were isolated from pcDNA3.1 template vectors by PCR amplification with Accuprime DNA polymerase. Double-enzyme digestion reactions (as depicted in Table 14) were performed depending on buffer compatibility and included either purified PCS2+ plasmid in ddH₂O or cleaned/purified PCR products in ddH₂O. To achieve maximum digestion and vector linearization, reactions were incubated for 3h at 37°C. Enzymatic reaction was stopped with DNA loading buffer. The digested DNA fragments were resolved in 0.8% agarose gels and the bands of interest (linearized vector and inserts) were excised from the gel, minimizing both excessive agarose removal and long UV exposure. DNA was gel-extracted with the QIAquick Gel Extraction kit (Qiagen) following the manufacturer's instructions. Cleaned DNAs were eluted in ddH₂O. Ligation procedures were performed as indicated in

Table 15 using the T4 DNA ligase from Promega for 2h at RT. 2 μ l of the reaction were used for transformation of competent *E. coli* cells. For ligation of gel-purified vector and insert fragments; the ligation volume was set to 50 μ l to compensate for buffer changes caused by residual gel TBE buffer.

Table 14. Standard double digestion reaction

Component	Amount
Plasmid DNA or PCR product	5-10 μ g (25-30 μ l)
BamHI (10 U/ μ l)	2 μ l
EcoRI (10 U/ μ l)	2 μ l
100x BSA	0.5 μ l
10x CutSmart Buffer	5 μ l
ddH ₂ O to the final volume of 50 μ l	

Table 15. Standard ligation reaction with T4 DNA ligase (Promega)

Component	Amount
10x Ligation buffer	5 μ l
T4 DNA ligase	2.5 μ l
Linearized vector	2 μ l
Insert	6x amount of vector
ddH ₂ O to the final volume of 50 μ l	

6.2.2.9. *In vitro* transcription of mRNA

To achieve protein OE in zebrafish, *CHP1* and *SLC18A3* WT or mutant mRNAs were synthesized *in vitro* from linearized PCS2+ plasmids. To do this, PCS2+ vectors (with the inserts of interest) were digested with the enzyme *NotI* in a reaction similar to the one described in Table 14 and the digestion products were cleaned as described in 6.2.2.4. Capped mRNAs were synthesized using the SP6 mMessage kit (Ambion) following manufacturer's instructions. The reaction for RNA transcription was prepared as indicated in Table 16 and incubated for 3 hours at 37°C. Synthesized RNAs were purified with the RNeasy isolation kit (Qiagen), as described in 6.2.2.2 and aliquoted to avoid thawing and freezing of the samples. To assess for RNA integrity and full PCS2+ plasmid removal, 1µl of RNA was loaded into LMA 0.8% gels. The detected ssRNA bands were confirmed to match expected transcript sizes. mRNA concentration was determined using the NanoDrop ND-1000 (6.2.2.2). Samples were stored at -80°C.

Table 16. Reaction set-up for *in vitro* mRNA transcription

Component	Amount
Linearized PCS2+ vectors	1µg (5-1µl)
2x NTP/CAP	10 µl
10x Reaction buffer	2 µl
Enzyme mix	2 µl
Nuclease-free water to the final volume of 20µl	

6.2.2.10. DNA sequencing

Sequencing of plasmid DNA and purified PCR products was performed at GATC Biotech. Nucleic acids were routinely sequenced using primers of own design or standard vector-primers provided by GATC. Sequence alignment and analysis was performed using the SeqMan application from the Lasergene Suite (DNASTar).

6.2.3. Microbiology work

All experimental procedures were performed under sterile conditions and in proximity to a Bunsen burner. Bacteria were cultivated under Ampicillin selection, as all plasmids used in this study were Ampicillin-resistant. To propagate the expression vectors, the *endA* deficient *E. coli* strains TOP10 and DH5α (Life Technologies) and the *endA/recA* XL1-Blue (Agilent) were used for transformation.

6.2.3.1. Transformation of DNA into competent *E.coli* cells

Upon arrival, cells were stored at -80°C and thawed on ice immediately before use. Transformation protocols were performed according to competent cells producer's instructions. Routinely, 2µl of ligation product or 50ng of plasmid DNA were added into the bacterial vial (provided) and gently mixed by tube inversion. The DNA-bacteria mix was incubated 20 minutes on ice and then heat shocked for 30 seconds at 42°C in a water bath (Heat shock times and reaction vials can vary slightly according to *E. coli* strains). Bacteria were directly transferred to ice and chilled for 2 minutes. Afterwards, 250µl of pre-warmed S.O.C medium (provided with competent cells) was added into bacterial vials. The small bacterial culture was incubated for 1 hour at 37°C in a shaking incubator. Different culture volumes (50µl to 200µl) were plated with a sterile Digrafsky spreader on Ampicillin-selective LB agar. Plates were incubated at 37°C overnight.

6.2.3.2. Colony PCR

Colony PCR was performed to identify bacterial clones successfully transformed with a vector of interest. The purpose of this PCR consisted in identify clones in which the orientation of the insert inside an expression vector is correct. Bacterial colonies from a selective agar plate were picked individually using a sterile pipette tip and resuspended in 20µl of sterile ddH₂O. From this solution, 5µl were used as template for colony PCR whereas the remaining suspension was used to inoculate 5ml of selective LB-cultures for further plasmidic DNA isolation (see 6.2.2.1). The colony PCR was based in the standard PCR setup described in 6.2.2.3.1, however to guarantee complete bacteria lysis, the initial denaturation step was increased up to 10 minutes. Most importantly, the primer pairs used for colony PCR were positioned on the vector sequence and within the insert, in order to detect the correct orientation of the insert.

6.2.3.3. Preparation of bacteria glycerol stocks

For long term storage of bacteria strains successfully transformed with the plasmid of interest, glycerol stocks were prepared from 5mL of bacterial culture growing in selective ampicillin media. Once the culture reached exponential phase (optical density 600nm – or slightly turbid to the observer), 750µl of culture were mixed with 250µl of sterile glycerol in cryo-conservation vials. Stocks were stored at -80°C. If necessary, selective bacterial cultures were inoculated with a small amount (ice scratched with a pipette tip) of frozen glycerol stock.

6.2.4. Gene identification methods

Whole Genome Linkage Analysis (WGLA) and Whole Exome Sequencing (WES) for the identification of novel ARCA genes were performed in collaboration with Drs. Giovanni Stevanin and Marie Coutelier, affiliated to INSERM (Institut du Cerveau et de la Moelle épinière) in Paris, France.

6.2.4.1. Whole genome linkage analysis

Linkage analysis is a method for the genetic mapping of loci within a family. The advantages of performing a WGLA combination with WES as well as the underpinnings of linkage analysis are described in the introduction section 2.3.

In a classic linkage analysis, polymorphic microsatellites or SNPs are used as markers for genome-wide linkage. The statistical analysis of linkage refers to the probability that a gene –relevant for disease- is linked to a genetic marker. This probability is studied through a LOD score (logarithm of the odds). This score compares the likelihood of obtaining the test data, in other words if two loci are linked (null hypothesis), to the likelihood of observing the same data by chance. A LOD score higher than 3.0 is generally accepted as statistical significant evidence of linkage; whereas a LOD score of -2 or below excludes linkage (Pulst, 1999).

In this study, WGLA was performed using Illumina LINKAGE_12 microarrays (6090 SNP markers). DNAs from 5 individuals were available (including the affected subjects, one unaffected sibling and their parents). Genotypes were determined using Beadstudio (Illumina) and analysed with MERLIN 1.0 (Abecasis et al, 2002). For statistical analysis, the following assumptions were considered: autosomal recessive transmission under a 0.90 penetrance model with equal allele frequencies, similar recombination fractions between males and females and a disease frequency of 0.00001.

6.2.4.2. Whole Exome Sequencing

The whole exome of four individuals, coded 1, 2, 6 and 8 in family AAR-087 pedigree (See Figure 11; where 1 and 2 are the parents and 6 and 8 are the affected siblings), was sequenced on the Illumina HiSeq 2000 as paired-end 100bp reads. Library preparation was performed with the SureSelect Human All Exon 50Mb v4 kit (Agilent). The reads were aligned to the human reference genome (UCSC hg19) using the Burrows-Wheeler Alignment tool (BWA) (Li & Durbin, 2009). The Broad Institute's Genome Analysis Toolkit

(GATK) was used for local re-alignments around indels, base-score recalibration and variant calling (McKenna et al, 2010). WES variants were annotated and imported into GEnomes Management Application (GEM.app), a web-based tool for NGS data analysis (genomics.med.miami.edu) (Gonzalez et al, 2013). Variants were filtered using the following criteria:

- I. Quality (GATK quality >50, maximal genotype quality in family >40).
- II. Effect on the coding sequence (missense, nonsense or splice variants, coding indels).
- III. Frequency in public databases. $\leq 2\%$ in dbSNP137 and $\leq 1\%$ in EVS-Exome Variant Server (NHLBI Exome Sequencing Project. <http://evs.gs.washington.edu/EVS>).
- IV. Conservation scores. GERP++ score >0 (Davydov et al, 2010) and PhastCons score >0.4 (Siepel et al, 2005).
- V. Internal frequency. Less than 5 families with the segregating variant among 892 families from the SPATAX exome database.
- VI. Homozygosity in the affected patients and heterozygosity in the parents.
- VII. Alternate allele homozygosity in the population. Genome Aggregation Database (GenomAD) (Lek et al, 2016).
- VIII. Mutation effect prediction scores. SIFT (Ng & Henikoff, 2003), Polyphen-2 HDIV and HVAR (Adzhubei et al, 2013), LRT (Chun & Fay, 2009) and Mutation Taster (Schwarz et al, 2010).

Variants were validated and segregation was assessed using Sanger sequencing. Primers design and PCR were performed following standard procedures.

6.2.4.3. Population screening for *CHP1* variants

6.2.4.3.1. Re-sequencing of *CHP1* exons 2 and 6

In order to unmask potentially undetected *CHP1* variants due to poor exon coverage, *CHP1* exons 2 and 6 were re-sequenced in all the 319 WES index cases with cerebellar ataxia (SPATAX cohort).

Primers for exons 2 and 6 were designed using Primer3Plus, and amplification was performed using either the DreamTaq or Accuprime-GC rich polymerases (both from Thermo Fischer). Amplicons were indexed using Fast-Start High-Fidelity polymerase (Roche) and subsequently sequenced on the Illumina MiSeq using 2x300bp paired-end read cycles. Sequence reads were processed as described above for WES sequences. Variants were annotated with Annovar (Wang et al, 2010) and sorted using the following criteria:

- I. Quality (GATK quality >30).
- II. Effect on the coding sequence of *CHP1*. Exonic non synonymous, SNVs or splice variants.
- III. Frequency in public databases. ≤1% in EVS, ExAC (Exome Aggregation Consortium <http://exac.broadinstitute.org/>) and bioRxiv (doi:<http://dx.doi.org/10.1101/030338>) databases.
- IV. Internal frequency in local exome database. Allele count ≤30, *i.e.* 4.7%.

6.2.4.3.2. Search for *CHP1* variants in a NMD cohort.

Focused screening for *CHP1* variants was additionally performed in our own WES cohort of 657 patients with NMDs. This search was performed by our colleague Mert Karakaya, MD.

6.2.5. Cell culture

All cell culture procedures were performed under a laminar flow workbench and sterile conditions. Routinely, cell growth media was supplemented with Penicillin, Streptomycin and Amphotericin B, unless noted otherwise, to avoid bacteria or fungi contamination. Cells were grown in sterile incubators at 37°C, 5 % CO₂ and 95% relative humidity.

6.2.5.1. Cultivation of eukaryotic cell lines

HEK293T, HeLa, NSC-34 and N2A cells were cultivated in DMEM (Dulbeccos's Modified Eagle Medium) complemented with 10% Fetal Calf Serum (FCS). PC12 cells were cultivated in DMEM-GlutaMAX (low glucose) supplemented with 10% horse serum and 5% FCS. Cells were cultivated in 75cm² flasks for maintenance and subcultured when 90% confluency was reached. For cell splitting and seeding into flasks, plates or well-plates, the cells were washed with PBS and detached by trypsinization using Trypsin-EDTA. Trypsin was neutralized upon addition of at least 1 volume of supplemented media. The cell suspension was homogenized and cells were distributed to new culture flasks or plates. Routinely, HEK293T, NSC-34 and PC12 cells were split 1:5 for maintenance. The faster-growing N2A cells were split 1:8.

6.2.5.2. Cell counting

As different experimental procedures required a defined number of cells *i.e.* specific confluency, a counting Neubauer chamber was used to determine the number of cells in suspension. After cell trypsinization and homogenization, 10 μ l of cell suspension were deposited on top of the chamber to calculate the number of cells per milliliter. The four large squares placed at the corners of the chamber were used for cell counting under the light microscope (cells touching the lower and right edges were not taken into account for quantification). The mean cell number of the four quadrants was multiplied by 10⁴ to calculate cells/ml.

6.2.5.3. Cryopreservation of cell lines

For long-term storage of cell lines in early passages, confluent 75cm² flasks were trypsinized (see 6.2.5.1) and collected by centrifugation at 3000 rpm for 5 min. The pelleted cells were resuspended in 2ml of growth medium containing DMSO as cryoprotective agent. The cells were frozen in a cryo-conservation container which allow slow cell freezing at a rate of approximately 1°C/min. For long term storage cells were transferred from -80°C freezer to liquid nitrogen tanks. To thaw frozen cells for new cell culture rounds, cryo-tubes were placed in a 37°C water bath for fast thawing and the liquid cell suspension was pipetted into 75cm² culture flasks with pre-warmed culture medium.

6.2.5.4. Cell transfection for transient protein overexpression

To transfect HEK293T, HeLa, N2A cells and PC12 cells the transfection reagent Lipofectamine2000 was used. For transfection of NSC-34 cells, the reagent DharmaFECT showed better transfection efficiencies. Depending on downstream applications, cells were seeded as shown in Table 17. Most importantly, for the cultivation of neuron-like cells, low confluency cultures were set to allow differentiation and neurite outgrowth (see next section).

Table 17. Cells seeding densities for transfection experiments

	HEK293T	HeLa	N2A	PC12	NSC-34
6-well plate	5x10 ⁵	-	3.5x10 ⁵	-	-
12-well plate	4.5x10 ⁴	4.5x10 ⁴	3x10 ⁵	4x10 ⁵	4x10 ⁵

Transfection reactions were prepared according to manufacturer's instructions. To transfect a 6-well plate, 2 μ g of plasmid DNA together with 4 μ l of transfection reagent were routinely

used. This transfection mix, in a final volume of 500 μ l (prepared in OPTIMEM media), was added on top of the cells and incubated during 20 minutes at RT. After this time, cells were filled with culture media without antibiotics, to a final cultivation volume of 2ml. Transfection mix was scaled-down according to the growth area (3.7cm²) and cultivation volume (1ml) of individual 12-well plate wells. Empty vectors were transfected as controls. For protein and RNA isolation, cells were harvested after 24, 48 or 72 hours. For immunostainings, cells were either fixed or differentiated after 24h of transfection.

6.2.5.5. Seeding and differentiation of neuron-like cells

For immunostaining purposes, all neuron-like cells were plated on coverslips coated with laminin to preserve neurite-like structures. Laminin was applied manually on top of the coverslips with a bended pipette tip. As the differentiation of neuron-like cells is density-dependent (once confluent they stop differentiation), cells were seeded in low densities (Table 17) to allow both 24 hours of transfection and subsequently 3-4 days of differentiation. After transfection, growth medium of NSC-34 cells was replaced for standard DMEM supplemented with 5 μ l/ml retinoic acid (RA) to trigger differentiation. PC12 growth media was supplemented with 25 μ l/ml NGF. As N2A cells differentiate under starvation conditions, media was replaced for 2% DMEM supplemented with 20 μ m/ml RA.

6.2.6. Protein biochemistry methods

Proteins were routinely isolated in RIPA buffer (Sigma-Aldrich) containing protease inhibitors (Complete Mini Protease Inhibitors, Roche). All experimental procedures with proteins were carried out at 4°C. After isolation, proteins were aliquoted and stored at -80°C. Thawing and freezing of protein samples was avoided.

6.2.6.1. Protein isolation from eukaryotic cells

Cells were seeded in variable amounts for protein isolation. After cell collection by trypsinization, cells were washed with PBS and transferred to eppendorf tubes. Ice cold RIPA buffer was used for cell lysis in variable amounts depending of the number of cells seeded (usually 50 μ l were used to lyse one well of a 6-well plate). After 30 minutes of RIPA incubation, cells were centrifuged for 25 minutes, at maximum speed at 4°C. Supernatants, with soluble proteins, were collected and aliquoted into new reaction tubes. If not immediately used, samples were stored at -80°C.

6.2.6.2. Subcellular fractionation of total protein lysates

HEK293T or undifferentiated N2A transiently expressing CHP1-V5 constructs were collected after 48 hours of transfection by trypsinization. After a PBS wash, cells were processed with the Subcellular Protein Fractionation Kit for cultured cells (Thermo Scientific) following manufacturer instructions. Subcellular fractionation consists in sequential incubations with different lysis buffers in order to collect proteins from different subcellular compartments. In this study, the soluble, membrane and cytoskeletal (insoluble) fractions were collected. As the fractionated proteins are recovered in high volumes (more than 250 μ L), samples were concentrated to an approximate volume of 50 μ l using Amicon® Ultra 0.5mL columns (Millipore).

6.2.6.3. Protein isolation from zebrafish

Protein lysates from zebrafish were prepared following the protocol described in (Hoyt, 2009) with some modifications. 20 fish larvae were manually dechorionized after ~32hpf, pooled in eppendorf tubes and resuspended in 60 μ L of ice cold RIPA buffer containing protease inhibitors. After 20 minutes of incubation on ice, fish were placed in soft-tissue homogenizing CK14-0.5ml columns (PeqLab) and homogenized in the Precellys24 (PeqLab) using the program for zebrafish recommended in the manufacturer's instructions booklet (1 round, 25 seconds at 5500 rpm). Fish lysates were centrifuged for 25 minutes, at maximum speed and 4°C. Supernatants, with soluble proteins, were collected and aliquoted into new reaction tubes. If not immediately used, samples were stored at -80°C.

6.2.6.4. Determination of protein concentration with Bradford

Protein concentration was determined by spectrophotometry using the Bradford assay (Bradford, 1976; Bradford & Williams, 1976). This colorimetric assay is based on the absorbance shift of the Coomassie Brilliant Blue G-250 dye. Under acidic conditions, *e.g.* protein amino acidic residues, the red form of the dye (with absorbance at 470nm) shifts into blue (absorbance at 595nm) upon protein binding. For protein concentration determination, 1 μ l of protein lysate was mixed with 499 μ l of Bradford reagent (Applichem) and incubated at room temperature for 10 minutes. The protein-Bradford mixture was transferred to spectrophotometric cuvettes and the concentration was determined by measuring the absorption at 595nm on a standard spectrophotometer (Eppendorf). A standard curve with known BSA concentrations (0.5-5 μ g) was generated for equipment calibration and protein concentration estimation.

6.2.6.5. Sodium Dodecyl Polyacrylamide Gel Electrophoresis SDS-PAGE

Gel electrophoresis of proteins with a polyacrylamide matrix, is one of the most widely used techniques to characterize complex protein mixtures. During SDS-PAGE, proteins are primarily separated by their molecular weight (MW) since the ionic detergent SDS denatures protein structure and also binds to proteins to make them negatively charged. When an electric current is applied, all SDS-bound proteins migrate through the polyacrylamide gel towards the anode (positively charged electrode). Small proteins, with less mass, travel more quickly through the gel than those with greater mass. Protein denaturation in the presence of the reducing compound β -Mercaptoethanol (added to the protein loading buffer; also termed Laemmli buffer) denatures hydrogen and disulfide bonds, *i.e.* secondary and tertiary protein structures (Laemmli, 1970).

Discontinuous SDS gels were prepared in this study using two different types of agarose namely stacking and separating. The higher stacking gel is slightly acidic (pH 6.8) and has a lower acrylamide concentration (4% was routinely used) making a porous gel, which do not separates protein but allows them to “concentrate” into thin and defined bands before separation. The lower separating gel, also termed resolving, is basic (pH 8.8) and has a higher polyacrylamide content (12% was routinely used), thus in this phase the gel’s pores are more narrow and proteins are separated by MW.

SDS gels were prepared between two glass plates. The resolving solution was poured first and once solidified, the stacking solution was poured on top. To obtain sharp resolving gel edges, isopropanol was applied on top of the resolving acrylamide solution and washed out prior to stacking addition (for gel compositions, see 0). Exceptionally, fractionated protein lysates were resolved in pre-casted SDS gradient gels (mini PROTEAN 4% to 20% from BioRad) to better resolve membrane proteins, which are more prone to aggregate and accumulate in the stacking phase. After protein concentration determination and prior to gel loading, protein lysates (between 5 μ g to 20 μ g) were mixed with 3x Laemmli buffer and boiled for 10 minutes. 10 μ L of the PageRuler™ Prestained Protein Ladder (Thermo) were loaded for estimation of relative protein sizes. Electrophoresis was performed at an initial voltage of 80V to allow proteins entrance into the stacking gel. Voltage was increased up to 180V for protein resolving.

6.2.6.6. Western blot

Once separated by electrophoresis, proteins can be transferred onto a nitrocellulose membrane for detection by Western blotting. All transfer procedures were performed as wet-transfer into transfer tanks (BioRad) filled with transfer buffer. Electrophoretic transfer

is performed using an electric field, oriented perpendicular to the surface of the gel, causing proteins to migrate from the gel towards the nitrocellulose membrane. For Western blotting, the membrane is placed between the gel surface and the positive electrode in a “sandwich” assembly. This sandwich includes both a sponge and filter papers at each end to protect the gel and blotting membrane. Protein transfer was carried out at 4°C for 1.5 hours at 110V or overnight at 30V. Successful transfer was confirmed with Ponceau S staining.

6.2.6.7. Protein immunodetection on Western Blot membranes

Western blotting uses specific antibodies to identify proteins that have been separated by SDS-PAGE. The nitrocellulose membrane is probed with primary antibody that recognizes a specific protein or epitope, however this antibody is not directly detectable. Therefore, horseradish peroxidase (HRP)-conjugated secondary antibodies are used to indirectly detect the target antigen.

After WB and Ponceu S staining, the nitrocellulose membrane was washed in TBST and blocked with blocking solution (5% milk powder and 1% BSA) at RT for 1 hour. Primary antibodies diluted in 1% blocking solution (1% milk powder and 0.2% BSA) were added to the membrane and routinely incubated overnight at 4°C (specific dilution and incubation conditions for all used antibodies are stated in 6.1.5). The next day, the membrane was washed 3 times for 10 minutes in TBST to remove unbound antibodies. Subsequently, the secondary HRP-conjugated antibodies, also diluted in 1% blocking solution, were supplied and incubated for 1h at RT. After 3 TBST washes of 10 minutes, the membrane was incubated for 5 minutes with the chemiluminescence detection substrate (Super Signal West Pico ECL Substrate from Thermo Scientific). Proteins were detected using the ChemiDoc XRS system (BioRAD) and densitometric analysis was performed using the ImageLab Software (BioRAD). When necessary, membranes were stripped to remove bound antibodies with the Restore Western Blot Stripping Buffer (Thermo Scientific). After 3 TBST washes of 10 minutes, immunodetection of proteins was performed as described above.

6.2.6.8. Size Exclusion Chromatography

Size Exclusion Chromatography (SEC) was performed in order to separate CHP1 WT and mutant protein complexes according to their MW. This assay was calibrated by our colleague Seyyed Mohsen Hosseini Barkoie.

For SEC, HEK293T cells transiently expressing CHP1-V5 constructs were collected after 48 hours of transfection by trypsinization (see 6.2.5.1) and lysed in 300µl of NP40 lysis

buffer. Cells were incubated for 20 minutes, sonicated and centrifuged at 13000 rpm for 15 min. SEC was performed with a Superose 6 10/300 GL column connected to an ÄKTA-pure FPLC system (both from GE Healthcare). The Superose 6 column was chosen for this analytical purpose, as it has a separation limit between 5 and 500KDa. For column equilibration, the same NP40 buffer without protease inhibitors was used. 250µl of total protein lysates were injected into the column and 500µl fractions were collected until no protein signal was detected (approximately 50 fractions). Collected proteins were snap-frozen and stored at -80°C. For Western blotting, 25µL of each fraction were processed as described in 6.2.6.5 and 6.2.6.6. To determine the elution volumes, and hence MW, of the separated CHP1 protein complexes, the Superose 6 column was calibrated with protein standards of known molecular weight (Table 18).

Table 18. Protein standards used for SEC column calibration

Standard	Size (kDa)	Range
Ribonuclease A	13.7 KDa	Low MW
Carbonic anhydrase	29 KDa	
Ovalbumin	43 KDa	
Aldolase	158 KDa	High MW
Ferritin	440 KDa	
Thyroglobulin	669 KDa	

6.2.6.9. Protein modelling

3D-protein modelling analyses were performed in collaboration with Christian Pichlo affiliated to the Institute of Biochemistry, University of Cologne. Cologne, Germany. The protein structures of free CHP1 (2CT9) and NHE1 bound CHP1 (2E30) were acquired from RCSB Protein Data Bank (<http://www.rcsb.org/pdb/home/home.do>). Cartoon representations were generated with PyMOL 1.5.0.4.

6.2.7. Fluorescence immunostaining

6.2.7.1. Immunostaining of eukaryotic cells

For fluorescence immunostainings HeLa, N2A, PC12 and NSC-34 cells transiently expressing various recombinant pcDNA3.1-GFP vectors (6.1.9) were seeded in coverslips or laminin-coated coverslips to preserve neurite-like structures, if necessary. As previously described, cells were transfected for 24 hours and differentiated, if necessary, during 4-5 days (see 6.2.5.4 and 6.2.5.5). Cells were washed with pre-warmed PBS (37°C) and fixed with 4% PFA for 15 min at RT. After three additional PBS washes of 10 minutes, cells were

permeabilized in PBST (0.2% Tween-20) for 5 minutes and blocked in blocking solution (PBST + 5% BSA and 1% FCS) during one hour at RT. Primary antibodies were diluted in blocking solution and used in the dilutions and incubation times described in section 6.1.5. After three PBST changes, cells were incubated 1h at RT with different combinations of Phalloidine and/or secondary antibodies, also diluted in blocking solution (see antibodies used in 6.1.5). After incubation, cells were washed three times with PBST and coverslips were rinsed in water prior mounting with ProLong mounting media with or without DAPI (Life Technologies).

6.2.7.2. Immunostaining of zebrafish

All fixation, washing and incubation procedures were performed on a horizontal rotating wheel, unless otherwise noted.

6.2.7.2.1. Visualization of Caudal Primary Motor Neurons (CaP-MN)

34hpf zebrafish were manually dechorionated, fixed in 4% PFA in 2ml eppendorf tubes overnight and long-term stored in methanol at -20°C. Immunostaining of fish larvae started by re-hydration in sequential and decreasing methanol solutions (in PBST 0.1% Tween20), namely 75%, 50% and 25%. Fish were incubated in each hydration solution for 5 minutes in a horizontal rack, subsequently permeabilized with 10µg/ml of Proteinase-K for 20 min and post-fixed in 4% PFA for 15 minutes at RT. To remove PFA, fish were washed 4 times with PBST for 5 minutes. Blocking was performed with blocking solution (PBST + 10% FCS and 1% DMSO) for at least 3 hours at RT. Primary mouse α - Znp1 antibody was diluted 1:150 in blocking solution and incubated overnight at 4°C. After multiple washes (5 minimum) of 1 hour with blocking solution, the secondary mouse α -AlexaFluor488 antibody was diluted 1:250 in blocking solution and incubated at 4°C overnight. Following 5 washes of 20 minutes each, stained fish were stored in 80% glycerol in PBS at 4°C.

For imaging of CaP-MN, fish were laterally embedded in 2% LMA microslides under the binocular microscope. Slides were analysed in the fluoresce microscope AxiolmagerM2 (Zeiss). The first 10 motor axons posterior to the yolk sac were considered for quantification (Figure 41). Based on overall appearance MN were classified as: normal, truncation (shortened axonal projection) or atrophy (absent axonal projection). Based on terminal branching, axons were classified as Normal, Mild (branching ventral from midline), Medium (2-3 or more branches at ventral or midline) or Severe (>3 branches ventral or dorsal from midline).

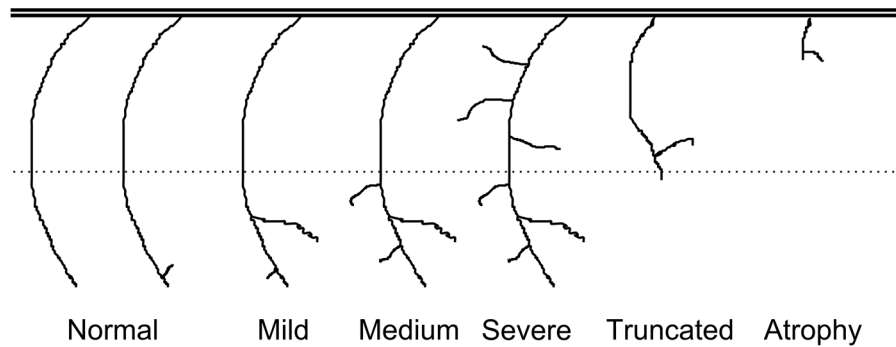


Figure 41. CaP-MN axon morphology. The first 10 motor axons posterior to the yolk sac were considered for quantification. Dotted line indicates the sensory mid-line.

6.2.7.2.2. Cerebellum visualization

~72hpf zebrafish were manually dechorionated, fixed in Dent's Fixative (80% methanol – 20% DMSO) and stored in this solution for maximum 1 week. After sequential re-hydration in different methanol solutions prepared in washing buffer (PBST 0.1% Tween20 + 1% BSA), fish were permeabilized with 10 μ g/ml of proteinase K (Sigma) for 30min and post-fixed in PFA as described in 6.2.7.2.1. After 4 washes of 5 minutes with washing buffer, fish were blocked in blocking solution (PBS + 1% BSA and 10% FCS) for at least one hour at RT. To visualize the cerebellum, fish were incubated overnight at 4°C with the primary antibodies: mouse α -acetylated tubulin 1:1000 and/or rabbit α -zebrafish-Chp1 1:150 diluted in blocking solution. Following 3 washes of 20 minutes with washing buffer, the corresponding AlexaFluor secondary antibodies (6.1.5) were diluted 1:250 in blocking solution and fish were incubated at 4°C overnight. Lastly, after 3 washes of 20 minutes with washing buffer, fish were long-term stored in 80% glycerol in PBS at 4°C. For imaging, fish were embedded dorsally in channeled-microslides under the binocular microscope. Lack of axonal density in the midline of the morphant's cerebellum was considered as cerebellar hypoplasia.

6.2.8. Microscopy

All images were acquired with a Zeiss fluorescence microscope AxioImager M2 equipped with the ApoTome2 system to mimic confocality and an AxioCam MRm camera. For cells imaging, 40x and 63x oil immersion objectives were used. Zebrafish images of CaP-MN and cerebellum were acquired with 10x and 20x objectives. Z-stacks were routinely generated to obtain quality images for representative pictures and colocalization analyses.

6.2.8.1. Colocalization analysis

Quantitative analysis of colocalization were performed with the in-built colocalization tool of the ZEN software. These analyses are performed on a pixel by pixel basis. Every pixel in the image is plotted in a scatter diagram based on its intensity level from each channel. Pixels with high intensities in the channels of interest, e.g. red and green, visible in one specific quadrant of the scatterplot, are considered to be colocalized. The ZEN software automatically analyze different measurement from this scatter plot to generate Pearson colocalization coefficients. The result of this analyses is +1 for perfect correlation, 0 for no correlation, and -1 for perfect anti-correlation.

6.2.9. Zebrafish methods

Zebrafish experiments were performed in collaboration with Dr. Mathias Hammerschmidt and Dr. Heiko Löhr from The Institute for Zoology / Developmental Biology of the University of Cologne (Germany). All procedures were approved by the local animal protection committee LANUV NRW; reference number 84-02.04.2012.A251 granted to Dr. Hammerschmidt. For visualization of CaP-MN embryos derived from TL/EK wild-type and *tg(mnx1-GFP)^{ml2TG}* (HB9-GFP) lines crossings were used (Flanagan-Steet et al, 2005). Embryos from TL/EK wild-type crossings were used for cerebellar analyses.

6.2.9.1. Zebrafish breeding and egg collection

To obtain zebrafish eggs for injection, zebrafish pairs were settled in mating tanks one day before injection. To do so, one female TL/EK wild-type and one male either HB9-GFP or TL/EK wild-type, depending on the intended analysis of CaP-MN or cerebellum, respectively, were placed together in a tank separated by a spacer. Depending on the fish strain, 5 to 8 tanks were prepared in order to collect enough eggs for injections. The next day and strictly before 10am –the most active period of the zebrafish- the fish tanks were refreshed with new water and the spacer was removed to allow egg fertilization. After 10-15 minutes, eggs were collected and placed in agarose injection plates under a binocular microscope. This plates have a series of 6 channels in which approximately 300 eggs can be immobilized for injection.

6.2.9.2. Zebrafish injection of Morpholinos (MOs) and mRNAs

Zebrafish eggs were injected with MOs (indicated in 6.1.8.4) and mRNAs as follows:

- *chp1* MO, *CHP1-WT* and *CHP1-K19del* mRNA were injected alone or in combination for CaP-MN and cerebellar morphology analyses.
- *VAcHt-WT* and *VAcHt-D147N* were injected for CaP-MN analysis.
- *chp1* and *smn* MOs were injected alone or in combination for CaP-MN analysis.

Specific concentrations of morpholinos and mRNAs were prepared for injection in a solution containing 1µl of Phenol Red (Sigma) and 1µl of Rhodamin-Dextran (Sigma) in a final volume of 10µl. The mixture was heated for 5 min at 65°C and afterwards transferred immediately to ice. 3µl of this solution were loaded into injection needles, prepared with anticipation with a microneedle puller device (Sutter Instrument Company). The needle was inserted into a pneumatic injector pump (World Precision Instruments) and the drop size, hence injection volume, was calibrated under the binocular (in 5x magnification) in a glass chamber containing dimethylpolysiloxane (Sigma). Routinely, a drop size of 0.1mm equivalent to 500pl was calibrated for injections. The injection plates, previously filled with fish eggs, were injected at the 1-to-4-cell division stage to guarantee maximum distribution of MO and/or mRNAs. The PhenolRed allows the visualization of injected eggs, at this step. After injection, plates were placed in a 28°C incubator. Later on the day of injection (6-7 hours) and taking advantage of the fluorescent Rhodamin-dextran dye included in the injection mix; embryos were sorted in order to select correctly-injected eggs. Embryos were analysed under a fluorescent binocular microscopy and only the eggs where homogenous dextran distribution was observed, were kept for further analysis. Positively selected embryos were reared in a clean petri dish filled with E3 embryo medium containing 200µM of 1-phenyl 2-thiourea (PTU Sigma) to prevent fish pigmentation. Fish embryos were kept in a 28°C incubator until processed for protein isolation (6.2.6.3) or immunostaining (6.2.7.2).

6.2.9.3. Zebrafish motor analysis

For motor analysis, ~34hpf zebrafish, still in chorion, were placed in 12-well plates (10 fish/well) containing E3 embryo medium and equilibrated for 5 min. The number of body contractions (spontaneous contractions) in 30 seconds was quantified manually for each fish from recorded videos. For data analysis, spontaneous contractions were categorized as: 0 (no contraction), 1 (one contraction in 30 sec), 2 or more (2 or more contractions in 30 sec). Videos of 34hpf or 72hpf fish larvae were recorded with a 16MP High Definition (30fps) camera (Samsung) attached to a Leica S8AP0 binocular.

6.2.10. Statistical analysis

Statistical analyses were performed in GraphPad Prism 6 (GraphPad Software). Precisely, for the analysis of RNA and protein levels, two tailed Student's t-tests were performed. Zebrafish data, defined by categorical variables, was analysed with Chi-square and Fisher's exact statistics tests, according to N size. Data is represented in percentage or as mean values \pm SEM. Levels of statistical significance are given in GraphPad Prism 6 format where: * $P \leq 0.05$, ** $P \leq 0.01$, *** $P \leq 0.001$ and **** $P \leq 0.0001$. Specific statistical tests, sample size, data representation (mean or percentage), and p values are indicated in results figure legends.

7. REFERENCES

- Abecasis GR, Altshuler D, Auton A, Brooks LD, Durbin RM, Gibbs RA, Hurles ME, McVean GA (2010) A map of human genome variation from population-scale sequencing. *Nature* 467: 1061-1073
- Abecasis GR, Cherny SS, Cookson WO, Cardon LR (2002) Merlin--rapid analysis of dense genetic maps using sparse gene flow trees. *Nat Genet* 30: 97-101
- Abs R, Van Vleymen E, Parizel PM, Van Acker K, Martin M, Martin JJ (1990) Congenital cerebellar hypoplasia and hypogonadotropic hypogonadism. *J Neurol Sci* 98: 259-265
- Ackerley S, James PA, Kalli A, French S, Davies KE, Talbot K (2006) A mutation in the small heat-shock protein HSPB1 leading to distal hereditary motor neuropathy disrupts neurofilament assembly and the axonal transport of specific cellular cargoes. *Hum Mol Genet* 15: 347-354
- Ackermann B, Krober S, Torres-Benito L, Borgmann A, Peters M, Hosseini Barkooie SM, Tejero R, Jakubik M, Schreml J, Milbradt J et al (2013) Plastin 3 ameliorates spinal muscular atrophy via delayed axon pruning and improves neuromuscular junction functionality. *Hum Mol Genet* 22: 1328-1347
- Adzhubei I, Jordan DM, Sunyaev SR (2013) Predicting functional effect of human missense mutations using PolyPhen-2. *Curr Protoc Hum Genet* Chapter 7: Unit7 20
- Akizu N, Cantagrel V, Zaki MS, Al-Gazali L, Wang X, Rosti RO, Dikoglu E, Gelot AB, Rosti B, Vaux KK et al (2015) Biallelic mutations in SNX14 cause a syndromic form of cerebellar atrophy and lysosome-autophagosome dysfunction. *Nat Genet* 47: 528-534
- Alfonso A, Grundahl K, Duerr JS, Han HP, Rand JB (1993) The *Caenorhabditis elegans* unc-17 gene: a putative vesicular acetylcholine transporter. *Science* 261: 617-619
- Allikmets R, Raskind WH, Hutchinson A, Schueck ND, Dean M, Koeller DM (1999) Mutation of a putative mitochondrial iron transporter gene (ABC7) in X-linked sideroblastic anemia and ataxia (XLSA/A). *Hum Mol Genet* 8: 743-749
- Andrade J, Pearce ST, Zhao H, Barroso M (2004a) Interactions among p22, glyceraldehyde-3-phosphate dehydrogenase and microtubules. *Biochem J* 384: 327-336
- Andrade J, Zhao H, Titus B, Timm Pearce S, Barroso M (2004b) The EF-hand Ca²⁺-binding protein p22 plays a role in microtubule and endoplasmic reticulum

organization and dynamics with distinct Ca²⁺-binding requirements. *Mol Biol Cell* 15: 481-496

Angerer LM, Angerer RC (2004) Disruption of gene function using antisense morpholinos. *Methods Cell Biol* 74: 699-711

Anheim M, Fleury M, Monga B, Laugel V, Chaigne D, Rodier G, Ginglinger E, Boulay C, Courtois S, Drouot N et al (2010) Epidemiological, clinical, paraclinical and molecular study of a cohort of 102 patients affected with autosomal recessive progressive cerebellar ataxia from Alsace, Eastern France: implications for clinical management. *Neurogenetics* 11: 1-12

Anheim M, Tranchant C, Koenig M (2012) The autosomal recessive cerebellar ataxias. *N Engl J Med* 366: 636-646

Antonellis A, Ellsworth RE, Sambuughin N, Puls I, Abel A, Lee-Lin SQ, Jordanova A, Kremensky I, Christodoulou K, Middleton LT et al (2003) Glycyl tRNA synthetase mutations in Charcot-Marie-Tooth disease type 2D and distal spinal muscular atrophy type V. *American journal of human genetics* 72: 1293-1299

Anttonen AK, Mahjneh I, Hamalainen RH, Lagier-Tourenne C, Kopra O, Waris L, Anttonen M, Joensuu T, Kalimo H, Paetau A et al (2005) The gene disrupted in Marinesco-Sjogren syndrome encodes SIL1, an HSPA5 cochaperone. *Nature Genetics* 37: 1309-1311

Anttonen AK, Siintola E, Tranebjaerg L, Iwata NK, Bijlsma EK, Meguro H, Ichikawa Y, Goto J, Kopra O, Lehesjoki AE (2008) Novel SIL1 mutations and exclusion of functional candidate genes in Marinesco-Sjogren syndrome. *European Journal of Human Genetics* 16: 961-969

Aran A, Segel R, Kaneshige K, Gulsuner S, Renbaum P, Oliphant S, Meirson T, Weinberg-Shukron A, HersHKovitz Y, Zeligson S et al (2017) Vesicular acetylcholine transporter defect underlies devastating congenital myasthenia syndrome. *Neurology* 88: 1021-1028

Babich V, Di Sole F (2015) The Na⁺/H⁺ Exchanger-3 (NHE3) Activity Requires Ezrin Binding to Phosphoinositide and Its Phosphorylation. *PloS one* 10

Babin PJ, Goizet C, Raldua D (2014) Zebrafish models of human motor neuron diseases: advantages and limitations. *Prog Neurobiol* 118: 36-58

Bading H (2013) Nuclear calcium signalling in the regulation of brain function. *Nat Rev Neurosci* 14: 593-608

- Bae YK, Kani S, Shimizu T, Tanabe K, Nojima H, Kimura Y, Higashijima S, Hibi M (2009) Anatomy of zebrafish cerebellum and screen for mutations affecting its development. *Dev Biol* 330: 406-426
- Ball LG, Xiao W (2005) Molecular basis of ataxia telangiectasia and related diseases. *Acta Pharmacol Sin* 26: 897-907
- Bansagi B, Griffin H, Whittaker RG, Antoniadi T, Evangelista T, Miller J, Greenslade M, Forester N, Duff J, Bradshaw A et al (2017) Genetic heterogeneity of motor neuropathies. *Neurology* 88: 1226-1234
- Barbeau A, Sadibelouiz M, Sadibelouiz A, Roy M (1984) A clinical classification of hereditary ataxias. *Can J Neurol Sci* 11: 501-505
- Barbosa J, Jr., Massensini AR, Santos MS, Meireles SI, Gomez RS, Gomez MV, Romano-Silva MA, Prado VF, Prado MA (1999) Expression of the vesicular acetylcholine transporter, proteins involved in exocytosis, and functional calcium signaling in varicosities and soma of a murine septal cell line. *J Neurochem* 73: 1881-1893
- Barroso MR, Bernd KK, DeWitt ND, Chang A, Mills K, Sztul ES (1996) A novel Ca²⁺-binding protein, p22, is required for constitutive membrane traffic. *J Biol Chem* 271: 10183-10187
- Baumgartel K, Mansuy IM (2012) Neural functions of calcineurin in synaptic plasticity and memory. *Learn Mem* 19: 375-384
- Beattie CE, Carrel TL, McWhorter ML (2007) Fishing for a mechanism: using zebrafish to understand spinal muscular atrophy. *J Child Neurol* 22: 995-1003
- Beaudin M, Klein CJ, Rouleau GA, Dupre N (2017) Systematic review of autosomal recessive ataxias and proposal for a classification. *Cerebellum Ataxias* 4: 3
- Becker-Catania SG, Chen G, Hwang MJ, Wang Z, Sun X, Sanal O, Bernatowska-Matuszkiewicz E, Chessa L, Lee EY, Gatti RA (2000) Ataxia-telangiectasia: phenotype/genotype studies of ATM protein expression, mutations, and radiosensitivity. *Mol Genet Metab* 70: 122-133
- Bedell VM, Westcot SE, Ekker SC (2011) Lessons from morpholino-based screening in zebrafish. *Brief Funct Genomics* 10: 181-188
- Beg AA, Ernstrom GG, Nix P, Davis MW, Jorgensen EM (2008) Protons act as a transmitter for muscle contraction in *C. elegans*. *Cell* 132: 149-160

Behra M, Cousin X, Bertrand C, Vonesch JL, Biellmann D, Chatonnet A, Strahle U (2002) Acetylcholinesterase is required for neuronal and muscular development in the zebrafish embryo. *Nature Neuroscience* 5: 111-118

Bell SM, Schreiner CM, Schultheis PJ, Miller ML, Evans RL, Vorhees CV, Shull GE, Scott WJ (1999) Targeted disruption of the murine Nhe1 locus induces ataxia, growth retardation, and seizures. *Am J Physiol* 276: C788-795

Ben Ammar Y, Takeda S, Hisamitsu T, Mori H, Wakabayashi S (2006) Crystal structure of CHP2 complexed with NHE1-cytosolic region and an implication for pH regulation. *Embo Journal* 25: 2315-2325

Bernier R, Golzio C, Xiong B, Stessman HA, Coe BP, Penn O, Witherspoon K, Gerds J, Baker C, Vulto-van Silfhout AT et al (2014) Disruptive CHD8 mutations define a subtype of autism early in development. *Cell* 158: 263-276

Berry-Kravis E, Abrams L, Coffey SM, Hall DA, Greco C, Gane LW, Grigsby J, Bourgeois JA, Finucane B, Jacquemont S et al (2007) Fragile X-associated tremor/ataxia syndrome: clinical features, genetics, and testing guidelines. *Mov Disord* 22: 2018-2030, quiz 2140

Bhatt JM (2016) The Epidemiology of Neuromuscular Diseases. *Neurol Clin* 34: 999-1021

Bidichandani SI, Ashizawa T, Patel PI (1998) The GAA triplet-repeat expansion in Friedreich ataxia interferes with transcription and may be associated with an unusual DNA structure. *American journal of human genetics* 62: 111-121

Bill BR, Petzold AM, Clark KJ, Schimmenti LA, Ekker SC (2009) A primer for morpholino use in zebrafish. *Zebrafish* 6: 69-77

Blackstone C (2012) Cellular pathways of hereditary spastic paraplegia. *Annu Rev Neurosci* 35: 25-47

Blakely RD, Edwards RH (2012) Vesicular and Plasma Membrane Transporters for Neurotransmitters. *Csh Perspect Biol* 4

Bodmer D, Ascano M, Kuruvilla R (2011) Isoform-specific dephosphorylation of dynamin1 by calcineurin couples neurotrophin receptor endocytosis to axonal growth. *Neuron* 70: 1085-1099

Borck G, Hog F, Dentici ML, Tan PL, Sowada N, Medeira A, Gueneau L, Thiele H, Kousi M, Lepri F et al (2015) BRF1 mutations alter RNA polymerase III-dependent transcription and cause neurodevelopmental anomalies. *Genome Res* 25: 155-166

- Botstein D, Risch N (2003) Discovering genotypes underlying human phenotypes: past successes for mendelian disease, future approaches for complex disease. *Nat Genet* 33 Suppl: 228-237
- Bowerman M, Shafey D, Kothary R (2007) Smn depletion alters profilin II expression and leads to upregulation of the RhoA/ROCK pathway and defects in neuronal integrity. *J Mol Neurosci* 32: 120-131
- Bradford MM (1976) Rapid and Sensitive Method for Quantitation of Microgram Quantities of Protein Utilizing Principle of Protein-Dye Binding. *Anal Biochem* 72: 248-254
- Bradford MM, Williams WL (1976) New, Rapid, Sensitive Method for Protein Determination. *Fed Proc* 35: 274-274
- Bradley JL, Blake JC, Chamberlain S, Thomas PK, Cooper JM, Schapira AH (2000) Clinical, biochemical and molecular genetic correlations in Friedreich's ataxia. *Hum Mol Genet* 9: 275-282
- Brandon EP, Lin W, D'Amour KA, Pizzo DP, Dominguez B, Sugiura Y, Thode S, Ko CP, Thal LJ, Gage FH et al (2003) Aberrant patterning of neuromuscular synapses in choline acetyltransferase-deficient mice. *J Neurosci* 23: 539-549
- Bretscher A, Reczek D, Berryman M (1997) Ezrin: a protein requiring conformational activation to link microfilaments to the plasma membrane in the assembly of cell surface structures. *Journal of cell science* 110: 3011-3018
- Brett CL, Donowitz M, Rao R (2005) Evolutionary origins of eukaryotic sodium/proton exchangers. *Am J Physiol-Cell Ph* 288: C223-C239
- Brosamle C, Halpern ME (2009) Nogo-Nogo receptor signalling in PNS axon outgrowth and pathfinding. *Mol Cell Neurosci* 40: 401-409
- Burglen L, Spiegel R, Ignatius J, Cobben JM, Landrieu P, Lefebvre S, Munnich A, Melki J (1995) SMN gene deletion in variant of infantile spinal muscular atrophy. *Lancet* 346: 316-317
- Burgoyne RD (2007) Neuronal calcium sensor proteins: generating diversity in neuronal Ca²⁺ signalling. *Nature Reviews Neuroscience* 8: 182-193
- Burns R, Majczenko K, Xu J, Peng W, Yapici Z, Dowling JJ, Li JZ, Burmeister M (2014) Homozygous splice mutation in CWF19L1 in a Turkish family with recessive ataxia syndrome. *Neurology* 83: 2175-2182

Campuzano V, Montermini L, Molto MD, Pianese L, Cossee M, Cavalcanti F, Monros E, Rodius F, Duclos F, Monticelli A et al (1996) Friedreich's ataxia: autosomal recessive disease caused by an intronic GAA triplet repeat expansion. *Science* 271: 1423-1427

Cardone RA, Casavola V, Reshkin SJ (2005) The role of disturbed pH dynamics and the Na⁺/H⁺ exchanger in metastasis. *Nat Rev Cancer* 5: 786-795

Casey JR, Grinstein S, Orlowski J (2010) Sensors and regulators of intracellular pH. *Nat Rev Mol Cell Biol* 11: 50-61

Cashman NR, Durham HD, Blusztajn JK, Oda K, Tabira T, Shaw IT, Dahrouge S, Antel JP (1992) Neuroblastoma x spinal cord (NSC) hybrid cell lines resemble developing motor neurons. *Dev Dyn* 194: 209-221

Chang HCH, Dimlich DN, Yokokura T, Mukherjee A, Kankel MW, Sen A, Sridhar V, Fulga TA, Hart AC, Van Vactor D et al (2008) Modeling Spinal Muscular Atrophy in *Drosophila*. *PLoS one* 3

Chen JC, Chesler M (1992) pH transients evoked by excitatory synaptic transmission are increased by inhibition of extracellular carbonic anhydrase. *Proc Natl Acad Sci U S A* 89: 7786-7790

Chen YZ, Bennett CL, Huynh HM, Blair IP, Puls I, Irobi J, Dierick I, Abel A, Kennerson ML, Rabin BA et al (2004) DNA/RNA helicase gene mutations in a form of juvenile amyotrophic lateral sclerosis (ALS4). *American journal of human genetics* 74: 1128-1135

Chesler M (2003) Regulation and modulation of pH in the brain. *Physiol Rev* 83: 1183-1221

Chesler M, Kaila K (1992) Modulation of pH by neuronal activity. *Trends Neurosci* 15: 396-402

Chiti F, Dobson CM (2006) Protein misfolding, functional amyloid, and human disease. *Annu Rev Biochem* 75: 333-366

Chow CW, Rincon M, Davis RJ (1999) Requirement for transcription factor NFAT in interleukin-2 expression. *Mol Cell Biol* 19: 2300-2307

Chun HH, Gatti RA (2004) Ataxia-telangiectasia, an evolving phenotype. *DNA Repair (Amst)* 3: 1187-1196

Chun S, Fay JC (2009) Identification of deleterious mutations within three human genomes. *Genome Res* 19: 1553-1561

Ciryam P, Tartaglia GG, Morimoto RI, Dobson CM, Vendruscolo M (2013) Widespread aggregation and neurodegenerative diseases are associated with supersaturated proteins. *Cell Rep* 5: 781-790

Clipstone NA, Crabtree GR (1992) Identification of calcineurin as a key signalling enzyme in T-lymphocyte activation. *Nature* 357: 695-697

Coleman WL, Bill CA, Simsek-Duran F, Lonart G, Samigullin D, Bykhovskaia M (2008) Synapsin II and calcium regulate vesicle docking and the cross-talk between vesicle pools at the mouse motor terminals. *J Physiol-London* 586: 4649-4673

Cossee M, Schmitt M, Campuzano V, Reutenauer L, Moutou C, Mandel JL, Koenig M (1997) Evolution of the Friedreich's ataxia trinucleotide repeat expansion: founder effect and premutations. *Proceedings of the National Academy of Sciences of the United States of America* 94: 7452-7457

Coutelier M, Stevanin G, Brice A (2015) Genetic landscape remodelling in spinocerebellar ataxias: the influence of next-generation sequencing. *J Neurol* 262: 2382-2395

Cox GA, Lutz CM, Yang CL, Biemesderfer D, Bronson RT, Fu A, Aronson PS, Noebels JL, Frankel WN (1997) Sodium/hydrogen exchanger gene defect in slow-wave epilepsy mutant mice. *Cell* 91: 139-148

D'Hooghe M, Selleslag D, Mortier G, Van Coster R, Vermeersch P, Billiet J, Bekri S (2012) X-linked sideroblastic anemia and ataxia: a new family with identification of a fourth ABCB7 gene mutation. *Eur J Paediatr Neurol* 16: 730-735

Davydov EV, Goode DL, Sirota M, Cooper GM, Sidow A, Batzoglou S (2010) Identifying a high fraction of the human genome to be under selective constraint using GERP++. *PLoS Comput Biol* 6: e1001025

de Castro BM, De Jaeger X, Martins-Silva C, Lima RD, Amaral E, Menezes C, Lima P, Neves CM, Pires RG, Gould TW et al (2009) The vesicular acetylcholine transporter is required for neuromuscular development and function. *Mol Cell Biol* 29: 5238-5250

De Michele G, Coppola G, Coccozza S, Filla A (2004) A pathogenetic classification of hereditary ataxias: is the time ripe? *J Neurol* 251: 913-922

De Michele G, Filla A (2012) Other autosomal recessive and childhood ataxias. *Handb Clin Neurol* 103: 343-357

De Michele G, Filla A, Striano S, Rimoldi M, Campanella G (1993) Heterogeneous findings in four cases of cerebellar ataxia associated with hypogonadism (Holmes' type ataxia). *Clin Neurol Neurosurg* 95: 23-28

Deenen JC, Horlings CG, Verschuuren JJ, Verbeek AL, van Engelen BG (2015) The Epidemiology of Neuromuscular Disorders: A Comprehensive Overview of the Literature. *J Neuromuscul Dis* 2: 73-85

Delatycki MB, Williamson R, Forrest SM (2000) Friedreich ataxia: an overview. *Journal of medical genetics* 37: 1-8

DeLong MR, Wichmann T (2007) Circuits and circuit disorders of the basal ganglia. *Arch Neurol* 64: 20-24

Di Donato S (1998) The complex clinical and genetic classification of inherited ataxias. I. Dominant ataxias. *Ital J Neurol Sci* 19: 335-343

Di Donato S, Gellera C, Mariotti C (2001) The complex clinical and genetic classification of inherited ataxias. II. Autosomal recessive ataxias. *Neurol Sci* 22: 219-228

Di Sole F, Babich V, Moe OW (2009) The Calcineurin Homologous Protein-1 Increases Na⁺/H⁺-Exchanger 3 Trafficking via Ezrin Phosphorylation. *J Am Soc Nephrol* 20: 1776-1786

Di Sole F, Vadnagara K, Moe OW, Babich V (2012) Calcineurin homologous protein: a multifunctional Ca²⁺-binding protein family. *Am J Physiol Renal Physiol* 303: F165-179

Dierick I, Baets J, Irobi J, Jacobs A, De Vriendt E, Deconinck T, Merlini L, Van den Bergh P, Rasic VM, Robberecht W et al (2008) Relative contribution of mutations in genes for autosomal dominant distal hereditary motor neuropathies: a genotype-phenotype correlation study. *Brain* 131: 1217-1227

Diering GH, Mills F, Bamji SX, Numata M (2011) Regulation of dendritic spine growth through activity-dependent recruitment of the brain-enriched Na⁺/H⁺ exchanger NHE5. *Molecular Biology of the Cell* 22: 2246-2257

Dietrich CJ, Morad M (2010) Synaptic acidification enhances GABAA signaling. *J Neurosci* 30: 16044-16052

Dimitriadi M, Sleigh JN, Walker A, Chang HC, Sen A, Kalloo G, Harris J, Barsby T, Walsh MB, Satterlee JS et al (2010) Conserved Genes Act as Modifiers of Invertebrate SMN Loss of Function Defects. *PLoS genetics* 6

Donowitz M, Tse CM, Fuster D (2013) SLC9/NHE gene family, a plasma membrane and organellar family of Na⁺/H⁺ exchangers. *Mol Aspects Med* 34: 236-251

Downes GB, Granato M (2004) Acetylcholinesterase function is dispensable for sensory neurite growth but is critical for neuromuscular synapse stability. *Developmental biology* 270: 232-245

Dubowitz V (1964) Infantile Muscular Atrophy. A Prospective Study with Particular Reference to a Slowly Progressive Variety. *Brain* 87: 707-718

Dubowitz V (2009) Ramblings in the history of spinal muscular atrophy. *Neuromuscul Disord* 19: 69-73

Durr A (2010) Autosomal dominant cerebellar ataxias: polyglutamine expansions and beyond. *The Lancet Neurology* 9: 885-894

Ekker SC, Larson JD (2001) Morphant technology in model developmental systems. *Genesis* 30: 89-93

Elinx-Benizri S, Glik A, Merkel D, Arad M, Freimark D, Kozlova E, Cabantchik I, Hassin-Baer S (2016) Clinical Experience With Deferiprone Treatment for Friedreich Ataxia. *J Child Neurol* 31: 1036-1040

Embirucu EK, Martyn ML, Schlesinger D, Kok F (2009) Autosomal recessive ataxias: 20 types, and counting. *Arq Neuropsiquiatr* 67: 1143-1156

Emery AE (1991a) Population frequencies of inherited neuromuscular diseases--a world survey. *Neuromuscul Disord* 1: 19-29

Emery AE (1991b) Population frequencies of neuromuscular diseases--II. Amyotrophic lateral sclerosis (motor neurone disease). *Neuromuscul Disord* 1: 323-325

Engel AG, Selcen D, Shen XM, Milone M, Harper CM (2016) Loss of MUNC13-1 function causes microcephaly, cortical hyperexcitability, and fatal myasthenia. *Neurol Genet* 2: e105

Engel AG, Shen XM, Selcen D, Sine SM (2015) Congenital myasthenic syndromes: pathogenesis, diagnosis, and treatment. *The Lancet Neurology* 14: 461

Engqvist-Goldstein AE, Drubin DG (2003) Actin assembly and endocytosis: from yeast to mammals. *Annu Rev Cell Dev Biol* 19: 287-332

Erickson JD, Varoqui H, Schafer MK, Modi W, Diebler MF, Weihe E, Rand J, Eiden LE, Bonner TI, Usdin TB (1994) Functional identification of a vesicular acetylcholine transporter and its expression from a "cholinergic" gene locus. *J Biol Chem* 269: 21929-21932

Evgrafov OV, Mersiyanova I, Irobi J, Van Den Bosch L, Dierick I, Leung CL, Schagina O, Verpoorten N, Van Impe K, Fedotov V et al (2004) Mutant small heat-shock protein 27 causes axonal Charcot-Marie-Tooth disease and distal hereditary motor neuropathy. *Nat Genet* 36: 602-606

Feldkotter M, Schwarzer V, Wirth R, Wienker TF, Wirth B (2002) Quantitative analyses of SMN1 and SMN2 based on real-time lightCycler PCR: fast and highly reliable carrier testing and prediction of severity of spinal muscular atrophy. *Am J Hum Genet* 70: 358-368

Filla A, De Michele G (2012) Overview of autosomal recessive ataxias. *Handb Clin Neurol* 103: 265-274

Finkel RS, McDermott MP, Kaufmann P, Darras BT, Chung WK, Sproule DM, Kang PB, Foley AR, Yang ML, Martens WB et al (2014) Observational study of spinal muscular atrophy type I and implications for clinical trials. *Neurology* 83: 810-817

Flanagan-Steet H, Fox MA, Meyer D, Sanes JR (2005) Neuromuscular synapses can form in vivo by incorporation of initially aneural postsynaptic specializations. *Development* 132: 4471-4481

Fogel BL, Perlman S (2007) Clinical features and molecular genetics of autosomal recessive cerebellar ataxias. *Lancet Neurol* 6: 245-257

Fridman V, Reilly MM (2015) Inherited Neuropathies. *Semin Neurol* 35: 407-423

Gallo G, Lefcort FB, Letourneau PC (1997) The trkA receptor mediates growth cone turning toward a localized source of nerve growth factor. *Journal of Neuroscience* 17: 5445-5454

Gallo G, Letourneau PC (1998) Localized sources of neurotrophins initiate axon collateral sprouting. *Journal of Neuroscience* 18: 5403-5414

Gey GO (1952) Tissue culture studies of the proliferative capacity of cervical carcinoma and normal epithelium. *Cancer Res* 12: 264-265

Ghysen A, Dambly-Chaudiere C (2004) Development of the zebrafish lateral line. *Curr Opin Neurobiol* 14: 67-73

Gilad S, Chessa L, Khosravi R, Russell P, Galanty Y, Piane M, Gatti RA, Jorgensen TJ, Shiloh Y, Bar-Shira A (1998) Genotype-phenotype relationships in ataxia-telangiectasia and variants. *American journal of human genetics* 62: 551-561

Gilissen C, Hoischen A, Brunner HG, Veltman JA (2012) Disease gene identification strategies for exome sequencing. *Eur J Hum Genet* 20: 490-497

Golzio C, Willer J, Talkowski ME, Oh EC, Taniguchi Y, Jacquemont S, Reymond A, Sun M, Sawa A, Gusella JF et al (2012) KCTD13 is a major driver of mirrored neuroanatomical phenotypes of the 16p11.2 copy number variant. *Nature* 485: 363-367

Gomez TM, Zheng JQ (2006) The molecular basis for calcium-dependent axon pathfinding. *Nature Reviews Neuroscience* 7: 115-125

Gonzalez MA, Lebrigio RF, Van Booven D, Ulloa RH, Powell E, Speziani F, Tekin M, Schule R, Zuchner S (2013) GENomes Management Application (GEM.app): a new software tool for large-scale collaborative genome analysis. *Hum Mutat* 34: 842-846

Grabczyk E, Usdin K (2000) The GAA*TTC triplet repeat expanded in Friedreich's ataxia impedes transcription elongation by T7 RNA polymerase in a length and supercoil dependent manner. *Nucleic acids research* 28: 2815-2822

Graham FL, Smiley J, Russell WC, Nairn R (1977) Characteristics of a human cell line transformed by DNA from human adenovirus type 5. *J Gen Virol* 36: 59-74

Greco CM, Berman RF, Martin RM, Tassone F, Schwartz PH, Chang A, Trapp BD, Iwahashi C, Brunberg J, Grigsby J et al (2006) Neuropathology of fragile X-associated tremor/ataxia syndrome (FXTAS). *Brain* 129: 243-255

Greene LA, Rein G (1977) Synthesis, storage and release of acetylcholine by a noradrenergic pheochromocytoma cell line. *Nature* 268: 349-351

Greene LA, Tischler AS (1976) Establishment of a noradrenergic clonal line of rat adrenal pheochromocytoma cells which respond to nerve growth factor. *Proceedings of the National Academy of Sciences of the United States of America* 73: 2424-2428

Grinstein S, Woodside M, Sardet C, Pouyssegur J, Rotin D (1992) Activation of the Na⁺/H⁺ antiporter during cell volume regulation. Evidence for a phosphorylation-independent mechanism. *J Biol Chem* 267: 23823-23828

Grohmann K, Schuelke M, Diers A, Hoffmann K, Lucke B, Adams C, Bertini E, Leonhardt-Horti H, Muntoni F, Ouvrier R et al (2001) Mutations in the gene encoding

immunoglobulin mu-binding protein 2 cause spinal muscular atrophy with respiratory distress type 1. *Nat Genet* 29: 75-77

Gu XQ, Yao H, Haddad GG (2001) Increased neuronal excitability and seizures in the Na(+)/H(+) exchanger null mutant mouse. *Am J Physiol Cell Physiol* 281: C496-503

Guissart C, Li X, Leheup B, Drouot N, Montaut-Verient B, Raffo E, Jonveaux P, Roux AF, Claustres M, Fliegel L et al (2015) Mutation of SLC9A1, encoding the major Na(+)/H(+) exchanger, causes ataxia-deafness Lichtenstein-Knorr syndrome. *Hum Mol Genet* 24: 463-470

Haberlova J, Claeys KG, De Jonghe P, Seeman P (2009) Cranial nerves palsy as an initial feature of an early onset distal hereditary motor neuropathy--a new distal hereditary motor neuropathy phenotype. *Neuromuscul Disord* 19: 427-428

Hadano S, Hand CK, Osuga H, Yanagisawa Y, Otomo A, Devon RS, Miyamoto N, Showguchi-Miyata J, Okada Y, Singaraja R et al (2001) A gene encoding a putative GTPase regulator is mutated in familial amyotrophic lateral sclerosis 2. *Nature Genetics* 29: 166-173

Hall A, Lalli G (2010) Rho and Ras GTPases in Axon Growth, Guidance, and Branching. *Csh Perspect Biol* 2

Hansen ST, Meera P, Otis TS, Pulst SM (2013) Changes in Purkinje cell firing and gene expression precede behavioral pathology in a mouse model of SCA2. *Human Molecular Genetics* 22: 271-283

Hantai D, Nicole S, Eymard B (2013) Congenital myasthenic syndromes: an update. *Current opinion in neurology* 26: 561-568

Hao LT, Wolman M, Granato M, Beattie CE (2012) Survival Motor Neuron Affects Plastin 3 Protein Levels Leading to Motor Defects. *Journal of Neuroscience* 32: 5074-5084

Harding AE (1983) Classification of the hereditary ataxias and paraplegias. *Lancet* 1: 1151-1155

Harding AE (1993) Clinical features and classification of inherited ataxias. *Adv Neurol* 61: 1-14

Harding AE (2005) Chapter 68 - Inherited Neuronal Atrophy and Degeneration Predominantly of Lower Motor Neurons* A2 - Dyck, Peter J. In *Peripheral Neuropathy (Fourth Edition)*, Thomas PK (ed) pp 1603-1621. Philadelphia: W.B. Saunders

Harding AE, Thomas PK (1980) Genetic aspects of hereditary motor and sensory neuropathy (types I and II). *Journal of medical genetics* 17: 329-336

Harding BN, Kariya S, Monani UR, Chung WK, Benton M, Yum SW, Tennekoon G, Finkel RS (2015) Spectrum of neuropathophysiology in spinal muscular atrophy type I. *Journal of neuropathology and experimental neurology* 74: 15-24

Harms MB, Ori-McKenney KM, Scoto M, Tuck EP, Bell S, Ma D, Masi S, Allred P, Al-Lozi M, Reilly MM et al (2012) Mutations in the tail domain of DYNC1H1 cause dominant spinal muscular atrophy. *Neurology* 78: 1714-1720

Heiney SA, Kim J, Augustine GJ, Medina JF (2014) Precise Control of Movement Kinematics by Optogenetic Inhibition of Purkinje Cell Activity. *Journal of Neuroscience* 34: 2321-2330

Hersheson J, Haworth A, Houlden H (2012) The inherited ataxias: genetic heterogeneity, mutation databases, and future directions in research and clinical diagnostics. *Hum Mutat* 33: 1324-1332

Higashijima S, Hotta Y, Okamoto H (2000) Visualization of cranial motor neurons in live transgenic zebrafish expressing green fluorescent protein under the control of the islet-1 promoter/enhancer. *J Neurosci* 20: 206-218

Hills LB, Masri A, Konno K, Kakegawa W, Lam AT, Lim-Melia E, Chandy N, Hill RS, Partlow JN, Al-Saffar M et al (2013) Deletions in GRID2 lead to a recessive syndrome of cerebellar ataxia and tonic upgaze in humans. *Neurology* 81: 1378-1386

Hipp MS, Park SH, Hartl FU (2014) Proteostasis impairment in protein-misfolding and -aggregation diseases. *Trends in cell biology* 24: 506-514

Holmes G (1908) A Form of Familial Degeneration of the Cerebellum. *Brain* 30: 466-489

Hoogerwerf WA, Tsao SC, Devuyst O, Levine SA, Yun CHC, Yip JW, Cohen ME, Wilson PD, Lazenby AJ, Tse CM et al (1996) NHE2 and NHE3 are human and rabbit intestinal brush-border proteins. *Am J Physiol-Gastr L* 270: G29-G41

Hornburg D, Drepper C, Butter F, Meissner F, Sendtner M, Mann M (2014) Deep proteomic evaluation of primary and cell line motoneuron disease models delineates major differences in neuronal characteristics. *Mol Cell Proteomics* 13: 3410-3420

Hosseini-barkoobe S, Peters M, Torres-Benito L, Rastetter RH, Hupperich K, Hoffmann A, Mendoza-Ferreira N, Kaczmarek A, Janzen E, Milbradt J et al (2016)

The Power of Human Protective Modifiers: PLS3 and CORO1C Unravel Impaired Endocytosis in Spinal Muscular Atrophy and Rescue SMA Phenotype. *Am J Hum Genet* 99: 647-665

Hosseinibarkooie S, Schneider S, Wirth B (2017) Advances in understanding the role of disease-associated proteins in spinal muscular atrophy. *Expert Rev Proteomics* 14: 581-592

Hosseinibarkooie SM (2016 - Thesis) Thesis: Identification and Characterization of molecular pathways underlying the modifier function of Plastin3 in neurodegenerative disorders In Mathematisch-Naturwissenschaftlichen Fakultät p 224. University of Cologne

Hoyt C (2009) Rapid, high-throughput homogenization of embryonic or larval zebrafish (*Danio rerio*).

Ingold E, Vom Berg-Maurer CM, Burckhardt CJ, Lehnherr A, Rieder P, Keller PJ, Stelzer EH, Greber UF, Neuhauss SC, Gesemann M (2015) Proper migration and axon outgrowth of zebrafish cranial motoneuron subpopulations require the cell adhesion molecule MDGA2A. *Biol Open* 4: 146-154

Inoue H, Nakamura Y, Nagita M, Takai T, Masuda M, Nakamura N, Kanazawa H (2003) Calcineurin homologous protein isoform 2 (CHP2), Na⁺/H⁺ exchangers-binding protein, is expressed in intestinal epithelium. *Biol Pharm Bull* 26: 148-155

Irobi J, Almeida-Souza L, Asselbergh B, De Winter V, Goethals S, Dierick I, Krishnan J, Timmermans JP, Robberecht W, De Jonghe P et al (2010) Mutant HSPB8 causes motor neuron-specific neurite degeneration. *Hum Mol Genet* 19: 3254-3265

Irobi J, Dierick I, Jordanova A, Claeys KG, De Jonghe P, Timmerman V (2006) Unraveling the genetics of distal hereditary motor neuropathies. *Neuromolecular Med* 8: 131-146

Irobi J, Van Impe K, Seeman P, Jordanova A, Dierick I, Verpoorten N, Michalik A, De Vriendt E, Jacobs A, Van Gerwen V et al (2004) Hot-spot residue in small heat-shock protein 22 causes distal motor neuropathy. *Nat Genet* 36: 597-601

Issa FA, Mock AF, Sagasti A, Papazian DM (2012) Spinocerebellar ataxia type 13 mutation that is associated with disease onset in infancy disrupts axonal pathfinding during neuronal development. *Dis Model Mech* 5: 921-929

Ito D, Suzuki N (2009) Seipinopathy: a novel endoplasmic reticulum stress-associated disease. *Brain* 132: 8-15

- Ivanov SV, Ward JM, Tessarollo L, McAreavey D, Sachdev V, Fananapazir L, Banks MK, Morris N, Djurickovic D, Devor-Henneman DE et al (2004) Animal model - Cerebellar ataxia, seizures, premature death, and cardiac abnormalities in mice with targeted disruption of the *Cacna2d2* gene. *American Journal of Pathology* 165: 1007-1018
- Iwata A, Christianson JC, Bucci M, Ellerby LM, Nukina N, Forno LS, Kopito RR (2005) Increased susceptibility of cytoplasmic over nuclear polyglutamine aggregates to autophagic degradation. *Proceedings of the National Academy of Sciences of the United States of America* 102: 13135-13140
- Jacoby D, Rusche J, Iudicello M, De Mercanti S, Clerico M, Gibbin M, Longo F, Miao W, Rai M, Piga A et al (2014) Epigenetic Therapy for Friedreich's Ataxia: A Phase I Clinical Trial (PL1.003). *Neurology* 82
- Janickova H, Prado VF, Prado MAM, El Mestikawy S, Bernard V (2017) Vesicular acetylcholine transporter (VACHT) over-expression induces major modifications of striatal cholinergic interneuron morphology and function. *J Neurochem*
- Janke M, Herrig A, Austermann J, Gerke V, Steinem C, Janshoff A (2008) Actin binding of ezrin is activated by specific recognition of PIP2-functionalized lipid bilayers. *Biochemistry* 47: 3762-3769
- Jayadev S, Bird TD (2013) Hereditary ataxias: overview. *Genet Med* 15: 673-683
- Jen JC (2008) Hereditary episodic ataxias. *Ann N Y Acad Sci* 1142: 250-253
- Jimenez-Vidal M, Srivastava J, Putney LK, Barber DL (2010) Nuclear-localized calcineurin homologous protein CHP1 interacts with upstream binding factor and inhibits ribosomal RNA synthesis. *J Biol Chem* 285: 36260-36266
- Kabashi E, Brusteian E, Champagne N, Drapeau P (2011) Zebrafish models for the functional genomics of neurogenetic disorders. *Biochim Biophys Acta* 1812: 335-345
- Kabashi E, Champagne N, Brusteian E, Drapeau P (2010) In the swim of things: recent insights to neurogenetic disorders from zebrafish. *Trends Genet* 26: 373-381
- Kaczmarek A, Schneider S, Wirth B, Riessland M (2015) Investigational therapies for the treatment of spinal muscular atrophy. *Expert Opin Investig Drugs* 24: 867-881
- Kalueff AV, Gebhardt M, Stewart AM, Cachat JM, Brimmer M, Chawla JS, Craddock C, Kyzar EJ, Roth A, Landsman S et al (2013) Towards a comprehensive catalog of zebrafish behavior 1.0 and beyond. *Zebrafish* 10: 70-86

Kariya S, Park GH, Maeno-Hikichi Y, Leykekhman O, Lutz C, Arkovitz MS, Landmesser LT, Monani UR (2008) Reduced SMN protein impairs maturation of the neuromuscular junctions in mouse models of spinal muscular atrophy. *Hum Mol Genet* 17: 2552-2569

Kasher PR, Namavar Y, van Tijn P, Fluiter K, Sizarov A, Kamermans M, Grierson AJ, Zivkovic D, Baas F (2011) Impairment of the tRNA-splicing endonuclease subunit 54 (*tSEN54*) gene causes neurological abnormalities and larval death in zebrafish models of pontocerebellar hypoplasia. *Hum Mol Genet* 20: 1574-1584

Kawahara G, Hayashi YK (2016) Characterization of Zebrafish Models of Marinesco-Sjogren Syndrome. *PLoS One* 11: e0165563

Kennerson M, Nicholson G, Kowalski B, Krajewski K, El-Khechen D, Feely S, Chu S, Shy M, Garbern J (2009) X-linked distal hereditary motor neuropathy maps to the *DSMAX* locus on chromosome Xq13.1-q21. *Neurology* 72: 246-252

Khaliq ZM, Gouwens NW, Raman IM (2003) The contribution of resurgent sodium current to high-frequency firing in Purkinje neurons: An experimental and modeling study. *Journal of Neuroscience* 23: 4899-4912

Kim MH, Hersh LB (2004) The vesicular acetylcholine transporter interacts with clathrin-associated adaptor complexes AP-1 and AP-2. *J Biol Chem* 279: 12580-12587

Kim MH, Lu M, Lim EJ, Chai YG, Hersh LB (1999) Mutational analysis of aspartate residues in the transmembrane regions and cytoplasmic loops of rat vesicular acetylcholine transporter. *J Biol Chem* 274: 673-680

Kim S, Jung U, Baek J, Lee S, Jung W, Kim J, Kang S (2013) Mouse neuroblastoma cell-based model and the effect of epileptic events on calcium oscillations and neural spikes. *Journal of Nanophotonics* 7: 073794-073794

Kitamoto T, Xie X, Wu CF, Salvaterra PM (2000) Isolation and characterization of mutants for the vesicular acetylcholine transporter gene in *Drosophila melanogaster*. *J Neurobiol* 42: 161-171

Klebe RJ, Ruddle RH (1969) Neuroblastoma - Cell Culture Analysis of a Differentiating Stem Cell System. *Journal of Cell Biology* 43: A69-&

Klein CJ, Duan X, Shy ME (2013) Inherited neuropathies: clinical overview and update. *Muscle Nerve* 48: 604-622

Klockgether T (2010) Sporadic ataxia with adult onset: classification and diagnostic criteria. *The Lancet Neurology* 9: 94-104

Klockgether T (2011) Update on degenerative ataxias. *Current opinion in neurology* 24: 339-345

Knierim E, Hirata H, Wolf NI, Morales-Gonzalez S, Schottmann G, Tanaka Y, Rudnik-Schoneborn S, Orgeur M, Zerres K, Vogt S et al (2016) Mutations in Subunits of the Activating Signal Cointegrator 1 Complex Are Associated with Prenatal Spinal Muscular Atrophy and Congenital Bone Fractures. *American journal of human genetics* 98: 473-489

Koenig M, Hoffman EP, Bertelson CJ, Monaco AP, Feener C, Kunkel LM (1987) Complete cloning of the Duchenne muscular dystrophy (DMD) cDNA and preliminary genomic organization of the DMD gene in normal and affected individuals. *Cell* 50: 509-517

Kohda M, Tokuzawa Y, Kishita Y, Nyuzuki H, Moriyama Y, Mizuno Y, Hirata T, Yatsuka Y, Yamashita-Sugahara Y, Nakachi Y et al (2016) A Comprehensive Genomic Analysis Reveals the Genetic Landscape of Mitochondrial Respiratory Chain Complex Deficiencies. *PLoS genetics* 12: e1005679

Kong L, Wang X, Choe DW, Polley M, Burnett BG, Bosch-Marce M, Griffin JW, Rich MM, Sumner CJ (2009) Impaired synaptic vesicle release and immaturity of neuromuscular junctions in spinal muscular atrophy mice. *J Neurosci* 29: 842-851

Kopito RR (2000) Aggresomes, inclusion bodies and protein aggregation. *Trends Cell Biol* 10: 524-530

Kugelberg E, Welander L (1956) Heredofamilial juvenile muscular atrophy simulating muscular dystrophy. *AMA Arch Neurol Psychiatry* 75: 500-509

Kuwahara H, Kamei J, Nakamura N, Matsumoto M, Inoue H, Kanazawa H (2003) The apoptosis-inducing protein kinase DRAK2 is inhibited in a calcium-dependent manner by the calcium-binding protein CHP. *J Biochem* 134: 245-250

Kwok AS, Phadwal K, Turner BJ, Oliver PL, Raw A, Simon AK, Talbot K, Agashe VR (2011) HspB8 mutation causing hereditary distal motor neuropathy impairs lysosomal delivery of autophagosomes. *J Neurochem* 119: 1155-1161

Laemmli UK (1970) Cleavage of Structural Proteins during Assembly of Head of Bacteriophage-T4. *Nature* 227: 680-&

Laing NG (2012) Genetics of neuromuscular disorders. *Crit Rev Clin Lab Sci* 49: 33-48

Lamar KM, McNally EM (2014) Genetic Modifiers for Neuromuscular Diseases. *J Neuromuscul Dis* 1: 3-13

Landrieu P, Baets J, De Jonghe P (2013) Hereditary motor-sensory, motor, and sensory neuropathies in childhood. *Handb Clin Neurol* 113: 1413-1432

Lara A, Damasceno DD, Pires R, Gros R, Gomes ER, Gavioli M, Lima RF, Guimaraes D, Lima P, Bueno CR, Jr. et al (2010) Dysautonomia due to reduced cholinergic neurotransmission causes cardiac remodeling and heart failure. *Mol Cell Biol* 30: 1746-1756

Lax NZ, Hepplewhite PD, Reeve AK, Nesbitt V, McFarland R, Jaros E, Taylor RW, Turnbull DM (2012) Cerebellar ataxia in patients with mitochondrial DNA disease: a molecular clinicopathological study. *Journal of neuropathology and experimental neurology* 71: 148-161

Lefebvre S, Burglen L, Reboullet S, Clermont O, Burlet P, Viollet L, Benichou B, Cruaud C, Millasseau P, Zeviani M et al (1995) Identification and characterization of a spinal muscular atrophy-determining gene. *Cell* 80: 155-165

Lek M, Karczewski KJ, Minikel EV, Samocha KE, Banks E, Fennell T, O'Donnell-Luria AH, Ware JS, Hill AJ, Cummings BB et al (2016) Analysis of protein-coding genetic variation in 60,706 humans. *Nature* 536: 285-291

LePage KT, Dickey RW, Gerwick WH, Jester EL, Murray TF (2005) On the use of neuro-2a neuroblastoma cells versus intact neurons in primary culture for neurotoxicity studies. *Crit Rev Neurobiol* 17: 27-50

Levy JR, Sumner CJ, Caviston JP, Tokito MK, Ranganathan S, Ligon LA, Wallace KE, LaMonte BH, Harmison GG, Puls I et al (2006) A motor neuron disease-associated mutation in p150Glued perturbs dynactin function and induces protein aggregation. *J Cell Biol* 172: 733-745

Lewis KE, Eisen JS (2003) From cells to circuits: development of the zebrafish spinal cord. *Prog Neurobiol* 69: 419-449

Li B, Duysen EG, Volpicelli-Daley LA, Levey AI, Lockridge O (2003) Regulation of muscarinic acetylcholine receptor function in acetylcholinesterase knockout mice. *Pharmacol Biochem Be* 74: 977-986

Li H, Durbin R (2009) Fast and accurate short read alignment with Burrows-Wheeler transform. *Bioinformatics* 25: 1754-1760

Lim J, Hao T, Shaw C, Patel AJ, Szabo G, Rual JF, Fisk CJ, Li N, Smolyar A, Hill DE et al (2006) A protein-protein interaction network for human inherited ataxias and disorders of Purkinje cell degeneration. *Cell* 125: 801-814

Lima R de F, Prado VF, Prado MA, Kushmerick C (2010) Quantal release of acetylcholine in mice with reduced levels of the vesicular acetylcholine transporter. *J Neurochem* 113: 943-951

Lin P, Li J, Liu Q, Mao F, Li J, Qiu R, Hu H, Song Y, Yang Y, Gao G et al (2008) A missense mutation in SLC33A1, which encodes the acetyl-CoA transporter, causes autosomal-dominant spastic paraplegia (SPG42). *American journal of human genetics* 83: 752-759

Lin X, Barber DL (1996) A calcineurin homologous protein inhibits GTPase-stimulated Na-H exchange. *Proc Natl Acad Sci U S A* 93: 12631-12636

Lin X, Sikkink RA, Rusnak F, Barber DL (1999) Inhibition of calcineurin phosphatase activity by a calcineurin B homologous protein. *J Biol Chem* 274: 36125-36131

Ling KK, Gibbs RM, Feng Z, Ko CP (2012) Severe neuromuscular denervation of clinically relevant muscles in a mouse model of spinal muscular atrophy. *Hum Mol Genet* 21: 185-195

Liu Y, Zaun HC, Orlowski J, Ackerman SL (2013) CHP1-mediated NHE1 biosynthetic maturation is required for Purkinje cell axon homeostasis. *J Neurosci* 33: 12656-12669

Lorson CL, Androphy EJ (2000) An exonic enhancer is required for inclusion of an essential exon in the SMA-determining gene SMN. *Hum Mol Genet* 9: 259-265

Lorson CL, Hahnen E, Androphy EJ, Wirth B (1999) A single nucleotide in the SMN gene regulates splicing and is responsible for spinal muscular atrophy. *Proceedings of the National Academy of Sciences of the United States of America* 96: 6307-6311

Lowenthal A, Bekaert J, Van Dessel F, van Hauwaert J (1979) Familial cerebellar ataxia with hypogonadism. *J Neurol* 222: 75-80

Lunn MR, Wang CH (2008) Spinal muscular atrophy. *Lancet* 371: 2120-2133

Lyon AN, Pineda RH, Hao LT, Kudryashova E, Kudryashov DS, Beattie CE (2014) Calcium binding is essential for plastin 3 function in Smn-deficient motoneurons. *Human Molecular Genetics* 23: 1990-2004

Ma E, Haddad GG (1997) Expression and localization of Na⁺/H⁺ exchangers in rat central nervous system. *Neuroscience* 79: 591-603

Ma J, Zeng F, Schultz RM, Tseng H (2006) Basonuclin: a novel mammalian maternal-effect gene. *Development* 133: 2053-2062

MacDonald BK, Cockerell OC, Sander JW, Shorvon SD (2000) The incidence and lifetime prevalence of neurological disorders in a prospective community-based study in the UK. *Brain* 123 (Pt 4): 665-676

Mackay DJG, Esch F, Furthmayr H, Hall A (1997) Rho- and Rac-dependent assembly of focal adhesion complexes and actin filaments in permeabilized fibroblasts: An essential role for ezrin/radixin/moesin proteins. *Journal of Cell Biology* 138: 927-938

Magrane J, Hervias I, Henning MS, Damiano M, Kawamata H, Manfredi G (2009) Mutant SOD1 in neuronal mitochondria causes toxicity and mitochondrial dynamics abnormalities. *Hum Mol Genet* 18: 4552-4564

Mahmood F, Mozere M, Zdebek AA, Stanescu HC, Tobin J, Beales PL, Kleta R, Bockenbauer D, Russell C (2013) Generation and validation of a zebrafish model of EAST (epilepsy, ataxia, sensorineural deafness and tubulopathy) syndrome. *Dis Model Mech* 6: 652-660

Maier O, Bohm J, Dahm M, Bruck S, Beyer C, Johann S (2013) Differentiated NSC-34 motoneuron-like cells as experimental model for cholinergic neurodegeneration. *Neurochemistry international* 62: 1029-1038

Maniti O, Carvalho K, Picart C (2013) Model membranes to shed light on the biochemical and physical properties of ezrin/radixin/moesin. *Biochimie* 95: 3-11

Manto M, Marmolino D (2009) Cerebellar ataxias. *Curr Opin Neurol* 22: 419-429

Margolin DH, Kousi M, Chan YM, Lim ET, Schmahmann JD, Hadjivassiliou M, Hall JE, Adam I, Dwyer A, Plummer L et al (2013) Ataxia, dementia, and hypogonadotropism caused by disordered ubiquitination. *N Engl J Med* 368: 1992-2003

Mark MD, Krause M, Bode HJ, Kruse W, Pollok S, Kuner T, Dalkara D, Koekkoek S, De Zeeuw CI, Herlitze S (2015) Spinocerebellar Ataxia Type 6 Protein Aggregates Cause Deficits in Motor Learning and Cerebellar Plasticity (vol 35, pg 8882, 2015). *Journal of Neuroscience* 35: 12606-12607

Markowitz JA, Tinkle MB, Fischbeck KH (2004) Spinal muscular atrophy in the neonate. *J Obstet Gynecol Neonatal Nurs* 33: 12-20

Martin E, Yanicostas C, Rastetter A, Alavi Naini SM, Maouedj A, Kabashi E, Rivaud-Pechoux S, Brice A, Stevanin G, Soussi-Yanicostas N (2012) Spatacsin and spastizin act in the same pathway required for proper spinal motor neuron axon outgrowth in zebrafish. *Neurobiol Dis* 48: 299-308

Mateo I, Llorca J, Volpini V, Corral J, Berciano J, Combarros O (2003) GAA expansion size and age at onset of Friedreich's ataxia. *Neurology* 61: 274-275

Matsushita M, Sano Y, Yokoyama S, Takai T, Inoue H, Mitsui K, Todo K, Ohmori H, Kanazawa H (2007) Loss of calcineurin homologous protein-1 in chicken B lymphoma DT40 cells destabilizes Na⁺/H⁺ exchanger isoform-1 protein. *Am J Physiol Cell Physiol* 293: C246-254

Matsushita M, Tanaka H, Mitsui K, Kanazawa H (2011) Dual functional significance of calcineurin homologous protein 1 binding to Na⁽⁺⁾/H⁽⁺⁾ exchanger isoform 1. *Am J Physiol Cell Physiol* 301: C280-288

Matusica D, Fenech MP, Rogers ML, Rush RA (2008) Characterization and use of the NSC-34 cell line for study of neurotrophin receptor trafficking. *J Neurosci Res* 86: 553-565

McDonald CM (2012) Clinical approach to the diagnostic evaluation of hereditary and acquired neuromuscular diseases. *Phys Med Rehabil Clin N Am* 23: 495-563

McEntagart M, Dunstan M, Bell C, Boltshauser E, Donaghy M, Harper PS, Williams N, Teare MD, Rahman N (2002) Clinical and genetic heterogeneity in peroneal muscular atrophy associated with vocal cord weakness. *J Neurol Neurosurg Psychiatry* 73: 762-765

McGeer PL, McGeer EG, Itagaki S, Mizukawa K (1987) Anatomy and pathology of the basal ganglia. *Can J Neurol Sci* 14: 363-372

McKenna A, Hanna M, Banks E, Sivachenko A, Cibulskis K, Kernytsky A, Garimella K, Altshuler D, Gabriel S, Daly M et al (2010) The Genome Analysis Toolkit: a MapReduce framework for analyzing next-generation DNA sequencing data. *Genome Res* 20: 1297-1303

McKinnon PJ (2004) ATM and ataxia telangiectasia. *EMBO Rep* 5: 772-776

McWhorter ML, Monani UR, Burghes AH, Beattie CE (2003) Knockdown of the survival motor neuron (Smn) protein in zebrafish causes defects in motor axon outgrowth and pathfinding. *J Cell Biol* 162: 919-931

Meera P, Pulst SM, Otis TS (2016) Cellular and circuit mechanisms underlying spinocerebellar ataxias. *J Physiol-London* 594: 4653-4660

Melki J, Lefebvre S, Burglen L, Burlet P, Clermont O, Millasseau P, Reboullet S, Benichou B, Zeviani M, Le Paslier D et al (1994) De novo and inherited deletions of the 5q13 region in spinal muscular atrophies. *Science* 264: 1474-1477

Mendoza-Ferreira N, Coutelier M, Janzen E, Hosseinibarkooie S, Lohr H, Schneider S, Milbradt J, Karakaya M, Riessland M, Pichlo C et al (2018) Biallelic CHP1 mutation causes human autosomal recessive ataxia by impairing NHE1 function. *Neurol Genet* 4: e209

Merlini L, Stagni SB, Marri E, Granata C (1992) Epidemiology of neuromuscular disorders in the under-20 population in Bologna Province, Italy. *Neuromuscul Disord* 2: 197-200

Misgeld T, Burgess RW, Lewis RM, Cunningham JM, Lichtman JW, Sanes JR (2002) Roles of neurotransmitter in synapse formation: development of neuromuscular junctions lacking choline acetyltransferase. *Neuron* 36: 635-648

Mishima M, Wakabayashi S, Kojima C (2007) Solution structure of the cytoplasmic region of Na⁺/H⁺ exchanger 1 complexed with essential cofactor calcineurin B homologous protein 1. *J Biol Chem* 282: 2741-2751

Murphy SM, Laura M, Fawcett K, Pandraud A, Liu YT, Davidson GL, Rossor AM, Polke JM, Castleman V, Manji H et al (2012) Charcot-Marie-Tooth disease: frequency of genetic subtypes and guidelines for genetic testing. *J Neurol Neurosurg Psychiatry* 83: 706-710

Murphy SM, Laura M, Reilly MM (2013) DNA testing in hereditary neuropathies. *Handb Clin Neurol* 115: 213-232

Nadeau JH (2001) Modifier genes in mice and humans. *Nat Rev Genet* 2: 165-174

Nadeau JH (2003) Modifier genes and protective alleles in humans and mice. *Curr Opin Genet Dev* 13: 290-295

Nagita M, Inoue H, Nakamura N, Kanazawa H (2003) Two nuclear export signals specify the cytoplasmic localization of calcineurin B homologous protein 1. *J Biochem* 134: 919-925

Nagy PM, Aubert I (2012) Overexpression of the vesicular acetylcholine transporter increased acetylcholine release in the hippocampus. *Neuroscience* 218: 1-11

Nakamura N, Miyake Y, Matsushita M, Tanaka S, Inoue H, Kanazawa H (2002) KIF1Bbeta2, capable of interacting with CHP, is localized to synaptic vesicles. *J Biochem* 132: 483-491

Naoe Y, Arita K, Hashimoto H, Kanazawa H, Sato M, Shimizu T (2005) Structural characterization of calcineurin B homologous protein 1. *J Biol Chem* 280: 32372-32378

Nasevicius A, Ekker SC (2000) Effective targeted gene 'knockdown' in zebrafish. *Nat Genet* 26: 216-220

Nehrke K (2003) A reduction in intestinal cell pH_i due to loss of the *Caenorhabditis elegans* Na⁺/H⁺ exchanger NHX-2 increases life span. *J Biol Chem* 278: 44657-44666

Neveling K, Martinez-Carrera LA, Holker I, Heister A, Verrips A, Hosseini-Barkooie SM, Gilissen C, Vermeer S, Pennings M, Meijer R et al (2013) Mutations in BICD2, which encodes a golgin and important motor adaptor, cause congenital autosomal-dominant spinal muscular atrophy. *American journal of human genetics* 92: 946-954

Ng PC, Henikoff S (2003) SIFT: Predicting amino acid changes that affect protein function. *Nucleic Acids Res* 31: 3812-3814

Norton WH, Mangoli M, Lele Z, Pogoda HM, Diamond B, Mercurio S, Russell C, Teraoka H, Stickney HL, Rauch GJ et al (2005) Monorail/Foxa2 regulates floorplate differentiation and specification of oligodendrocytes, serotonergic raphe neurones and cranial motoneurones. *Development* 132: 645-658

O'Grady GL, Verschuuren C, Yuen M, Webster R, Menezes M, Fock JM, Pride N, Best HA, Benavides Damm T, Turner C et al (2016) Variants in SLC18A3, vesicular acetylcholine transporter, cause congenital myasthenic syndrome. *Neurology* 87: 1442-1448

Okano HJ, Park WY, Corradi JP, Darnell RB (1999) The cytoplasmic Purkinje onconeural antigen *cdr2* down-regulates c-Myc function: implications for neuronal and tumor cell survival. *Genes Dev* 13: 2087-2097

Oprea GE, Krober S, McWhorter ML, Rossoll W, Muller S, Krawczak M, Bassell GJ, Beattie CE, Wirth B (2008) Plastin 3 is a protective modifier of autosomal recessive spinal muscular atrophy. *Science* 320: 524-527

Ouyang YB, Mellergard P, Kristian T, Kristianova V, Siesjo BK (1994) Influence of Acid-Base Changes on the Intracellular Calcium-Concentration of Neurons in Primary Culture. *Exp Brain Res* 101: 265-271

Palau F, Espinos C (2006) Autosomal recessive cerebellar ataxias. *Orphanet J Rare Dis* 1: 47

Pandolfo M (2008) Friedreich ataxia. *Arch Neurol* 65: 1296-1303

Pandolfo M (2009) Friedreich ataxia: the clinical picture. *J Neurol* 256 Suppl 1: 3-8

Pang T, Hisamitsu T, Mori H, Shigekawa M, Wakabayashi S (2004) Role of calcineurin B homologous protein in pH regulation by the Na⁺/H⁺ exchanger 1: tightly bound Ca²⁺ ions as important structural elements. *Biochemistry* 43: 3628-3636

Pang T, Su X, Wakabayashi S, Shigekawa M (2001) Calcineurin homologous protein as an essential cofactor for Na⁺/H⁺ exchangers. *J Biol Chem* 276: 17367-17372

Pang TX, Wakabayashi S, Shigekawa M (2002) Expression of calcineurin B homologous protein 2 protects serum deprivation-induced cell death by serum-independent activation of Na⁺/H⁺ exchanger. *Journal of Biological Chemistry* 277: 43771-43777

Pang ZP, Sudhof TC (2012) Cell biology of Ca²⁺-triggered exocytosis. *Curr Opin Cell Biol* 22: 496-505

Pastore A, Puccio H (2013) Frataxin: a protein in search for a function. *J Neurochem* 126 Suppl 1: 43-52

Paulson HL, Miller VM (2005) Breaks in coordination: DNA repair in inherited ataxia. *Neuron* 46: 845-848

Pedersen SF, Hoffmann EK, Novak I (2013) Cell volume regulation in epithelial physiology and cancer. *Front Physiol* 4: 233

Perera EM, Martin H, Seeherunvong T, Kos L, Hughes IA, Hawkins JR, Berkovitz GD (2001) Tescalcin, a novel gene encoding a putative EF-hand Ca(2⁺)-binding protein, Col9a3, and renin are expressed in the mouse testis during the early stages of gonadal differentiation. *Endocrinology* 142: 455-463

Pfeiffer J, Johnson D, Nehrke K (2008) Oscillatory transepithelial H(+) flux regulates a rhythmic behavior in *C. elegans*. *Curr Biol* 18: 297-302

Pick U, Karlsh JD (1982) Regulation of the Conformational Transition in the Ca-ATPase from Sarcoplasmic-Reticulum by Ph, Temperature, and Calcium-Ions. *Journal of Biological Chemistry* 257: 6120-6126

Pierce SB, Walsh T, Chisholm KM, Lee MK, Thornton AM, Fiumara A, Opitz JM, Levy-Lahad E, Klevit RE, King MC (2010) Mutations in the DBP-deficiency protein HSD17B4 cause ovarian dysgenesis, hearing loss, and ataxia of Perrault Syndrome. *Am J Hum Genet* 87: 282-288

Pollard TD, Borisy GG (2003) Cellular motility driven by assembly and disassembly of actin filaments. *Cell* 112: 453-465

Pouyssegur J, Sardet C, Franchi A, L'Allemain G, Paris S (1984) A specific mutation abolishing Na⁺/H⁺ antiport activity in hamster fibroblasts precludes growth at neutral and acidic pH. *Proc Natl Acad Sci U S A* 81: 4833-4837

Prado VF, Martins-Silva C, de Castro BM, Lima RF, Barros DM, Amaral E, Ramsey AJ, Sotnikova TD, Ramirez MR, Kim HG et al (2006) Mice deficient for the vesicular acetylcholine transporter are myasthenic and have deficits in object and social recognition. *Neuron* 51: 601-612

Prado VF, Roy A, Kolisnyk B, Gros R, Prado MA (2013) Regulation of cholinergic activity by the vesicular acetylcholine transporter. *Biochem J* 450: 265-274

Puccio H, Koenig M (2000) Recent advances in the molecular pathogenesis of Friedreich ataxia. *Hum Mol Genet* 9: 887-892

Puls I, Jonnakuty C, LaMonte BH, Holzbaur EL, Tokito M, Mann E, Floeter MK, Bidus K, Drayna D, Oh SJ et al (2003) Mutant dynactin in motor neuron disease. *Nat Genet* 33: 455-456

Pulst SM (1999) Genetic linkage analysis. *Arch Neurol* 56: 667-672

Purves D (2004) *Neuroscience*, Sunderland, Mass.: Sinauer Associates, Publishers

Putney LK, Denker SP, Barber DL (2002) The changing face of the Na⁺/H⁺ exchanger, NHE1: structure, regulation, and cellular actions. *Annu Rev Pharmacol Toxicol* 42: 527-552

Pyati UJ, Look AT, Hammerschmidt M (2007) Zebrafish as a powerful vertebrate model system for in vivo studies of cell death. *Semin Cancer Biol* 17: 154-165

Qin K, Zhao L, Tang Y, Bhatta S, Simard JM, Zhao RY (2006) Doppel-induced apoptosis and counteraction by cellular prion protein in neuroblastoma and astrocytes. *Neuroscience* 141: 1375-1388

Raman IM, Bean BP (1999) Ionic currents underlying spontaneous action potentials in isolated cerebellar Purkinje neurons. *Journal of Neuroscience* 19: 1663-1674

Rideout HJ, Lang-Rollin I, Stefanis L (2004) Involvement of macroautophagy in the dissolution of neuronal inclusions. *Int J Biochem Cell Biol* 36: 2551-2562

Riessland M, Kaczmarek A, Schneider S, Swoboda KJ, Lohr H, Bradler C, Gysko V, Dimitriadi M, Hosseinibarkooie S, Torres-Benito L et al (2017) Neurocalcin Delta Suppression Protects against Spinal Muscular Atrophy in Humans and across Species by Restoring Impaired Endocytosis. *Am J Hum Genet* 100: 297-315

Ross CA, Poirier MA (2004) Protein aggregation and neurodegenerative disease. *Nat Med* 10 Suppl: S10-17

Rossoll W, Jablonka S, Andreassi C, Kroning AK, Karle K, Monani UR, Sendtner M (2003) Smn, the spinal muscular atrophy-determining gene product, modulates axon growth and localization of beta-actin mRNA in growth cones of motoneurons. *Journal of Cell Biology* 163: 801-812

Rossor AM, Kalmar B, Greensmith L, Reilly MM (2012) The distal hereditary motor neuropathies. *J Neurol Neurosurg Psychiatry* 83: 6-14

Ruano L, Melo C, Silva MC, Coutinho P (2014) The global epidemiology of hereditary ataxia and spastic paraplegia: a systematic review of prevalence studies. *Neuroepidemiology* 42: 174-183

Ruffin VA, Salameh AI, Boron WF, Parker MD (2014) Intracellular pH regulation by acid-base transporters in mammalian neurons. *Frontiers in physiology* 5

Ruiz R, Casanas JJ, Torres-Benito L, Cano R, Tabares L (2010) Altered intracellular Ca²⁺ homeostasis in nerve terminals of severe spinal muscular atrophy mice. *J Neurosci* 30: 849-857

Sacca F, Puorro G, Antenora A, Marsili A, Denaro A, Piro R, Sorrentino P, Pane C, Tessa A, Brescia Morra V et al (2011) A combined nucleic acid and protein analysis in Friedreich ataxia: implications for diagnosis, pathogenesis and clinical trial design. *PLoS one* 6: e17627

Saporta AS, Sottile SL, Miller LJ, Feely SM, Siskind CE, Shy ME (2011) Charcot-Marie-Tooth disease subtypes and genetic testing strategies. *Ann Neurol* 69: 22-33

Savitsky K, Bar-Shira A, Gilad S, Rotman G, Ziv Y, Vanagaite L, Tagle DA, Smith S, Uziel T, Sfez S et al (1995) A single ataxia telangiectasia gene with a product similar to PI-3 kinase. *Science* 268: 1749-1753

Schaefer AW, Schoonderwoert VTG, Ji L, Mederios N, Danuser G, Forscher P (2008) Coordination of actin filament and microtubule dynamics during neurite outgrowth. *Dev Cell* 15: 146-162

Schlachetzki JC, Saliba SW, Oliveira AC (2013) Studying neurodegenerative diseases in culture models. *Rev Bras Psiquiatr* 35 Suppl 2: S92-100

Schmid S, Azzopardi E, De Jaeger X, Prado MA, Prado VF (2011) VACHT knock-down mice show normal prepulse inhibition but disrupted long-term habituation. *Genes Brain Behav* 10: 457-464

Schofield D, Alam K, Douglas L, Shrestha R, MacArthur DG, Davis M, Laing NG, Clarke NF, Burns J, Cooper ST et al (2017) Cost-effectiveness of massively parallel sequencing for diagnosis of paediatric muscle diseases. *npj Genomic Medicine* 2: 4

Schreij AM, Fon EA, McPherson PS (2016) Endocytic membrane trafficking and neurodegenerative disease. *Cell Mol Life Sci* 73: 1529-1545

Schulz JB, Boesch S, Burk K, Durr A, Giunti P, Mariotti C, Pousset F, Schols L, Vankan P, Pandolfo M (2009) Diagnosis and treatment of Friedreich ataxia: a European perspective. *Nat Rev Neurol* 5: 222-234

Schwarz JM, Rodelsperger C, Schuelke M, Seelow D (2010) MutationTaster evaluates disease-causing potential of sequence alterations. *Nat Methods* 7: 575-576

Scoles DR, Meera P, Schneider MD, Paul S, Dansithong W, Figueroa KP, Hung GN, Rigo F, Bennett CF, Otis TS et al (2017) Antisense oligonucleotide therapy for spinocerebellar ataxia type 2. *Nature* 544: 362-+

Sekerkova G, Kim JA, Nigro MJ, Becker EBE, Hartmann J, Birnbaumer L, Mugnaini E, Martina M (2013) Early Onset of Ataxia in Moonwalker Mice Is Accompanied by Complete Ablation of Type II Unipolar Brush Cells and Purkinje Cell Dysfunction. *Journal of Neuroscience* 33: 19689-19694

Seminara SB, Acierno JS, Jr., Abdulwahid NA, Crowley WF, Jr., Margolin DH (2002) Hypogonadotropic hypogonadism and cerebellar ataxia: detailed phenotypic characterization of a large, extended kindred. *J Clin Endocrinol Metab* 87: 1607-1612

Senderek J, Krieger M, Stendel C, Bergmann C, Moser M, Breitbach-Faller N, Rudnik-Schoneborn S, Blaschek A, Wolf NI, Harting I et al (2005) Mutations in SIL1 cause Marinesco-Sjogren syndrome, a cerebellar ataxia with cataract and myopathy. *Nature Genetics* 37: 1312-1314

Sendtner M (2010) Therapy development in spinal muscular atrophy. *Nat Neurosci* 13: 795-799

Shafer TJ, Atchison WD (1991) Transmitter, ion channel and receptor properties of pheochromocytoma (PC12) cells: a model for neurotoxicological studies. *Neurotoxicology* 12: 473-492

Shen XM, Selcen D, Brengman J, Engel AG (2014) Mutant SNAP25B causes myasthenia, cortical hyperexcitability, ataxia, and intellectual disability. *Neurology* 83: 2247-2255

Shiloh Y (2006) The ATM-mediated DNA-damage response: taking shape. *Trends Biochem Sci* 31: 402-410

Siepel A, Bejerano G, Pedersen JS, Hinrichs AS, Hou M, Rosenbloom K, Clawson H, Spieth J, Hillier LW, Richards S et al (2005) Evolutionarily conserved elements in vertebrate, insect, worm, and yeast genomes. *Genome Res* 15: 1034-1050

Signorini S, Liao YJ, Duncan SA, Jan LY, Stoffel M (1997) Normal cerebellar development but susceptibility to seizures in mice lacking G protein-coupled, inwardly rectifying K⁺ channel GIRK2. *Proceedings of the National Academy of Sciences of the United States of America* 94: 923-927

Sin WC, Moniz DM, Ozog MA, Tyler JE, Numata M, Church J (2009) Regulation of early neurite morphogenesis by the Na⁺/H⁺ exchanger NHE1. *J Neurosci* 29: 8946-8959

Sinning A, Hubner CA (2013) Minireview: pH and synaptic transmission. *Febs Lett* 587: 1923-1928

Smith KR, Bromhead CJ, Hildebrand MS, Shearer AE, Lockhart PJ, Najmabadi H, Leventer RJ, McGillivray G, Amor DJ, Smith RJ et al (2011) Reducing the exome search space for mendelian diseases using genetic linkage analysis of exome genotypes. *Genome Biol* 12: R85

Son EJ, Moon IS, Kim SH, Kim SJ, Choi JY (2009) Interferon-gamma Suppresses Na⁺-H⁺ Exchanger in Cultured Human Endolymphatic Sac Epithelial Cells. *J Cell Biochem* 107: 965-972

Stiess M, Bradke F (2011) Neuronal Polarization: The Cytoskeleton Leads the Way. *Dev Neurobiol* 71: 430-444

Storbeck M, Horsberg Eriksen B, Unger A, Holker I, Aukrust I, Martinez-Carrera LA, Linke WA, Ferbert A, Heller R, Vorgerd M et al (2017) Phenotypic extremes of

BICD2-opathies: from lethal, congenital muscular atrophy with arthrogryposis to asymptomatic with subclinical features. *Eur J Hum Genet* 25: 1040-1048

Sudhof TC (2004) The synaptic vesicle cycle. *Annu Rev Neurosci* 27: 509-547

Sugita S, Fleming LL, Wood C, Vaughan SK, Gomes MP, Camargo W, Naves LA, Prado VF, Prado MA, Guatimosim C et al (2016) VACHT overexpression increases acetylcholine at the synaptic cleft and accelerates aging of neuromuscular junctions. *Skelet Muscle* 6: 31

Synofzik M, Hufnagel RB, Zuchner S (1993) PNPLA6-Related Disorders. In *GeneReviews(R)*, Pagon RA, Adam MP, Ardinger HH, Wallace SE, Amemiya A, Bean LJH, Bird TD, Ledbetter N, Mefford HC, Smith RJH et al (eds). Seattle (WA)

Tabares L, Betz B (2010) Multiple Functions of the Vesicular Proton Pump in Nerve Terminals. *Neuron* 68: 1020-1022

Takata RI, Speck Martins CE, Passosbueno MR, Abe KT, Nishimura AL, Da Silva MD, Monteiro A, Jr., Lima MI, Kok F, Zatz M (2004) A new locus for recessive distal spinal muscular atrophy at Xq13.1-q21. *Journal of medical genetics* 41: 224-229

Tarnutzer AA, Gerth-Kahlert C, Timmann D, Chang DI, Harmuth F, Bauer P, Straumann D, Synofzik M (2015) Boucher-Neuhauser syndrome: cerebellar degeneration, chorioretinal dystrophy and hypogonadotropic hypogonadism: two novel cases and a review of 40 cases from the literature. *J Neurol* 262: 194-202

Taylor JP, Hardy J, Fischbeck KH (2002) Toxic proteins in neurodegenerative disease. *Science* 296: 1991-1995

Tesson C, Koht J, Stevanin G (2015) Delving into the complexity of hereditary spastic paraplegias: how unexpected phenotypes and inheritance modes are revolutionizing their nosology. *Hum Genet* 134: 511-538

Thomas AC, Williams H, Seto-Salvia N, Bacchelli C, Jenkins D, O'Sullivan M, Mengrelis K, Ishida M, Ocaka L, Chanudet E et al (2014) Mutations in SNX14 cause a distinctive autosomal-recessive cerebellar ataxia and intellectual disability syndrome. *American journal of human genetics* 95: 611-621

Timm S, Titus B, Bernd K, Barroso M (1999) The EF-hand Ca²⁺-binding protein p22 associates with microtubules in an N-myristoylation-dependent manner. *Mol Biol Cell* 10: 3473-3488

Tsai PT, Hull C, Chu YX, Greene-Colozzi E, Sadowski AR, Leech JM, Steinberg J, Crawley JN, Regehr WG, Sahin M (2012) Autistic-like behaviour and cerebellar dysfunction in Purkinje cell Tsc1 mutant mice. *Nature* 488: 647-+

Tsuiko O, Noukas M, Zilina O, Hensen K, Tapanainen JS, Magi R, Kals M, Kivistik PA, Haller-Kikkatalo K, Salumets A et al (2016) Copy number variation analysis detects novel candidate genes involved in follicular growth and oocyte maturation in a cohort of premature ovarian failure cases. *Hum Reprod* 31: 1913-1925

Utine GE, Haliloglu G, Salanci B, Cetinkaya A, Kiper PO, Alanay Y, Aktas D, Boduroglu K, Alikasifoglu M (2013) A homozygous deletion in GRID2 causes a human phenotype with cerebellar ataxia and atrophy. *J Child Neurol* 28: 926-932

Valdmanis PN, Meijer IA, Reynolds A, Lei A, MacLeod P, Schlesinger D, Zatz M, Reid E, Dion PA, Drapeau P et al (2007) Mutations in the KIAA0196 gene at the SPG8 locus cause hereditary spastic paraplegia. *American journal of human genetics* 80: 152-161

Valerio M, Colosimo A, Conti F, Giuliani A, Grottesi A, Manetti C, Zbilut JP (2005) Early events in protein aggregation: molecular flexibility and hydrophobicity/charge interaction in amyloid peptides as studied by molecular dynamics simulations. *Proteins* 58: 110-118

van Blitterswijk M, Landers JE (2010) RNA processing pathways in amyotrophic lateral sclerosis. *Neurogenetics* 11: 275-290

Vanhoutteghem A, Delhomme B, Herve F, Nondier I, Petit JM, Araki M, Araki K, Djian P (2016) The importance of basonuclin 2 in adult mice and its relation to basonuclin 1. *Mech Dev* 140: 53-73

Varshavsky A (2012) The ubiquitin system, an immense realm. *Annu Rev Biochem* 81: 167-176

Vedanarayanan VV (2003) Mitochondrial disorders and ataxia. *Semin Pediatr Neurol* 10: 200-209

Venkatraman A, Hu YS, Didonna A, Cvetanovic M, Krbanjevic A, Bilesimo P, Opal P (2014) The histone deacetylase HDAC3 is essential for Purkinje cell function, potentially complicating the use of HDAC inhibitors in SCA1. *Hum Mol Genet* 23: 3733-3745

Viollet L, Barois A, Rebeiz JG, Rifai Z, Burlet P, Zarhrate M, Vial E, Dessainte M, Estournet B, Kleinknecht B et al (2002) Mapping of autosomal recessive chronic distal spinal muscular atrophy to chromosome 11q13. *Ann Neurol* 51: 585-592

Viollet L, Zarhrate M, Maystadt I, Estournet-Mathiaut B, Barois A, Desguerre I, Mayer M, Chabrol B, LeHeup B, Cusin V et al (2004) Refined genetic mapping of autosomal recessive chronic distal spinal muscular atrophy to chromosome 11q13.3

and evidence of linkage disequilibrium in European families. *Eur J Hum Genet* 12: 483-488

Vissers LE, de Ligt J, Gilissen C, Janssen I, Steehouwer M, de Vries P, van Lier B, Arts P, Wieskamp N, del Rosario M et al (2010) A de novo paradigm for mental retardation. *Nat Genet* 42: 1109-1112

Voncken M, Ioannou P, Delatycki MB (2004) Friedreich ataxia-update on pathogenesis and possible therapies. *Neurogenetics* 5: 1-8

Wagner J, Allman E, Taylor A, Ulmschneider K, Kovanda T, Ulmschneider B, Nehrke K, Peters MA (2011) A calcineurin homologous protein is required for sodium-proton exchange events in the *C. elegans* intestine. *Am J Physiol Cell Physiol* 301: C1389-1403

Walter JT, Alvina K, Womack MD, Chevez C, Khodakhah K (2006) Decreases in the precision of Purkinje cell pacemaking cause cerebellar dysfunction and ataxia. *Nature Neuroscience* 9: 389-397

Wang K, Li M, Hakonarson H (2010) ANNOVAR: functional annotation of genetic variants from high-throughput sequencing data. *Nucleic Acids Res* 38: e164

Warr A, Robert C, Hume D, Archibald A, Deeb N, Watson M (2015) Exome Sequencing: Current and Future Perspectives. *G3 (Bethesda)* 5: 1543-1550

Whittaker RG, Herrmann DN, Bansagi B, Hasan BA, Lofra RM, Logigian EL, Sowden JE, Almodovar JL, Littleton JT, Zuchner S et al (2015) Electrophysiologic features of SYT2 mutations causing a treatable neuromuscular syndrome. *Neurology* 85: 1964-1971

Willems PJ, Van Roy BC, Kleijer WJ, Van der Kraan M, Martin JJ (1993) Atypical clinical presentation of ataxia telangiectasia. *Am J Med Genet* 45: 777-782

Willoughby D, Thomas RC, Schwiening CJ (2001) The effects of intracellular pH changes on resting cytosolic calcium in voltage-clamped snail neurones. *J Physiol-London* 530: 405-416

Wirth B (2000) An update of the mutation spectrum of the survival motor neuron gene (SMN1) in autosomal recessive spinal muscular atrophy (SMA). *Hum Mutat* 15: 228-237

Wirth B, Brichta L, Schrank B, Lochmuller H, Blick S, Baasner A, Heller R (2006) Mildly affected patients with spinal muscular atrophy are partially protected by an increased SMN2 copy number. *Hum Genet* 119: 422-428

Wirth B, Garbes L, Riessland M (2013) How genetic modifiers influence the phenotype of spinal muscular atrophy and suggest future therapeutic approaches. *Curr Opin Genet Dev* 23: 330-338

Wirth B, Mendoza-Ferreira N, Torres-Benito L (2017) Chapter 12 - Spinal Muscular Atrophy Disease Modifiers A2 - Sumner, Charlotte J. In *Spinal Muscular Atrophy*, Paushkin S, Ko C-P (eds) pp 191-210. Academic Press

Wolf NI, Koenig M (2013) Progressive cerebellar atrophy: hereditary ataxias and disorders with spinocerebellar degeneration. *Handb Clin Neurol* 113: 1869-1878

Wolosker H, Rocha JBT, Engelender S, Panizzutti R, DeMiranda J, deMeis L (1997) Sarco/endoplasmic reticulum Ca²⁺-ATPase isoforms: Diverse responses to acidosis. *Biochemical Journal* 321: 545-550

Woods CG, Bunday SE, Taylor AM (1990) Unusual features in the inheritance of ataxia telangiectasia. *Hum Genet* 84: 555-562

Wu CH, Fallini C, Ticozzi N, Keagle PJ, Sapp PC, Piotrowska K, Lowe P, Koppers M, McKenna-Yasek D, Baron DM et al (2012) Mutations in the profilin 1 gene cause familial amyotrophic lateral sclerosis. *Nature* 488: 499-+

Xia Y, Zhao P, Xue J, Gu XQ, Sun XL, Yao H, Haddad GG (2003) Na⁺ channel expression and neuronal function in the Na⁺/H⁺ exchanger 1 null mutant mouse. *Journal of neurophysiology* 89: 229-236

Yao H, Ma EB, Gu XQ, Haddad GG (1999) Intracellular pH regulation of CA1 neurons in Na⁺/H⁺ isoform 1 mutant mice. *J Clin Invest* 104: 637-645

Yi L, Donsante A, Kennerson ML, Mercer JF, Garbern JY, Kaler SG (2012) Altered intracellular localization and valosin-containing protein (p97 VCP) interaction underlie ATP7A-related distal motor neuropathy. *Hum Mol Genet* 21: 1794-1807

Zatloukal K, Stumptner C, Fuchsbichler A, Heid H, Schnoelzer M, Kenner L, Kleinert R, Prinz M, Aguzzi A, Denk H (2002) p62 Is a common component of cytoplasmic inclusions in protein aggregation diseases. *Am J Pathol* 160: 255-263

Zerres K, Rudnik-Schoneborn S, Forkert R, Wirth B (1995) Genetic basis of adult-onset spinal muscular atrophy. *Lancet* 346: 1162

Zeviani M, Simonati A, Bindoff LA (2012) Ataxia in mitochondrial disorders. *Handb Clin Neurol* 103: 359-372

Zh LX, Zhou RH, Mettler S, Wu T, Abbas A, Delaney J, Forte JG (2007) High turnover of ezrin T567 phosphorylation: conformation, activity, and cellular function. *Am J Physiol-Cell Ph* 293: C874-C884

Zhang X, Chou W, Haig-Ladewig L, Zeng W, Cao W, Gerton G, Dobrinski I, Tseng H (2012) BNC1 is required for maintaining mouse spermatogenesis. *Genesis* 50: 517-524

Zhang ZS, Nguyen KT, Barrett EF, David G (2010) Vesicular ATPase Inserted into the Plasma Membrane of Motor Terminals by Exocytosis Alkalinizes Cytosolic pH and Facilitates Endocytosis. *Neuron* 68: 1097-1108

Zhao LH, Longo-Guess C, Harris BS, Lee JW, Ackerman SL (2005) Protein accumulation and neurodegeneration in the woozy mutant mouse is caused by disruption of SIL1, a cochaperone of BiP. *Nature Genetics* 37: 974-979

Zhou J, Tawk M, Tiziano FD, Veillet J, Bayes M, Nolent F, Garcia V, Servidei S, Bertini E, Castro-Giner F et al (2012) Spinal muscular atrophy associated with progressive myoclonic epilepsy is caused by mutations in *ASAH1*. *American journal of human genetics* 91: 5-14

Zhou W, Qian Y, Kunjilwar K, Pfaffinger PJ, Choe S (2004) Structural insights into the functional interaction of KChIP1 with Shal-type K(+) channels. *Neuron* 41: 573-586

Zoupa M, Machera K (2017) Zebrafish as an Alternative Vertebrate Model for Investigating Developmental Toxicity-The Triadimefon Example. *Int J Mol Sci* 18

8. PUBLICATIONS, PRESENTATIONS, SCHOLARSHIPS AND AWARDS

Publications

- **Mendoza-Ferreira N**, Coutelier M, Janzen E, Hosseinibarkooie SM, Löhr H, Schneider S, Milbradt J, Karakaya M, Riessland M, Pichlo C, Torres-Benito L, Singleton A, Zuchner S, Brice A, Durr A, Hammerschmidt M, Stevanin G, Wirth B.
Biallelic CHP1 mutation causes human autosomal recessive ataxia by impairing NHE1 function. Neurology® Genetics, 2018, 4:e209
- Wirth B, **Mendoza-Ferreira N**, Torres-Benito L.
Chapter: Spinal Muscular Atrophy Disease Modifiers. In Book: Spinal Muscular Atrophy. Edited by Sumner CJ, Paushkin S and Ko CP. Academic Press (Elsevier), 2017, pp. 191-210
- Hosseinibarkooie SM, Peters M, Torres-Benito L, Rastetter RH, Hupperich K, Hoffmann A, **Mendoza-Ferreira N**, Kaczmarek A, Janzen E, Milbradt J, Lamkemeyer T, Rigo F, Bennett CF, Guschlbauer C, Büschges A, Hammerschmidt M, Riessland M, Jeong MK, Clemen CS, Wirth B.
The power of human protective modifiers: PLS3 and CORO1C unravel impaired endocytosis in spinal muscular atrophy and rescue SMA phenotype. American Journal of Human Genetics, 2016, 99, pp. 647-665.

Oral presentations

- **Mendoza-Ferreira N**, Coutelier M, Janzen E, Hosseinibarkooie SM, Löhr H, Schneider S, Milbradt J, Karakaya M, Riessland M, Pichlo C, Torres-Benito L, Singleton A, Zuchner S, Brice A, Durr A, Hammerschmidt M, Stevanin G, Wirth B.
Identification and Functional Characterization of a CHP1, a new causative gene of ARCA
March, 2017. 1st Cologne Neuroscience Day. Cologne, Germany.
- **Mendoza-Ferreira N**, Coutelier M, Janzen E, Hosseinibarkooie SM, Löhr H, Schneider S, Milbradt J, Riessland M, Pichlo C, Torres-Benito L, Brice A, Durr A, Hammerschmidt M, Stevanin G, Wirth B.
Identification and Functional Characterization of a CHP1, a new ARCA-causative gene.
October, 2016. 6th Annual Human Genetics Meeting, University of Cologne. Cologne, Germany.
- **Mendoza-Ferreira N**, Coutelier M, Janzen E, Hosseinibarkooie SM, Milbradt J, Torres-Benito L, Riessland M, Hammerschmidt M, Stevanin G, Wirth B.
Identification and Functional Characterization of CHP1, a new potential causative gene of Autosomal Recessive Ataxia with Hypergonadotropic Hypogonadism
April, 2015. 2nd Joint Annual NeurOmics Meeting, Palma de Mallorca, Spain.

Poster presentations

- **Mendoza-Ferreira N**, Coutelier M, Janzen E, Hosseinibarkooie SM, Löhr H, Schneider S, Milbradt J, Riessland M, Pichlo C, Torres-Benito L, Brice A, Durr A, Hammerschmidt M, Stevanin G, Wirth B.
Identification and Functional Characterization of a CHP1, a new ARCA-causative gene.
May, 2017. 4th Joint Annual NeurOmics Meeting. Berlin, Germany.

- **Mendoza-Ferreira N**, Coutelier M, Janzen E, Hosseinibarkooie SM, Löhr H, Schneider S, Milbradt J, Riessland M, Pichlo C, Torres-Benito L, Brice A, Durr A, Hammerschmidt M, Stevanin G, Wirth B.
Identification and Functional Characterization of a CHP1, a new ARCA-causative gene. October, 2016. Annual Human Genetics Meeting, University of Cologne. Cologne, Germany.
- **Mendoza-Ferreira N**, Janzen E, Coutelier M, Hosseinibarkooie SM, Schneider S, Milbradt J, Torres-Benito L, Riessland M, Hammerschmidt M, Stevanin, G, Wirth, B.
Identification and Functional Characterization of CHP1, a new potential causative gene of Autosomal Recessive Ataxia with Hypogonadism.
April, 2016. Cold Spring Harbor Laboratory meeting in: Protein Homeostasis in Health and Disease. Cold Spring Harbor, New York.
- **Mendoza-Ferreira N**, Coutelier M, Janzen E, Hosseinibarkooie SM, Milbradt J, Torres-Benito L, Riessland M, Hammerschmidt M, Stevanin G, Wirth B.
Identification and Functional Characterization of CHP1, a new potential causative gene of Autosomal Recessive Ataxia with Hypergonadotropic Hypogonadism
April, 2015. 2nd Joint Annual NeurOmics Meeting. Palma de Mallorca, Spain.
- **Mendoza-Ferreira N**, Coutelier M, Haberlova J, Janzen E, Neveling K, Milbradt J, Martinez-Carrera L, Hosseinibarkooie SM, Torres-Benito L, Riessland M, Seeman P, Stevanin G, Wirth B.
Identification and functional characterization of the genetic cause in one family with hereditary motor neuropathy and one with recessive ataxia.
May, 2014. 5th Annual Human Genetics Meeting, University of Cologne. Cologne, Germany.
- **Mendoza-Ferreira N**, Haberlova J, Neveling K, Martinez-Carrera L, Riessland M, Seeman P, Wirth B.
Functional Analysis of a Distal Motor Neuropathy – Related Mutation of *SLC18A3*. A Zebrafish Model Approach.
February, 2013. 1st Joint Annual NeurOmics, EURenOmics and RDConnect Meeting. Heidelberg, Germany.

Scholarships and Awards

- Best poster prize. 4th Joint Annual NeurOmics Meeting. Berlin, German, March, 2017.
- Financial aid to attend the Cold Spring Harbor Laboratory meeting in: Protein Homeostasis in Health and Disease. Funds from Cold Spring Harbor Laboratory. Cold Spring Harbor, New York, April, 2016.
- Best poster prize. 1st Joint Annual NeurOmics, EURenOmics and RDConnect Meeting. Prize awarded by Faculty1000 Research Ltd, April, 2015.
- Course and Travel Scholarship to attend the 27th Course in Medical Genetics. European Society of Human Genetics. Bertinoro de Romagna, Italy, May, 2014.

ACKNOWLEDGMENTS

I would like to express my deep gratitude to my supervisor Professor. Dr. Brunhilde Wirth for giving me the opportunity and support to work in her group, for her guidance, enthusiastic encouragement, optimism and knowledge. I am more than grateful for the freedom she granted me to develop and pursue my scientific interests, for helping me grow as a scientist and for her generous support to attend international meetings and further training. I would also like to thank her for always having time and being available. Her passionate dedication to science was –and still is- an inspiration for me.

I thank my examiner Professor Dr. Elena Rugarli for kindly agreeing to review my thesis and Professor Dr. Ansgar Büschges for taking the chair in my thesis defense.

I would like to thank our collaborators from the SPATAX network (Drs. Giovani Stevanin, Alexandra Durr, Marie Coutelier and Alexis Brice) for our work together in the “CHP1 project” and to Drs. Pavel Seeman and Konny Neveling in the “VACHT project”. I am extremely grateful to all participating patients and family members, without whom this research would not be possible. I also thank Prof. Matthias Hammerschmidt and Dr. Heiko Löhr for their supervision and support on the Zebrafish work. Further, I thank Christian Pichlo for the great protein modelling (magic) work together.

A huge thanks to all members of the RG. Wirth ☺. I am especially grateful to my fish team Janine (J) and Svenja for all those endless injections together (fire alarm included!) and for all the good times we shared (earrings business, writing cave...). I thank Lilian and Störtl for their initial supervision (I learned a lot!), for welcoming me in the “small lab” and not being angry at me and my stationery-stealing habit. Thanks to Mohsen for his help with the chromatography, and the buffer, and the blot, and... just thanks for taking care of my proteins as your own. I further thank Laura (Mari) for... so much! For your always valuable input and all the moments of bliss, and not so much bliss, we have shared together. Eva, my CHP1-team pal, thanks for all the input you brought to my project and for helping me to find the same antibody one thousand times. I thank our talented technicians Vanessa and Theresa for helping me with the small things (maybe not so small), when I need it the most. My words of gratitude are also extensive to former and current members: Anna, Miri, Markus Riessland (who introduced me to the fish world), Nassim, Ludwig, Mert, Kristina, Andrea Hoffman, Aaradhita, Irmgard, Andrea Delle Vedove, Eike and Anixa. I have enjoyed working next to all of you.

I would also like to thank the members of the RG Kye: Wiebke, Max, Joanna and especially Ines (Nes) for all the happy moments, for your kindness and for the warmest welcome I could've ever had. I also thank Min for all the scientific and pseudo-scientific conversations

and her valuable advice. Further, I thank the entire Institute of Human Genetics as well as Dr. Uwe Becker, for making of my German “bureaucratic” issues something manageable.

The following acknowledgment words go to my family. To my parents Donaldo and Angela and my little brother Camilo for their love, constant support, endless motivation and faith in me. Thanks for finding the way to remain closer, despite the distance. To my lifelong lasting friends: Lina, Isabel and *mis parseros* Lina and Pata for your unconditional friendship and for that crazy way of believing in me. To Anne und Thomas, for taking care of me as a daughter. Finally, I thank Enrico Piras for being my love and my best friend, for always finding a way to uplift my spirit, for his constant support and motivation and for building with me a place we feel like home.

EIDESSTATTLICHE ERKLÄRUNG

Ich versichere, dass ich die von mir vorgelegte Dissertation selbstständig angefertigt, die benutzten Quellen und Hilfsmittel vollständig angegeben und die Stellen der Arbeit – einschließlich Tabellen, Karten und Abbildungen – die anderen Werken im Wortlaut oder im Sinn nach entnommen sind, in jedem Einzelfall als Entlehnung kenntlich gemacht habe; dass diese Dissertation noch an keiner anderen Fakultät oder Universität zur Prüfung vorgelegen hat; dass sie –abgesehen von den angegebenen Teilpublikationen- noch nicht veröffentlicht worden ist sowie, dass ich eine solche Veröffentlichung vor Abschluss des Promotionsverfahrens nicht vornehmen werde. Die Bestimmungen dieser Promotionsordnung sind mir bekannt. Die von mir vorgelegte Dissertation ist von Prof. Dr. Brunhilde Wirth betreut worden.

Teilpublikationen sind in Kapitel 8 angegeben.

Ich versichere, dass ich alle Angaben wahrheitsgemäß nach bestem Wissen und Gewissen gemacht haben und verpflichte mich, jedmögliche, die obigen Angaben betreffenden Veränderungen, dem Promotionsausschuss unverzüglich mitzuteilen.

.....

Datum

.....

Unterschrift

LEBENS LAUF

· Persönliche Daten

Name Mendoza-Ferreira
 Vorname Natalia
 Geburtsdatum 21.01.1985
 Geburtsort Popayán, Cauca, Kolumbien
 Nationalität Kolumbianisch

· Schulische Ausbildung

1989 – 2001 Besuch des „San Jose de Tarbes“ Gymnasium in Popayán, Cauca (Kolumbien). Erwerb der allgemeinen Hochschulzugangsberechtigung

· Akademische Ausbildung

2001 – 2007 Studium der Biologie an der Universität „del Cauca“ in Popayán, Cauca, (Kolumbien)
 - Thema der Bachelorarbeit: *DNA damage assessment in car painters occupationally exposed to organic solvents*

2008 – 2010 Studium der Molekularbiologie an der Universität „de Valencia“ in Valencia, (Spanien)
 - Akademischer Abschluss: Master of Science. *Master in cellular and molecular biology and Genetics*
 - Thema der Masterarbeit: *Functional characterization of the C-terminal region of MnME, a modifying-tRNA protein*

· Praktika und Berufserfahrung

2012 – 2013 Praktikum am Leibniz Institut für Altersforschung in Jena, (Deutschland)
 - Forschungsprojekt: *Virus-induced oncogenesis*

2010 – 2012 Wissenschaftliche Lehrbeauftragte an der Universität „del Rosario“ in Bogotá, Kolumbien

2008 – 2010 Wissenschaftlicher Mitarbeiter am Forschungsinstitut „Principe Felipe“ in Valencia (Spanien). Stipendium „*Santiago Grisolia*“ for young researchers
 - Forschungsprojekt: *tRNA post-transcriptional modification and mitochondrial disorders*

2009 Biologie Dozentin am Gymnasium „Fundación Educativa Integral“ in Popayán, Cauca, (Kolumbien)

· Dissertation

2013 – 2017 Promotionsstudium im Fach Genetik am Institut für Humangenetik der Universitätsklinik Köln unter der Anleitung von Prof. Dr.rer.nat Brunhilde Wirth. Köln, (Deutschland).
 - Titel der Dissertation: *Uncovering and Functional Analysis of Novel Genes and Potential Genetic Modifiers for Neuromuscular Disorders*